

THÈSE

Présentée à

L'UNIVERSITÉ BORDEAUX 1

ÉCOLE DOCTORALE DES SCIENCES CHIMIQUES DE BORDEAUX

POUR OBTENIR LE GRADE DE:

DOCTEUR EN SCIENCE

Par

M. Pengxiang ZHAO

SPÉCIALITÉ: CHIMIE MOLECULAIRE

Thèse dirigée par le Professeur Didier ASTRUC

ISM, Groupe Nanosciences et Catalyse, Université Bordeaux 1

Titre de la thèse:

NANOPARTICULES D'OR : FONCTIONNALISATIONS ET APPLICATIONS EN NANOMEDECINE ET NANOMATERIAUX

Soutenue le 31 Aout 2012 devant la commission d'examen

COMPOSITION DU JURY

M. Jaques Robert	Professeur à l'Université Bordeaux 2	Rapporteur
M^{me}. Gillian Barratt	Directeur de Recherche CNRS à Université de Paris 11	Rapporteur
M^{me}. Maria Csiba-Dalko	Directeur de Recherche à L'Oréal, Paris	Membre
M. Jean-François Létard	Directeur de Recherche CNRS à l'Université Bordeaux 1	Membre
M. Jaime Ruiz	Ingénieur de Recherche CNRS à l'Université Bordeaux 1	Membre
M. Lionel Salmon	Chargé de Recherche CNRS au LCC de Toulouse	Membre
M. Didier Astruc	Professeur à l'Université Bordeaux 1, Membre de l'Institut Universitaire de France	Directeur de thèse

<<Je suis de ceux qui pensent que la science a une grande beauté. Un savant dans son laboratoire n'est pas seulement un technicien : c'est aussi un enfant en face de phénomènes naturels qui l'impressionnent comme un conte de fées.>>

-----Marie Curie

Je tiens à exprimer mes remerciements à mon père et ma mère, merci pour votre amour et votre support inconditionnel dans ces trois années de thèse.

Remerciements

Ce travail a été effectué dans le Groupe Nanosciences et Catalyse, ISM, Université de Bordeaux 1 (CNRS UMR 5255), sous la direction scientifique du Professeur Didier Astruc, Membre de l'Institut Universitaire de France.



Je remercie beaucoup Monsieur le Professeur Didier Astruc pour m'avoir donné l'opportunité de réaliser ma thèse sur "Nanoparticules d'or" dans son laboratoire. C'est lui qui m'a rendu amoureux de la chimie. Durant les trois années passées, il m'a permis de me familiariser avec les nanosciences. Je le remercie pour tout l'enthousiasme avec lequel il a dirigé cette thèse, pour les nombreux conseils et les bonnes idées qu'il m'a donnés au quotidien. Il m'a toujours encouragé quand j'ai rencontré les difficultés et m'a donné la force de continuer. Il est comme un père et un ami qui a essayé de m'aider à la fois dans les sciences et dans la vie quotidienne. Je lui exprime toute ma gratitude pour tout ce qu'il a fait pour moi durant les trois années.



J'adresse mes sincères remerciements à Mme. Gillian Barratt, Directeur de Recherche CNRS à l'Université de Paris 11 et à M. Jaques Robert Professeur à l'Université Bordeaux 2 pour avoir accepté d'être rapporteurs de ce manuscrit et pour leurs précieux conseils et corrections.

J'exprime toute ma reconnaissance à M. Lionel Salmon, Chargé de Recherche CNRS au LCC de Toulouse pour sa participation à ce jury et pour toute son aide cruciale et ses excellents conseils.

Que Mme. Maria Csiba-Dalko Resercher à L'Oréal, Paris et M. Jean-François Létard Professeur à l'Université de Bordeaux 1, qui m'ont fait l'honneur de bien vouloir participer à mon jury, en soient bien remerciés.



J'exprime toute ma gratitude à M. Jaime Ruiz, Ingénieur de Recherche du CNRS, qui m'a encadré tout au long de ces trois ans passés dans ce groupe. Il a eu beaucoup de patience à m'apprendre la manipulation expérimentale et à m'aider dans la vie quotidienne. Bien que j'ai rencontré plusieurs difficultés au cours de ma thèse, il m'a toujours encouragé et m'a donné beaucoup de force pour surmonter les difficultés. Je le remercie pour tous ces moments passés ensemble et je ne les oublierai jamais.



Je remercie du fond du coeur toutes les personnes qui ont participé de près ou de loin à ce travail de recherche: je remercie entre autres, M. Jean Michel et M. Noël Pinaud pour leurs conseils en RMN, M. Lionel Salmon pour les analyses TEM et M. Nicolas Guidolin pour les analyses DLS.

Je tiens à remercier tout le personnel de l'ISM, en particulier Karine Ndiaye, Bernadette Spinadel, Thierry Bataille, Michel Colomes, et Fabrice Folini.



Enfin, mes salutations amicales à tous les étudiants présents ou qui l'ont été dans notre groupe: Abdou, Rodrique, Lily, Alison, Maxime, Frida. Je vous souhaite à tous beaucoup de bonheur et beaucoup de réussite dans la vie.

J'exprime toute ma gratitude à Lily pour son aide et sa patience lorsque je suis arrivé en France. Je remercie du fond du coeur Amalia, Christophe, Dong et Yanlan, pour leur gentillesse, leur soutien et leurs précieux conseils. Je remercie aussi tout particulièrement Na et Maxime pour leur amicale collaboration durant la fin de ma thèse.

J'ai été très heureux de travailler avec tous ces membres de notre groupe et leur amitié m'est très précieuse. Je vous souhaite à tous une bonne continuation et la réussite dans tous les domaines de l'existence pour le futur.



Pour finir, je n'oublie pas d'adresser tous mes remerciements à mon Professeur de Master, M. Wuyong CHEN, Directeur du Département à l'Université de Sichuan à Chengdu, Chine, qui m'a donné l'opportunité de venir en France, ainsi qu'à l'administration de mon pays qui a assuré le financement de la thèse.

Nanoparticules d'or: fonctionnalisations et applications vers la nanomédecine et les nanomatériaux

Résumé:

La thèse a été consacrée à la synthèse, fonctionnalisations et application biomédicales et pour les matériaux de nouvelles nanoparticules d'or. Le manuscrit comporte d'abord des contributions substantielles à leur étude bibliographique ainsi qu'à la vectorisation du docétaxel. Sur le plan expérimental, des nanoparticules d'or fonctionnelles ont été synthétisées avec pour objectif l'élaboration de nanomatériaux pour applications biomédicales et propriétés physiques originales. L'étude de la fonctionnalisation a conduit à utiliser la chimie "click" entre des nanoparticules d'or portant des ligands thiolates azotés et des alcynes terminaux en utilisant un catalyseur au cuivre (I) dont le centre métallique est stabilisé et électroniquement enrichi par un ligand tétra-azoté, ce qui a permis d'introduire des fonctions très variées. En particulier le récepteur folate a été greffé de façon covalente pour la synthèse de nouveaux vecteurs du docétaxel, un puissant agent anti-cancéreux dont l'étude in vitro vis-à-vis de cellules cancéreuses est menée en collaboration par les laboratoires de l'Institut Bergonié de Bordeaux et la Faculté de Pharmacie de Chatenay-Malabry. Des nanoparticules d'or fonctionnelles ont aussi servi de support pour le greffage de complexes du fer (II) à transition de spin, ce qui a permis de réaliser l'étude en 2D par différentes techniques physiques en collaboration avec l'équipe d'Azzedine Bousseksou à Toulouse. Enfin les nanoparticules d'or ont servi de templates pour l'encapsulation de vitamines variées et un nouveau ligand azoté a été mis au point pour la synthèse de nanoparticules d'or originales avec diverses applications en synthèse de nanomatériaux et reconnaissance moléculaire (ATP et vitamine C).

Gold Nanoparticles : Functionalizations and Applications in Nanomedicine and Nanomaterials

Abstract

The thesis was devoted to the synthesis, functionalization and biomedical application for gold nanoparticles. The first chapter of this manuscript includes the contributions to the literature review of gold nanoparticles and the vectorization of docetaxel. Experimentally, functional gold nanoparticles were synthesized with the aim of developing nanomaterials for biomedical applications and original physical properties. The study of functionalization by "click" was carried out between gold nanoparticles with thiolate ligands azides and terminal alkynes using a copper catalyst (I). The metal center of the catalyst is electronically stabilized and enriched by a

tetra-nitrogen ligand, which has introduced a variety of functions of gold nanoparticles. In particular, the folate receptor was covalently introduced to for vectorizing docetaxel, a potent anticancer agent whose *in vitro* study on cancer cells is conducted in collaboration with the laboratories of the Bergonie Institute of Bordeaux and the Faculty of Pharmacy of Chatenay-Malabry. Functional gold nanoparticles have also served as a support for grafting complex of iron (II) spin transition, which helped conduct the study in 2D by various physical techniques in collaboration with the team Azzedine Bousseksou in Toulouse. Finally the gold nanoparticles were used as templates for encapsulation of various vitamins and a new nitrogen ligand has been developed for the synthesis of gold nanoparticles with various original synthetic applications of molecular recognition and nanomaterials (ATP and vitamin C).

Keywords: Gold nanoparticles, Docetaxel, Vitamins, Biosensors, Catalyst, Nanomedicine

List of published or submitted thesis publications

1. **P. Zhao**, D. Astruc, Docetaxel nanotechnology in anti-cancer therapy, *ChemMedChem* **2012**, DOI: 10.1002/cmdc.201200052.
2. **P. Zhao**, M.Grillaud, L. Salmon, J. Ruiz, D. Astruc, Click Functionalization of Gold Nanoparticles Using the Very Efficient CatalystCopper^I(Hexabenzyl)Tris-(2-aminoethyl) Amine Bromide, *Adv. Syn. Catal.* **2012**, 354, 1001-1011.
3. **P. Zhao**, N, Li, D. Astruc, State the art in gold nanoparticle synthesis, **2012**, submitted
4. **P. Zhao**, L. Salmon, J. Ruiz, D. Astruc, Encapsulation of Water-soluble Vitamins by Gold Nanoparticles in Hydrophobic Media, **2012**, submitted.
5. G. Molnár, I. A. Gural'skiy, C. Quintero, A. Akou, K. Abdul-kader, G. Félix, M. Lopes, L. Salmon, W. Nicolazzi, **P. Zhao**, D. Astruc, A. Bousseksou, Detection of Molecular Spin State Changes in Ultra-thin Films by Photonic Methods, **2012**, submitted.

Table des matières- Table of Content

General Introduction (English).....	9
Chapter 1	12
Overview on the Preparation of Gold Nanoparticles and Nanotechnology on Docetaxel delivery.....	12
1.1 Introduction.....	13
1.2 State of the Art in Gold Nanoparticle Synthesis	14
1.3 Docetaxel nanotechnology in anti-cancer therapy.....	73
Chapter 2	94
The improvement of Functionalization of AuNPs by “Click” Chemistry	94
2.1 Introduction.....	95
2.2 Click Functionalization of Gold Nanoparticles Using the very Efficient Datalyst Copper (I) (Hexabenzyl) tris (2-aminoethyl)- amine Bromide	95
Chapter 3	111
Biomedical Applications of Gold Nanoparticles.....	111
3.1 Introduction.....	112
3.2 Gold Nanoparticles on Docetaxel Drug Delivery Systems.....	112
3.3 Encapsulation of Water-soluble Vitamins by Gold Nanoparticles in Hydrophobic Media.....	127
Chapter 4	138
The Application of AuNPs on the Device of Spin Transition.....	138
4.1 Introduction.....	139
4.2 Gold Nanoparticles on Spin Transition Device.....	143
Conclusions and Perspectives	158

Introduction générale - General Introduction

Les nanoparticules d'or (AuNPs) ont suscité de tous temps beaucoup d'intérêt et de curiosité, et les recherches dans ce domaine se considérablement accélérées durant ces dernières années en raison de leurs applications en optique (liées à leur absorption plasmonique), catalyse et nanomédecine (diagnostic et thérapie)¹. La chimie se situe au cœur de ce domaine car l'ingénierie qui préside à la mise en place d'applications est entre les mains des chimistes. C'est pourquoi cette thèse est consacrée à de nouvelles stratégies de synthèses et de fonctionnalisations des AuNPs dans la perspective d'applications en nanomédecine² (vectorisation) et dans le champ des matériaux (transition de spin³). On peut d'ailleurs aussi envisager que ces travaux de thèse sur l'ingénierie des AuNPs trouveront encore d'autres applications (optique, diagnostic, capteurs, catalyse; voir la conclusion et les perspectives).

Le premier chapitre, bibliographique, comprend deux mises au point substantielles: l'une, soumise à publication, sur les différentes approches de synthèse des AuNPs, l'autre, publiée à ChemMedChem⁴, sur la vectorisation du docétaxel, un puissant anticancéreux de la famille des taxanes découvert et mis en œuvre par Pierre Potier. Trois chapitres expérimentaux suivent.

Le deuxième chapitre concerne l'amélioration de la fonctionnalisation des AuNPs par catalyse par un nouveau complexe du cuivre (I) de la principale réaction dite "click", c'est-à-dire de la réaction de Huisgen entre un alcyne terminal et un azoture⁵. Ce nouveau catalyseur permet de diminuer de façon considérable la quantité de Cu(I) mis en jeu, d'éviter l'agrégation des AuNPs et est appliqué ici à des fonctionnalisations très variées.⁶

Le troisième chapitre décrit la fonctionnalisation de façon biocompatible (à terminaisons polyéthylène glycols) des AuNPs avec pour objectif direct la vectorisation dite "active" (c'est-à-dire comportant un récepteur, l'acide folique) du docétaxel vers des cellules cancéreuses^{2,4}. Cette vectorisation "active" s'ajoute à la vectorisation dite "passive" (moins spécifique) procurée par l'effet de perméabilité accrue des micro vaisseaux formés dans les tissus cancéreux qui attirent préférentiellement les polyéthylène glycols.^{2,7}

Le quatrième chapitre concerne la fixation de complexes du Fe(II) à transition de spin³ (entre l'état bas spin 0 à basse température (T) et l'état haut spin 2 à haute T) sur des AuNPs afin d'assurer la formation d'un réseau induisant une coopérativité responsable d'une hystérésis (matériaux à mémoire) entre la structure électronique moléculaire et ce réseau organisé. L'équipe d'Azzedine Bousseksou au LCC de Toulouse a utilisé la spectroscopie Raman exacerbée par la surface des AuNPs (dite SERS, Surface Enhanced Raman Spectroscopy) pour tenter de caractériser la transition de spin dans ces matériaux.

En fin de mémoire, les “Conclusion et perspectives” résumant les avancées de nos travaux de thèse sur l’ingénierie de fonctionnalisation des AuNPs et leurs applications potentielles. Les perspectives résident dans les propriétés biomédicales des AuNPs y compris les travaux actuels en collaboration sur la vectorisation du docétaxel et, à terme, dans les propriétés concernant le diagnostic, la photo thérapie, les capteurs, les matériaux à propriétés optiques et la catalyse

English

Gold nanoparticles (AuNPs) have raised great interest, and research in this area has accelerated dramatically in recent years due to their applications in optics (related to their plasmon absorption), catalysis and nanomedicine (diagnosis and therapy).¹ Chemistry at the heart of this area treat as engineering who presides over the development of applications in the hands of chemists. That is why this thesis is devoted to new strategies for synthesis and functionalization of AuNPs with a broad applications in nanomedicine² (vectorization) and in materials fields (spin cross-over³). We can also consider that this work on the engineering of AuNPs opens other potential applications (optical diagnostics, sensors, catalysis, see the conclusion and perspectives).

The first chapter, literature research contains two subsections: the first subject was the publication on the different approaches to synthesis of AuNPs, the other one, published in ChemMedChem⁴ was vectorization of docetaxel. Docetaxel is a powerful anti-cancer drug of the taxane family discovered and developed by Pierre Potier. Three experimental chapters will follow.

The second chapter concerns the improvement of functionalization on AuNPs catalyzed by a new complex of copper (I) catalyst for the main reaction called “click”, i. e. the Huisgen reaction between a terminal alkyne and azide⁵. This new catalyst reduces significantly the amount of Cu (I) involved, avoid the aggregation of AuNPs and yielded a variety of functionalizations.⁶

The third chapter describes the biocompatible (polyethylene glycol terminated) functionalized AuNPs with docetaxel as "active" vectorization (that is to say comprising a receptor, folic acid) for cancer cells.^{2,4} This "active" vectorization stands together with the "passive" vectorization (less specific) provided by the enhanced permeability and rétention (EPR) effect of micro-vessels formed in cancerous tissues that have higher affinity for polyethylene glycols than normal cells do.^{2,7}

The fourth chapter concerns the design of nanodevices involving Fe (II) spin cross-over complexes³ (transition between the low spin state 0 at low temperature (T) and the high spin state 2 at high T) on AuNPs to ensure formation of a network for

inducing cooperativity between the molecular electronic structure and lattice resulting in hysteresis (memory materials). The team of Azzedine Bousseksou at LCC in Toulouse has used Raman spectroscopy enhanced by the surface of AuNPs (called SERS, Surface Enhanced Raman Spectroscopy) in attempts to characterize the spin cross-over materials.

At the end of the thesis manuscript, the "Conclusion and Perspectives" section summarizes the progress resulting from our thesis work concerning the engineering of functionalization of AuNPs and their potential applications. Prospects lie in the biomedical properties of AuNPs including current work collaboratively on the vectorization of docetaxel and finally on the diagnosis, the photo therapy, sensors, optical properties of materials and catalysis.

References

- (1) M. C. Daniel, D. Astruc. Gold Nanoparticles: Assembly, Supramolecular Chemistry, Quantum-size Related Properties, and Applications towards Biology, Catalysis and Nanotechnology. *Chem. Rev.* **2004**, *104*, 293-346.
- (2) A. Llevot, D. Astruc. Application of gold nanoparticles to the diagnostic and therapy of cancer. *Chem. Soc. Rev.* **2012**, *41*, 245-257.
- (3) A. Bousseksou, G. Molnár, L. Salmon, W. Nicolazzi. Molecular Spin Crossover Phenomenon: Recent Achievements and Prospects. *Chem. Soc. Rev.* **2011**, *40*, 3313.
- (4) P. Zhao, D. Astruc, Docetaxel Nanotechnology in Anti-cancer Therapy, *ChemMedChem* **2012**, *7*, DOI: 10.1002/cmdc.201200052.
- (5) L. Liang, D. Astruc. The Copper(I)-catalyzed Alkyne-Azide Cycloaddition (CuAAC) "Click" Reaction and its Applications. An Overview. *Coord. Chem. Rev.* **2011**, *255*, 2933-2945.
- (6) P. Zhao, M. Grillaud, L. Salmon, J. Ruiz, D. Astruc. Click Functionalization of Gold Nanoparticles Using the Very Efficient Catalyst Copper^I(Hexabenzyl)Tris-(2-aminoethyl) Amine Bromide. *Adv. Syn. Catal.* **2012**, *354*, 1001-1011.
- (7) A. Francois, A. Laroche, N. Pinaud, L. Salmon, J. Ruiz, D. Astruc. Encapsulation of Docetaxel into PEGylated Gold Nanoparticles for Vectorization to Cancer Cells and In Vitro Results. *ChemMedChem* **2011**, *6*, 2003-2008.



Chapter 1
Overview on the Preparation of Gold Nanoparticles and
Nanotechnology on Docetaxel delivery

1.1 Introduction

Two literature reviews are included in this chapter. The first work is the review prepared in collaboration with Li Na on the synthesis of AuNPs. AuNPs have attracted considerable interest and driven a variety of potential applications in catalysis, biology, and optics. Indeed, more than 70 000 publications have appeared on AuNPs up to date. In 2004, our group has published a comprehensive review entitled “*Gold Nanoparticles: Assembly, Supramolecular Chemistry, Quantum-size Related Properties, and Applications towards Biology, Catalysis and Nanotechnology*” also including in its introduction the fascinating historical aspects since antiquity. This review was cited more than 4000 times up to now, thus it appeared necessary to write a new updated review on the synthetic aspects including recent improvements which have recently been disclosed in the literature on the synthesis of AuNPs of various types.

The second review concerns the current docetaxel nanotechnology. Docetaxel has gained consideration since it was discovered and developed by Pierre Potier at the CNRS in France during his work on the improvements of the production of taxol. Compared with other present anticancer drugs, docetaxel has a broad spectrum of activity against a variety of tumors. Thus, it is essential to concentrate on the docetaxel delivery systems in cancer therapy. Otherwise, our group and the group in Chatenay-Malabry have collaboration work on prostate cancer therapy. Thus, this literature research can also help us to understand the role of AuNPs and docetaxel on prostate tumor cells. (see the first part of chapter 3)

1.2 State of the Art in Gold Nanoparticle Synthesis

State of the Art in Gold Nanoparticle Synthesis

Pengxiang Zhao, Na Li, Didier Astruc*

ISM, Univ. Bordeaux, 351 Cours de la Libération, 33405 Talence Cedex, France.

E-mail: d.astruc@ism.u-bordeaux1.fr

Abstract

General principles and recent developments in the synthesis of gold nanoparticles (AuNPs) are reviewed. The “*in situ*” Turkevitch-Fens and Schiffrin-Brust methods are still major synthetic routes, with citrate and thiolate ligands respectively, that have been improved and extended to macromolecules including biomacromolecules with a large biomedical potential of optical and theranostic applications. Along this line, however, recently developed seed-growth methods have allowed a precise control of AuNP sizes in a broad range and multiple shapes. AuNPs and core@shell bimetallic MAuNPs loosely stabilized by nitrogen and oxygen atoms of embedding polymers and dendrimers and composite solid-state materials containing AuNPs with supports including oxides, carbons, mesoporous materials and molecular organic frameworks (MOFs) have attracted much interest because of their catalytic applications.

Keywords: Gold, nanoparticle, cluster, seed-growth, core@shell, thiol, oxide, dendrimer, polymer

Contents

1. Introduction
2. *In situ* syntheses
 - 2.1. AuNPs stabilized by simple molecules
 - 2.1.1 Turkevitch method
 - 2.1.1.1. Citrate as both stabilizing and reducing agent
 - 2.1.1.2. Citrate as a stabilizing agent only
 - 2.1.1.3. Reversed addition method
 - 2.1.2. Brust-Schiffrin method
 - 2.1.2.1. Synthetic procedure
 - 2.1.2.2. Purification of precise Au clusters from AuNPs
 - 2.1.2.3. Determination of the number of thiolate ligands
 - 2.1.2.4. Other sulfur ligands
 - 2.1.2.5. Methods offunctionalization
 - 2.1.2.5.1. Reactions of AuNP-citrate with thiols
 - 2.1.2.5.2. Brust-Schiffrin method with functional thiols
 - 2.1.2.5.3 Thiolate-thiol ligand substitution reaction

-
- 2.1.2.5.4. Functionalization of pre-formed AuNPs
 - 2.1.3. Schmid's Au₅₅cluster and phosphorus ligands
 - 2.1.4. Other ligands
 - 2.2. Macromolecule-stabilized AuNPs
 - 2.2.1. Polymers
 - 2.2.2. Dendrimers
 - 2.3. Surfactants and reverse micelles
 - 2.3.1. Surfactant-stabilized AuNPs without reverse micelle formation
 - 2.3.2. Surfactant-stabilized AuNPs with reverse micelle formation
 - 2.3.3. Polymer reverse micelles
 - 2.3.4. Liposomes
 - 2.4. Biosynthesis and "green chemistry"
 - 2.4.1. Natural-source extracts
 - 2.4.2. Chitosan
 - 2.4.3. Microbes
 - 3. Seed-growth method
 - 3.1. Principle of the seed-growth method
 - 3.2. Spherical or quasi-spherical AuNPs
 - 3.3. Gold nanorods (AuNRs)
 - 3.4. Other shapes of AuNPs
 - 4. Other synthetic methods
 - 4.1. Pulse radiolysis
 - 4.2. Top-down methods
 - 4.3. Supported AuNPs
 - 4.3.1. Oxides
 - 4.3.2. Carbon
 - 4.3.3. Mesoporous materials and MOFs
 - 4.3.3.1. Mesoporous materials
 - 4.3.3.2. MOFs
 - 5. Bimetallic AuNPs
 - 5.1. Core@shell AuNPs
 - 5.2. Bimetallic alloy AuNPs
 - 6. Conclusion and outlook
 - 7. Abbreviations

1. Introduction

Metal nanoparticles (NPs) have long been considered to disclose unique physical and chemical properties different from those of the bulk state or atoms, due to the quantum size effect resulting in specific electronic structures.¹⁻⁷ Gold nanoparticles (AuNPs) are probably the most remarkable member of the metal NP groups.⁸⁻¹¹ They have attracted considerable interest and driven a variety of potential applications in catalysis,¹²⁻²¹ biology,²²⁻²⁶ and optics.²⁷⁻²⁹ Indeed, more than 70 000 publications have appeared on AuNPs up to date. In 2004, one of us together with M.-C. Daniel published a comprehensive review entitled "*Gold Nanoparticles: Assembly,*

Supramolecular Chemistry, Quantum-size Related Properties, and Applications towards Biology, Catalysis and Nanotechnology ” also including in its introduction the fascinating historical aspects since antiquity. Here we are specifically focusing on the principles and most recent improvements disclosed in the literature on the synthesis of AuNPs of various types.

After the seminal report by Faraday in 1857⁸ of the reduction of a tetrachloroaurate solution by phosphorous in carbon disulfide (a biphasic reaction), the preparation of AuNPs with controlled sizes and shapes has raised increased attention during the second half of the XXth century. The breakthroughs have been those by Turkevitch in 1951 with the citrate method improved by Fens in 1973, then in 1981 with Schmid’s report of a Au₅₅-phosphine cluster and the notion of quantum dot, then by Mulvaney and Giersing in 1993 with the first synthesis and stabilization of AuNPs by thiolates, and finally by the Schiffrin group in 1994 with the report of the illustrious and most convenient Brust-Schiffrin biphasic method of thiolate-stabilized AuNPs.⁹ Sophistications of these methods during the last decade have now led to promising applications.

AuNPs can be prepared by both “top down” and “bottom up” approaches. For “top down” procedures, a bulk state Au is systematically broken down to generate AuNPs of desired dimensions. In this case, particle assembly and formation is controlled by a pattern or matrix. However, the “top down” method is limited concerning the control of the size and shape of particles as well as further functionalization.³⁰ In contrast, in the “bottom up” strategy, the formation of AuNPs originates from individual molecules, because it involves a chemical or biological reduction.³¹ This chemical reduction method involves two steps: nucleation and successive growth. When the nucleation and successive growth are completed in the same process, it is called *in situ* synthesis; otherwise it is called seed-growth method. For the *in situ* synthesis method, we will focus on the preparation of spherical or quasi-spherical AuNPs. For the seed-growth method, we will concentrate on the preparation of AuNPs having various sizes and shapes. In addition, we will discuss methods of AuNP functionalization. This review is not comprehensive, but it is limited to the essential and most useful preparation methods of AuNPs and their improvements, in particular the most recent development.

2. *In situ* synthesis

In general, the preparation of AuNPs by chemical reduction contains two major parts: (i) reduction using agents such as borohydrides, aminoboranes, hydrazine, formaldehyde, hydroxylamine, saturated and unsaturated alcohols, citric and oxalic acids, polyols, sugars, hydrogen peroxide, sulfites, carbon monoxide, hydrogen, acetylene, and monoelectronic reducing agents including electron-rich transition-metal sandwich complexes; (ii) stabilization by agents such as trisodium citrate dehydrate, sulfur ligands, phosphorous ligands, nitrogen-based ligands, oxygen-based ligands, dendrimers and polymers. The *in situ* synthesized AuNPs are also used for the seedgrowth or further functionalization. In this section, we will review the various *in situ* methods and their improvements.

2.1 AuNPs stabilized by simple molecules

2.1.1 Turkevitch method

2.1.1.1. Citrate as both stabilizing and reducing agent

Among all the *in situ* syntheses of AuNPs by reduction of HAuCl_4 , citrate-stabilized AuNPs has been regarded as the most popular ones for a long time, since their introduction by Turkevitch in 1951.³² The synthetic route is shown in Figure 1. The HAuCl_4 solution is boiled, and the trisodium citrate dihydrate is then quickly added under vigorous stirring. After a few minutes, the wine-red colloidal suspension is obtained, and the AuNP size is about 20 nm. In 1973, Frens³³ reported an improvement, i.e. a broad size range of AuNPs (from 15 to 150 nm) was obtained by controlling the trisodium citrate to Au ratio. However, particles larger than 20 nm were always polydispersed. The histogram of size distribution could be readily determined by transmission electron microscopy (TEM).

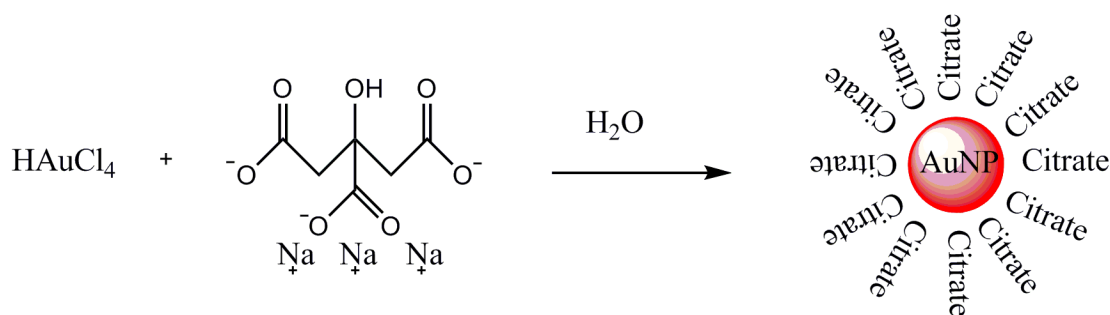


Figure 1. Synthetic route for the Turkevitch method.

Recently, several research groups have improved the Turkevitch-Frens method in order to promote the convenient use of citrate-stabilized AuNPs. In particular, the mechanism of AuNPs formation using this synthetic route has been examined in details.³⁴⁻³⁸ Kimiling *et al.* indicated that a high concentration of citrate more rapidly stabilizes the AuNPs of smaller size, whereas a low concentration of citrate leads to large-size AuNPs and even to the aggregation of AuNPs.³⁴ Kumar *et al.* showed the variation of AuNPs size with various ratios of initial citrate concentration to HAuCl_4 .³⁷ Peng's group³⁸ reported that the presence of a citrate salt changes the pH of the system and influences the size and size distribution of AuNPs. On this basis, they synthesized nearly monodispersed AuNPs with sizes ranging from 20 to 40 nm by simply varying the solution pH. Inspired by Peng's work, other groups considered the pH influence on citrate-capped AuNPs.³⁹⁻⁴² Other improvements of the Turkevitch method, such as controlling the temperature of the process,⁴³ introducing the fluorescent light irradiation,⁴⁴ and using high-power ultrasounds^{45,46} were recently reported.

The size of citrate-stabilized AuNPs was always greater than 10 nm, due to the poor reducing ability of trisodium citrate dihydrate. An intriguing result about citrate-stabilized AuNPs was reported in 2010 by Puntès's group.⁴⁷ D_2O was used as

the solvent instead of H₂O during the synthesis of AuNPs. As shown in Figure 2, the size of the AuNPs was tailored to 5 nm. It was concluded that D₂O increased the reducing strength of citrate.

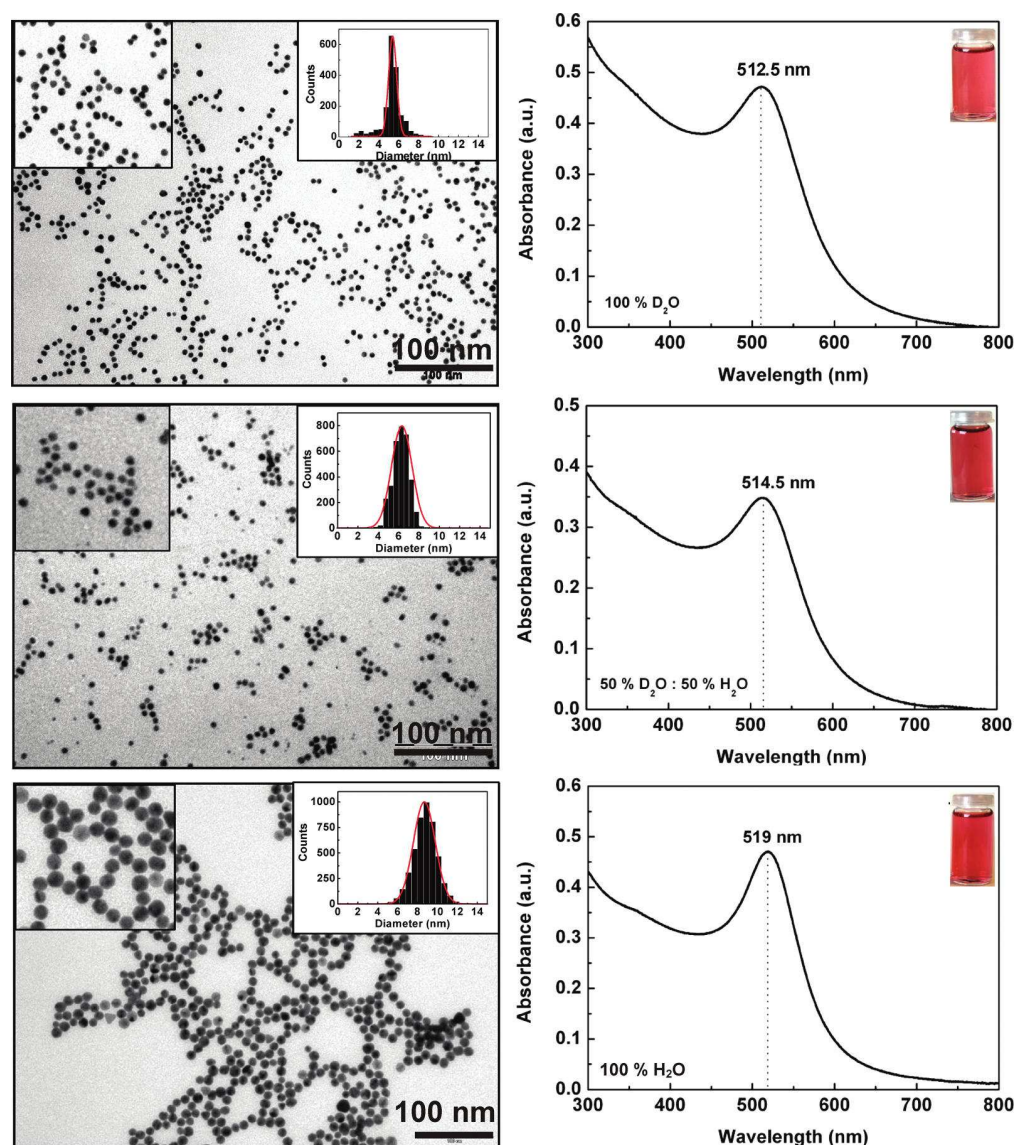


Figure 2. Optical (UV-vis. spectroscopy) and morphological (TEM) characterization of AuNPs synthesized using various solvents: 100% D₂O (top), 50% D₂O/H₂O (middle), and 100% H₂O (bottom). Inset graphs in TEM images show the size distribution measurements of Au NPs. Inset images in UV-vis. spectra show colors of AuNPs solutions. These figures are representative of three separated experiments. Reprinted with permission from ref 47(Puntes's group). Copyright 2010 American Chemical Society.

2.1.1.2. Citrate as a stabilizing agent only

In general, citrate plays a role not only as a stabilizing agent but also as a reducing

agent. As discussed above, due to the poor reducing capacity of trisodium citrate dihydrate, the preparation of AuNPs requires a high temperature. Slot discovered a new way to prepare AuNPs using a mixture of tannic acid/citrate solution. In this case, tannic acid plays the role of a reducing agent instead of citrate, and the AuNPs are obtained at 60°C.⁴⁸ Then Natan's group introduced a method using citrate as a stabilized agent only and NaBH₄ as a reducing agent.⁴⁹ The AuNPs were obtained upon adding the NaBH₄/citrate mixture into the HAuCl₄ solution at room temperature. With this method, the size of AuNPs is tailored to 6 nm, which compares with sizes beyond 20 nm using the traditional Turkevitch method.

2.1.1.3. Reversed addition method

Very recently, another remarkable modification of the Turkevitch method was reported. The experiments involved the reversed order of addition that was conducted by adding HAuCl₄ to the citrate solution, producing monodispersed AuNPs with small size (less than 10 nm).^{50, 51}

In summary, the size of the citrate-stabilized AuNPs produced by *in situ* synthesis is between 5 nm and 150 nm. When the size is decreased, relatively monodispersed AuNPs are obtained, whereas when with the size is increased (especially > 20 nm) polydispersed AuNPs are obtained. Citrate-stabilized AuNPs were also used in further preparation or functionalization such as ligand substitution reaction and seed-growth.

2.1.2 Brust-Schiffrin method

2.1.2.1. Synthetic procedure

Thiolate-stabilized AuNPs were first reported by Mulvaney and Giersig,⁵² who showed the possibility of using alkylthiols with various chain lengths to stabilize the AuNPs. The two-phase Brust-Schiffrin method, published in 1994, was the first reported method to prepare the thiolate-stabilized AuNPs *via in situ* synthesis, and has therefore met a great success.⁵³ Its high impact is due to (i) facile synthesis in ambient condition; (ii) relative high thermal and air stability of the AuNPs prepared in this way; (iii) repeated isolation and re-dissolution without aggregation or decomposition; (iv) control of the small size (less than 5 nm) with narrow dispersity; (v) relatively easily functionalization and modification by ligand substitution. In this Brust-Schiffrin procedure, as shown in Figure 3, anionic Au^{III}, in the form of AuCl₄⁻, is transferred to the toluene phase by ion pairing with the lipophilic tetra(octylammonium) cation of the phase-transfer agent tetra(octylammonium) bromide (TOAB). Then the freshly prepared reducing agent NaBH₄ is quickly and dropwise added with vigorously stirring in the presence of dodecanethiol. The color changes from orange to deep brown, which indicates the formation of AuNPs. AuNPs are stabilized by relatively strong Au-thiolate bonds, their diameters are in the 2-5 nm range, and their shapes are cuboctahedral and icosahedral. Due to the nucleation-growth-passivation kinetics model by which the sulfur-containing agents inhibit the growth process,^{54,55} larger S/Au mole ratios give smaller average core sizes. Fast NaBH₄ addition and cooled solutions also produce smaller, more monodispersed AuNPs. During the reaction of the thiol with growing Au⁰NPs, the H atom of the thiol is lost, presumably by

oxidative addition of the S-H bond onto two contiguous Au⁰ atoms of the AuNP surface. The fluxional properties of the Au-H bonds on the AuNP surface can provide the fast walking path of the H atoms on the surface until two Au-H bonds become contiguous for H₂ reductive elimination. Given the above advantages, the Brust-Schiffrin method is now much in use for the preparation and application on thiolate-liganded AuNPs.⁵⁶⁻⁶² Precise Au clusters have been synthesized using this method and purified (see § 2.1.2.2). From the nomenclature point of view, it is best to call clusters such small “NPs” that are precisely defined without polydispersity (single molecules), and to reserve the NP nomenclature to the cases for which there is some dispersity (mixture of several clusters), even if it is low.⁶³

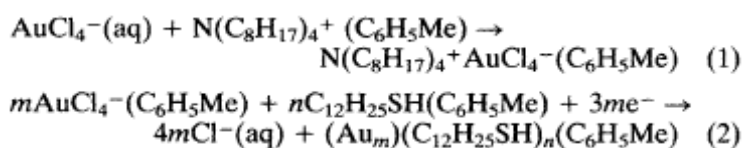


Figure 3. Scheme of the Brust-Schiffrin method for AuNP synthesis. Reprinted with permission from ref 53 (Schiffrin’s group). Copyright 1994 Royal Society of Chemistry.

The Brust-Schiffrin method was extended in 1995 to an improved procedure upon which the *p*-mercaptophenol-stabilized AuNPs were synthesized in methanol solution without the phase-transfer agent TAOB.⁶⁴ In this way, the introduction of TAOB impurities was avoided. Indeed, methanol is an excellent solvent for a single-phase system, because both HAuCl₄ and *p*-mercaptophenol are soluble. Any thiol that is soluble in the same solvent as HAuCl₄ such as methanol, ethanol or water allows the use of a single-phase system for AuNP synthesis. In the following years, a variety of publications concentrated on functional thiol ligand-stabilized AuNPs using the single-phase procedure.^{54,55,65-67} Brust’s group prepared biocompatible and water-soluble AuNPs capped by (1-mercaptoundec-11-yl) tetraethylene glycol⁶⁸ with less than 10 nm. Due *inter alia* to the hydrophobic alkanethiol interior and tetra (ethylene glycol) (TEG) hydrophilic shell, AuNPs are of great biomedical interest,⁶⁹⁻⁷¹ in particular in the form of AuNPs capped with thiolated polyethylene glycols (PEGs).^{72,73}

Very recently, a series of thiolate-stabilized AuNPs were prepared by a modified single-phase method. Sardar and Shumaker-Parry introduced 9-borabicyclo [3.3.1] nonane (9-BBN) as a mild reducing agent for the synthesis of a series of ω-functionalized alkylthiolate-stabilized AuNPs.⁷⁴ The use of other thiolate ligands such as bifunctional alkanethiolate,⁷⁵⁻⁷⁷ arenethiolate⁷⁸⁻⁸² and other functional thiolate-stabilized AuNPs⁸³ involving their synthesis from the corresponding thiols have also been reported.

The strength of the reducing agent used in Brust-Schiffrin method is much larger than

that of citrate used in the Turkevitch method, and according to Marcus theory the reaction rate in AuNPs synthesis using NaBH_4 is much larger than that of the Turkevitch AuNP synthesis using citrate reduction. A direct consequence is that the size of the AuNPs synthesized using the NaBH_4 reductant is much smaller than that of Turkevitch method using the citrate reductant.

2.1.2.2. Purification of precise Au clusters from AuNPs

Various methods of purification and isolation of precise Au clusters from AuNPs that are more or less polydispersed mixtures of such clusters have been experimented. AuNPs with precise number of Au atoms and ligands such as $\text{Au}_{140}(\text{SC6})_{53}$ (SC6 = hexanethiol)⁸⁴ and $\text{Au}_{144}(\text{SCH}_2\text{CH}_2\text{Ph})_{60}$ ⁸⁵ have been synthesized using the Brust-Schiffrin method. Murray's group^{63, 86, 87} has prepared $\text{Au}_{25}(\text{SCH}_2\text{CH}_2\text{Ph})_{18}$ by a modified version of the Brust-Schiffrin procedure. In this synthesis, AuCl_4^- was phase-transferred from water to toluene, reacted with $\text{HSCH}_2\text{CH}_2\text{Ph}$, and then reduced by adding aqueous NaBH_4 . The crude product $\text{Au}_m(\text{SCH}_2\text{CH}_2\text{Ph})_n$ was purified by precipitation. For instance, the $\text{Au}_{25}(\text{SCH}_2\text{CH}_2\text{Ph})_{18}$ and $\text{Au}_{140}(\text{SCH}_2\text{CH}_2\text{Ph})_{53}$ were isolated from the crude product by precipitation in acetonitrile, $\text{Au}_{25}(\text{SCH}_2\text{CH}_2\text{Ph})_{18}$ being soluble in acetonitrile unlike $\text{Au}_{140}(\text{SCH}_2\text{CH}_2\text{Ph})_{53}$. The formation of $[\text{oct}_4\text{N}^+][\text{Au}_{25}(\text{SCH}_2\text{CH}_2\text{Ph})_{18}^-]$ was confirmed by ^1H NMR, UV-vis., and mass spectrometry, and the X-ray crystal structure is illustrated in Figure 4. Further, the yield was improved up to 50% by tuning the temperature and duration of the various steps, and the formation of oxidized neutral $\text{Au}_{25}\text{L}_{18}$ was avoided. Sweeney *et al.*⁸⁸ reported the purification and separation of water-soluble thiolated 3-nm AuNPs. In this procedure, the solution of AuNPs is removed using a peristaltic pump through a diafiltration membrane. Small molecule impurities or small NPs are eluted in the permeate, while the large NPs are retained. The expanded view is that of a hollow-fiber-type diafiltration membrane depicting the elution of small impurities and NPs and the retention of larger particles. Kornberg's group^{89,90} introduced the precipitation method to obtain of $\text{Au}_{102}(\text{P-MBA})_{44}$ (MBA: *p*-mercaptobenzoic acid). The prepared *P*-MBA-protected AuNPs are precipitated by addition of ammonium acetate or NaCl and methanol and then collected in a microfuge by centrifugation. The pellets are allowed to dry in air, and they redissolved in water and purified by fractional precipitation. The solution is adjusted using appropriate amounts of ammonium acetate and methanol, and centrifuged for a few minutes. The supernatant is centrifuged repeatedly until no further precipitate is formed, adjusted to appropriate amounts of ammonium acetate, 80% methanol, and centrifuged to give the purified $\text{Au}_{102}(\text{P-MBA})_{44}$. The final Au cluster products are characterized by SEM, MALDI-TOF MS, TGA and XPS.^{89,90}

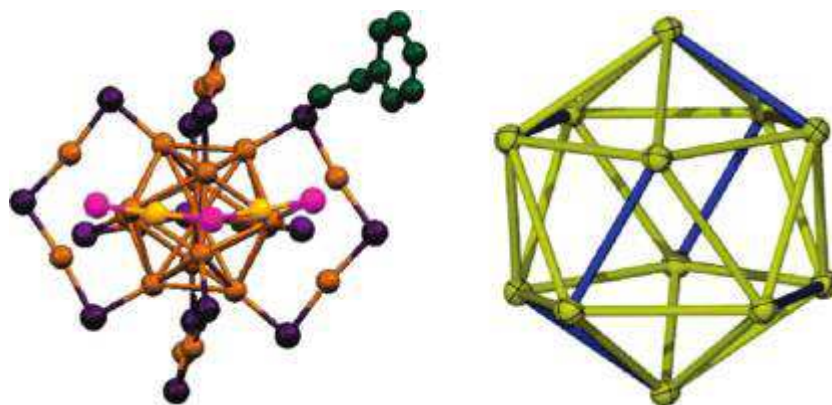


Figure 4. (left) X-ray crystal structure of $[\text{oct}_4\text{N}^+][\text{Au}_{25}(\text{SCH}_2\text{CH}_2\text{Ph})_{18}]^-$.¹⁶ The icosahedral Au_{13} core is surrounded by six $\text{Au}_2(\text{SR})_3$ semi-rings that are slightly puckered in the reduced AuNPs as shown for the semi-ring with more pronounced yellow and pink colors (right). The icosahedral Au_{13} core (minus the center Au) is slightly distorted; the blue Au-Au bonds lying directly below the center of each semi-ring are on average 0.12 \AA shorter than the yellow Au-Au bonds (average 2.96 \AA). Overall Au-Au average 2.93 \AA . Au_{13} core diameter 9.8 \AA ; overall AuNP diameter 23.9 \AA . Reprinted with permission from ref 63 (Murray's group). Copyright 2010 American Chemical Society.

2.1.2.3. Determination of the number of thiolate ligands

For the thiolate ligand-stabilized AuNPs, the surface ligand coverage is determined using theoretical and experimental methods. A most commonly employed theoretical method is that reported by Leff and co-workers⁹¹ for spheric AuNPs in 1995. In their assumption, the thiolate ligands are close-packed on the AuNP as a spherical surface. It was also assumed that each gold atom had a constant volume, $v_g = 17 \text{ \AA}^3$, and each thiol occupied an area of $S_{\text{sulfur}} = 21.4 \text{ \AA}^2$ on the surface, so that both the number of Au atoms ($n_{\text{Au}} = 4\pi(R-\delta)^3 / 3v_g$, $R-\delta \approx D/2$) and the number of thiolate ligands ($n_{\text{thiol}} = 4\pi(R-\delta)^2 / S_{\text{sulfur}}$) were obtained through a simple measurement of the AuNP diameter by TEM followed by statistical calculations. For example, the average core diameter of 2.7 nm AuNP resulted in 577 Au atoms and 103 thiol ligands at the periphery.⁹²

In 1995, Murray's group⁹³ reported the spherical AuNP-core model that introduced a functional relationship between the thiolate ligand coverage (ratio of alkanethiolates to surface Au atoms, γ) and the mass fraction of alkanethiolate (χ_{organic}) in the cluster with a given Au core radius (eq. 1). The surface ligand coverage was calculated using the measurement of χ_{organic} by elemental and TGA analyses, and R_{core} by TEM or SAXS. Murray et al. also pointed out that the calculated result of spherical core was not very different⁹³ from those predicted for the face-centered cubic cuboctahedral model that was determined by Brust et al.⁵³ through the HRTEM measurement. As an example, an AuNP with a core radius $R_{\text{core}} = 1.19 \text{ nm}$ and coverage $\gamma = 0.66$ contains 409 Au atoms and 126 alkanethiolate ligands in each AuNP.

$$\chi_{\text{organic}} = \frac{4\pi(R_{\text{core}} - R_{\text{Au}})^2(\rho_{\text{HCP}})(MW_{\text{thiol}})\gamma}{4\pi(R_{\text{core}} - R_{\text{Au}})^2(\rho_{\text{HCP}})(MW_{\text{thiol}})\gamma + \frac{4}{3}\pi R_{\text{core}}^3(\rho_{\text{Au}})(AW_{\text{Au}})}$$

eq.1

In equation 1, χ_{organic} is the mass fraction of alkanethiolate in the AuNP, R_{Au} is the crystallographic radius of a gold atom (0.145 nm), ρ_{HCP} is the density of surface gold atoms (13.89 atoms/nm², assuming hexagonal close packing), MW_{thiol} is the alkanethiolate molecular weight in mass/molecule, γ is the coverage (ratio of alkanethiolates to surface Au atoms), ρ_{Au} is the atom density of bulk gold (58.01 atoms/nm³), and AW_{Au} is the Au atomic weight in mass/atom.

In a previous work of our group,⁹⁴ it was experimentally determined that through the measurement of the AuNP core radius by TEM and the organic fraction determined by element analysis, the thiolate ligand number and total gold atom number could be calculated, and the result was in relatively good agreement with the reports by Murray and Brust. From these various determination methods, it results that Leff's theoretical method leads to an underestimation of the actual number of thiolate ligands. If the thiolated AuNPs are well washed to remove excess free thiol (a key condition), i.e. if the Au/S ratio is correctly provided by elemental analysis or thermogravimetric analysis, the AuNP size determination by TEM leads to the correct number of AuNP ligands. The AuNP surface coverage by thiolate ligands depends on the geometry and size and varies between one thiolate ligand per two surface Au atoms to 2 thiolate ligands per 3 Au surface atoms.

2.1.2.4. Other sulfur ligands

Other sulfur ligands such as disulfides,⁹⁵⁻¹⁰⁰ xanthates,¹⁰¹ thioacetates,¹⁰² dithiocarbamates,¹⁰³ trithiolates,¹⁰⁴ benzenesulfonate (SDBS),¹⁰⁵ and thioctic acid¹⁰⁶ have been also used in synthesis of AuNPs *via* the Brust-Schiffrin two-phase method or improved single-phase method. Some of these ligands are considered to bind less readily than thiolates to the AuNP cores of AuNPs.¹⁰⁷⁻¹⁰⁹ An opposite view was reported by Lee's group, however, who recently observed that the alkanethioacetates stabilized-AuNPs were as stable as alkanethiol-stabilized AuNPs.¹⁰² Alkanethioacetate ligands stabilize AuNPs with loss of the S-acetyl moiety and covalent attachment of the sulfur atoms as thiolates to the Au surface.

2.1.2.5. Methods of functionalization

2.1.2.5.1. Reactions of AuNP-citrate with thiols

Due to the weakness of the Au-citrate bonds, the citrate-stabilized AuNPs are easily functionalized upon substitution of the citrate ligands by stronger thiolate ligands; this substitution is experimentally very simple and involves reaction of the precursor citrate-AuNPs with the corresponding functional thiols under ambient conditions. Compared to the Brust-Schiffrin method of direct synthesis, the AuNPs prepared from AuNP-citrate are larger, which allows potential applications of the latter in nanomedicine; therefore the plasmon band,¹¹⁰ observed only for AuNPs larger than 2 nm, is key to the diagnostic. Mulvaney and Giersig initiated this method to synthesize

thiolate-stabilized AuNPs by substituting the citrate ligands by thiolate ligands using the corresponding thiols.⁵² This research area is already largely developed. Mirkin's group has used this strategy to load AuNPs with thiolated DNA.¹¹¹ In a recent example, citrate-stabilized AuNPs have been functionalized with thiolated PEG and the PEGylated AuNPs formed in this way have been used as contrast agent for in vivo X-ray computed tomography imaging.¹¹² Very recently, Daniel's group¹¹³ synthesized robust AuNP-cored nitrile- and amine-terminated dendrimers by reaction between 19.5-nm AuNP-citrate and poly (propyleneimine) dendronic thiols as efficient platforms for drug delivery (Figure 5).



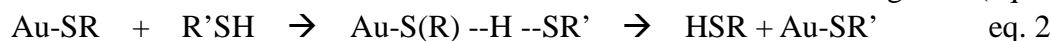
Figure 5. The synthetic routes for the thiol-dendron-stabilized AuNPs. Reprinted with permission from ref 113 (Daniel's group). Copyright 2011 Royal Society of Chemistry.

2.1.2.5.2. Brust-Schiffrin method with functional thiols

Since the seminal report by Brust *et al.*,⁶⁴ it is known that some functional thiols can be used in the Brust-Schiffrin AuNP synthesis (§ 2.1.2.1) if the functional group of the thiol is compatible with the reactions conditions, in particular the reductant. This strategy has thus been largely exploited. A recent example was reported with the synthesis of 16-mercaptohexadecanoic acid-capped AuNPs used for immobilization onto silica.¹¹⁴ Thiol-functionalized polymers or dendrimers are also used to stabilize AuNPs *via* Brust-Schiffrin synthesis (see § 2.2.1 and 2.2.2). The direct synthesis of AuNPs with functional thiols sometimes avoids the aggregation that may result from the post-functionalization method (§ 2.1.2.5.4).

2.1.2.5.3. Thiolate-thiol ligand substitution reaction: functionalization

The ligand-substitution reaction (occasionally called “place exchange” reaction) was first initiated by Murray's group who first substituted alkylthiolate ligands by functional alkyl thiolate ligands using the corresponding functional thiols for the synthesis of functional AuNPs.^{115, 116} The reaction at the AuNP core surface involves transfer of the SH hydrogen atom of the incoming functional thiol to the AuNP surface-bonded S atom of the coordinated thiolate to form the leaving thiol (eq. 2).



The thiolate ligand substitution is conducted by introducing excess thiol ligands. This method has been widely used,¹¹⁷ because it avoids using the reducing conditions of

the direct Brust-Schiffrin synthesis with functional thiols. Usually, the excess of functional thiol and the exchanged non-functional alkylthiol are separated by dissolution in methanol or ethanol in which the AuNPs are not soluble. Examples include amidoferrocenyl functionalized alkanethiol groups that were introduced into AuNPs for the redox recognition of oxoanions,¹¹⁸ azide- or bromo-functionalized thiols for further “click” functionalization of AuNPs,¹¹⁹⁻¹²⁴ carboxylic acid-functionalized thiols for controlled preparation of carboxylated AuNPs,¹²⁵ and small thiolate molecules for the identification of antibiotics.¹²⁶ Recently, Lennox’s group developed a new ligand substitution reaction called “thiol-for-DMAP exchange”.¹²⁷⁻¹²⁹ They used thiol ligands for substituting the DMAP-capped AuNPs for the synthesis of liquid crystal (LC)-capped AuNPs,¹²⁷ and polymer-capped AuNPs.¹²⁸ However, the ligand-substitution reaction has some drawbacks that are (i) risk of irreversible aggregation of AuNPs, (ii) incomplete ligand substitution, (iii) in some cases experimental difficulty in the determination of the amount of exchanged ligands, (iv) possible incompatibilities between the initial medium of the AuNPs and new capping molecules, such as tolerance of the new potential ligands towards solvent.¹¹⁹ Nevertheless, it remains very useful.

2.1.2.5.4. Functionalization of pre-formed AuNPs

Various functionalizations of pre-formed AuNPs by direct synthesis or ligand substitution have been conducted such as halide nucleophilic substitution reactions,¹¹⁷ nucleophilic addition reaction,¹³⁰ carboxylic acid-alcohol-coupling reactions,¹³¹ polymerizations,¹³² and “click” functionalization.^{133,134} For example, AuNPs stabilized by 4-aminothiophenol are functionalized with folic acid by condensation reaction, with potential application in cancer therapy.^{135,136} In our group, “click” functionalization of AuNPs has been applied for usage in drug delivery systems (Figure 6).^{124,136} This functionalization of pre-functionalized AuNPs has the inconvenience, however, that aggregation often occurs in the course of reactions, in particular if a catalyst is used. Nevertheless, it remains very useful, because the aggregated AuNPs are easily separated by precipitation.

In summary, due to the strong Au-S bond (47 kcal/mol),¹³⁷ sulfur ligand-stabilized AuNPs have gained considerable interest for functionalization with thousands of publications since their discovery. These four functionalization methods are all currently used and complementary.

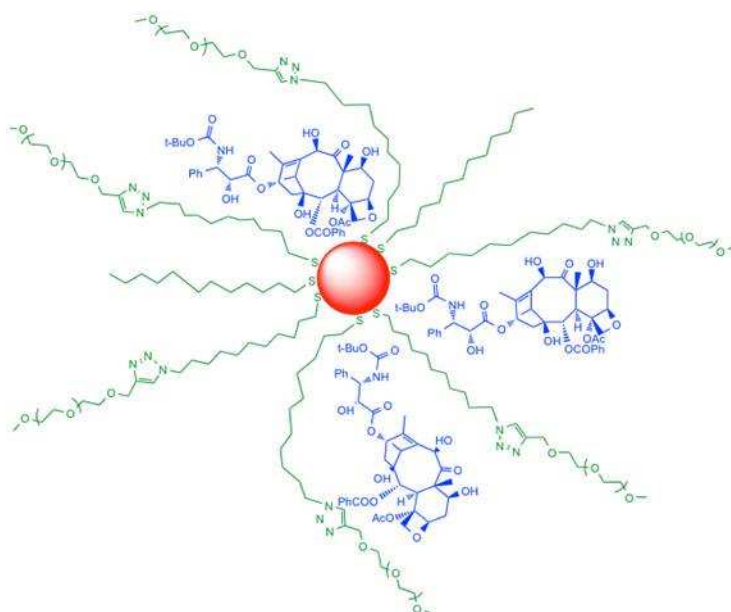


Figure 6. Encapsulation of docetaxel in PEGylated AuNPs considerably increases its solubility in water (Astruc's group). Reprinted with permission from ref 124. Copyright 2011 Wiley-VCH.

2.1.3. Schmid's Au₅₅cluster and the phosphorus ligands

The phosphorus ligand-stabilized AuNPs have possible future applications in catalysis, imaging, sensing, and new therapeutic approaches.¹³⁸⁻¹⁵¹ They are also excellent precursors for ligand-substitution reactions towards the functionalization of AuNPs and for building bimetallic cores of AuNPs.^{152,153} In the early 1980s, Schmid reported a phosphine-stabilized Au₅₅cluster that is known as Schmid's cluster with narrow dispersity (1.4±0.4 nm).¹¹ Schmid Au cluster was defined as [Au₅₅(PPh₃)₁₂Cl₆], was well characterized by X-ray crystal structure and showed the properties of a quantum-dot particle for the first time.¹⁵⁴ Weare and Hutchison¹⁵³ improved the Schmid method in 2000 using HAuCl₄ and N(C₈H₁₅)₄Br in a water-toluene mixture to which PPh₃ and NaBH₄ (instead of diborane in Schmid's method) were added. The cluster [Au₁₀₁(PPh₃)₂₁Cl₅] formed with [Au(PPh₃)Cl] as an impurity. Later, Moores et al. used the precursor complex [AuCl(SMe₂)] instead of HAuCl₄ as the gold source and sodium naphthalenide (C₁₀H₈Na) instead of NaBH₄ as the reducing agent, to synthesize phosphinine-stabilized AuNPs. Phosphinines are well adapted to the coordination to Au⁰ and are suitable for AuNPs formation. Very recently, the mild reducing agent 9-borabicyclo-[3.3.1]nonane (9-BBN) was used in a new simple and versatile method for the synthesis of triphenylphosphine-stabilized AuNPs with diameters of 1.2-2.8 nm and narrow size distribution (Figure 7).¹³⁸ Other recent examples of the synthesis of AuNPs stabilized by phosphines or phosphine derivatives are (i) triphenylphosphine-stabilized small Au clusters where triphenylphosphine is considered as a proactive etching agent,¹⁵⁵ (ii) calixarene phosphine-stabilized AuNPs that were used for catalysis,^{156, 157} (iii) 1,1'-binaphthyl-2,2'-dithiol-stabilized AuNPs

for optics,¹⁵⁸ and (iv) tetrakis(hydroxymethyl)phosphonium chloride (THPC)-stabilized AuNPs for further preparation of bimetallic nanoshells.¹⁵⁹ In addition, proteins and lipids contains many phosphorus atoms that also stabilize AuNPs with these bioligands (see § 2.2.1).

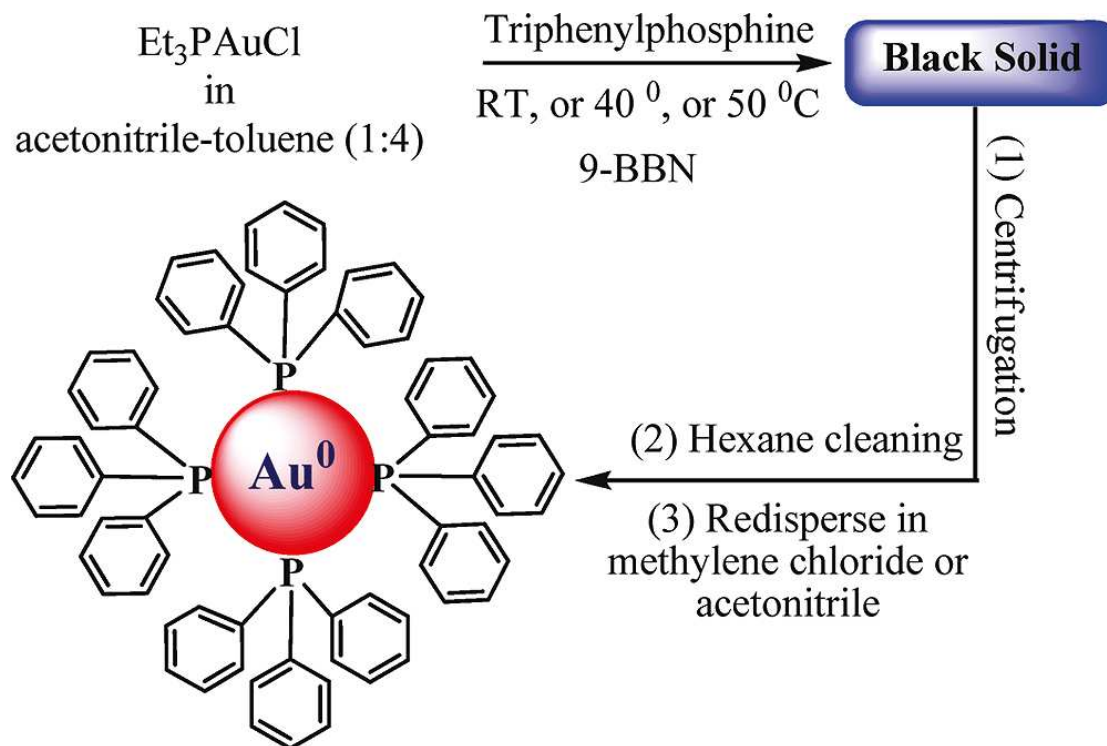


Figure 7. Synthesis pathway for TPP-stabilized AuNPs. Reprinted with permission from ref 138 (Shumaker-Parry's group). Copyright 2009 American Chemical Society.

2.1.4. Other ligands

The other possible AuNP ligands are oxygen- and nitrogen-based ligands containing electronegative groups such as amine (or amino), carboxyl, carbonyl and phenol groups. In particular, amines have been popular AuNP ligands for a long time due to their presence in biological and environmental systems.¹⁶⁰⁻¹⁶⁶ For instance, Crooks's group has reported octadecyl amine-capped AuNPs in 1993.¹⁶⁰ A series of aminoalcohol-stabilized AuNPs¹⁶², amine-stabilized AuNPs used as bioprobes^{163,164} (Figure 8) and cyclic phenylazomethine (CPA)-stabilized AuNPs used as electrochemical probes for metal ion sensing are known.¹⁶⁵ Among them, 4-(*N,N*-dimethylamino) pyridine (DMAP) is a frequent AuNP ligand, and DMAP-stabilized AuNPs have found broad used in AuNP ligand-substitution reactions¹⁶⁷ and heterogeneous catalysis.¹⁶⁸ DMAP-liganded AuNPs were first reported in 2001 by Caruso's group^{168,169} and recently gained increased attention.¹⁷⁰⁻¹⁷³ These AuNPs are obtained by adding an aqueous DMAP solution into the TOAB-stabilized AuNPs via phase transfer. Two other key nitrogen ligands, TOAB and CTAB will be discussed in § 2.3.1.

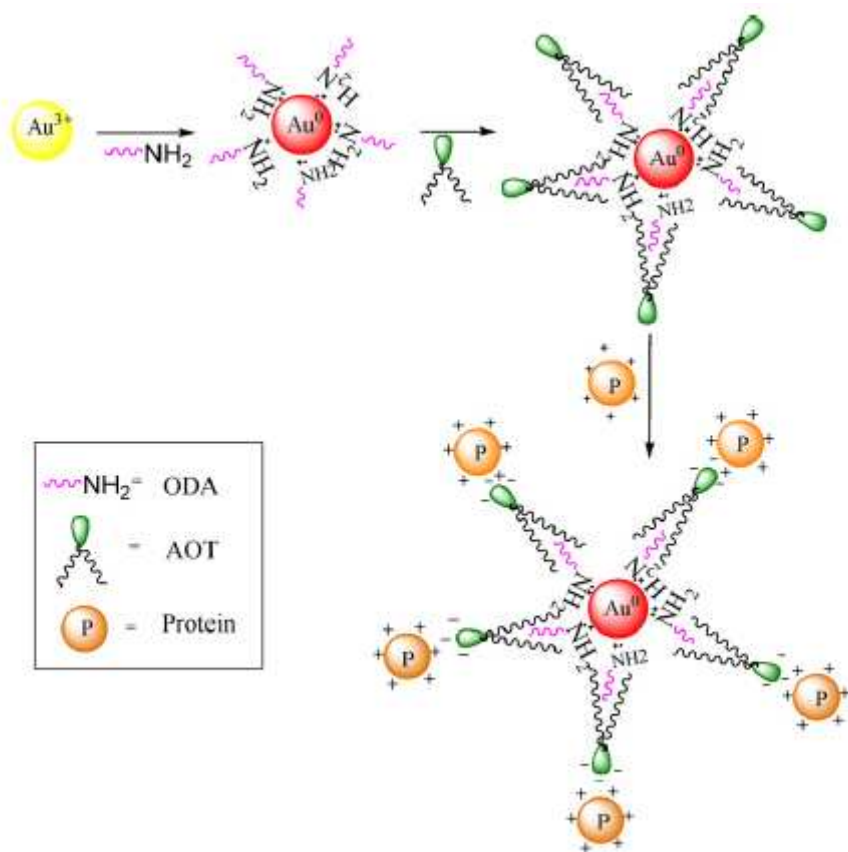


Figure 8. Synthesis pathway for TPP-stabilized AuNPs. Reprinted with permission from ref 164 (Suri's group). Copyright 2008 Elsevier.

Among oxygen ligands, carboxyl derivatives and phenol were reported as AuNP stabilizer. For instance, folic acid stabilizes AuNPs via a carboxyl group, which is useful for nanomedicinal applications.¹⁷⁴ The other carbonyl stabilizers include *N*-vinylpyrrolidone¹⁷⁵ and *N*-2-hydroxyethylpiperazine-*N*-2-ethanesulphonic acid (HEPES); the latter stabilizes flower-like AuNPs with its carbonyl and phenolate groups.¹⁷⁶

2.2. Macromolecule-stabilized AuNPs

Macromolecules stabilize AuNPs by both steric embedding effect and ligand interactions of their heteroatoms (N, O, P and S donors) with the AuNP surface.¹⁷⁷

2.2.2. Polymers

As reviewed by Shan and Tenhu, using polymers as AuNP stabilizers has various advantages: (i) enhancement of long-term AuNP stability, (ii) adjustment of their solubility, (iii) increased amphiphilicity, (iv) high and tunable surface density of shell/brush, (v) tailored properties of AuNPs, and (vi) compatibility and processibility.¹⁷⁸ Polymer-stabilized AuNPs date from Helcher's treatise in 1718¹⁷⁹ that indicated starch-stabilized water-soluble Au particles. With the rapid development of nanotechnology, polymer-stabilized AuNPs are becoming actively and widely used in

catalysis,¹⁸⁰ optics¹⁸¹ and biology.¹⁸² The two major synthetic routes to polymer-stabilized AuNPs are the “grafting to” and “grafting from” techniques.^{183,184-190} With the latter method, polymerization occurs at the Au surface in the presence of initiators; thus it can be viewed as a method of AuNP functionalization. The “grafting to” method involves direct AuNP synthesis by attachment of polymers onto the Au surface. There are two strategies for the “grafting to” method. The first one uses functionalized polymers with sulfur, nitrogen or other ligands at the end or in the middle of polymers to stabilize the AuNPs. This synthetic route is relevant to the Brust-Schiffrin method or the ligand substitution reaction. For the Brust-Schiffrin route that is often used with polymers, the HAuCl₄ solution is mixed with the functionalized polymers, and the reducing agent is added to form the AuNPs (both in one phase or two phases). For instance, the polymeric AuNP ligands used in this way include thiolate end-capped polystyrene (PS),¹⁹¹⁻¹⁹³ thiolate poly(ethylene glycol) (PEG),¹⁹⁴ five-arm PEG-b-PCL star block copolymers,¹⁹⁵ thiolate poly(*N*-isopropylacrylamide) (PNIPAM),¹⁹⁶ thiolate poly(vinyl pyridine) (PVP),¹⁹⁷ polypeptide with disulfide termini,¹⁹⁸ poly(acryloylaminophenylarsonic acid) (PAAPHA) with amine and arsenic acid group,¹⁹⁹ poly(ethylenimine) (PEI) with amine groups,³¹ thioether-functionalized polymer ligands (DDT-PVAc and PTMP-PVAc),²⁰⁰ ionic polymers,²⁰¹ and *O*-ethyl-*S*-(1-methoxycarbonyl)ethyl dithiocarbonate functionalized poly(*N*-vinyl caprolactam) (PVCL) (Figure 9).²⁰² The AuNP size is controlled by the polymer/ Au ratio that is detected by the change of intensity of the plasmon absorption in the UV-vis spectra.²⁰³ Some polymers such as PS and PAAPHA act as both reducing agents and stabilizers. Thus, they form AuNPs without additional reducing agents, but the AuNPs formed with such weak reducing agents are much larger than those formed using NaBH₄.



Figure 9. Synthesis of PVCL and coating of AuNPs. Reprinted with permission from ref 202(Marty's group). Copyright 2011 Royal Chemical Society.

The functionalized co-polymers are also used as templates in AuNP synthesis. For instance, Suzuki developed thermosensitive hybrid core-shell AuNPs *via in situ* synthesis. Figure 10 shows the route used in this study. Thiol- and amino-functionalized poly(*N*-isopropylacrylamide) (NIPAM)-b-(glycidyl methacrylate) (GMA) (poly NIPAM-b-GMA) have been used as templates to stabilize AuNPs inside the polymer shells.²⁰⁴

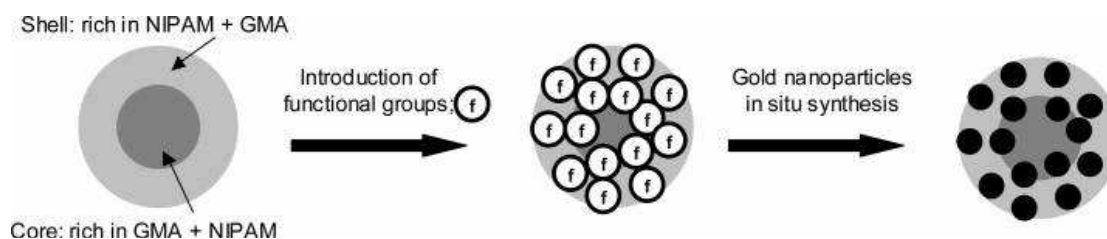


Figure 10. Schematic representation of the synthesis of thermosensitive hybrid core-shell particles containing AuNPs. Reprinted with permission from ref 204 (Kawaguchi's group). Copyright 2005 American Chemical Society.

The ligand-substitution reaction for the synthesis of polymer-stabilized AuNPs has a significant advantage in that the pre-prepared AuNPs therefore lead to relatively monodispersed AuNPs by the Turkevitch or Brust method. Thus, after the ligand-substitution reaction by polymers, the polymer-stabilized AuNPs are also relatively monodispersed, because the AuNP core does not undergo size change (Ostwald ripening) during the ligand-substitution process. Azzam *et al.* reported a typical ligand substitution reaction: PEO-b-PS-b-P4VP was added into the TOAB-stabilized AuNP solution in toluene and stirred for 24h, and the PEO-b-PS-b-P4VP-stabilized AuNPs were obtained.²⁰⁵ Recent examples have been reported.²⁰⁶⁻²⁰⁸ The other “grafting-to” strategy uses the polymer as a template to stabilize the AuNPs as core-shell NPs. This method is also defined as polymer-surfactant- or reverse micelle-stabilization of AuNPs, and is discussed in section §2.2.4.

2.2.3. Dendrimers

Dendrimers are highly branched, cauliflower-shaped monodispersed, synthetic macromolecules with well defined composition, dimension and structures.^{209,210} Dendrimer- or dendron-stabilized AuNPs are classified in three parts: (i) AuNPs that are entrapped into the dendrimers or dendrons by the functional groups (containing S, N, P and O) and the steric embedding effects. These AuNPs are also called dendrimer-encapsulated AuNPs (Au DENs), and are sometimes used in electrocatalysis;²¹¹⁻²¹⁹ (ii) AuNPs that are surrounded by several small dendrimers at their periphery are called dendrimer-stabilized AuNPs (Au DSNs); (iii) AuNPs prepared as dendrimer cores and stabilized by coordinating ligands located at the focal points of dendrons. With functional groups located at the dendron periphery, the AuNP assembly provides AuNP-cored dendrimers containing peripheral functional groups such as redox groups that are broadly used as redox sensors.²²⁰⁻²²⁵

Au DENs were first reported by Crooks's and Tomalia's groups using the polyamidoamine (PAMAM) dendrimers as stabilizers,²²⁶⁻²²⁸ followed by a number of reports dealing with the preparation of dendrimer-stabilized AuNPs of various kinds. The size distribution of dendrimer-stabilized AuNPs depends on the initial dendrimer to Au ratio²²⁹⁻²³¹ and dendrimer generation.^{232,233} The synthesis of dendrimer-stabilized AuNPs with AuNP cores bound to other sulfur groups²³⁴⁻²⁴⁴

(Figure 11), hydroxyl groups,^{245,246} benzyl ethers,²⁴⁷ and amine groups,²⁴⁸ has been reported. “Click” PEG dendrimer-stabilized AuNPs have recently been reported by our group. In these AuNPs, stabilization is provided by 1,2,3-triazole coordination, and the AuNPs are encapsulated in the dendrimers when the latter are large enough or surrounded by several dendrimers when the latter are too small (zeroth generation).^{249,250}

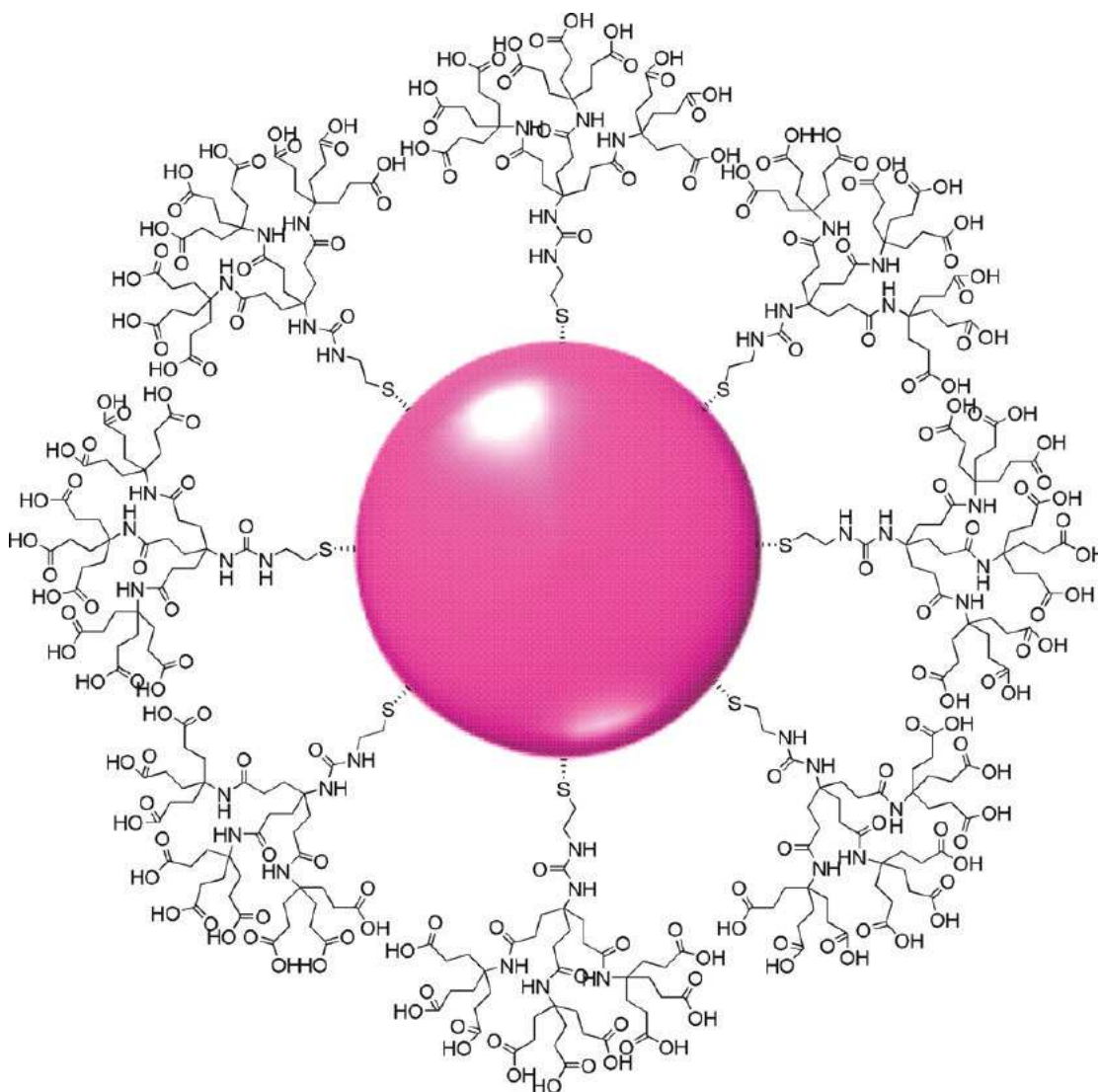


Figure 11. Newkone-type dendron-stabilized AuNPs. Reprinted with permission from ref 244 (Hackley's group). Copyright 2010 American Chemical Society.

Jia et al., reported the synthesis of AuNPs that are stabilized by phosphorylcholine-functionalized dendrimers. Their stability and controllable surface properties indicated potential use in biosensing (Figure 12).²⁵¹ AFM and TEM were used to demonstrate the morphology and size distribution of the AuNPs formed. Recently, the technique NICISS, reported by Voelcker's group, was useful to

understand the inner structure of dendrimer-stabilized AuNPs.²³³

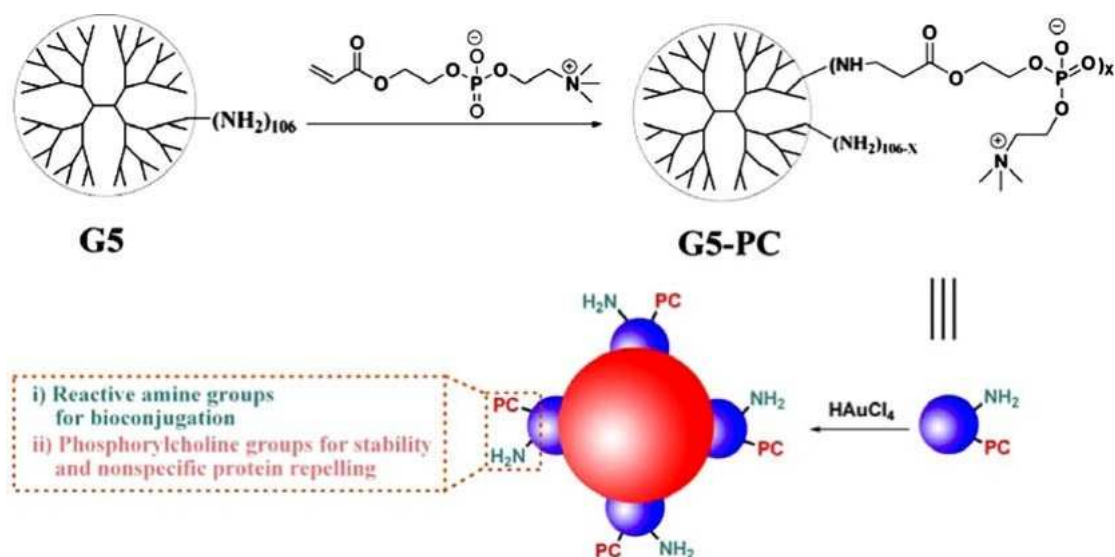


Figure 12. Schematic representation of the synthesis of Au DSNs. Reprinted with permission from ref 251 (Ji's group). Copyright 2011 Springer

2.3. Surfactants and reverse micelles

2.3.1 Surfactant-stabilized AuNPs without reverse micelle formation

Surfactants stabilize the AuNPs by electrostatic bonding between the Au surface and the surfactant heads. The surfactant TOAB is normally used in the Brust-Schiffrin two-phase method as a phase-transfer agent, and it also acts as AuNP stabilizer. The TOAB-capped AuNPs is obtained by the Brust-Schiffrin two-phase method without adding the additional stabilizer and utilized in further functionalization or self-assembly.²⁵²⁻²⁵⁵ Another example is the synthesis of cetyltrimethylammonium bromide (CTAB)-stabilized AuNPs,²⁵⁶⁻²⁵⁹ that was first reported by Nikoobakht *et al.* in 2001.²⁵⁷ The AuNPs are obtained by quickly adding an ice-cold NaBH_4 solution into the mixture of CTAB and HAuCl_4 solution, yielding AuNPs of average size up to 4 nm with a net positive interfacial charge. It is frequently used as a seed for the preparation of monodispersed gold nanorods (AuNRs)^{256,257} and size- and shape-controlled AuNPs.^{260, 261}

2.3.2 Surfactant-stabilized AuNPs with reverse micelle formation

Besides the electrostatic bonding, surfactants are also used to form reverse micelles for AuNPs synthesis. Reverse micelle solutions are transparent, isotropic, thermodynamically stable water-in-oil microemulsions that are dispersed in a continuous oil phase and stabilized by surfactant molecules at the water/oil interface.²⁶²⁻²⁶⁴ Water is readily solubilized in the polar core of reverse micelles,

forming so-called water pools that play the role of templates for AuNP formation and also prevent the aggregation of AuNPs.²⁶⁵ The size of the AuNPs is defined by the micelle volume. Both low-molecular-weight surfactants and copolymer surfactants form reverse micelles for the synthesis of AuNPs.

Sodium bis(2-ethylhexyl) sulfosuccinate (AOT) is a widely used low-molecular-weight surfactant in AuNPs synthesis. The reverse micelle is thus prepared by adding water/AOT/n-heptane²⁶⁶ or water/ATO/isooctane^{267,268} into an appropriate amount of HAuCl₄ or a gold salt. Then, the reducing agent hydrazine is added into the mixture to form the AuNPs. Recently, catanionic surfactants (mixture of octanoic acid and octylamine) such as lecithin,^{269,270} and trichromophoric dye-reverse micelle-stabilized AuNPs were also reported (Figure 13).²⁷¹ However, the use of water/oil microemulsions for the synthesis of AuNPs has a major drawback. Large amounts of surfactant are required to stabilize the AuNPs, which introduces impurities. Very recently, Hollamby *et al.* reported the purification of reverse micelle-stabilized AuNPs in a single step. In this case, the AuNPs are stabilized by the microemulsion that forms in water/octane with butanol as co-additive. After adding excess water, the AuNPs are concentrated into the upper octane-rich phase and the impurities remain in the water-rich lower phase.²⁷²

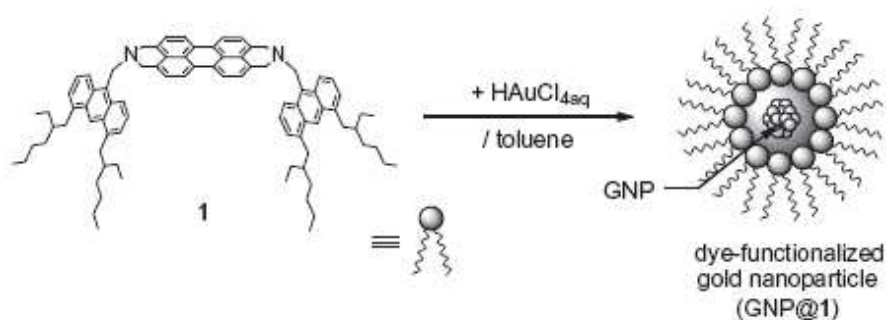


Figure 13. Scheme of dye-functionalized AuNPs (GNP = AuNP). Reprinted with permission from ref 271 (Yoda's group). Copyright 2011 Elsevier.

2.3.3. Reverse micelles

Compared with classical surfactant-formed micelles, the copolymer surfactant-formed micelles have several advantages. First, the critical micelle concentration (cmc) of copolymers is much smaller, and their kinetic stability is larger than that of low-molecular-weight surfactants. Second, the size and shape of copolymer micelles is easily tuned by varying the composition of the copolymer, the length of the constituent blocks, and the architecture of the copolymer. Third, the stability of the AuNPs is enhanced upon increasing the length of the coronal blocks.^{195, 273}

A large number of studies are available in polymer micelle-stabilized AuNPs, therefore only a few representative or recent examples are mentioned here. Poly (styrene)-block-poly (vinylpyridine) (PS-*b*-PVP)²⁷⁴⁻²⁷⁹ and poly (ethylene oxide)-poly (propylene oxide)-poly (ethylene oxide) (PEO-PPO-PEO)²⁸⁰⁻²⁸⁷ are the most widely

used polymer micelles for AuNPs synthesis, and these AuNPs are applied in catalysis²⁷⁵⁻²⁷⁷ and biosensing.²⁸⁷ PS-b-PVP micelle-stabilized AuNPs are typically synthesized as described by Möller's group. A solution of the block copolymer in dry toluene is mixed with HAuCl₄ in appropriate amount. The mixture is stirred for at least 24 h in order to allow complete dissolution of the gold salt in the core of the block copolymer micelle. The reducing agent hydrazine is added under vigorous stirring to form the AuNPs (Figure 14).^{274, 278} Very recently, Papp *et al.*²⁷⁹ showed that various reducing agents introduced into PS-b-PVP micelle systems resulted in the formation of AuNPs of various sizes. The morphology, size and size distribution of the AuNPs formed were determined by AFM, DLS, and TEM. In addition, microcalorimetry was used to investigate AuNP formation in the copolymer micelles. PEO-PPO-PEO-stabilized AuNPs have been synthesized through the route reported by Sakai and Alexandridis.²⁸⁰ AuNPs are prepared in an efficient one-pot aqueous-phase synthesis from the reduction of Au salts by using PEO-PPO-PEO both as reducing agent and stabilizer. The formation of AuNPs from Au salts comprises three steps: (i) initial reduction of Au ions in crown ether-like domains formed by block copolymer in solution, (ii) absorption of block copolymer on AuNPs and further reduction of Au ions on the surface of these AuNPs, and (iii) growth of particles stabilized by block copolymers.²⁸⁴ Increasing the PEO chain length favors the reduction of Au salts and formation of AuNPs.²⁸⁴

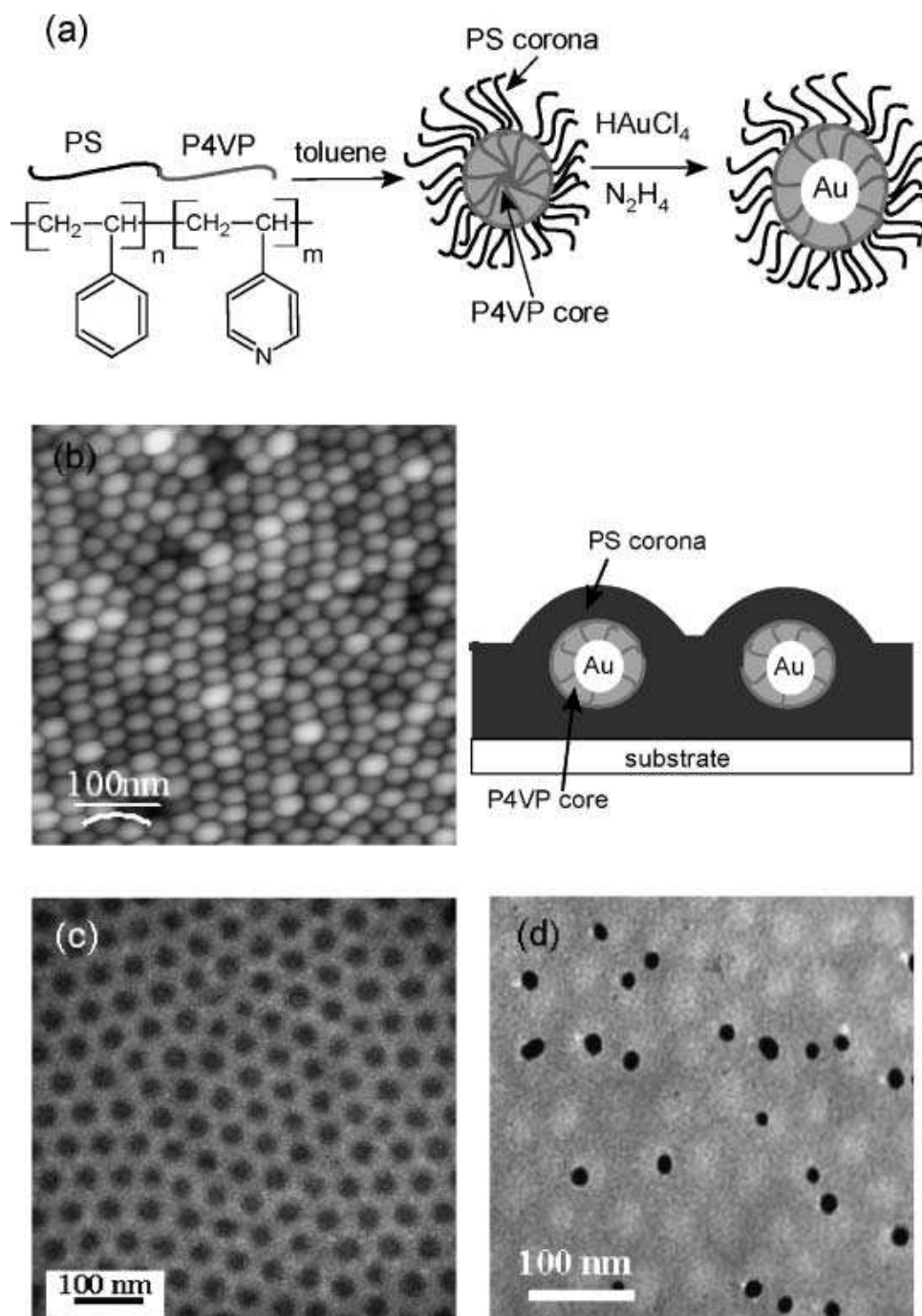


Figure 14. a) Molecular structure of the PS-*b*-P4VP copolymer and schematic illustration of the micellation process with *in-situ* synthesis of AuNPs in PS-*b*-P4VP. b) Topography image of the surface (from AFM) of a spin-coated PS-*b*-P4VP film along with a schematic illustration of a self-assembled PS-*b*-P4VP (with AuNPs) micellar film on a substrate. c) TEM image of PS-*b*-P4VP. The copolymer film is made up of a continuous bright PS matrix and dark spherical P4VP cores. d) TEM image of PS-*b*-P4VP with AuNPs; PS-*b*-(P4VP/Au). The molar ratio of H₂AuCl₄:P4VP is 0.1. Reprinted with permission from ref 278(Leong's group). Copyright 2008 Wiley-VCH.

In addition, the temperature,²⁸⁵ micelle environment²⁸⁶, and shapes and sizes of micelles²⁸⁶ are also considered to be the main contribution factors in the overall growth kinetics leading to a specific morphology of AuNPs.²⁸⁶ For example, the smaller micelle size with few surface cavities produced small AuNPs (Figure 15).²⁸⁶ Other polymer reverse micelle-stabilized AuNPs were also recently prepared using similar approaches. For example, poly (ethylene oxide)-b-poly (ϵ -caprolactone) (PEO-b-PCL)-stabilized AuNPs with 5-7 nm core size have potential for the exploration of drug-delivery systems with biodegradable PCL units and biocompatible PEO units.²⁸⁸ Polyethylenimine-g-hydrocaffeic acid (PEI-C)-AuNPs are also the subject of biomedical applications.²⁸⁹

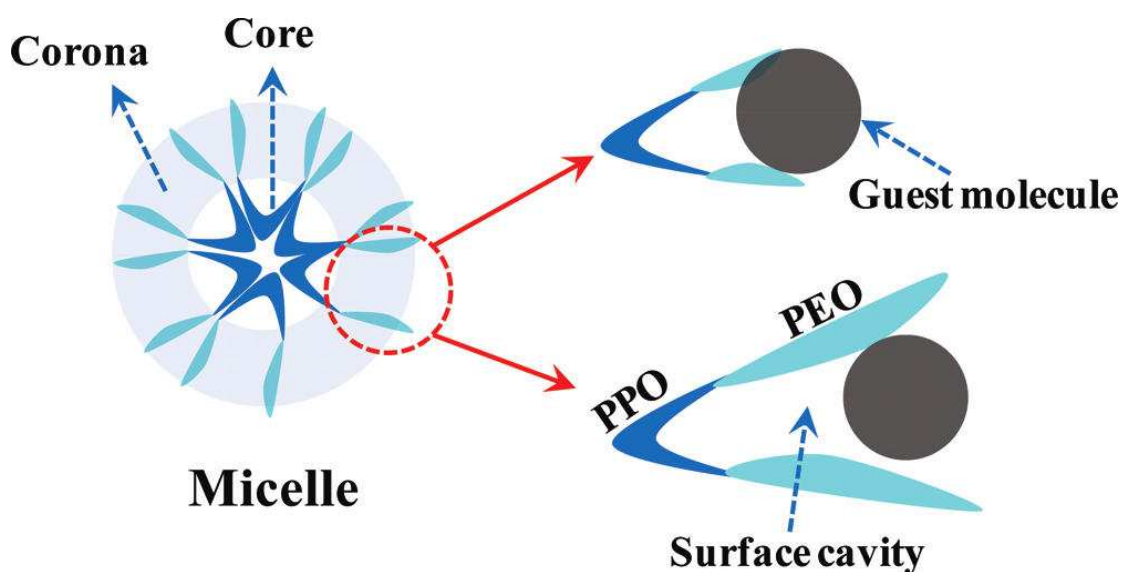
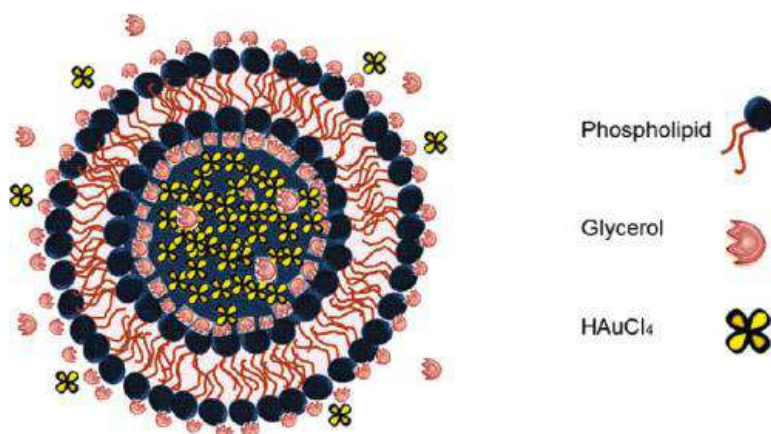


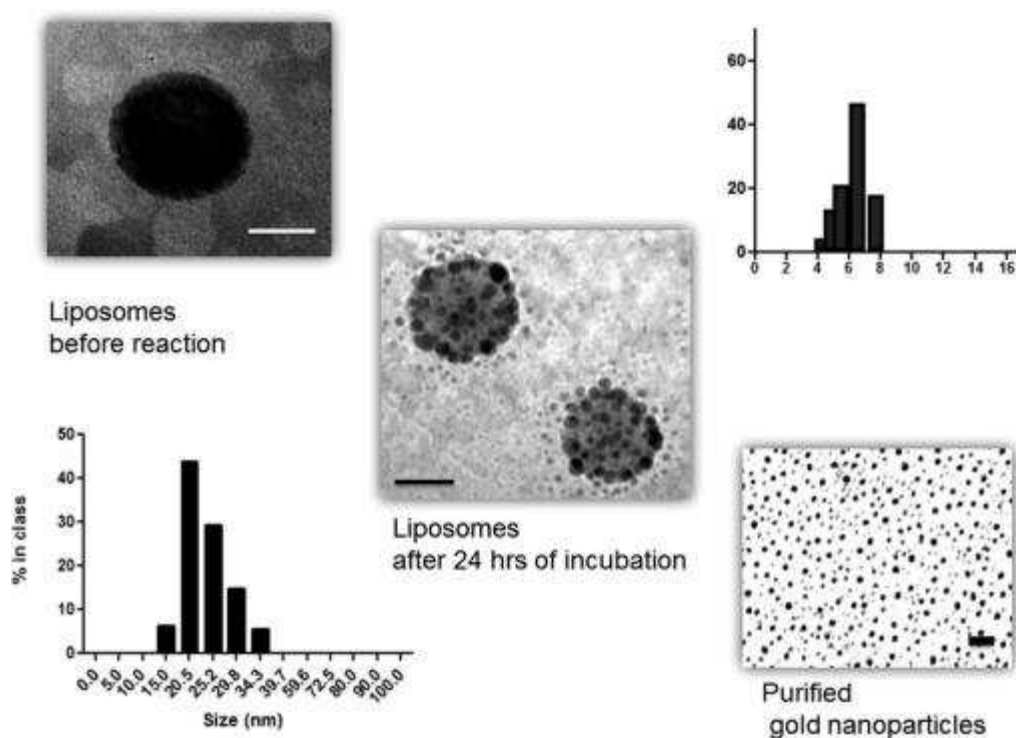
Figure 15. A PEO-PPO-PEO micelle with the core occupied by PPO units and the corona constituted by PEO units. Reprinted with permission from ref 286 (Bakshi's group). Copyright 2011 American Chemical Society.

2.3.4 Liposomes

Liposomes, supramolecular assemblies of amphiphilic lipids, can be used as reverse micelles to prepare AuNPs. Early syntheses of liposome-stabilized AuNPs have been conducted by adding NaBH_4 to mixtures of HAuCl_4 and liposomes.²⁹⁰ This method easily provides size-controlled AuNPs, but NaBH_4 is toxic and can modify the biological function.²⁹¹ Recently, Sau *et al.* reported a “green” and efficient methodology that yields liposome-stabilized AuNPs in a simple, rapid, and controlled way. The AuNPs are obtained by adding ascorbic acid as reducing agent into the mixture of liposome-based giant unilamellar vesicles (similar to micelles) and HAuCl_4 .²⁹¹ Similarly, AuNP synthesis using the biocompatible reducing agent glycerol was reported by O’Sullivan’s group (Figure 16).^{292, 293}



(a)



(b)

Figure 16. a) Designed liposomal nanoreactor. b) Formation stages of AuNPs inside the glycerol-incorporated (15% v/v) liposomes: liposomes before reaction (top left), liposomes during the reaction (middle) (scale bars = 10 nm), and purified AuNPs synthesized in the nanoreactor (bottom right, scale bar 20 nm). Photon correlation spectroscopy graph of the liposome size distribution before the reaction, PI = 0.232 (bottom left corner) and graph of the calculated AuNP size distribution using TEM (top right corner). Reprinted with permission from ref 293 (O’Sullivan’s group). Copyright 2011 American Chemical Society.

2.4 Biosynthesis and “green chemistry”

Biosyntheses and “green” syntheses of AuNPs are another remarkable area in AuNPs preparation via *in situ* synthesis. In these syntheses, the biomolecule directly acts both as a stabilizer and reducing agent to form the AuNPs. The sources for bio- and green preparations of AuNPs are natural source extracts, chitosan, and microbes.

2.4.1. Natural-source extracts

Due to the abundance of carboxyl, carbonyl, hydroxyl and phenol groups, the natural-source extracts reduce Au^{III} and stabilize the AuNPs with these groups. Since Goia and Marijevic synthesized gum arabic (originated from a natural plant) stabilized AuNPs in 1999,²⁹⁴ many environmentally friendly AuNP syntheses were reported, especially by Sastry’s group.²⁹⁵⁻²⁹⁷ In these reports (Table 1), non toxic chemicals from natural source extracts were used in the syntheses in order to avoid adverse effects in medical and biology applications. These AuNP syntheses using natural-source extracts are simple, just mixing the extracts with aqueous HAuCl₄ until the color changes to red or purple.²⁹⁵ Besides this green-chemistry aspect, AuNPs stabilized by natural-source extracts are also used in other fields involving AuNPs assembly.³⁰⁶

Table 1. AuNPs stabilized by natural-source extracts

Natural source	Groups for stabilizing AuNPs	Publication year
Gum arabic ²⁹⁴	phenol	1999
Lemongrass ²⁹⁵	hydroxyl and carbonyl	2004
Emblica officinalis ²⁹⁶	carbonyl and phenol	2005
Alove vera plant ²⁹⁷	carbonyl and phenol	2006
Cinnamomum camphora ²⁹⁸	carbonyl	2007
Gellan gum ²⁹⁹	carboxy, carbonyl and phenol	2008
Castor oil ³⁰⁰	carboxyl	2008
Volvariella volvacea ³⁰¹	phenol	2009
Hibiscus ³⁰²	phenol	2010
Bayberry tannin (BT) ³⁰³	phenol and carbonyl	2010
Tannic acid ³⁰⁴	phenol and carboxyl	2010
Zingiber officinale ³⁰⁵	carbonyl and phenol	2011

2.4.2. Chitosan

Chitosan, the second-most abundant natural polymer in the world, is known as the deacetylated chitin and has a good water solubility and biocompatibility.^{307,308} Chitosan stabilizes AuNPs with the amine groups and the steric effect of its own structure. Yoshimura’s group first reported chitosan-stabilization of AuNPs by adding NaBH₄ as a reducing agent.³⁰⁸ Further, Huang’s group³⁰⁹ used chitosan both as a stabilizing agent and reducing agent, and obtained AuNPs by 2h heating of HAuCl₄ and chitosan mixture with a 70°C water bath, a fully “green” synthesis. From then on, the chitosan-stabilized AuNPs have been widely used in catalysis,³¹⁰ biomedicine,³¹¹ and sensing.¹⁶² In addition, carboxymethyl chitosan has

later also been used to synthesize AuNPs, due to its higher sorption of metal ions than that of chitosan.³¹²

2.4.3. Microbes

The stabilization by microbes provides a remarkable mode of AuNP biosynthesis that has been studied for more than three decades. In 1980, Beveridge and Murray reported that the *Bacillus subtilis* reduces Au^{III} to AuNPs with a size range of 5-25 nm sizes inside the cell wall.³¹³ Up to now, four major microbes have been used for AuNPs synthesis: bacteria, fungi, actinomycete and yeast. The abundance of carboxyl groups in microbes is considered to play a major role in the reduction of Au^{III}.³¹³ Moreover, the abundant electronegative groups in microbes (amine, carboxyl, thiol, disulfur, etc.) contribute to the microbe stabilization of AuNPs. The synthesis of AuNPs with microbes follows two procedures: extracellular production and intracellular production. For the extracellular production, Au^{III} is reduced by the cell wall reducing enzymes or soluble secreted enzymes. For the intracellular production, reduction occurs inside the cell. The extracellular production of AuNPs has wider applications than intracellular accumulation in optoelectronics, electronics, bioimaging and sensor technology.³¹⁴

In Table 2, some identified data from ref 314 are recollected together with some newest data showing recent microbe-stabilized AuNPs.

Table 2. Microbe-stabilized AuNPs

Microbe type	Microbe	Localization	Size	Reference
Bacteria	Sulfate-reducing bacteria	intracellular	< 10 nm	315
	Shewanella algae	intracellular	10-20 nm	316
	Plectonema	intracellular	10 nm	317
	Rhodopseudomonas capsulata	extracellular	50-400 nm	318
Fungi	Verticillium sp.	intracellular	20±8 nm	319
	Fusarium oxysporum	extracellular	20-40 nm	320
Actinomycete	streptomyces viridogens strain HM10	intracellular	18-20 nm	321
	Thermomonospora sp.	extracellular	8 nm	322
Yeast	Extremophilic Yeasts	intracellular	30-100 nm	323
	Yarrowia lipolyrica NCIM 3580	intracellular	15 nm	324

3. Seed-growth method

3.1. Principle of the seed-growth method

The seed growth method is another popular technique for AuNP synthesis that has been used for more than a century. Compared with the *in situ* synthesis, the seed-growth method enlarges the particles step by step, and it is easier to control the sizes and shapes of formed AuNPs. Thus, this procedure is widely used in the most recent size- and shape-controlled AuNPs syntheses.

The seed growth usually involves two steps. In the first step, small-size AuNP seeds are prepared. In the second step, the seeds are added to a “growth” solution containing

HAuCl₄ and the stabilizing and reducing agents, then the newly reduced Au⁰ grows on the seed surface to form large-size AuNPs. The reducing agents used in the second step are always mild ones that reduce Au^{III} to Au⁰ only in the presence of Au seeds as catalysts, thus the newly reduced Au⁰ can only assemble on the surface of the Au seeds, and no new particle nucleation occurs in solution. Moreover, due to the use of a mild reducing agent, the second step is much slower than the first one, and it can be repeated to continue the growth process.

In the course of the seed-growth synthesis of AuNPs, the formation of seeds takes a significant place correlated to the size, shape and surface properties that are controlled by the amount and nature of reducing agent and stabilizer, and their ratio to the Au precursor. The earliest gold nano seeds were proposed by Natan,³²⁵ using citrate reductant and capped spherical Au seeds with diameter 12 nm for the overgrowth of spherical AuNPs. In 2001, Jana and co-workers³²⁶ synthesized 3.5 nm citrate-capped gold seeds by dropping an ice-cold aqueous solution of NaBH₄ into a solution of a mixture of HAuCl₄ and citrate. These seeds were originally used for the formation of AuNRs. This procedure of Au seed formation was modified by El-Sayed³²⁷ in 2003 using hexadecyltrimethylammonium bromide (CTAB) as the stabilizer instead of citrate. These Au seeds with a diameter smaller than 4 nm were used to promote the narrow dispersity of AuNRs. Subsequently, this seed formation was regarded as the most primary nucleation process in the synthesis of AuNPs. Other monodispersed, large-sized, spherical or quasi-spherical AuNPs, AuNRs, and other shaped AuNPs have been synthesized using the seed-growth method, as follows.

3.2. Spherical or quasi-spherical AuNPs

The traditional *in situ* synthesis provides spherical or quasi-spherical AuNPs. The disadvantage is, however, that when the size increases it becomes out of control, and the shape is not controlled either. Therefore, the seed-growth strategy has emerged as a very efficient method to synthesize monodispersed AuNPs with large sizes (up to 300 nm) precisely and with well-defined shapes.³²⁸⁻³³⁰

Natan and co-workers,^{325,331,332} pioneered the seed-growth method reported in an European patent.³³³ In this procedure, the AuNPs between 20 nm and 100 nm were prepared by adding citrate-capped, NaBH₄-reduced seeds into a “growth” solution containing a mild reducing agent such as citrate^{331,332} or hydroxylamine.³²⁹ This results provided an improvement of physical properties compared to the Turkevitch and Frens method. However, this synthetic route also generated a small population of rod-shaped AuNPs as impurities. Later, Murphy’s group³³⁴ improved the method by using ascorbic acid as a reducing agent as mild as citrate in growth solution and using CTAB as a stabilizer to synthesize monodispersed spherical AuNPs up to 40 nm (the citrate-stabilized AuNPs with a relative standard deviation that was lower than 10% were considered as monodisperse^{334,335}). This method was later used for the synthesis of icosahedral AuNPs with controlled size (from 10 nm to 90 nm) by Han’s group (Figure 17).³³⁶

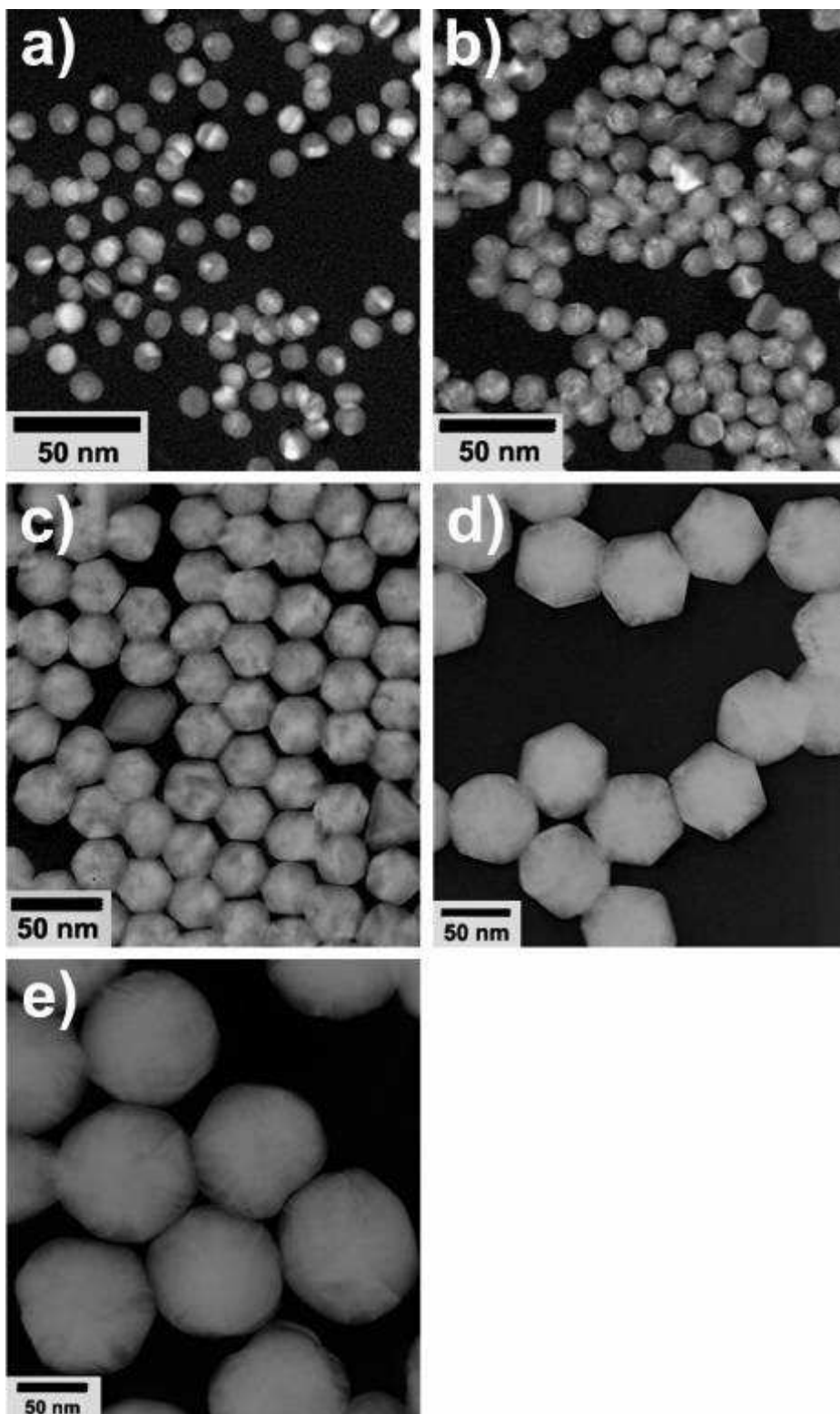


Figure 17. TEM images of AuNPs in solution a) 11.0 ± 0.8 nm, b) 13.3 ± 2.0 nm, c) 32.2 ± 1.8 nm, d) 69.0 ± 3.7 nm and e) 87.3 ± 12.1 nm. Reprinted with permission from ref 336(Han's group). Copyright 2007 American Chemical Society.

Recently, highly monodispersed, spherical, citrate-stabilized AuNPs were synthesized up to 300 nm by using hydroquinone³²⁹ or ascorbic acid (Figure 18)³³⁷ as reducing agent in the seed-growth process. Reaction conditions such as temperature,³³⁰ pH,³³⁰ Au precursor to seed particle concentration³³⁰ and citrate concentration³³⁵ were considered to affect the size distribution and shape of the AuNPs.

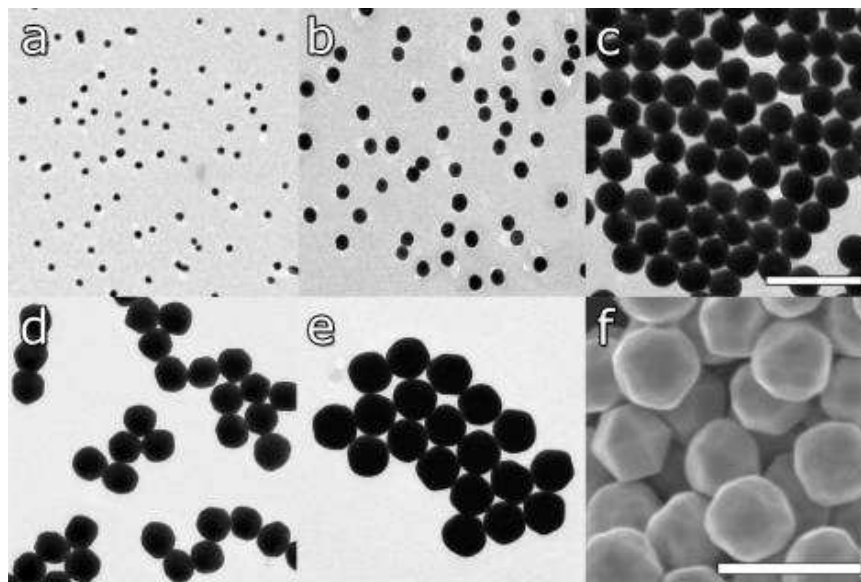


Figure 18. TEM images of AuNPs in solutions a) 15 ± 2 nm, b) 31 ± 3 nm, c) 69 ± 3 nm, d) 121 ± 10 nm, e) 151 ± 8 nm and e) 294 ± 17 nm. Scale bars are 200 nm for parts a-c and 500 nm for parts d-f. Reprinted with permission from ref 337 (Eychmüller's group). Copyright 2011 American Chemical Society.

3.3. Gold nanorods (AuNRs)

The AuNRs show two plasmon bands: a strong longitudinal band in the near-infrared region and a weak transverse band, similar to that of gold nanospheres, in the visible region. The band in the near-infrared region, where tissue absorption is minimal, is very useful for potential *in vivo* applications. Consequently, due to their specific structure and shape, the AuNRs exhibit wide potential use in nanomedicine.^{338, 339, 340} During the last few decades, AuNRs had been prepared using electrochemical and photochemical reduction methods in aqueous surfactant media and nanoporous templates.³⁴¹⁻³⁴³ However, the seed-growth method now clearly appears as the most favorable one for synthesizing AuNRs, because it can easily generate high yields of well-defined and monodispersed AuNRs.

The current seed-growth method was first reported by Murphy's group in 2001.³²⁶ Briefly, 3-4 nm citrate capped AuNPs are used as seeds, then the seeds are added into the growth solution containing appropriate HAuCl_4 , CTAB and freshly prepared ascorbic acid, without further stirring or agitation. After 5 to 10 min, AuNRs with 4.6 ± 1 aspect ratio are generated in the solution. AuNRs with a high aspect ratio

(up to approximate 20) are obtained by three-step growth: the first-step forms AuNRs that are used as seeds for the second growth, and the second-step-formed AuNRs are used as seeds for the third growth (Figure 19).^{326,344,345} The AuNRs obtained are purified and form other-shaped AuNPs by centrifugation. However, this method has the disadvantage that large amounts of AuNPs of sphere and other shapes are formed as by-products, which greatly reduces the AuNR yield. Nikoobakht and EI-Sayed improved the method in 2003, efficiently overcoming the drawbacks. The CTAB-capped seeds are used instead of citrate-capped seeds, and silver nitrate is used in the seed-growth process to control the aspect ratio of AuNRs. This protocol results in high yield of AuNRs (99%) with ratios from 1.5 up to 5 and generates only traces of spherical AuNPs.³²⁷

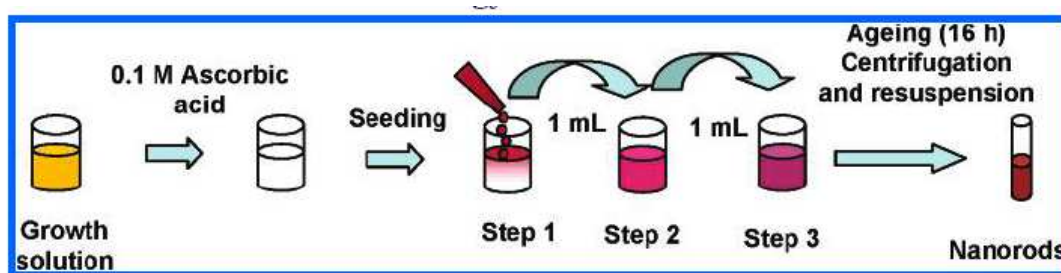


Figure 19. General methodology for the generation of AuNRs. Reprinted with permission from ref 345 (Murphy's group). Copyright 2004 American Chemical Society.

In order to better understand the formation of AuNRs, the scientists have concentrated on the parameters that affect the yield, monodispersity and size of AuNRs. For instance, Huang's group^{346,347} reported that nitric acid added into the growth solution leads to a high yield of AuNRs. Korgel's group^{348,349} and Manohar' group³⁵⁰ noticed that the presence of iodide at ppm concentrations in CTAB prevents the formation of AuNRs in the growth media. In a recent report, it was disclosed that the micelle nature of CTAB was a key factor in NR purification from other shapes due to depletion attraction forces of surfactant micelles.³⁵¹ Then Garg *et al.* showed that bromide anions of the CTAB surfactant played a greater role than the CTA⁺ cations for the process of AuNRs formation.³⁵² Furthermore, Si *et al.* figured out that bromide anions played a crucial role in the formation of rod-like AuNPs in the sense that there was a critical [Br⁻]/[Au^{III}] ratio (around 200) to form AuNRs with a maximum aspect ratio; beyond this value, the aspect ratio of AuNRs decreased (Figure 20).³⁵³ Details of the mechanism of AuNR formation have been carefully reviewed by the EI-Sayed³³⁸ and Murphy groups³³⁹.

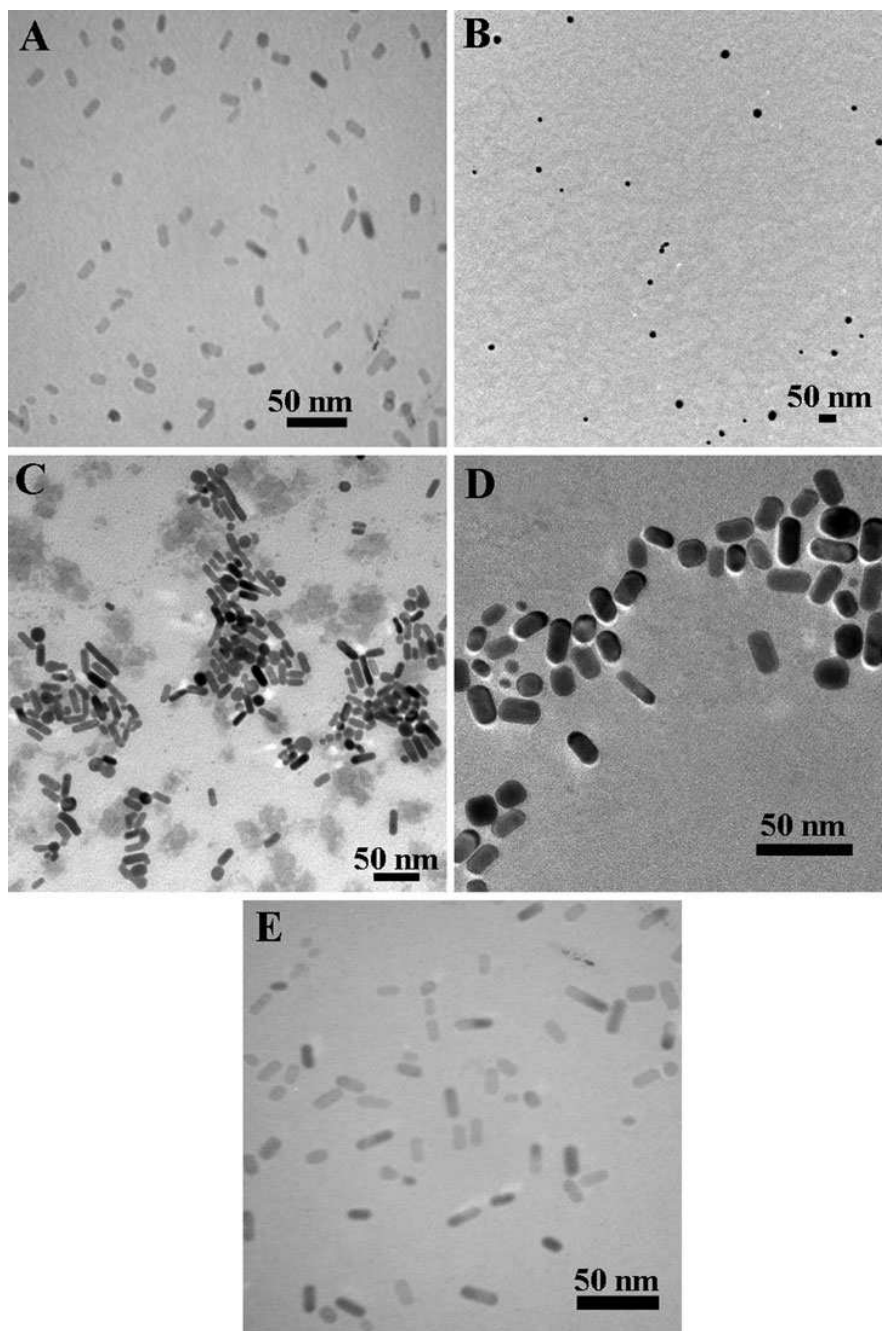


Figure 20. TEM image of AuNRs prepared with A) 100 [size: $(18\pm3) \times (8.5\pm1)$ nm], B) 200 [spheres (26 ± 5) nm in diameter], and C) 20 mM CTAB [size: $(23\pm5) \times (8\pm1)$ nm]; D) 20 mM CTAB+80 mM NaBr [size: $(21\pm3) \times (11\pm1)$ nm] and E) after 24 h reaction with 100 mM CTAB. The concentration of HAuCl_4 was 8×10^{-2} mM in all reactions. Reprinted with permission from ref 353 (Lounis's group). Copyright 2012 Wiley-VCH.

3.4. Other shapes of AuNPs

Besides spherical or quasi-spherical AuNPs, anisotropic AuNPs have also recently been reported and widely used in biomedicine³⁵⁴ and nanotherapy.³⁵⁵ Among the

shape-controlled strategies,³⁵⁶ seed growth is an efficient method for the synthesis of anisotropic AuNPs. It allows rational design of nanocrystal shape, size distribution and monodispersity through the adaption of nucleation and growth conditions. In particular, reported anisotropic AuNPs include AuNRs,⁵⁷ Au nanocubes,³⁵⁷ Au nanohexapods,³⁵⁸ Au nanoribbons,³⁵⁹ Au hollow nanocages,³⁶⁰ Au nanobranches,³⁶¹⁻³⁶³ and Au nanopolyhedrons.³⁶⁴⁻³⁶⁶

Herein we are focusing on the main examples of anisotropic AuNP syntheses and their improvements. A seminal report of a solution-based “chemical” route to multiple shaped-controlled AuNPs in 2004 is that of Murphy³⁵⁷ and co-workers. In a typical procedure, a HAuCl₄ solution is added to a CTAB solution followed by addition to the growth solution of an aqueous solution containing AgNO₃, ascorbic acid, and HAuCl₄. In given conditions, nanorods, and other particles with triangular and square outlines were formed and, by increasing the ascorbic acid concentration, hexagonal nanocrystal appeared. Then, upon further increase in ascorbic acid, cube-shaped particles were formed in high yield (90%). A variation of branched AuNPs were also synthesized by controlling the various combinations of [seed]/[Au^{III}] ratio or the concentrations of CTAB and ascorbic acid.

Huang's³⁶⁷ group reported a systematic shape evolution process from CTAC-capped truncated cubic Au seeds to trioctahedral and rhombic dodecahedral AuNPs *via* a two-step seed growth process. Systematic shape evolutions from truncated cube to cubic, trisoctahedral, and rhombic dodecahedral structures have been controlled upon addition of various amounts of ascorbic acid.

Xia³⁵⁸ and coworkers reported a facile method for the formation of thermodynamically unfavorable Au nano-hexapods by using *N,N*-dimethylformamide (DMF) to reduce HAuCl₄ in the presence of single crystal of octahedral Au as the seed. The shapes of the hexapods have been controlled by variation of the amount of HAuCl₄ in the growth solution or changing the reaction temperature. Polyhedron is another shape of AuNPs that has recently been obtained by adding the CTAC-capped Au seeds into the growth solution containing HAuCl₄, CTAC, and various salts, followed by reduction using ascorbic acid. The shapes of the AuNPs formed are controlled by the nature of various salts in the growth solution. For example, NaBr is used for rhombic dodecahedra, and KI is used for octahedral.³⁶⁶ Very recently, Mirkin's group³⁶¹ reported a method to synthesize octahedral AuNPs with hollow features. In the growth process, Au concave nanocubes are prepared as seeds,³⁶² and the reaction is initiated by the addition of the seeds to the growth solution containing the appropriate ratio of HCl, HAuCl₄, AgNO₃, ascorbic acid, and cetyltrimethylammonium chloride (CTAC). The yield is higher than 90%, and the structure of the Au hollow is well characterized (Figure 21 shows some examples of anisotropic AuNPs).

The growth mechanism of anisotropic nanocrystal formations was scrutinized, and it was found that the temperature, pH, Au precursors/surfactants ratio and salts used in the growth solution influenced the growth of Au seeds on each facet, and finally affected the size and shapes of the AuNPs.³⁶⁸⁻³⁷¹

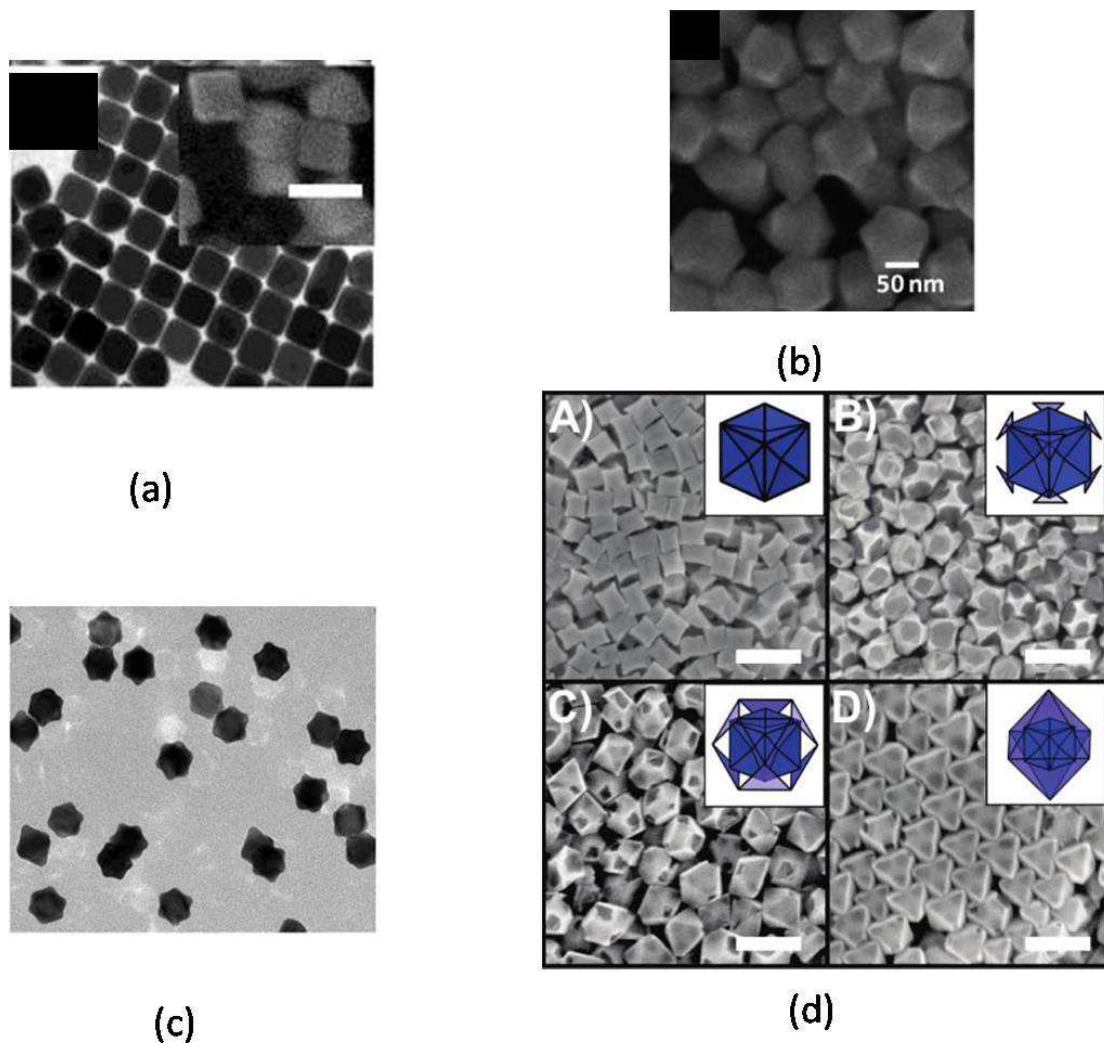


Figure 21. a) Cubic AuNPs. Reprinted with permission from ref 357 (Murphy's group). Copyright 2004 American Chemical Society.

b) Trisoctahedra AuNPs. Reprinted with permission from ref 367 (Huang's group). Copyright 2010 American Chemical Society.

c) Star-like AuNPs. Reprinted with permission from ref 358 (Xia's group). Copyright 2011 Wiley-VCH.

d) SEM images of (A) the concave cube seeds and the products of the octahedra reaction with (B) 50, (C) 100, and (D) 150 μL of a 10 mM HAuCl_4 solution. Scale bars: 100 nm. Reprinted with permission from ref 361 (Mirkin's group). Copyright 2011 American Chemical Society.

4. Other AuNP synthetic methods

Other methods involve both "top down" and "bottom up" strategies and are discussed here. They also include supported AuNPs and bimetallic AuNPs.

4.1. Pulse radiolysis

Pulse-radiolysis is another “bottom-up” method that involves gamma-ray irradiation for the reduction of Au^{III} instead of the traditional addition of a chemical reductant.³⁷² As a suggested mechanism, radiolysis generates radicals by ionization and excitation of the solvent (usually water). A radical scavenger is introduced in order to trap the primary radical formed (OH[•]) to give a new radical that is unable to oxidize the gold ions but exhibits strong reducing power, such as the radicals of secondary alcohols (2-propanol is the most-commonly used one). This is followed by the disproportionation of Au^{II} species giving Au^I and Au^{III} species. Meanwhile, the mild reducing agent reduces Au^{III} to Au^{II}, and Au^I to Au⁰. During this stepwise process, Au^{III} is progressively reduced to Au⁰, and the formation of AuNPs proceeds in the presence of a stabilizer that is required in order to avoid the overgrowth and aggregation of the AuNPs.³⁷³ The stabilizer must be unable to reduce the gold salt directly before the irradiation. For instance, poly(vinyl alcohol) (PVA), octadecylamine(OA), and polyvinyl pyrrolidone (PVP) were used as stabilizers.

In a recent example, Abidi *et al.*³⁷⁴ reported a one-pot radiolytic synthesis of AuNRs of well-controlled aspect ratios in a CTAB micelle. The synthetic procedure involved addition of HAuCl₄ and TOAB to a stirred aqueous CTAB solution; after further stirring for 1h at 50 °C, acetone, cyclohexane, and AgNO₃ were successively added into the previous solution, and then flushed with nitrogen and irradiated by a ⁶⁰Co panoramic gamma source. A series of AuNRs with various aspect ratios were obtained by variation of the Ag^I concentration.

The radiolysis strategy has also been reported for the synthesis of spherical AuNPs with diameters 6 nm and 13 nm³⁷⁵ bimetallic Au-Pd³⁷⁶ and Au-Ag³⁷⁷ NPs, but altogether rather few reports are known.

4.2. Top-down methods

The top-down strategies start with a bulk gold substrate (generally film or pellet), followed by a nanoscale patterning procedure during which most portion of the gold film is removed, yielding AuNPs with predetermined scale and shape.³³⁸ One of the most commonly utilized top-down techniques is the electron-beam lithographic method that results in the formation of multiple-shaped nanostructures with dimensional control on tens of nanometer length scale.³⁷⁸ Another most popular top-down technique is the laser-based ablation,³⁷⁹ first introduced by Cotton *et al.*³⁸⁰ As an recent example, Meunier's³⁸¹ group developed a two-step femtosecond laser-assisted technique producing size-controlled, low dispersed (20%), and functionalized spherical Au NPs in aqueous solution in the size range of 2 to 80 nm. In the first step, seeds were obtained by ablating a gold pellet substrate immersed in aqueous dextran (as stabilizer ligand) solutions. The seed-growth proceeds under femtosecond laser irradiation for 1h.

4.3. Supported AuNPs

As in the synthesis of ligand-stabilized AuNPs, the primary role of the support is to

avoid the aggregation of AuNPs. Moreover, the support also plays a direct or indirect role at the AuNP-support interface in gold-catalyzed reactions. AuNPs supported by mesoporous oxides including TiO₂, CeO₂, SiO₂, Fe₃O₄, Al₂O₃, ZrO₂, the forms of carbon, and metal-organic framework (MOFs) have broad applications in homogeneous and heterogeneous catalysis.³⁸²

4.3.1. Oxides

The most widely used procedure for the preparation of AuNPs supported on these insoluble oxides solids is the precipitation–deposition method. Starting from an aqueous solution of HAuCl₄, addition of a base leads to precipitation of a mixture of Au(OH)₄ or Au(OH)_x⁻Cl_{4-x}⁻. Related gold oxy/hydroxides that adsorb into the solid are then reduced to metallic Au by boiling the adsorbed species in methanol or any other alcohol. After adsorption on the solid surface, AuNP formation occurs by nucleation and growth. The pH of the precipitation and the other experimental conditions (nature of the alcohol, temperature and time of the reduction, calcination procedure, etc.) provides a certain control of the particle size of the resulting NPs.³⁸³ The ideal solid oxide support should have a high density of hydroxyl groups and a large surface area according to the deposition-precipitation mechanism in order to achieve the formation of AuNPs with narrow size distribution.^{382,384-392} Characterization techniques for the oxide-supported AuNPs include TEM, SEM, XRD, Raman and UV-vis spectroscopies. Since Haruta's seminal discovery³⁸³ in the 1980's of CO oxidation by O₂ to CO₂ at low temperature using TiO₂-supported AuNPs that are smaller than 5 nm, these oxide-stabilized AuNPs are widely studied in catalysis for aerobic oxidations of various substrates including alcohol oxidation, CO oxidation, and hydrolytic dehydrogenation and for hydrogenation reactions.³⁸⁴⁻³⁹²

4.3.2. Carbon

In the family of activated carbons, carbon blacks, graphites and carbon nanotubes (CNTs) have been reported to support AuNPs for catalytic applications³⁹³ and sensing.³⁹⁴ The precipitation–deposition method that is very useful with oxide supports results instead in aggregation with carbon supports.³⁸² Thus, in order to deposit AuNPs on carbons, two steps are required. This first step is the synthesis of the AuNPs by either the Turkevitch method or the Brust method using a stabilizer such as citrate, thiol, polymer, *i.e.* The second step is the immobilization of preformed AuNPs on the surface of active carbons (also carbon blacks and graphite) or into the matrixes of CNTs. Concerning the immobilization step, as shown by the group of Prati and Rossi,^{15,395} the carbon support is added into a sol of preformed AuNPs with vigorous stirring, and the AuNPs are immobilized on the support with a certain amount of AuNP loading. A high stabilizer/Au ratio maintains the original sizes of the AuNPs during the immobilization step.³⁹⁵ Sol-carbon interactions are critical to control the resulting AuNP size.^{395, 396}

4.3.3. Mesoporous materials and MOFs

4.3.3.1. Mesoporous materials

Mesoporous material-supported AuNPs are widely used as catalysts. The production of these types of catalysts leads to high surface-area systems, in which the shape-selective behavior of mesoporous materials can be combined with the catalytic action of metal particles. This shape selectivity cannot be achieved with amorphous oxide-supported metal catalysts.^{397,398} Among all the mesoporous materials, the mesoporous silicas have gained great attention due to the properties of MCM-41 (MCM: Mobil Composition of Matters) and related materials, including highly ordered mesopores, controlled pore size, specific surface areas and pore volumes.^{382,399,400} An early synthesis of silica-coated AuNPs was reported in 1996 by Mulvaney' group. The silane coupling agent (3-aminopropyl)-trimethoxysilane was used to render the gold surface vitreophilic. After the formation of a thin silica layer in aqueous solution, the particles were transferred into ethanol for further growth using the Stober method. Varying the silica shell thickness and the refractive index of the solvent allowed control over the optical properties of the dispersions.¹¹⁰ The use of task-specific ligands with calcining as post-treatment provides AuNPs that are encapsulated into the mesoporous channels or loaded on the surface of silica spheres.^{382,401} For example, Corma's group⁴⁰² reported task-specific ligands containing a cetylammonium moiety to act as structure-directing agent that reacts with AuNPs containing a trialkoxysilyl group. The latter co-condenses with tetraethoxysilane (TEOS) to form mesoporous silica. (Figure 22) In another recent example, it was reported⁴⁰² that a $-NH_2$ and $-NH$ functionalized mesoporous carbon nitride (MCN) stabilizes AuNPs. The synthesis involved the reduction of $AuCl_4$ by $NaBH_4$ in water suspension in the presence of MCN.

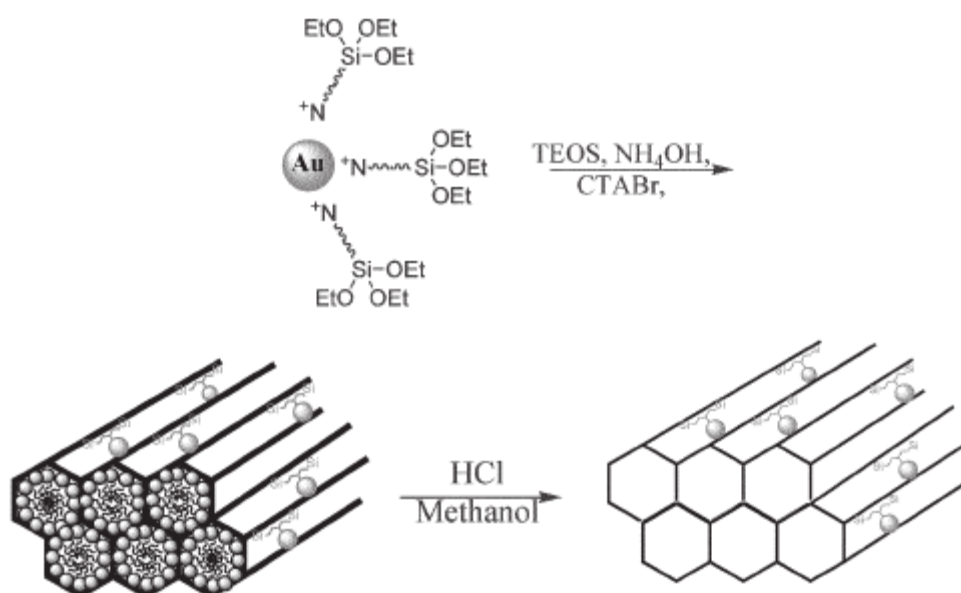


Figure 22. Synthesis of AuNPs encapsulated in mesoporous silica. Reprinted with permission from ref 402 (Corma's group). Copyright 2005 Royal Chemical Society.

Besides task-specific ligands, the AuNPs are also coated with polymers and then encapsulated by mesoporous materials as core-shell AuNPs. For instance, Jan et al.⁴⁰³ reported a preparation of AuNP/mesoporous silica tubular nanostructures. Poly(L-lysine) (PLL) and poly(L-glutamic acid) (PLGA) multilayer-coated membranes are immersed in a HAuCl₄ solution to form AuNP/PLL/PLGA multilayers. Subsequently the membranes are taken out from the solution and inserted in a freshly prepared orthosilicic acid solution for 6-12 h, in order to allow precipitation of silica in this multilayer. After thoroughly rinsing with water and drying at room temperature, the as-prepared AuNP/meso-SiO₂/PLL/PLGA multilayer is obtained and purified by calcination (Figure 23).

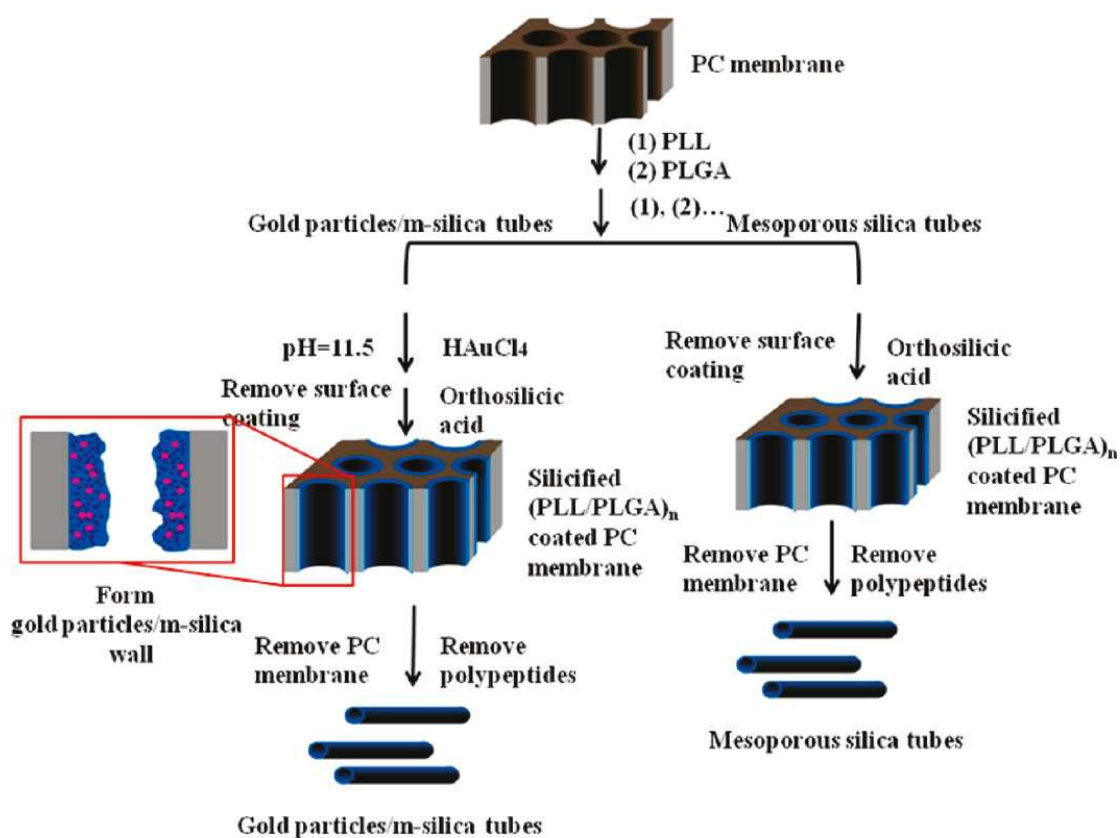


Figure 23. Procedure used for preparing mesoporous silica and AuNP/meso-silica tubes. Reprinted with permission from ref 403 (Jan's group). Copyright 2011 American Chemical Society.

4.3.3.2. MOFs

MOFs are another form of mesoporous materials that are thermally robust and in many cases highly porous. It is expected that the crystalline porous structures of MOFs limit the migration and aggregation of AuNPs. Thus, MOF-supported AuNPs have gained progressive attention since their first report by Fisher and co-workers in 2005.⁴⁰⁴ In Fisher's method, the precursor AuNPs are mixed with MOF-5 and loaded

into MOF-5 both by thermal metal organic chemical vapor deposition (MOCVD) and photo MOCVD. Then Ishida *et al.*⁴⁰⁵ reported a new method for the synthesis of MOF-5-encapsulated AuNPs by solid grinding without organic solvent (Figure 24). Very recently, Xu' group^{406, 407} published the synthesis of ZIF-8-encapsulated AuNPs ($\text{Zn}(\text{MeIM})_2$ MeIM = 2-methylimidazole). The pretreated ZIF-8 is dispersed in a $\text{HAuCl}_4/\text{MeOH}$ solution, and the mixture is pumped for 1-2 h to be mushy, then suitable amounts of MeOH are added into the slurry, and NaBH_4 in MeOH is added under vigorous stirring for the complete reduction of AuCl_4^- . The solid is recovered by filtration and thoroughly washed with MeOH. Very weak diffractions were detected from powder XRD patterns, indicating the formation of small AuNPs that was confirmed by TEM and HADDF-STEM.

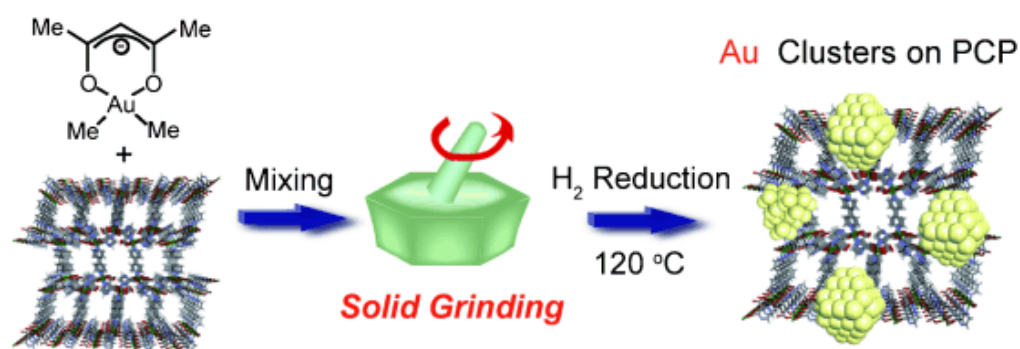


Figure 24. Synthetic procedure of MOF-5-encapsulated AuNPs. (PCP: porous coordination polymer) Reprinted with permission from ref 405 (Haruta's group). Copyright 2008 Wiley-VCH.

5. Bimetallic AuNPs

Au bimetallic NPs are classified in two types of mixing patterns: core@shell NPs and alloy bimetallic NPs. The core@shell NPs consist of a metal shell surrounding a gold core, or gold shell surrounding another metal core. These NPs could be considered as heterogeneous. The alloy bimetallic NPs consists of a homogeneous mixture of gold and another metal in the NP. Many Au bimetallic NPs have been reported with Ag, Pd, Pt, Zn, Cu, ZrO_2 , CdS, Fe_2O_3 , Eu, Ni, and Rh.⁹

5.1. Core@shell NPs

Core@shell heterobimetallic NPs have appeared in the 1970's,^{408,409} and Toshima^{410,411} has synthesized PVP-stabilized Au@Pd and Pd@Au NP catalysts, characterized them by X-ray absorption fine structures and shown that Au@PdNPs were more active than PdNPs for catalytic hydrogenation reactions, due to synergistic electronic effects.⁴¹²⁻⁴¹⁴ The Au- Fe_3O_4 bimetallic NPs are attractive materials for biological and medical areas, due to their theranostic (therapy + diagnostic) properties involving magnetic resonance imaging (MRI) and hyperthermia.^{415, 416}

The Au-core@other metal-shell NPs are generally synthesized by sequential reduction

of appropriate precursors.⁴¹⁷ For example, Crooks's group reported various ways of forming Au-Pd bimetallic NPs in dendrimers. The reduction of metallic precursors is initiated either by the polyol method or by addition of NaBH₄. The co-complexation of dendritic PAMAM interior ligands followed by reduction results in a core@shell structure. For instance, the polyol reduction often results in the formation of Au-core@Pd-shell NPs, because of the difference in the reduction potentials of Au and Pd. The Au^{III} precursor is easier to reduce than various transition metal cations including Pd^{II} and provides a seed for Pd^{II} to be reduced on for the synthesis of Au@Pd NPs. The sizes of the core and shell are controlled by the Au/Pd ratio used during the synthetic procedure. Alternatively, an elegant method used by Crooks is galvanic displacement that involves the redox reaction between a DEN and metal ions of another metal.⁴¹⁷ Recently, Xie et al. reported the synthesis of Au@Pt@Au nano raspberries for catalysis.⁴¹⁸ As shown in Figure 25, the first step is the formation of an Ag shell around the Au core. The conversion from Au@Ag to Au@Pt particles is achieved via the galvanic displacement of Ag by Pt through the addition of hexa-chloroplatinic(IV) acid. Silver is deposited on the Pt surface in a second coating step, again using AgNO₃ and sodium citrate as reducing agent. In the last step of the synthesis, raspberry-like Au@Pt@Au NPs are formed via the concerted action of both reagent reduction and galvanic replacement (*vide infra*). As shown in the SEM image in Figure 25b, this approach leads to the growth of the desired Au protuberances instead of the formation of a complete and smooth Au shell.

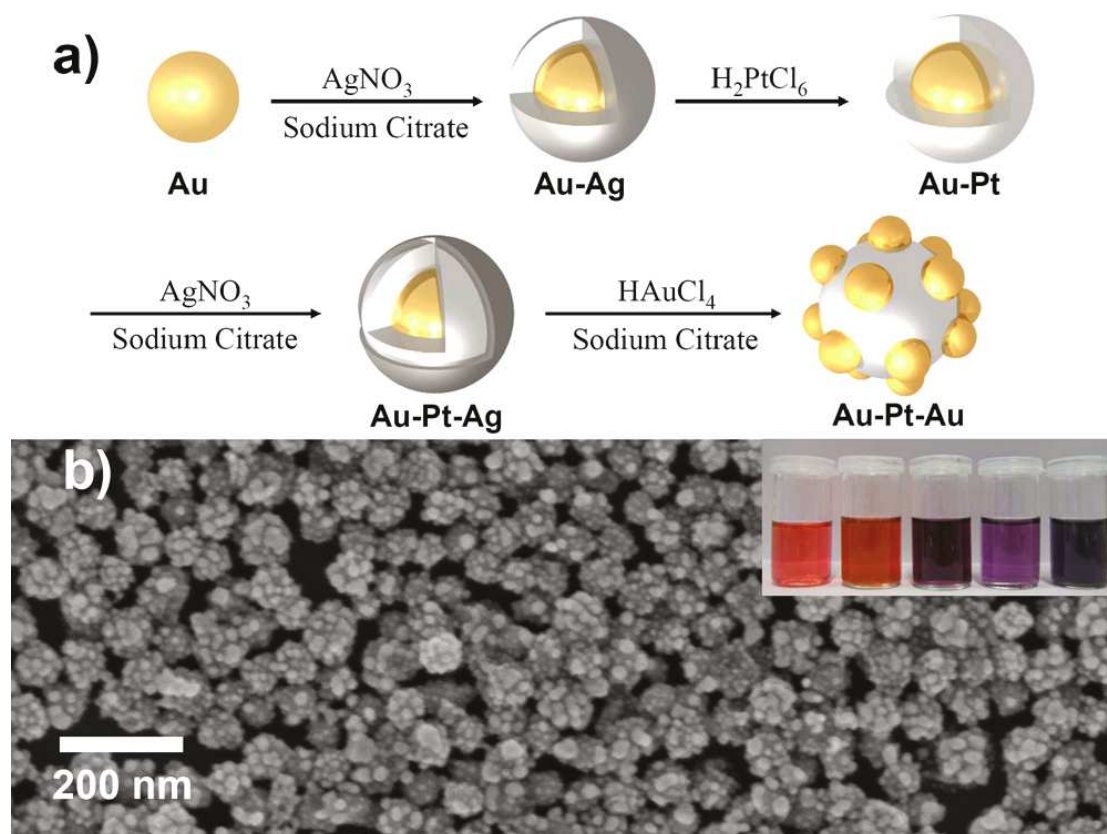


Figure 25. a) Reaction scheme showing morphological and structural changes involved

in the fabrication of Au/Pt/Au core/shell nanoraspberries and b) SEM image of the product Au@Pt@Au. Reprinted with permission from ref 418 (Schlücker's group). Copyright 2011 American Chemical Society.

The other metal-core@Au-shell NPs are usually synthesized by forming the Au shell on the other metal core, i.e. sequential loading and reduction of the metals leads to the choice of core and shell, because the metal that is first introduced forms the core.⁴¹⁷ A variation involves core surface modification with functional groups serving as templates for the nucleation of Au.^{408, 419} For example, small Fe₃O₄ NPs (5-15 nm) were first synthesized by reduction of Fe(acac)₃ by 1,6-hexadecanediol in the presence of the capping agents oleic acid (OA) and oleylamine. Then, the Fe₃O₄ NPs served as seeds for the coating of the Au shell. Oleylamine is a crucial surfactant, providing an amine functional group that coordinates to the Au atoms, which is followed by reduction of Au(CH₃COO)₃ by 1,6-hexadecanediol in the presence of oleylamine. As a result, the HR-TEM confirmed the formation of monodispersed Fe_xO_y@Au NPs with a 5-15 nm core and 0.5-2 nm Au shell thickness.⁴²⁰ Core@shell AuNPs are also known with AuNPs coated with silica shells (§ 4.3.3.1). Murphy *et al.* disclosed silica nanospheres with a nanoscale overcoat of gold ("nanoshells") that have tunable absorption in the visible and NIR regions, which leading to remarkable potential use of these AuNPs in cellular imaging.⁴²¹

5.2. Bimetallic alloy NPs

The bimetallic Au alloy NPs are generally synthesized by simultaneous reduction of appropriate precursors.^{422,423} For instance, Liu and Walker reported a Au-Cu nanocube that was formed by simultaneous reduction of copper(II) acetylacetonate and HAuCl₄ by 1,2-hexadecanediol in diphenyl ether in the presence of 1-adamantanecarboxylic acid, 1-hexadecylamine, and 1-dodecanethiol. The TEM image showed that the as-prepared particles were perfectly cubic in shape and uniform in size, averaging 23 nm, and the EDX spectroscopy line scanning analysis showed a homogeneous distribution of copper and gold across the entire nanocube.⁴²⁴

Recently, Negishi *et al.* synthesized the precise alloy clusters Au_{25-n}Ag_n(SC₁₂H₂₅)₁₈ by reducing various ratios of HAuCl₄/AgNO₃ mixtures and purified them by precipitation in acetonitrile. The structures were confirmed by MALDI and LDI mass spectra.⁴²⁵ Later, Kumara and Dass⁴²⁶ developed this method to obtain the alloy clusters Au_{144-n}Ag_n(SR)₆₀ (SR = SCH₂CH₂Ph, SC₆H₁₃ or SC₁₂H₂₅) by etching of the pre-formed Au/Ag clusters with excess thiol. The optical absorption spectra of the nanoalloy clusters in the UV-vis. region exhibit three distinct features: a "plasmonic" peak around 430 nm (2.9 eV) and two shoulders around 310 (4.0 eV) and 560 nm (2.2 eV). The higher is the n value, the clearer is the appearance of these features (Figure 26).^{426,427}

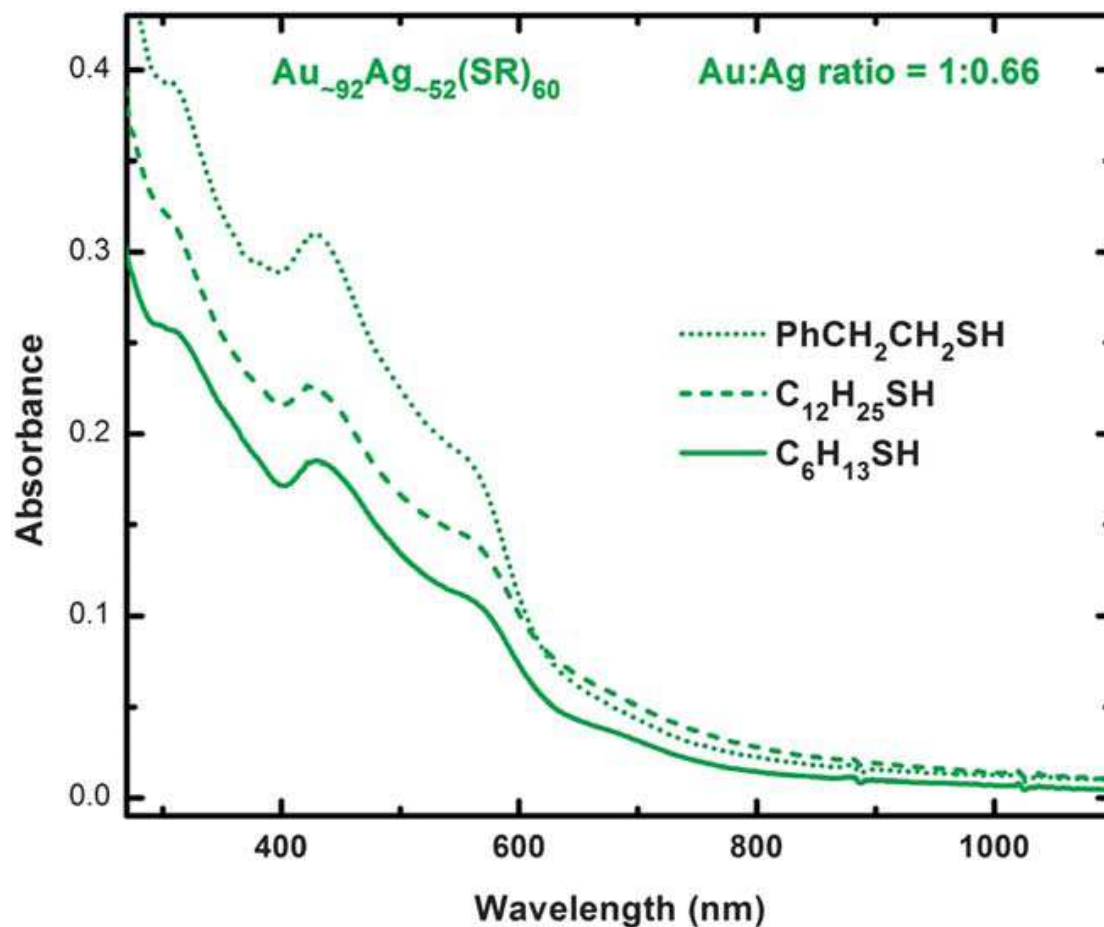


Figure 26. UV-vis. spectra of Au₉₂Ag₅₂(SR)₆₀ clusters for Au / Ag precursor ratio of 1:0.66 with phenylethane thiol (dotted), hexane thiol (dashed), and dodecane thiol (solid). Reprinted with permission from ref 426 (Dass's group). Copyright 2011 Royal Chemical Society.

6. Conclusion and outlook

The preparation of AuNPs that has been known for a very long time has met a considerable amount of variations involving multiple materials from biology to functional molecules and finally the solid state. The engineering of AuNPs has become finely tuned with size and shape control towards targeted applications. The intrinsic lack of toxicity of the AuNP cores and their topological, optical, sensing, catalytic and biomedical properties will obviously lead to a huge expansion of their applications in nanotechnology.⁴²⁸⁻⁴³⁰

In summary, AuNPs with size below 10 nm are easily prepared by the Brust-Schiffrin method or by high-temperature reduction with oxide and other solid supports for catalytic applications with supported AuNPs smaller than 5 nm. In molecular chemistry, thiolate ligands provide robust AuNPs of 1-10 nm size, and direct syntheses, ligand substitution reactions with functional thiols and post functionalizations using for instance olefin metathesis, click reaction and amide bond

formation provide rich means of multiple functionalizations for potential biomedical applications.^{431,432}

AuNPs larger than 2 to 3 nm present the plasmon band resulting from the interaction of light with the collective conducting surface electrons of the AuNPs that is not observed for AuNPs smaller than 2 nm due to the localization of electron in molecular Au cluster bonds. The plasmon band of relatively large AuNPs is thus most useful for various imaging and other optics techniques. Therefore the improved Turkevitch method using citrate Au^{III} reduction is still much in use for the synthesis of such AuNPs in the 10-50 nm-size range that are functionalized with biomolecules, drugs, receptors and imaging agents for diagnostic and therapy applications. The seed-growth method with recent progress, however, is now considered as more precise than the Turkevitch method, because it provides narrower size distributions. For the synthesis of AuNPs larger than 100 nm, the seed-growth method is also specifically efficient. AuNPs with various shapes (rods, cubes, triangles, hexapods, ribbons, hollow cages, branches, polyhedrons) are synthesized using this method by careful controlling of the synthesis conditions.

The technology of solid state-supported AuNPs that started with glass decoration (e. g. the IVth-century Lycurgus cup) continues to fascinate scientists with the remarkable catalytic properties of *inter alia* oxide-supported AuNPs. The latter, pioneered by Haruta 25 years ago, is still expanding using a variety of solids including mesoporous materials, MOFs and heterobimetallic NPs towards promising “green-chemistry” applications.

7. Abbreviations

9-BBN: 9-borabicyclo[3.3.1] nonane

AFM: atomic force microscopy

ATO: sodium bis (2-ethylhexyl) sulfosuccinate

AuNP: gold nanoparticle

AuNR: gold nanorod

CNT: carbon nanotube

CPA: cyclic phenylazomethine

CTAB: cetyltrimethylammonium bromide

DENs: dendrimer encapsulated NPs

DLS: dynamic light scattering

DMAP: 4-(*N,N*-dimethylamino) pyridine

EDX: energy-dispersive X-ray

GMA: glycidyl methacrylate

GUVs: giant unilamellar vesicles

HADDF-STEM: high-angle annular dark-field scanning transmission electron microscopy

HEPES: *N*-2-hydroxyethylpiperazine-*N*-2-ethanesulphonic acid

HR-TEM: high-resolution transmission electron microscopy

LDI: laser desorption ionization

MALDI: matrix-assisted laser desorption ionization

MOCVD: metal organic vapor deposition
MOF: molecular organic framework
MRI: magnetic resonance imaging
NICISS: neutral impact collision ion scattering spectroscopy
NIPM: poly (*N*-isopropylacrylamide)
NIR: near infra red
NP: nanoparticle
PAAPHA: poly (acryloylaminophenylarsonic acid)
PCL: poly (caprolactone)
PEG: poly (ethylene glycol)

PEI: poly (ethylenimine)
PEO: poly (ethylene oxide)
PPO: poly(propylene oxide)
PS: polystyrene
PVCL: poly (*N*-vinyl caprolactam)
PVP: poly (vinyl pyridine)
SDBS: benzenesulfonate
TAOB: tetra (octylammonium) bromide
TEM: transmission electron microscopy
TEG: tetra (ethylene glycol)
THPC: tetrakis(hydroxymethyl) phosphonium chloride
TGA: thermogravimetric analysis
XRD: X-ray diffraction

Acknowledgement

Financial support from the China Scholarship Council (CSC) of the People's Republic of China (Ph. D. grants to Na Li and Pengxiang Zhao), the Université Bordeaux 1, the Centre National de la Recherche Scientifique (CNRS) and the Agence Nationale pour la Recherche (ANR) is gratefully acknowledged.

References

1. L. M. Liz-Marzan, P. V. Kamat. *Nanoscale materials*. Kluwer Academic Publishers, New York, **2003**.
2. V. Rotello (ed). *Nanoparticles. Building block for nanotechnology*, Kluwer Academic Publishers, New York, **2004**.
3. G. Schmid (ed.), *Nanoparticles: from theory to application*, Wiley-VCH, Weinheim, **2006**.
4. F. Caruso. *Colloids and colloid assemblies*, WILEY-VCH, Weinheim, **2004**.
5. C. Burda, X. Chen, R. Narayanan, M. A. El-Sayed, *Chem. Rev.* **2005**, *105*, 1025-1102.
6. X. Chen, S. S. Mao, *Chem. Rev.* **2007**, *107*, 2891-2959.
7. Y. Xia, Y. Xiong, B. Lim, S. E. Skrabalak, *Angew. Chem., Int. Ed.* **2009**, *48*, 60-103.

-
8. M. Faraday, *Philos. Trans.* **1857**, *147*, 145-181.
 9. M.-C. Daniel, D. Astruc, *Chem. Rev.* **2004**, *104*, 293-346.
 10. G. J. Hutchings, M. Brust, H. Schmidbaur, *Chem. Soc. Rev.* **2008**, *37*, 1759-1765.
 11. C. Louis in *Nanoparticles and Catalysis*, (Ed. D. Astruc) Wiley-VCH, Weinheim, **2008**, pp. 507-530.
 12. M. Haruta, M. Date, *Appl. Catal. A* **2001**, *222*, 427- 437.
 13. A. Corma, P. Serna, *Science* **2006**, *313*, 332- 333.
 14. A. S. K. Hashmi, G. J. Hutchings, *Angew. Chem., Int. Ed.* **2006**, *45*, 7896- 7936.
 15. F. Porta, L. Prati, M. Rossi, G. Scari, *J. Catal.* **2002**, *210*, 464- 469.
 16. C. G. Bond, D. T. Thompson, *Gold Bull.* **2000**, *33*, 41.
 17. C. K. Costello, J. H. Yang, H. Y. Law, Y. Wang, J. N. Lin, L. D. Marks, M. D. Kung, H. H. Kung, *Appl. Catal. A* **2003**, *243*, 15-24.
 18. M. S. Chen, D. W. Goodman, *Acc. Chem. Res.* **2006**, *39*, 739-746.
 19. G. C. Bond, C. Louis, D. Thompson, *Catalysis by Gold*, Imperial College Press, London, **2006**.
 20. B. K. Min, C. M. Friend, *Chem. Rev.* **2007**, *107*, 2709-2724.
 21. N. Dimitratos, J. A. Lopez-Sanchez, G. J. Hutchings, *Chem. Sci.* **2012**, *3*, 20-44.
 22. P. K. Jain, I. H. El-Sayed, M. A. El-Sayed, *Nano Today* **2007**, *2*, 18-29.
 23. R. A. Sperling, P. Rivera-Gil, F. Zhang, M. Zanella, W. J. Parak, *Chem. Soc. Rev.* **2008**, *37*, 1896-1908.
 24. M. A. El-Sayed, *Acc. Chem. Res.* **2004**, *37*, 326-333.
 25. A. Schroeder, D. A. Heller, M. M. Winslow, J. E. Dahlman, G. W. Pratt, R. Langer, T. Jacks, D. G. Anderson, *Nat. Rev. Cancer.* **2012**, *12*, 39-50.
 26. K. Saha, S. S. Agasti, C. Kim, X. Li, V. M. Rotello, *Chem. Rev.* **2012**, DOI: 10.1021/cr2001178.
 27. J. L. West, N. J. Halas, *Annu. Rev. Bioeng.* **2003**, *5*, 285-292.
 28. G. C. Schatz, *Proc. Natl. Acad. Sci.* **2007**, *104*, 6885-6892.
 29. R. Elghanian, J. J. Storhoff, R. C. Mucic, R. L. Letsinger, C. A. Mirkin, *Science* **1997**, *277*, 1078-1081.
 30. D. T. Nguyen, D. J. Kim, K. S. Kim, *Micron* **2011**, *42*, 207-227.
 31. H. Parab, C. Jung, M. A. Woo H. G. Park, *J. Nanopart. Res.* **2011**, *13*, 2173-2180.
 32. J. Turkevich, P. C. Stevenson, J. Hillier, *Discuss. Faraday. Soc.* **1951**, *11*, 55-75.
 33. G. Frens, *Nature: Phys. Sci.* **1973**, *241*, 20-22.
 34. J. Kimling, M. Maier, B. Okenve, V. Kotaidis, H. Ballot, A. Plech, *J. Phys. Chem. B* **2006**, *110*, 15700-15707.
 35. B. K. Pong, H. I. Elim, J. X. Chong, W. Ji, B. L. Trout, J. Y. Lee, *J. Phys. Chem. C* **2007**, *111*, 6281-6287.
 36. J. Polte, T. T. Ahner, F. Delissen, S. Sokolov, F. Emmerling, A. F. Thunemann, R. Kraehnert, *J. Am. Chem. Soc.* **2010**, *132*, 1296-1301.
 37. S. Kumar, K. S. Gandhi, R. Kumar, *Ind. Eng. Chem. Res.* **2007**, *46*, 3128-3136.
 38. X. Ji, X. Song, J. Li, Y. Bai, W. Yang, X. Peng, *J. Am. Chem. Soc.* **2007**, *129*, 13939-13948.
 39. C. Li, D. Li, G. Wan, J. Xu, W. Hou, *Nanoscale Res. Lett.* **2011**, *6*, 440.
 40. M. R. Rahman, F. S. Saleh, T. Okajima, T. Ohsaka, *Langmuir* **2011**, *27*,

5126-5135.

41. H. Xia, S. Bai, J. Hartmann, D. Wang, *Langmuir***2010**, *26*, 3585-3589.
42. W. Patungwasa, J. H. Hodak, *Mater. Chem. Phys.***2008**, *108*, 45-54.
43. A. Rohiman, I. Anshori, A. Surawijaya, I. Idris, *AIP Conf. Proc.***2011**, *1415*, 39-42.
44. J. H. Kim, B. W. Lavin, R. D. Burnett, B. W. Boote, *Nanotechnol.***2011**, *22*, article number: 285602.
45. L. M. C. Aguilera, M. F. Romano, M. L. A. Gil, I. N. Rodriguez, J. L. Hidalgo-Hidalgo de Cisneros, J. M. P. Santander, *Untrason. Sonochem.* **2011**, *18*, 789-794.
46. C. H. Su, P. L. Wu, C. S. Yeh, *J. Phy. Chem. B***2003**, *107*, 14240-14243.
47. I. Ojea-Jimenez, F. M. Romero, N. G. Bastus, V. Puentes, *J. Phys. Chem. C***2010**, *114*, 1800-1804.
48. J. W. Slot, H. J. Geuze, *Eur. J. Cell Biol.***1985**, *38*, 87-93.
49. K. R. Brown, A. P. Fox, M. J. Natan, *J. Am. Chem. Soc.* **1996**, *118*, 1154-1157.
50. S. K. Sivaraman, S. Kumar, V. Santhanam, *J. Colloid Interface Sci.***2011**, *361*, 543-547.
51. D. Philip, *Spectrochim. Acta. A: Mol. Biomol. Spectrosc.***2008**, *71*, 80-85.
52. M. Giersig, P. Mulvaney, *Langmuir***1993**, *9*, 3408-3413.
53. M. Brust, M. Walker, D. Bethell, D. J. Schiffrin, R. J. Whyman, *J. Chem. Soc., Chem. Commun.***1994**, 801-802.
54. M. J. Hostetler, S. J. Green, J. J. Stockes, R. W. Murray, *J. Am. Chem. Soc.* **1996**, *118*, 4212-4213.
55. A. C. Templeton, W. P. Wuelfing, R. W. Murray, *Acc. Chem. Res.***2000**, *33*, 27-36
56. O. Zaluzhna, Y. Li, C. Zangmeister, T. C. Alison, Y. J. Tong, *Chem. Commun.*, **2012**, *48*, 362-364.
57. F. Vitale, I. Fratoddi, C. Battocchio, E. Piscopiello, L. Tapfer, M. V. Russo, G. Polzonetti, C. Giannini, *Nanoscale Res. Lett.***2011**, *6*, 103.
58. H. Häkkinen, B. Yoon, U. Landman, X. Li, H.-J. Zhai, L.-S. Wang, *J. Phys. Chem. A***2003**, *107*, 6168-6175.
59. J. Akola, M. Walter, R. L. Whetten, H. Häkkinen, H. Grönbeck, *J. Am. Chem. Soc.* **2008**, *130*, 3756-3757.
60. O. Toikkanen, V. Ruiz, G. Ronnholm, N. Kalkkinen, P. Liljeroth, B. M. Quinn, *J. Am. Chem. Soc.***2008**, *132*, 11049-11055.
61. V. J. Gandubert, R. B. Lennox, *Langmuir***2005**, *21*, 6532-6539.
62. P. J. G. Goulet, R. B. Lennox, *J. Am. Chem. Soc.***2010**, *132*, 9582-9584.
63. J. F. Parker, C. A. Fields-Zinna, R. W. Murray, *Acc. Chem. Res.* **2010**, *43*, 1289-1296.
64. M. Brust, J. Fink, D. Bethell, D. J. Schiffrin, C. J. Kiely, *J. Chem. Soc., Chem. Commun.***1995**, 1655-1656.
65. S. Chen, *Langmuir***1999**, *15*, 7551-7557.
66. S. Chen, R. W. Murray, *Langmuir***1999**, *15*, 682-689.
67. R. S. Ingram, M. J. Hostetler, R. W. Murray, *J. Am. Chem. Soc.***1997**, *119*, 9175-9178.

-
68. A. G. Kanaras, F. S. Kamounah, K. Schaumburg, C. J. Kiely, M. Brust, *Chem. Commun.* **2002**, 20, 2294-2295.
69. B. Duncan, C. Kim, V. M. Rotello, *J. Control. Release* **2010**, 148, 122-127.
70. E. Glogowski, R. Tangirala, H. Jinbo, T.P. Russell, T. Emrick, *Nano Lett.* **2007**, 7, 389-393.
71. C. Miesch, I. Kosif, E. Lee, J. K. Kim, T. P. Russell, R. C. Hayward, T. Emrick, *Angew. Chem., Int. Ed.* **2011**, 51, 145-149.
72. M. Zheng, Z. Li, X. Huang, *Langmuir* **2004**, 20, 4226-4235.
73. Y. Hao, X. Yang, S. Song, M. Huang, C. He, M. Cui, J. Chen, *Nanotechnol.* **2012**, 23, no. 045103.
74. R. Sardar, J. S. Shumaker-Parry, *Chem. Mater.* **2009**, 21, 1167-1169.
75. G. Chen, M. Takezawa, N. Kawazoe, T. Tateishi, *Open Biotechnol. J.* **2008**, 2, 152-156.
76. A. J. Di-Pasqua, R. E. Mishler, Y. L. Ship, J. C. Davrowiak, T. Asefa, *Mater. Lett.* **2009**, 63, 1876-1879.
77. A. F. G. Leontowich, C. F. Calver, M. Dasog, R. W. J. Scott, *Langmuir* **2010**, 26, 1285-1290.
78. M. Busby, C. Chiorboli, F. Scandola, *J. Phys. Chem. B* **2006**, 110, 6020-6026.
79. R. K. Gupta, M. P. Srinivasan, R. Dharmarajan, *Colloid. Surface. A* **2011**, 390, 149-156.
80. E. R. Zubarev, J. Xu, A. Sayyad, J. D. Gibson, *J. Am. Chem. Soc.* **2006**, 128, 4958-4959.
81. R. M. Pattabi, M. Pattabi, *Spectrochim. Acta. A* **2009**, 74, 195-199.
82. C. J. Ackerson, P. D. Jadzinsky, J. Z. Sexton, D. A. Bushnell, R. D. Kornberg, *Bioconjug. Chem.* **2010**, 21, 214-218.
83. C. I. Müller, C. Lambert, *Langmuir* **2011**, 27, 5029-5039.
84. D. T. Miles, R. W. Murray, *Anal. Chem.* **2003**, 75, 1251-1257.
85. B. M. Quinn, P. Liljeroth, V. Ruiz, T. Laaksonen, K. Kontturi, *J. Am. Chem. Soc.* **2003**, 125, 6644-6645.
86. R. L. Donkers, D. Lee, R. W. Murray, *Langmuir* **2004**, 20, 1945-1952.
87. J. B. Tracy, G. Kalyuzhny, M. C. Crowe, R. Balasubramanian, J.-P. Choi, R. W. Murray, *J. Am. Chem. Soc.* **2007**, 129, 6706-6707.
88. S. F. Sweeney, G. H. Woehrle, J. E. Hutchison, *J. Am. Chem. Soc.* **2006**, 128, 3190-3197.
89. Y. L. Kalisman, P. D. Jadzinsky, N. Kalisman, H. Tsunoyama, T. Tsukuda, D. A. Bushnell, R. D. Kornberg, *J. Am. Chem. Soc.* **2011**, 133, 2976-2982.
90. P. D. Jadzinsky, G. Calero, C. J. Ackerson, D. A. Bushnell, R. D. Kornberg, *Science* **2007**, 318, 430-433.
91. D. V. Leff, P. C. Ohara, J. R. Heath, W. M. Gelbart, *J. Phys. Chem.* **1995**, 99, 7036-7041.
92. P. Zhao, M. Grillaud, L. Salmon, J. Ruiz, D. Astruc, *Adv. Synth. Catal.* **2012** DOI: 10.1002/adsc.201100865.
93. R. H. Terrill, T. A. Postlethwaite, C. H. Chen, C. D. Poon, A. Terzis, A. Chen, J. E. Hutchison, M. R. Clark, G. Wignall, J. D. Londono, R. Superfine, M. Falvo, C. S.

-
- Johnson Jr., E. T. Samulski, R.W. Murray, *J. Am. Chem. Soc.* **1995**, *117*, 12537-12548.
94. A. Labande, J. Ruiz, D. Astruc, *J. Am. Chem. Soc.* **2002**, *124*, 1782-1789.
95. L. A. Jr. Porter, D. Ji, S. L. Westcott, M. Graupe, R. S. Czernuzewicz, N. J. Halas, T. R. Lee, *Langmuir* **1998**, *14*, 7378-7386.
96. T. Yonezawa, K. Yasui, N. Kinizuka, *Langmuir* **2001**, *17*, 271-273.
97. E. Oh, K. Susumu, R. Goswami, H. Mattoussi, *Langmuir* **2010**, *26*, 7604-7613.
98. A. Manna, P. Chen, H. Akiyama, T. Wei, K. Tamada, W. Knoll, *Chem. Mater.* **2003**, *15*, 20-28.
99. Y. Li, O. Zaluzhna, Y. Tong, *Chem. Commun.* **2011**, *47*, 6033-6035.
100. Z. Tang, B. Xu, B. Wu, M. W. Germann, G. Wang, *J. Am. Chem. Soc.* **2010**, *132*, 3367-3374.
101. O. Tzhayik, P. Sawant, S. Efrima, E. Kovalev, J. T. Klug, *Langmuir* **2002**, *18*, 3364-3369.
102. S. Zhang, G. Leem, T. R. Lee, *Langmuir* **2009**, *25*, 13855-33860.
103. M. S. Vickers, J. Cookson, P. D. Beer, P. T. Bishop, B. Thiebaut, *J. Mater. Chem.* **2006**, *16*, 209-215.
104. Y. Tan, Y. Li, D. Zhu, *Langmuir* **2002**, *18*, 3392-3395.
105. S. Wang, K. Qian, X. Bi, W. Huang, *J. Phys. Chem. C* **2009**, *113*, 6505-6510.
106. A. A. Volkert, V. Subramaniam, M. R. Ivanov, A. M. Goodman, A. J. Haes, *ACS Nano* **2011**, *5*, 4570-4580.
107. Y. Kang, D. J. Won, S. R. Kim, K. Seo, H. S. Choi, G. Lee, Z. Noh, T. S. Lee, C. Lee, *Mater. Sci. Eng. C* **2004**, *24*, 43-46.
108. M. I. Bethencourt, L. Srisombat, P. Chinwangso, T. R. Lee, *Langmuir* **2009**, *25*, 1265-1271.
109. E. J. Shelley, D. Ryan, S. R. Johnson, M. Couillard, D. Fitzmaurice, P. D. Nellist, Y. Chen, R. E. Palmer, J. A. Preece, *Langmuir* **2002**, *18*, 1791-1795.
110. M. Liz-Marzan, M. Giersig, P. Mulvaney, *Langmuir* **1996**, *12*, 4329-4335.
111. D. A. Giljohann, D. S. Seferos, W. L. Daniel, M. D. Massich, P. C. Patel, C. A. Mirkin, *Angew. Chem., Int. Ed.* **2010**, *49*, 3280-3294.
112. D. K. Kim, S. J. Park, J. H. Lee, Y. Y. Jeong, S. Y. Jon, *J. Am. Chem. Soc.* **2007**, *129*, 7661-7665.
113. M.-C. Daniel, M. E. Grow, H. Pan, M. Bednarek, W. E. Ghann, K. Zabetakis, J. Cornish, *New J. Chem.* **2011**, *35*, 2366-2374.
114. R. K. Gupta, M. P. Srinivasan, R. Dharmarajan, *Mater. Lett.* **2012**, *67*, 315-319.
115. A. C. Templeton, M. J. Hostetler, C. T. Kraft, R. W. Murray, *J. Am. Chem. Soc.* **1998**, *120*, 1906-1911.
116. M. J. Hostetler, A. C. Templeton, R. W. Murray, *Langmuir* **1999**, *15*, 3782-3789.
117. Y. S. Shon, H. Choo, *C. R. Chime* **2003**, *6*, 1009-1018.
118. A. Labande, D. Astruc, *Chem. Commun.* **2000**, 1007-1008.
119. D. Baranov, E. N. Kadnikova, *J. Mater. Chem.* **2011**, *21*, 6152-6157.
120. Y. Zhou, S. Wang, K. Zhang, X. Jiang, *Angew. Chem., Int. Ed.* **2008**, *47*, 1-5.
121. J. L. Brennan, N. S. Hatzakis, T. R. Tshikhudo, N. Dirvianskyte, V. Razumas, S. Patkar, J. Vind, A. Svendsen, R. J. M. Nolte, A. E. Rowan, M. Brust, *Bioconj.*

-
- Chem.***2006**,*17*, 1373-1375.
122. E. Boisselier, L. Salmon, J. Ruiz, D. Astruc, *Chem. Commun.* **2008**, 5788-5790.
 123. D. A. Fleming, C. J. Thode, M. E. Williams, *Chem. Mater.* **2006**,*18*, 2327-2334.
 124. A. François, A. Laroche, N. Pinaud, L. Salmon, J. Ruiz, J. Robert, D. Astruc, *ChemMedChem* **2011**, *6*, 2003-2008.
 125. A. W. Shaffer, J. G. Worden, Q. Huo, *Langmuir* **2004**, *20*, 8343-8351.
 126. J. Bresee, K. E. Maier, C. Melander, D. L. Feldheim, *Chem. Commun.* **2010**,*46*, 7516-7518.
 127. J. Milette, V. Toader, L. Reven, R. B. Lennox, *J. Mater. Chem.***2011**, *21*, 9043-9050.
 128. S. Rucareanu, M. MacCarini, L. J. Shepherd, R. B. Lennox, *J. Mater. Chem.* **2008**, *18*, 5830-5834.
 129. S. Rucareanu, V. J. Gandubert, R. B. Lennox, *Chem. Mater.***2006**, *18*, 4674-4680.
 130. Y. S. Shon, H. Choo, *Chem Commun.* **2002**, 2560-2561.
 131. F. P. Zamborini, S. M. Gross, R. W. Murray, *Langmuir***2001**,*17*, 481-488.
 132. J. Raula, J. Shan, M. Nuopponen, A. Nishanen, H. Jiang, E. Kauppinen, H. Tenhu, *Langmuir***2003**, *19*, 3499-3504.
 133. L. Liang, D. Astruc, *Coord. Chem. Rev.***2011**, *255*, 2933-2945.
 134. D. Astruc, E. Boisselier, C. Ornelas, *Chem. Rev.***2010**, *110*, 1857-1959.
 135. A. Shakeri-Zadeh, M. Ghasemifard, G. A. Mansoori, *Phys. E: Low-dim. Sys. Nanostr.***2010**, *42*, 1272-1280.
 136. P. Zhao, D. Astruc, *ChemMedChem***2012**DOI: 10.1002/cmdc.201200052.
 137. R. D. Felice, A. J. Selloni, *J. Chem. Phys.***2004**, *120*,4906-4914.
 138. P. M. Shem, R. Sardar, J. S. Shumaker-Parry, *Langmuir***2009**, *25*, 13279-13283.
 139. R. W. Burgess, V. J. Keast, *J. Phys. Chem. C***2011**, *115*, 21016-21021.
 140. J. Ramirez, M. Sanau, E. Fernandez, *Angew. Chem., Int. Ed.* **2008**, *47*, 5194-5197.
 141. A. Fürstner, L. Morency, *Angew. Chem., Int. Ed.* **2008**, *47*, 5030-5033.
 142. M. Walter, J. Akola, O. Lopez-Acevedo, P. D. Jadzinsky, G. Calero, C. J. Ackerson, R. L. Whetten, H. Gronbeck, H. Häkkinen, *PNAS* **2008**, *105*, 9157-9162.
 143. J. F. Hainfield, *Science* **1987**, *236*, 450-453.
 144. C. J. Ackerson, P. D. Jadzinsky, G. J. Jensen, R. D. Kornberg, *J. Am. Chem. Soc.* **2006**, *128*, 2635-2640.
 145. G. Schmid, U. Simon, *Chem. Commun.* **2005**, 697-710.
 146. P. D. Jadzinsky, G. Calero, C. J. Ackerson, D. A. Bushnell, R. D. Kornberg, *Science***2007**, *318*, 430-433.
 147. M. H. Heaven, A. Dass, P. S. White, K. M. Holt, R. W. Murray, *J. Am. Chem. Soc.***2008**,*130*, 3754-3755.
 148. P. Gruene, D. M. Rayner, B. Redlich, Van der Meer, A. F. G., J. T. Lyon, G. Meijer, A. Fielicke, *Science***2008**, *321*, 674-676.
 149. M. Zhu, C. M. Aikens, F. J. Hollander, G. C. Schatz, R. Jin, *J. Am. Chem. Soc.* **2008**, *130*, 5883-5885.

-
150. S. W. Chen, R. S. Ingram, M. J. Hostetler, J. J. Pietron, R. W. Murray, T. G. Schaaff, J. T. Khoury, M. M. Alvarez, R. L. Whetten, *Science***1998**, *280*, 2098-2101.
 151. D. Boyer, P. Tamarat, A. Maali, B. Lounis, M. Orrit, *Science***2002**, *297*, 1160-1163.
 152. N. Zheng, J. Fan, G. D. Stucky, *J. Am. Chem. Soc.***2006**, *128*, 6550-6551.
 153. W. W. Weare, S. M. Reed, M. G. Warner, J. E. Hutchison, *J. Am. Chem. Soc.* **2000**, *122*, 12890-12891.
 154. G. Schmid, R. Pfeil, R. Boese, F. Bandermann, S. Meyer, G. H. M. Calis, J. W. A. van der Velden, *Chem. Ber.***1981**, *114*, 3634-3642.
 155. J. M. Pettibone, J. W. Hudgens, *ACS Nano* **2011**, *5*, 2989-3002.
 156. N. De-Silva, J. M. Ha, A. Solovyov, M. M. Nigra, I. Ogino, S. W. Yeh, K. A. Durkin, A. Katz, *Nat. Chem.***2010**, *2*, 1062-1068.
 157. J. M. Ha, A. Solovyov, A. Katz, *Langmuir***2009**, *25*, 10548-10553.
 158. C. Gautier, R. Taras, S. Gladiali, T. Burgi, *Chirality***2008**,*20*, 486-493.
 159. T. Pham, J. B. Jackson, N. J. Halas, T. R. Lee, *Langmuir***2002**,*18*, 4915-4920.
 160. C. Xu, L. Sun, L. J. Kepley, R. M. Crooks, *Anal. Chem.* **1993**, *65*, 2102-2107.
 161. A. Kumar, S. Mandal, P. R. Selvakannan, R. Paricha, A. B. Mandale, M. Sastry, *Langmuir***2003**, *19*, 6277-6282.
 162. F. Porta, Z. Krpetic, L. Prati, A. Gaiassi, G. Scari, *Langmuir***2008**, *24*, 7061-7065.
 163. N. Wangoo, K. K. Bhasin, R. Boro, C. R. Suri, *Anal. Chim. Acta.***2008**, *610*, 142-148.
 164. N. Wangoo, K. K. Bhasin, S. K. Mehta, C. R. Suri, *J. Colloid Interf. Sci.***2008**, *323*, 247-254.
 165. R. Shomura, K. J. Chung, H. Iwai, M. Higuchi, *Langmuir***2011**,*27*, 7972-7975.
 166. N. Wangoo, K. J. Kaushal, K. Bhasin, S. K. Mehta, C. R. Suri, *Chem. Commun.***2006**, *46*, 5755-5757.
 167. F. Griffin, D. Fitzmaurice, *Langmuir***2007**,*23*, 10262-10271.
 168. D. I. Gittins, F. Caruso, *Angew. Chem., Int. Ed.***2001**, *40*, 3001-3004.
 169. A. Yu, Z. Liang, J. Cho, F. Caruso, *Nano Lett.***2003**, *3*, 1203-1207.
 170. V. J. Gandubert, R. B. Lennox, *Langmuir* **2005**, *21*, 6532-6539.
 171. B. C. Barlow, I. J. Burgess, *Langmuir* **2007**, *23*, 1555-1563.
 172. H. Lange, J. Maultzsch, W. Meng, D. Mollenhauer, B. Paulus, N. Peica, S. Schlecht, C. Thomsen, *Langmuir***2011**, *27*, 7258-7264.
 173. M. A. Raj, S. B. Revin, S. A. John, *Colloid. Surf. B***2011**, *87*, 353-360.
 174. G. Li, D. Li, L. Zhang, J. Zhai, E. Wang, *Chem. Eur. J.* **2009**, *15*, 9868-9873.
 175. M. S. Yavuz, W. Li, Y. Xia, *Chem. Eur. J.* **2009**, *15*, 13181-13187.
 176. B. Kumar-Jean, C. R. Raj, *Langmuir* **2007**, *23*, 4064-4070.
 177. N. T. K. Thanh, L. A. W. Green, *Nano Today* **2010**, *5*, 213-230.
 178. J. Shan, H. Tenhu, *Chem. Commun.* **2007**, 4580-4598.
 179. H. H. Helcher, *Aurum Postabile oder Gold Tinstur*, J. Herbord Klossen: Breslau, Leipzig, **1718**.
 180. Z. Tuzar, P. Kratochvil, *Surface and Colloid Science*, Plenum Press: New York,

-
- 1993, pp. 1-83
181. R. Shenhar, T. B. Norsten, V. M. Rotello, *Adv. Mater.* **2005**, *17*, 657-669.
 182. T. Sun, G. Qing, *Adv. Mater.* **2011**, *23*, H57-H77.
 183. *Adv. Polym. Sci.* **2006**, *198* (Ed. R. Jordan).
 184. A. Kotal, T. K. Mandal, D. R. Walt, *J. Polym. Sci.:Part A: Polym. Chem.* **2005**, *43*, 3631-3642.
 185. T. K. Mandal, M. S. Fleming, D. R. Walt, *Nano Lett.* **2002**, *2*, 3-7.
 186. D. J. Kim, S. M. Kang, B. Kong, W.-J. Kim, H.-J. Paik, H. Choi, I. S. Choi, *Macromol. Chem. Phys.* **2005**, *206*, 1941-1946.
 187. D. Li, Q. He, Y. Cui, K. Wang, X. Zhang, J. Li, *Chem. Eur. J.* **2007**, *13*, 2224-2229.
 188. D. Li, Q. He, Y. Cui, J. Li, *Chem. Mater.* **2007**, *19*, 412-417.
 189. C. Kruger, S. Agarwal, A. Greiner, *J. Am. Chem. Soc.* **2008**, *130*, 2710-2711.
 190. A. M. Alkilany, P. K. Nagaria, M. D. Wyatt, C. J. Murphy, *Langmuir* **2010**, *26*, 9328-9333.
 191. M. K. Corbierre, N. S. Cameron, R. B. Lennox, *Langmuir* **2004**, *20*, 2867-2873.
 192. S. K. Bae, S. Y. Lee, S. C. Hong, *React. Funct. Polym.* **2011**, *71*, 187-194.
 193. A. Buonerba, C. Cuomo, S. O. Sanchez, P. Canton, A. Grassi, *Chem. Eur. J.* **2012**, *18*, 709-715.
 194. C. Gentilini, F. Evangelista, P. Rudolf, P. Franchi, M. Lucarini, L. Pasquato, *J. Am. Chem. Soc.* **2008**, *130*, 15678-15682.
 195. C. A. Fustin, C. Colard, M. Filali, P. Guillet, A. S. Duwez, M. A. R. Meier, U. S. Schubert, J. F. Gohy, *Langmuir* **2006**, *22*, 6690-6695.
 196. J. Shan, M. Nupponen, H. Jiang, T. Viitala, E. Kauppinen, K. Kontturi, H. Tenhu, *Macromol.* **2005**, *38*, 2918-2926.
 197. J. J. Chiu, B. J. Kim, E. J. Kramer, D. J. Pine, *J. Am. Chem. Soc.* **2005**, *127*, 5036-5037.
 198. N. Higashi, J. Kawahara, M. Niwa, *J. Colloid Interf. Sci.* **2005**, *288*, 83-87.
 199. J. G. Serrano, U. Pal, A. M. Herrera, P. Salas, C. A. Chavez, *Chem. Mater.* **2008**, *20*, 5146-5153.
 200. X. Huang, B. Li, H. Zhang, I. Hussain, L. Liang, B. Tan, *Nanoscale* **2011**, *3*, 1600-1607.
 201. I. Biondi, G. Laurencay, P. J. Dyson, *Inorg. Chem.* **2011**, *50*, 8038-8045.
 202. M. Beija, J. D. Marty, M. Destarac, *Chem. Commun.* **2011**, *47*, 2826-2828.
 203. I. Hussain, S. Graham, Z. Wang, B. Tan, D. C. Sherrington, S. P. Rannard, A. I. Cooper, M. Brust, *J. Am. Chem. Soc.* **2005**, *127*, 16398-16399.
 204. D. Suzuki, H. Kawaguchi, *Langmuir* **2005**, *21*, 8175-8179.
 205. T. Azzam, L. Bronstein, A. Eisenberg, *Langmuir* **2008**, *24*, 6521-6529.
 206. C. D. Gasselin, M. Capelot, N. Sanson, N. Lequeux, *Langmuir* **2010**, *26*, 12321-12329.
 207. D. Miyamoto, M. Oishi, K. Kojima, K. Yoshimoto, Y. Nagasaki, *Langmuir* **2008**, *24*, 5010-5017.
 208. N. S. Jeong, K. Brebis, L. E. Daniel, R. K. O'Reilly, M. I. Gibson, *Chem. Commun.* **2011**, *47*, 11627-11629.

-
209. G. R. Newkome, C. N. Moorefield, F. Vögtle, *Dendrimers and dendrons: concepts, synthesis, applications*, VCH: Weinheim, Germany, **2001**.
210. J. M. J. Fréchet and D. A. Tomalia, *Dendrimers and other dendritic polymers*, John Wiley and Sons, New York, **2002**.
211. K. Esumi, K. Miyamoto, T. Yoshimura, *J. Colloid Interf. Sci.***2002**, *254*, 402-405.
212. K. Esumi, H. Houdatsu, T. Yoshimura, *Langmuir***2004**, *20*, 2536-2538.
213. D. Astruc, F. Lu, J. Ruiz, *Angew. Chem., Int. Ed.***2005**, *44*, 7852-7872.
214. T. Endo, T. Yoshimura, K. Esumi, *J. Colloid. Interf. Sci.* **2005**, *286*, 602-609.
215. N. Krasteva, I. Besnard, B. Guse, R. E. Bauer, K. Müllen, A. Yasuda, T. Vossmeier, *Nano Lett.***2002**, *2*,551-555.
216. J. A. He, R. Valluzzi, K. Yang, T. Dolukhanyan, C. Sung, J. Kumar, S. K. Tripathy, *Chem. Mater.* **1999**, *11*, 3268-3274.
217. J. Won, K. J. Ihn, Y. S. Kang, *Langmuir***2002**, *18*, 8246-8249.
218. D. F. Yancey, E. V. Carino, R. M. Crooks, *J. Am. Chem. Soc.***2010**, *132*, 10988-10989.
219. C. Ornelas, D. Méry, E. Cloutet, J. Ruiz, D. Astruc, *J. Am. Chem. Soc.* **2008**, *130*, 1495-1506.
220. D. Astruc, *Nat. Chem.* **2012**,*4*, 255-267.
221. A. Labande, J. Ruiz, D. Astruc, *J. Am. Chem. Soc.***2002**, *124*, 1728-1735.
222. M. C. Daniel, J. Ruiz, S. Nlate, J. C. Blais, D. Astruc, *J. Am. Chem. Soc.***2003**,*125*, 2617-2628.
223. D. Astruc, M. C. Daniel, J. Ruiz, *Chem. Commun.* **2004**, 2637-2649.
224. J. Ruiz, C. Belin, D. Astruc, *Chem. Commun.***2007**, 3456-3458.
225. D. Astruc. *Electron transfer and radical processes in transition metal chemistry*. VCH, New York, 1995. Chap. 3.
226. L. Balogh, R. Valluzzi, K. S. Laverdure, S. P. Gido, G. L. Hagnauer, D. A. Tomalia, *J. Nanopart. Res.* **1999**, *1*, 353-368.
227. M. E. Garcia, L. A. Baker, R. M. Crooks, *Anal. Chem.* **1999**,*71*, 256-258.
228. V. Chechik, R. M. Crooks, *Langmuir* **1999**, *15*, 6364-6369.
229. A. Manna, T. Imae, K. Aoi, M. Okada, T. Yogo, *Chem. Mater.* **2001**, *13*, 1674-1681.
230. X. Sun, X. Jiang, S. Dong, E. Wang, *Macromol. Rapid Commun.***2003**, *24*, 1024-1028.
231. Y. G. Kim, S. K. Oh, R. M. Crooks, *Chem. Mater.***2004**, *16*, 167-172.
232. C. S. Love, V. Chechik, D. K. Smith, C. Brennan, *J. Mater. Chem.* **2004**, *14*, 919-923.
233. L. W. Hoffman, G. G. Andersson, A. Sharma, S. R. Clarke, N. H. Voelcker, *Langmuir* **2011**, *27*, 6759-6767.
234. M. C. Daniel, J. Ruiz, J. Nlate, J. Palumbo, J. C. Blais, D. Astruc, *Chem. Commun.***2001**, 2000-2001.
235. M. C. Daniel, J. Ruiz, S. Nlate, J. C. Blais, D. Astruc, *J. Am. Chem. Soc.***2003**, *125*, 2617-2628.
236. D. Astruc, L. Liang, A. Rapakousiou, J. Ruiz, *Acc. Chem. Res.* **2012**, DOI:

10.1021/ar200235m

237. R. Wang, J. Yang, Z. Zheng, M. D. Carducci, J. Jiao, S. Seraphin, *Angew. Chem., Int. Ed.* **2001**, *40*, 549-552.
238. M. K. Kim, Y. M. Jeon, W. S. Jeon, H. J. Kim, S. G. Hong, C. G. Park, K. Kim, *Chem. Commun.* **2001**, 667-668.
239. K. R. Gopidas, J. K. Whitesell, M. A. Fox, *J. Am. Chem. Soc.* **2003**, *125*, 6491-6502.
240. A. Taubert, U. M. Wiesler, K. Müllen, *J. Mater. Chem.* **2003**, *13*, 1090-1093.
241. M. R. Knecht, J. C. M. Garcia, R. M. Crooks, *Langmuir* **2005**, *21*, 11981-11986.
242. S. Deng, T. M. Fulghum, G. Krueger, D. Parron, J. Y. Park, R. C. Advincula, *Chem. Eur. J.* **2011**, *17*, 8929-8940.
243. J. P. Hermes, F. Sander, T. Peterle, R. Urbani, T. Pfohl, D. Thompson, M. Mayor, *Chem. Eur. J.* **2011**, *17*, 13473-13481.
244. T. J. Cho, R. A. Zangmeister, R. I. Mac-Cuspie, A. K. Patri, V. A. Hackley, *Chem. Mater.* **2011**, *23*, 2665-2676.
245. C. Bao, M. Jin, R. Lu, T. Zhang, Y. Y. Zhao, *Mater. Chem. Phys.* **2003**, *81*, 160-165.
246. H. Namazi, A. M. P. Fard, *Mater. Chem. Phys.* **2011**, *129*, 189-194.
247. G. Jiang, L. Wang, T. Chen, H. Yu, C. Chen, *Mater. Chem. Phys.* **2006**, *98*, 76-82.
248. E. Murugan, R. Rangasamy, *J. Poly. Sci. A: Poly. Chem.* **2010**, *48*, 2525-2532.
249. E. Boisselier, A. K. Diallo, L. Salmon, J. Ruiz, D. Astruc, *Chem. Commun.* **2008**, *39*, 4819-4821.
250. E. Boisselier, A. K. Diallo, L. Salmon, C. Ornelas, D. Astruc, *J. Am. Chem. Soc.* **2010**, *132*, 2729-2742.
251. L. Jia, L. P. Lv, J. P. Xu, J. Ji, *J. Nanopart. Res.* **2011**, *13*, 4075-4083.
252. Y. Chaikin, H. Leader, R. Popovitz-Biro, A. Vaskevich, I. Rubinstein, *Langmuir* **2011**, *27*, 1298-1307.
253. S. S. Nair, S. A. John, T. Sagara, *Electrochim. Acta.* **2009**, *54*, 6837-6843.
254. M. Wanunu, R. Popovita-Biro, H. Cohen, A. Vaskevich, I. Rubinstein, *J. Am. Chem. Soc.* **2005**, *127*, 9207-9215.
255. M. Brust, R. Etchenique, E. J. Calvo, G. J. Gordillo, *Chem. Commun.* **1996**, 1949-1950.
256. J. A. Edgar, A. M. McDonaph, M. B. Cortie, *ACS Nano* **2012**, *6*, 1116-1125.
257. B. Nikoobakht, M. A. El-Sayed, *Langmuir* **2001**, *17*, 6368-6374.
258. A. Swami, A. Kumar, M. Sastry, *Langmuir* **2003**, *19*, 1168-1172.
259. K. T. Yong, M. T. Swihart, H. Ding, P. N. Prasad, *Plasmonics* **2009**, *4*, 79-93.
260. S. Pyrpassopoulos, D. Niarchos, G. Nounesis, N. Boukos, I. Zafiropuolou, V. Tzitzios, *Nanotechnol.* **2007**, *18*, number: 485604.
261. S. Y. Moon, T. Kusunose, T. Sekino, *Mater. Lett.* **2009**, *63*, 2038-2040.
262. M. Wu, D. Chen, T. Huang, *Langmuir* **2001**, *17*, 3877-3883.
263. M. P. Pileni, *J. Phys. Chem.* **1993**, *97*, 6961-6973.
264. P. L. Luisi, M. Giomini, M. P. Pileni, B. H. Robinson, *Biochem. Biophys. Acta* **1988**, *947*, 209-246.

-
265. C. J. Murphy, T. K. Sau, A. Gole, C. J. Orendorff, *MRS Bulletin***2005**, *30*, 349-355.
266. F. Aliotta, V. Arcoletto, S. Buccoler, G. L. Manna, V. T. Liver, *Thermochim. Acta.* **1995**,*265*, 15-23.
267. C. L. Chiang, *J. Colloid Interf. Sci.***2000**, *230*, 60-66.
268. A. P. Herrera, O. Resto, J. G. Briano, C. Rinaldi, *Nanotechnol.***2005**, *16*, S618-S625.
269. P. Calandra, C. Giordano, A. Longo, V. T. Liveri, *Mater. Chem. Phys.* **2006**, *98*, 494-499.
270. B. Abecassis, F. Testard, T. Zemb, *Soft Matter***2009**, *5*, 974-978.
271. M. Takahashi, S. Ohno, N. Fujita, T. Sengoku, H. Yoda, *J. Colloid Interf. Sci.* **2011**, *356*, 536-542.
272. M. J. Hollamby, J. Eastoe, A. Chemelli, O. Glatter, S. Rogers R. K. Heenan, I. Grillo, *Langmuir***2010**, *26*, 6989-6994.
273. G. Riess, *Prog. Polym. Sci.* **2003**, *28*, 1107-1170.
274. J. Spatz, S. Mößmer, M. Möller, *Chem. Eur. J.* **1996**, *2*, 1552-1555.
275. J. Spatz, S. Mößmer, M. Möller, M. Kocher, D. Neher, G. Wegner, *Adv. Mater.* **1998**, *10*, 473-475.
276. T. F. Jaramillo, S. H. Baeck, B. R. Cuenya, E. W. McFarland, *J. Am. Chem. Soc.* **2003**, *125*, 7148-7149.
277. B. R. Cuenya, S. H. Baeck, T. F. Jaramillo, E. W. McFarland, *J. Am. Chem. Soc.***2003**, *125*, 12928-12934.
278. W. L. Leong, P. S. Lee, A. Lohani, Y. M. Lan, T. Chen, *Adv. Mater.* **2008**, *20*, 2325-2331.
279. S. Papp, L. Korösi, B. Gool, T. Dederichs, P. Mela. M. Möller, I. Dékány, *J. Therm. Anal. Calorim.* **2010**, *101*, 865-872.
280. T. Sakai, P. Alexandridis, *Langmuir***2004**,*20*, 8426-8430.
281. M. S. Bakshi, A. Kaura, P. Bhandari, G. Kaur, K. Torgoe, K. Esumi, *J. Nanosci. Nanotechnol.* **2006**, *6*, 1405-1410.
282. S. Chen, C. Guo, G. H. Hu, J. Wang, J. H. Ma, X. F. Liang, L. Zheng, H. Z. Liu, *Langmuir***2006**, *22*, 9704-9711.
283. S. G. Lopez, E. Castro, P. Taboada, V. Mosquera, *Langmuir***2008**, *24*, 13186-13196.
284. T. Sakai, P. Alexandridis, *J. Phys. Chem. B***2005**, *109*, 7766-7777
285. P. Khullar, A. Mahal, V. Singh, T. S. Banipal, G. Kaur, M. S. Bakshi, *Langmuir* **2010**, *26*, 11363-11371.
286. P. Khullar, V. Singh, A. Mahal, H. Kaur, V. Singh, T. S. Banipal, G. Kaur, M. S. Bakshi, *J. Phys. Chem. C***2011**,*115*, 10442-10454.
287. J. Liu, J. Niu, L. Yin, F. Jiang, *Analyst* **2011**, *136*, 4802-4808.
288. T. Azzam, A. Eisenberg, *Langmuir* **2007**,*23*, 2126-2132.
289. Y. Lee, T. G. Park, *Langmuir***2011**,*27*, 2965-2971.
290. P. He, M. W. Urban, *Biomacromol.***2005**, *6*, 1224-1225.
291. T. K. Sau, A. S. Urban, S. K. Dondapati, M. Fedoruk, M. R. Horton, A. L. Rogach, F. D. Stefani, J. O. Radler, J. Feldmann, *Colloid. Surf. A.* **2009**, *342*,

-
- 92-96.
292. R. Genc, M. Ortiz, C. K. O'Sullivan, *Langmuir* **2009**, *25*, 12604-12613.
293. R. Genc, G. Clergeaud, M. Ortiz, C. K. O'Sullivan, *Langmuir* **2011**, *27*, 10894-10900.
294. D. V. Goia, E. Marijevic, *Colloid. Surface. A* **1999**, *146*, 139-152.
295. S. S. Shankar, A. Rai, B. Ankamwar, A. Singh, A. Ahmad, M. Sastry, *Nat. Mater.* **2004**, *3*, 482-488.
296. B. Ankamwar, C. Damle, A. Ahmad, M. Sastry, *J. Nanosci. Nanotechnol.* **2005**, *5*, 1665-1671.
297. S. P. Chandran, M. Chaudhary, R. Pasricha, A. Ahmad, M. Sastry, *Biotechnol. Progr.* **2006**, *22*, 577-583.
298. J. Huang, Q. Li, D. Sun, Y. Lu, Y. Su, X. Yin, H. Wang, Y. Wang, W. Shao, N. He, J. Hong, C. Chen, *Nanotechnol.* **2007**, *18*, 105104-105114.
299. S. Dhar, E. M. Reddy, A. Shiras, V. Pokharkar, B. L. V. Prasad, *Chem, Eur, J.* **2008**, *14*, 10244-10250.
300. E. C. da Silva, M. G. A. da Silva, S. M. P. Meneghetti, G. Machado, M. A. R. C. Alencar, J. M. Hickmann, M. R. Meneghetti, *J. Nanopart Res.* **2008**, *10*, 201-208.
301. D. Philip, *Spectrochim. Acta. A* **2009**, *73*, 374-381.
302. D. Philip, *Physica E.* **2010**, *42*, 1417-1424.
303. S. K. Sivaraman, S. Kumar, V. Santhanam, *Gold Bull.* **2010**, *43*, 275-286.
304. X. Huang, H. Wu, X. Liao, B. Shi, *Green Chem.* **2010**, *12*, 395-399.
305. K. P. Kumar, W. Paul, C. P. Sharma, *Process Biochem.* **2011**, *46*, 2007-2013.
306. H. Wang, N. J. Halas, *Adv. Mater.* **2008**, *20*, 820-825.
307. M. Mathew, A. Sureshkumar, N. Sandhyarani, *Colloid. Surf. B.* **2012** ASAP.
308. K. Esumi, N. Takei, T. Yoshimura, *Colloid. Surf. B.* **2003**, *32*, 117-123.
309. H. Huang, X. Yang, *Biomacromolecules* **2004**, *5*, 2340-2346.
310. A. Primo, F. Quignard, *Chem. Commun.* **2010**, *46*, 5593-5595.
311. L. C. Cheng, J. H. Huang, H. M. Chen, T. C. Lai, K. Y. Yang, R. S. Liu, M. Hsiao, C. H. Chen, L. J. Her, D. P. Tsai, *J. Mater. Chem.* **2012**, *22*, 2244-2253.
312. M. J. Laudenslager, J. D. Schirrmann, G. L. Schauer, *Biomacromol.* **2008**, *9*, 2682-2685.
313. T. J. Beveridge, R. G. E. Murray, *J. Bacteriol.* **1980**, *141*, 876-887.
314. K. B. Narayanan, N. Sakthivel, *Adv. Colloid Interf. Sci.* **2010**, *156*, 1-13.
315. M. Lengke, G. Southam, *Geochim. Cosmochim. Acta.* **2006**, *70*, 3646-3661
316. Y. Konishi, T. Tsukiyama, T. Tachimi, N. Saitoh, T. Nomura, S. Nagamine, *Electrochim. Acta.* **2007**, *53*, 186-192.
317. M. Lengke, M. E. Fleet, G. Southam, *Langmuir* **2006**, *22*, 2780-2787.
318. S. He, Z. Guo, Y. Zhang, S. Zhang, J. Wang, N. Gu, *Mater. Lett.* **2007**, *61*, 3984-3987.
319. P. Mukherjee, A. Ahamd, D. Mandal, S. Senapati, S. R. Sainkar, M. I. Khan, R. Ramani, R. Parischa, P. V. Ajayakumar, M. Alam, M. Sastry, R. Kumar, *Angew. Chem., Int. Ed.* **2001**, *40*, 3585-3588.
320. A. Ahamd, S. Senapati, M. I. Khan, R. Kumar, M. Sastry, *J. Biomed.*

-
- Nanotechnol.***2005**, *1*, 47-53.
321. R. Balagurunathan, M. Radhakrishnan, R. B. Rajendran, D. Velmurugan, *Indian J. Biochem. Bio.* **2011**, *48*, 331-335.
322. A. Ahamd, S. Senapati, M. I. Khan, R. Kumar, M. Sastry, *Langmuir***2003**,*19*, 3550-3553.
323. A. Mourato, M. Gadanho, A. R. Lino, R. Tenreiro, *Bioinorg. Chem. Appl.***2011** doi:10.1155/2011/546074.
324. M. Agnihotri, S. John, A. R. Kumar, S. Zinjarde, S. Kulkarni, *Mat. Lett.***2009**,*63*, 1231-1234.
325. K. R. Brown, M. J. Natan, *Langmuir***1998**,*14*, 726-728.
326. N. R. Jana, L. Gearheart, C. J. Murphy, *J. Phys. Chem. B.* **2001**, *105*, 4065-4067.
327. B. Nikoobakht, M. A. El-Sayed, *Chem. Mater.* **2003**,*15*, 1957-1962.
328. N. C. Bigall, T. Halrtling, M. Klose, P. Simon, L. M. Eng, A. Eychmuller, *Nano Lett.* **2008**,*8*, 4588-4592.
329. S. D. Perrault, W. C. W. Chan, *J. Am. Chem. Soc.***2009**,*131*, 17042-17043.
330. N. G. Bastus, J. Comenge, V. Puentes, *Langmuir* **2011**, *27*, 11098-11105.
331. K. R. Brown, D. G. Walter, M. J. Natan, *Chem. Mater.***2000**, *12*, 306-313.
332. K. R. Brown, L. A. Lyon, A. P. Fox, B. D. Reiss, M. J. Natan, *Chem. Mater.* **1999**, *12*, 314-323.
333. E. G. Schutt, *Eur. Patent Application* 90317671.4, filled Sept. 25, **1990**.
334. N. R. Jana, L. Gearheart, C. J. Murphy, *Langmuir***2001**, *17*, 6782-6786.
335. A. A. Volkert, V. Subramaniam, A. J. Haes, *Chem. Commun.***2011**, *47*, 478-480.
336. K. Kwon, K. Y. Lee, Y. W. Lee, M. Kim, J. Heo, S. J. Ahn, S. W. Han, *J. Phys. Chem. C***2007**, *111*, 1161-1165.
337. C. Ziegler, A. Eychmüller, *J. Phys. Chem. C* **2011**, *115*, 4502-4506.
338. X. Huang, S. Neretina, M. A. El-Sayed, *Adv. Mater.* **2009**, *21*, 4880-4910.
339. C. J. Murphy, L. B. Thompson, D. J. Chernak, J. A. Yang, S. T. Sivapalan, S. P. Boulos, J. Huang, A. M. Alkilany, P. N. Sisco, *Curr. Opin. Colloid Interfac. Sci.***2011**, *16*, 128-134.
340. J. P. Juste, I. P. Santos, L. M. L. Marzan, P. Mulvaney, *Coord. Chem. Rev.***2005**, *249*, 1870-1901.
341. Y. Y. Yu, S. S. Chang, C. L. Lee, C. R. C. Wang, *J. Phys. Chem. B***1997**, *101*, 6661-6664.
342. K. Esumi, K. Matsuhisa, K. Torigoe, *Langmuir***1995**, *11*, 3285-3287.
343. A. Govindaraj, B. C. Satishkumar, M. Nath, C. N. R. Rao, *Chem. Mater.***2000**, *12*, 202-205.
344. B. D. Busbee, S. O. Obare, C. J. Murphy, *Adv. Mater.***2003**, *15*, 414-416.
345. A. Gole, C. J. Murphy, *Chem. Mater.***2004**, *16*, 3633-3640.
346. H. Y. Wu, H. C. Chu, T. J. Kuo, C. L. Kuo, M. H. Huang, *Chem. Mater.***2005**, *17*, 6447-6451.
347. H. Y. Wu, W. L. Huang, M. H. Huang, *Cryst. Growth Des.***2007**, *7*, 831-835.
348. D. K. Smith, B. A. Korgel, *Langmuir***2008**, *24*, 644-649.
349. D. K. Smith, N. R. Miller, B. A. Korgel, *Langmuir***2009**, *25*, 9518-9524.

-
350. R. G. Rayavarapu, C. Ungureanu, P. Krystek, T. G. van Leeuwen, S. Manohar, *Langmuir***2010**, *26*, 5050-5055.
351. K. Park, H. Koerner, R. A. Vaia, *Nano Lett.* **2010**, *10*, 1433-1439.
352. N. Grag, C. Scholl, A. Mohanty, R. Jin, *Langmuir***2010**, *26*, 10271-10276.
353. S. Si, C. Leduc, M.-H. Delville, B. Lounis, *ChemPhysChem***2012**, *13*, 193-202.
354. S. R. Beeram, F. P. Zamborini, *J. Am. Chem. Soc.***2009**, *131*, 11689-11691.
355. W. T. Lu, A. K. Singh, A. A. Khan, D. Senapati, H. T. Yu, P. C. Ray, *J. Am. Chem. Soc.***2010**, *132*, 18103-18114.
356. J. Y. Xiao and L. M. Qi, *Nanoscale***2011**, *3*, 1383-1396.
357. T. K. Sau, C. J. Murphy, *J. Am. Chem. Soc.***2004**, *126*, 8648-8649
358. D. Y. Kim, T. Yu, E. C. Cho, Y. Ma, O. O. Park, Y. Xia, *Angew. Chem., Int. Ed.* **2011**, *50*, 6328-6331.
359. M. S. Bakshi, F. Possmayer, N. O. Petersen, *J. Phys. Chem. C***2008**, *112*, 8259-8265.
360. Y. Zhang, F. G. Xu, Y. J. Sun, C. L. Guo, K. Cui, Y. Shi, Z. W. Wen, Z. Li, *Chem. Eur. J.***2010**, *16*, 9248-9256.
361. M. R. Langille, M. L. Personick, J. Zhang, C. A. Mirkin, *J. Am. Chem. Soc.***2011**, *133*, 10414-10417.
362. J. A. Zhang, M. R. Langille, M. L. Personick, K. Zhang, S. Y. Li, C. A. Mirkin, *J. Am. Chem. Soc.***2010**, *132*, 14012-14014.
363. X. S. Kou, Z. H. Sun, Z. Yang, H. J. Chen, J. F. Wang, *Langmuir***2009**, *25*, 1692-1698.
364. G. H. Jeong, M. Kim, Y. W. Lee, W. Choi, W. T. Oh, Q. H. Park, S. W. Han, *J. Am. Chem. Soc.***2009**, *131*, 1672-1673.
365. J. Li, L. H. Wang, L. Liu, L. Guo, X. D. Han, Z. Zhang, *Chem. Commun.***2010**, *46*, 5109-5111.
366. H. L. Wu, H. R. Tsai, Y. T. Hung, K. Un. Lao, C. W. Liao, P. J. Chung, J. S. Huang, I. C. Chen, M. H. Huang, *Inorg. Chem.***2011**, *50*, 8106-8111
367. H. L. Wu, C. H. Kuo, M. H. Huang, *Langmuir***2010**, *26*, 12307-12313.
368. W. X. Niu, S. L. Zheng, D. W. Wang, X. Q. Liu, H. J. Li, S. Han, J. Chen, Z. Y. Tang, G. B. Xu, *J. Am. Chem. Soc.***2009**, *131*, 697-703.
369. T. Ming, W. Feng, Q. Tang, F. Wang, L. D. Sun, J. F. Wang, C. H. Yan, *J. Am. Chem. Soc.***2009**, *131*, 16350-16351
370. X. G. Peng, J. Wickham, A. P. Alivisatos, *J. Am. Chem. Soc.***1998**, *120*, 5343-5344.
371. M. M. Mariscal, J. J. V. Salazar, M. J. Yacaman, *Cryst. Eng. Comm.***2012**, *14*, 544-549.
372. J. Belloni, M. Mostafavi, H. Remita, J. L. Marignier, M. O. Delcourt, *New J. Chem.***1998**, *22*, 1239-1255
373. E. Gachard, H. Remita, J. Khatouri, B. Keita, L. Nadjjo, J. Belloni, *New J. Chem.***1998**, *22*, 1257-1265.
374. W. Abidi, P. R. Selvakannan, Y. Guillet, I. Lampre, P. Beaunier, B. Pansu, B. Palpant, H. Remita, *J. Phys. Chem. C***2010**, *114*, 14794-14803.
375. N. Misra, J. Biswal, A. Gupta, J. K. Sainis, S. Sabharwal, *Radiat. Phys.*

-
- Chem.***2012**, *81*,195-200.
376. K. Roy, S. Lahiri, *Anal. Chem.***2008**, *80*, 7504-7507.
377. M. Treguer, C. de Cointet, H. Remita, J. Khatouri, M. Mostafavi, J. Amblard, J. Belloni, *J. Phys. Chem. B***1998**, *102*, 4310-4321.
378. M. Hu, F. S. Ou, W. Wu, I. Naumov, X. M. Li, A. M. Bratkovsky, R. S. Williams, Z. Y. Li, *J. Am. Chem. Soc.***2010**, *132*, 12820-12822.
379. W. Y. Huang, W. Qian, M. A. El-Sayed, *J. Am. Chem. Soc.***2006**, *128*, 13330-13331.
380. J. Neddersen, G. Chumanov, T. M. Cotton, *Appl. Spectrosc.***1993**, *47*, 1959-1964.
381. S. Besner, A. V. Kabashin, F. M. Winnik, M. Meunier, *J. Phys. Chem. C***2009**, *113*, 9526-9531.
382. A. Corma, H. García, *Chem. Soc. Rev.***2008**, *37*, 2096-2126.
383. M. Haruta, N. Yamada, T. Kobayashi, S. Iijima, *J. Catal.***1989**, *115*, 301-309.
384. J. M. Yan, X. B. Zhang, T. Akita, Haruta, M, Xu, Q, *J. Am. Chem. Soc.***2010***132*, 5326-5327.
385. T. Fujitani, I. Nakamura, T. Akita, M. Okumura, M. Haruta, *Angew. Chem., Int. Ed.***2009**, *48*, 9515-9518.
386. A. Leyva-Perez, A. Corma, *Angew. Chem., Int. Ed.***2012**, *51*, 614-635.
387. H. Yoshida, Y. Kuwauchi, J. R. Jinschek, K. Sun, S. Tanaka, M. Kohyama, S. Shimada, M. Huruta, S. Takeda, *Science***2012**, *335*, 317-319.
388. Y. Wei, J. Liu, Z. Zhao, A. Duan, G. Jiang, *J. Catal.***2012**, *287*, 13-29.
389. H. Y. Kim, H. M. Lee, G. Henkelman, *J. Am. Chem. Soc.***2012**, *134*, 1560-1570.
390. R. Zanella, S. Giorgio, C. H. Shin, C. R. Henry, C. Louis, *J. Catal.***2004**, *222*, 357-367.
391. A. Hugon, N. El-Kolli, C. Louis, *J. Catal.***2010**, *274*, 239-250.
392. Y. Borensztein, L. Delannoy, A. Djedidi, R. G. Barrera, C. Louis, *J. Phys. Chem. C***2010**, *114*, 9008-9021.
393. L. Alves, B. Ballesteros, M. Boronat, J. R. Cabrero-Antonino, P. Concepcion, A. Corma, M. A. Correa-Duarte, E. Mendoza, *J. Am. Chem. Soc.* **2011**, *133*, 10251-10261.
394. M. Ding, D. C. Sorescu, G. P. Kotchey, A. Star, *J. Am. Chem. Soc.***2012**, *134*, 3472-3479.
395. L. Prati, A. Villa, A. R. Lupini, G. M. Veith, *Chem. Chem. Phys.***2012**, *14*, 2969-2978.
396. L. Prati, F. Porta, *Appl. Catal. A: General***2005**, *291*, 199-203
397. Z. Konya, V. F. Puentes, I. Kiricsi, J. Zhu, J. W. Ager, M. K. Ko, H. Frei, P. Alivisatos, G. A. Somorjai, *Chem. Mater.***2003**, *15*, 1242-1248
398. P. McMorn, G. J. Hutchings, *Chem. Soc. Rev.* **2004**, *33*, 108-122.
399. C. T. Kresge, M. E. Leonowicz, W. J. Roth, J. C. Varuli, J. S. Beck, *Nature***1992**, *359*, 710-712.
400. J. S. Beck, J. C. Varuli, W. J. Roth, M. E. Leonowicz, C. T. Kresge, K. D. Schmitt, C. T. -W. Chu, D. H. Olson, E. W. Sheppard, S. B. McCullen, J. B. Higgins, J. L. Schlenker, *J. Am. Chem. Soc.***1992**, *114*, 10834-10843.

-
401. J. C. Hu, L. F. Chen, K. Zhu, A. Suchopar, R. Richards, *Catal. Today***2007**, *122*, 277-283.
402. C. Aprile, A. Abad, H. Garcia, A. Corma, *J. Mater. Chem.***2005**, *15*, 4408-4413.
403. J. S. Jan, T. H. Chuang, P. J. Chen, H. Teng, *Langmuir***2011**, *27*, 2834-2843.
404. S. Hermes, M. K. Schroter, R. Schmid, L. Khodeir, M. Muhler, A. Tissler, R. W. Fischer, R. A. Fischer, *Angew. Chem., Int. Ed.***2005**, *44*, 6237-6241.
405. T. Ishida, M. Nagaoka, T. Akita, M. Haruta, *Chem. Eur. J.* **2008**, *14*, 8456-8460.
406. H. L. Jiang, B. Liu, T. Akita, M. Haruta, H. Sakurai, Q. Xu, *J. Am. Chem. Soc.* **2009**, *131*, 11302-11303.
407. H. L. Jiang, T. Akita, T. Ishida, M. Haruta, Q. Xu, *J. Am. Chem. Soc.***2011**, *133*, 1304-1306.
408. K. C. F. Leung, S. Xuan, X. Zhu, D. Wang, C. P. Chak, S. F. Lee, W. K. W. Ho, B. C. C-T. Chung, *Chem. Soc. Rev.* **2012**, *41*, 1911-1928.
409. Y. Sun, Y. Xia, *Science***2002**, *298*, 2176-2179.
410. H. Zhang, N. Toshima, *Appl. Catal. A: General***2011**, *400*, 9-13.
411. H. Zhang, T. Watanabe, M. Okumura, M. Haruta, N. Toshima, *Nat. Mater.***2012**, *11*, 49-52.
412. R. W. J. Scott, O. M. Wilson, R. M. Crooks, *J. Phys. Chem B***2005**, *109*, 692-704.
413. O. M. Wilson, R. W. J. Scott, J. C. García-Martinez, R. M. Crooks, *J. Am. Chem. Soc.***2005**, *127*, 1015-1024.
414. D. F. Yancey, L. Zhang, R. M. Crooks, G. Henkelman, *Chem. Sci.***2012**, *3*, 1033-1040.
415. I. García, J. Gallo, N. Genicio, D. Padro, S. Penádes, *Bioconjugate Chem.***2011**, *22*, 264-273.
416. D. Kim, M. K. Yu, T. S. Lee, J. J. Park, Y. Y. Jeong, S. Jon, *Nanotechnology***2011**, *22*, number: 155101
417. M. R. Knecht, M. G. Weir, A. I. Frenkel, R. M. Crooks, *Chem. Mater.***2008**, *20*, 1019-1028.
418. W. Xie, C. Herrmann, K. Kömpe, M. Haase, S. Schlücker, *J. Am. Chem. Soc.***2011**, *133*, 19302-19305.
419. Y. D. Jin, C. X. Jia, S. W. Huang, M. O'Donnell, X. H. Gao, *Nat. Commun.***2010**, *1*, number: 41.
420. L. Y. Wang, H. Y. Park, S. I. I. Lim, M. J. Schadt, D. Mott, J. Luo, X. Wang, C. J. Zhong, *J. Mater. Chem.* **2008**, *18*, 2629-2635.
421. C. J. Murphy, A. M. Golet, J. W. Stone, P. N. Sisco, A. M. Alkilany, E. C. Goldsmith, S. C. Baxter, *Acc. Chem. Res.***2008**, *41*, 1721-1730.
422. C. Wang, H. Yin, R. Chan, S. Peng, S. Dai, S. Sun, *Chem. Mater.***2009**, *21*, 433-435.
423. S. Link, Z. L. Wang, M. A. El-Sayed, *J. Phys. Chem. B***1999**, *103*, 3529-3533.
424. Y. Liu, A. R. H. Walker, *Angew. Chem., Int. Ed.***2010**, *49*, 6781-6785.
425. Y. Negishi, T. Iwai, M. Ide, *Chem. Commun.***2010**, *46*, 4713-4715.
426. C. Kumara, A. Dass, *Nanoscale***2011**, *3*, 3064-3067.
427. S. Malola, H. Häkkinen, *J. Phys. Chem. Lett.***2011**, *2*, 2316-2321.

-
428. A. Travesset, *Science***2011**, *334*, 183-184.
429. Z. Qin, J. C. Bischof, *Chem. Soc. Rev.***2012**, *41*, 1191-1217.
430. A. Llevot, D. Astruc, *Chem. Soc. Rev.***2012**, *41*, 242-257.

1.3 Docetaxel nanotechnology in anti-cancer therapy

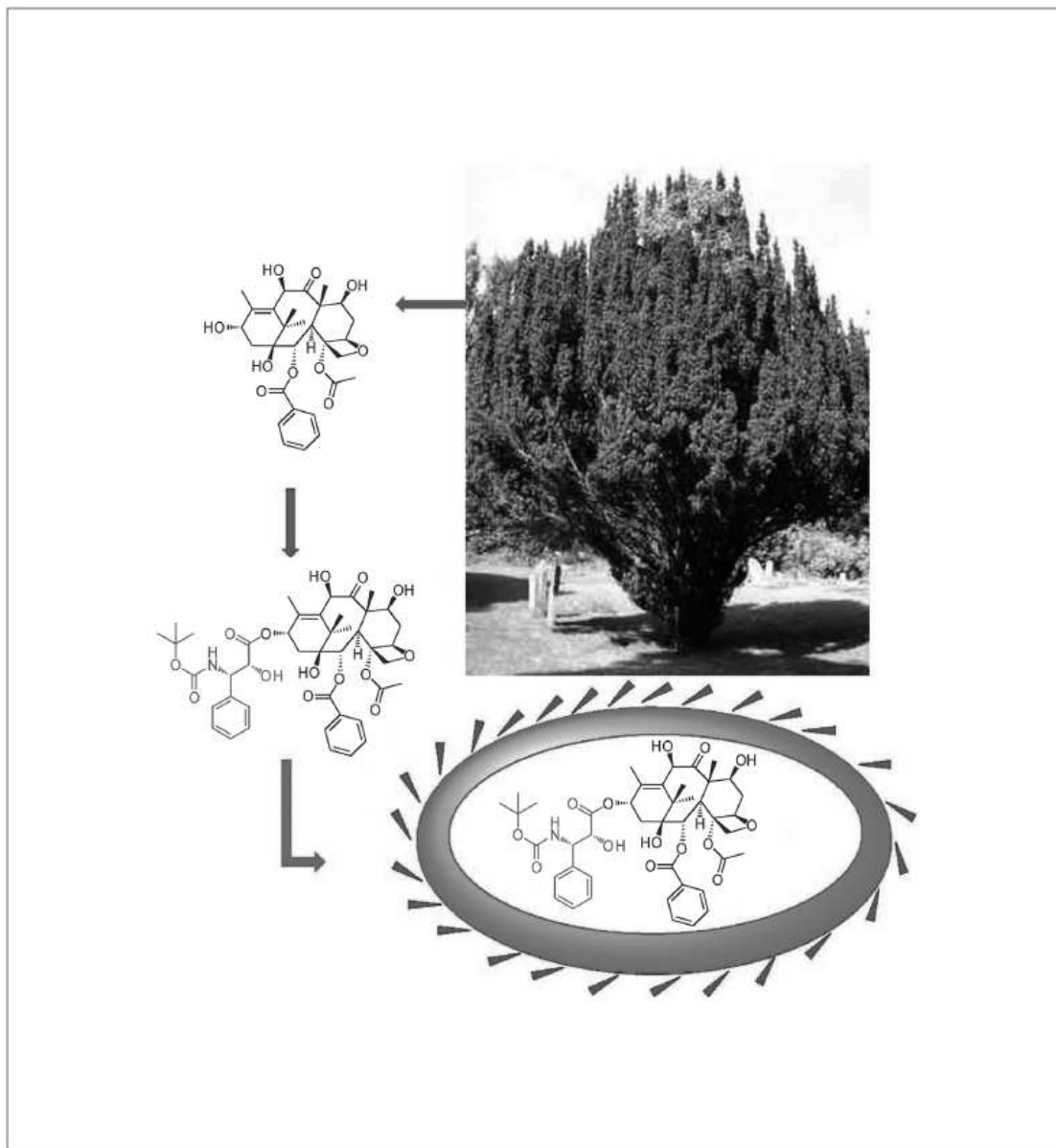
CHEMMEDCHEM

DOI: 10.1002/cmdc.201200052

Docetaxel Nanotechnology in Anticancer Therapy

Pengxiang Zhao and Didier Astruc*^[a]

Dedicated to the memory of Pierre Potier (1934–2006)



Taxanes have been recognized as a family of very efficient anticancer drugs, but the formulation in use for the two main taxanes—Taxol for paclitaxel and Taxotere for docetaxel—have shown dramatic side effects. Whereas several new formulations for paclitaxel have recently appeared, such as Abraxane and others currently in various phases of clinical trials, there is no new formulation in clinical trials for the other main taxane, docetaxel, except BIND-014, a polymeric nanoparticle, which recently entered phase I clinical testing. Therefore, we review herein the state of the art and recent abundance in published results of academic approaches toward nanotechnology-based drug-delivery systems containing nanocarriers and targeting agents for docetaxel formulations. These efforts will certainly enrich the spectrum of docetaxel treatments in the near

future. Taxotere's systemic toxicity, low water solubility, and other side effects are significant problems that must be overcome. To avoid the limitations of docetaxel in clinical use, researchers have developed efficient drug-delivery assemblies that consist of a nanocarrier, a targeting agent, and the drug. A wide variety of such engineered nanosystems have been shown to transport and eventually vectorize docetaxel more efficiently than Taxotere *in vitro*, *in vivo*, and in pre-clinical administration. Recent progress in drug vectorization has involved a combined therapy and diagnostic ("theranostic") approach in a single drug-delivery vector and could significantly improve the efficiency of such an anticancer drug as well as other drug types.

Introduction

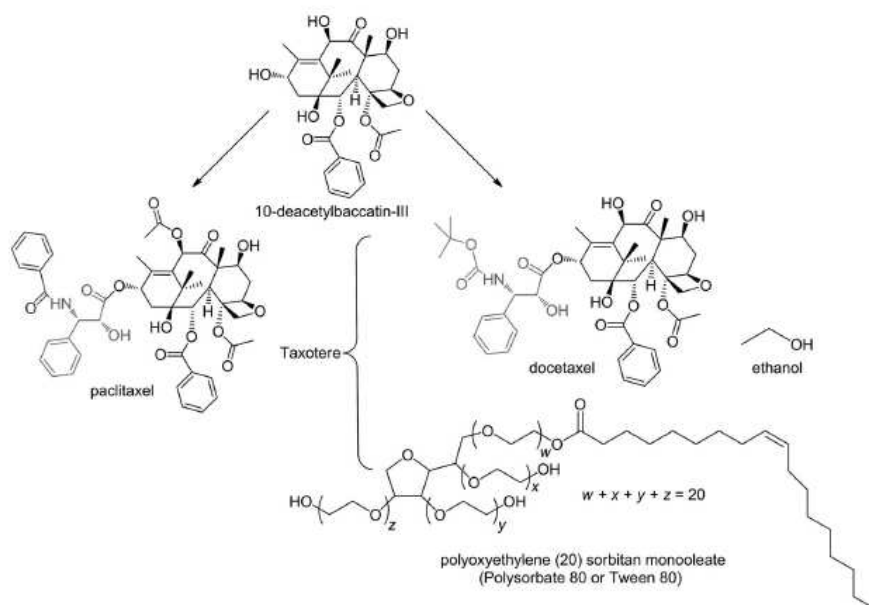
Among all diseases, cancer is one of the main causes of death.^[1a] Traditional cancer treatments such as surgery, radiotherapy, and chemotherapy are limited.^[1b–d] In chemotherapy with anticancer drugs administered by classical formulations, 95% of the therapeutic agent is taken up by healthy tissues and cells, and only 2–5% reaches tumors. Adverse side effects are a crucial problem and limit drug doses. Consequently, effective vectorization of anticancer drug therapies is required, and the past few years have witnessed much progress involving nanotechnology approaches toward vectorization strategies. Nanovectors can be defined as an association between a drug, a nanocarrier, and a targeting agent. The latter allows the selective transport of the drug to the exact organ, tissue, or cell where its activity is required. In addition, the vector–drug association must be labile under suitable conditions upon reaching the targeted location. Drug targeting is another expression for drug vectorization. The vectors must be water soluble and must impart water solubility to drugs that are, for the most part, hydrophobic. They must also be stable and should have prolonged persistence in blood circulation after intravascular administration. Nanotechnology tools (tools in the size range of a few nanometers to ~100 nm) include micelles, liposomes, polymers, steroids, peptides, hyaluronic acid, folate, fatty acids, antigens, dendrimers, nanotubes, and various types of nanoparticles (NPs). Vectorization can be passive with supramolecular encapsulation (weak drug–vector bonds) or active (covalent drug–vector bonds that are selectively cleaved at the target site). In the latter case, covalent incorporation of a specific receptor that is overexpressed at the cancer cell surface will specifically guide the drug–vector assembly to cancer cells. Finally, drug delivery by the vector at the cell surface may be effective before or after endocytosis.

Traditional anticancer drug therapies have been classified as chemotherapy, hormone therapy, or immunotherapy.^[2] Nowadays, researches are focused on anticancer drug delivery and on the use of chemotherapy drugs such as doxorubicin, daunorubicin, fluorouracil, taxanes, and many others. Among them, docetaxel has gained considerable attention since its

discovery and development by Pierre Potier at the CNRS in France during his work on improving the production of Taxol.^[3] Docetaxel belongs to the family of taxoids or taxanes, which are diterpenes produced by the plants of the genus *Taxus* (yews).^[4] The best-known derivative of the taxanes is paclitaxel, which was originally available from the bark of the Pacific yew (*Taxus brevifolia*); direct extraction of this natural product was an ecologically detrimental and unsustainably laborious process (see Scheme 1). Paclitaxel later became accessible through total synthesis, although this process is impractical.^[5,6] Pierre Potier was the first to address the problem of yield. In the early 1980s, he demonstrated the facile and ecologically sound isolation of large quantities of 10-deacetylbaccatin-III, the potential precursor of paclitaxel, from the needles of *Taxus baccata* (the European yew); in 1988 he published the semi-synthesis of this key compound from these needles.^[7,8] However, paclitaxel is currently produced by plant cell fermentation technology. Whereas the original formulation of paclitaxel, Taxol, involved the solvent Cremophor, which caused high toxicity, a now clinically approved formulation is an albumin-bound paclitaxel marketed as Abraxane. The human serum albumin used in Abraxane facilitates endothelial transcytosis of plasmatic components and paclitaxel transport through endothelial cells.^[9] Thus, the tolerated dose is higher than that of the Cremophor formulation, leading to increased efficiency.

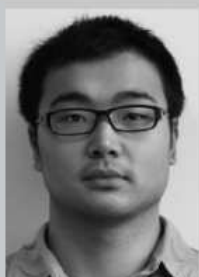
Potier's research into an efficient synthesis of paclitaxel also included the motivation to access closely related taxanes from 10-deacetylbaccatin-III, and in this manner Potier discovered docetaxel, which he made available by semi-synthesis in a few steps from the needles of *Taxus baccata*. Docetaxel has shown better bioavailability and superior activity than paclitaxel in some *in vitro* and *in vivo* assays,^[8] and frequently even in clinical settings.^[10] Docetaxel is now a major anticancer drug, especially for the treatment of breast, gastric, ovarian, prostate

[a] P. Zhao, D. Astruc
ISM, UMR CNRS No. 5255
Univ. Bordeaux, 33405 Talence Cedex (France)
E-mail: d.astruc@ism.u-bordeaux1.fr



Scheme 1. The taxoid anticancer drugs docetaxel and paclitaxel stemming from their natural precursor 10-deacetylbaccatin-III; also shown is Taxotere (one docetaxel formulation).

Pengxiang Zhao was born near Chengdu, southwest China. He carried out graduate studies on leather chemistry and engineering with Prof. Wuyong Chen at Sichuan University in Chengdu before joining the research group of Prof. Didier Astruc at the University of Bordeaux 1, where he is presently in the final stage of his PhD work. His research is devoted to the functionalization and engineering of gold nanoparticles for applications in nanomedicine and nanomaterials.



Didier Astruc is Professor of Chemistry at the University of Bordeaux 1 and is a Member of the *Institut Universitaire de France*. Born in Versailles, he studied in Rennes (Brittany) for his PhD with Prof. R. Dabard. He then carried out postdoctoral research with Prof. R. R. Schrock at the Massachusetts Institute of Technology in Cambridge (USA). He also spent a year sabbatical at the University of California at Berkeley with Prof. K. P. C. Vollhardt. His research interests are in inorganic chemistry and nanomaterials including molecular electronics, catalysis, sensors, and nanomedicine.



(metastasis), and non-benign lung cancer.^[11–14] Annual sales in 2010 (Sanofi-Aventis) were € 2.122 billion (\$US 3.1 billion).

As shown in Scheme 1, docetaxel is related to paclitaxel in terms of structure and neighboring activity, but it differs from paclitaxel particularly in its toxicity and antitumor efficacy. As with paclitaxel, docetaxel is an anti-neoplastic agent that acts by disrupting cellular microtubule networks that are essential for mitotic and interphase functions. The anticancer mechanism of docetaxel and paclitaxel can be described briefly as follows: they bind free tubulin and promote its assembly into stable microtubules, while simultaneously inhibiting disassembly; this leads to the production and stabilization of microtubule bundles that lack normal function. Thus, these compounds prevent cancerous cells from dividing, leading to their death.^[11,15] Relative to other anticancer drugs in current use, docetaxel has a broad spectrum of activity against a variety of tumors. Furthermore, docetaxel is considered to be as or more effective than doxorubicin, paclitaxel, and fluorouracil as a cytotoxic anti-microtubule agent. For instance, docetaxel is up to fivefold more potent than paclitaxel *in vitro* with regard to promoting microtubule formation and inhibition of depolymerization.^[16] Docetaxel has both anti-angiogenic and antitumor efficacy. Therefore, this review is limited to docetaxel in drug-delivery systems.

Despite the success of docetaxel against several tumor types, there are still severe limitations for docetaxel and other anticancer drugs, including poor aqueous solubility (normally at the level of $\mu\text{g mL}^{-1}$) and the systematic toxicity mentioned above.^[16–18] To address these problems and to use anticancer

drugs more efficiently in cancer therapy, researchers have focused their attention on the design of nanovectors for anticancer drug-delivery systems.^[19] Drug-delivery systems should not only impart anticancer drugs with improved water solubility, but should also target the anticancer drugs directly to tumor tissues in order to minimize their side effects (see Figure 1).^[20–23]

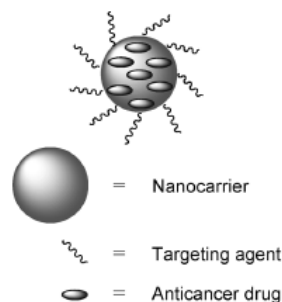


Figure 1. General view of a docetaxel delivery system.

The most common potential nanocarriers of docetaxel and other anticancer drug-delivery systems are polymers, dendrimers, inorganic NPs, and liposomes.^[24–35] The main targeting agents used for receptor recognition are monoclonal antibodies, peptides, folates, hyaluronic acid, fatty acids, and transferrin.^[36–48] Herein we discuss nanocarriers for docetaxel delivery, then consider targeting agents that would assist docetaxel in recognizing receptors at the surface of cancer cells. Ideal nanocarriers have transport properties including good water solubility, appropriate size, biocompatibility, biodegradability, and suitable pharmacokinetics. The nanocarrier transports both the drug and targeting agent that has selectivity (passive or active vectorization) for distribution to cancer cells rather than to normal cells.

A. Nanocarriers for docetaxel delivery

Various nanocarrier types for docetaxel delivery have been investigated *in vitro* and *in vivo*. Extensive clinical research with docetaxel has been carried out over the last decade using the classic formulation of Polysorbate 80; on the other hand, only very few vectorizing formulations have entered phase I clinical trials. There are two fundamental kinds of conjugation between nanocarriers and docetaxel: noncovalent and covalent. For each type of conjugation, the following properties have been sought: 1) good solubility under physiological conditions, 2) good stability until the drug arrives at the target cancer cells, 3) selectivity and efficiency in targeting tumor cells, 4) slow release in tumor cells, and 5) minimal side effects toward other cells. Thus, some nanocarriers also come equipped with a targeting agent (see below). For the noncovalent linkage approach, the greatest challenge is encapsulation by the nanocarriers and stability before arrival at tumor cells. For the covalent approach, prodrugs linked to the nanocarriers

should be stable throughout the bloodstream, readily cleaved to the active state, and released upon reaching the cancer cells.

1. Polymers

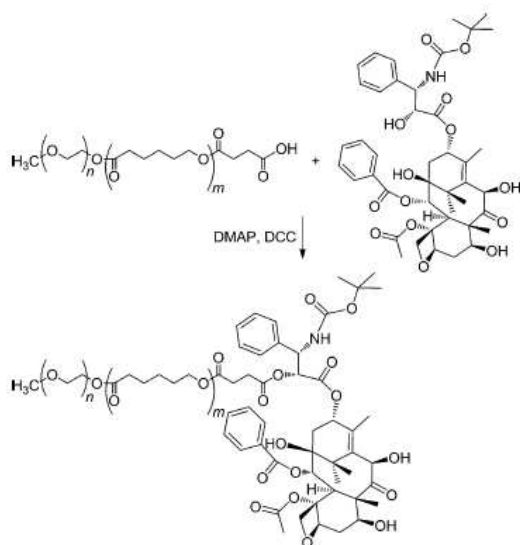
The advantages of drug biostability in polymeric nanocarriers were initially illustrated by Ringsdorf in 1975.^[49,50] Subsequently, because of their small size and low cost, polymers have been the most widely used nanocarriers, and in particular many water-soluble polymers have been tested for drug delivery.^[51] In recent years, along the discovery and development of docetaxel, polymers have played an important role as nanocarriers.^[30,31,52–57] The conjugation between polymer nanocarriers and docetaxel can be organized by either covalent bond or by micelle formation. The former conjugation is defined as a polymer–drug system, and the latter as a polymeric NP.

1.1. Poly(ethylene glycol)

Among a variety of hydrophilic polymers, poly(ethylene glycol) (PEG), also referred to poly(ethylene oxide) (PEO), has emerged as one of the most promising nanocomponents^[19,50,58–61] in drug-delivery systems, particularly because of its good water solubility, biocompatibility, steric protection of micelles, and enhanced permeability and retention (EPR) effect.^[62] As a main polymer in nanomedicine, PEG and PEG derivatives (including PEG copolymers) have been widely used as drug-loaded micelles to incorporate not only docetaxel, but also other anticancer drugs such as doxorubicin, cisplatin, haloperidol, paclitaxel, and indomethacin.^[63,64]

Due to its hydrophilicity, PEG used as a nanocarrier can increase the solubility of docetaxel. For example, Mikhail and Allen^[30] reported the physicochemical characteristics of a biocompatible block copolymer composed of poly(ethylene glycol)-*b*-poly(ϵ -caprolactone) (PEG-*b*-PCL) and a copolymer–docetaxel conjugate (PEG-*b*-PCL–docetaxel) linked by a covalent bond. In this case, the conjugation of the drug was found to have a profound effect on drug loading, which was 1840-fold higher than the free drugs in water. PEG-*b*-PCL–docetaxel was released over the course of one week, indicating its excellent capacity for sustained drug release (see Scheme 2 and Figure 2). Similarly, Shin et al.^[52] conjugated docetaxel with poly(ethylene glycol)-block-poly(D,L-lactic acid) (PEG-*b*-PLA) to increase the solubility from the $\mu\text{g mL}^{-1}$ range to the level of mg mL^{-1} .

Moreover, PEG has one active hydroxy group located at each end of the polymer chain, which means that it can be easily hetero-bifunctionalized at the two termini. Thus, researchers have been able to introduce the drug and the targeting agent at each terminus of the PEG molecule. A remarkable application of PEG in docetaxel delivery was demonstrated by Zhang's research group.^[65] They situated a peptide, the Asn-Gly-Arg (NGR) motif, as a targeting agent at the hydrophilic termini of the PEG-*b*-PLA copolymer, and anticancer drugs were encapsulated by the hydrophobic termini (PLA) of the copolymer to form a polymeric NPs as NGR-PM–docetaxel (see



Scheme 2. Synthesis of PEG-b-PCL-docetaxel. Reprinted with permission from ref. [30], Copyright 2010 American Chemical Society.

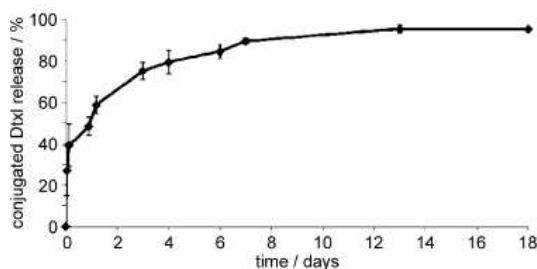


Figure 2. Release of chemically conjugated docetaxel (Dtxl) from PEG-b-PCL-docetaxel micelles at 10 mg mL^{-1} (2.4 mg mL^{-1} Dtxl equivalent) in PBS (pH 7.4). Reprinted with permission from ref. [30], Copyright 2010 American Chemical Society.

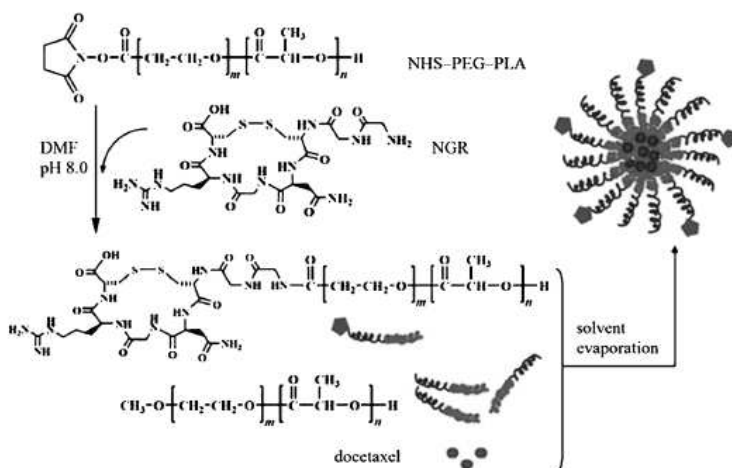
Table 1. Inhibition of PC3 and DU145 cell growth after incubation with docetaxel and docetaxel-NPs for 24, 48, and 72 h.

Time [h]	PC3		DU145	
	Docetaxel	Docetaxel-NPs	Docetaxel	Docetaxel-NPs
24	11.79 ± 1.091	9.914 ± 1.104	10.34 ± 1.090	7.877 ± 1.126
48	7.087 ± 1.112	5.054 ± 1.117	6.619 ± 1.110	4.399 ± 1.107
72	4.313 ± 1.179	2.571 ± 1.195	3.710 ± 1.152	2.472 ± 1.141

[a] Data from ref. [66].

Scheme 3). Compared with other formulations, NGR-PM-docetaxel has excellent *in vivo* antitumor activity, which can be seen in Figure 3. It was concluded that NGR-PEG-b-PLA-docetaxel is a potential vehicle for the delivery of hydrophobic chemotherapeutic agents to CD13-overexpressing tumors. PEGs have also been covalently attached to inorganic NPs to form a nanocarrier. For example, [1,2-distearoyl-*sn*-glycero-3-phosphoethanolamine-*N*-carboxy(PEG)₂₀₀₀ (DSPE-PEG-COOH) stabilized oleic acid coated hydroxyapatite NPs can encapsulate do-

docetaxel into the NPs (see Scheme 4). As shown in Table 1, this formulation, with docetaxel inside and oleic acid as targeting agent at the NP periphery retained the pharmacological effects of docetaxel while enhancing the therapeutic efficiency of the encapsulated drug *in vitro*.^{66]} Very recently, PEGylated poly(*n*-butylcyanoacrylate) (PBCA) NPs prepared by the emulsion polymerization method were reported. This method has the unique advantage of single-step *in situ* polymerization, nanoparticle formation, as well as PEGylation. It is also helpful for ligand or antibody conjugation using the amine groups of PEG derivatives as initiators of polymerization reactions. The pharmacological profiles of these docetaxel-containing NPs have been studied. The results of *in vitro* cell line studies demonstrated the effectiveness of this carrier as a nanocarrier for drug delivery, and *in vivo* animal studies showed the clear advantage of this formulation over other formulations in terms of lower blood clearance, lower liver uptake, high blood concentration, and prolonged plasma half-life.^{67]}



Scheme 3. Synthesis of NGR-PEG-b-PLA copolymer and strategy of docetaxel encapsulation. Reprinted with permission from ref. [65], Copyright 2009 Elsevier.

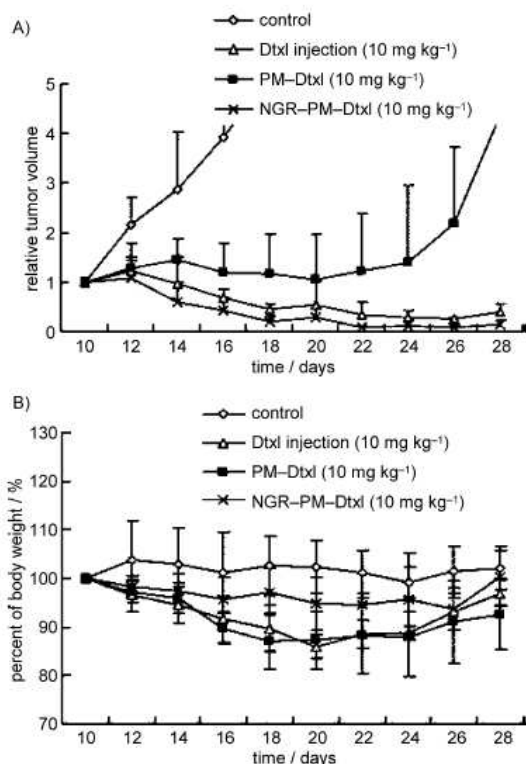
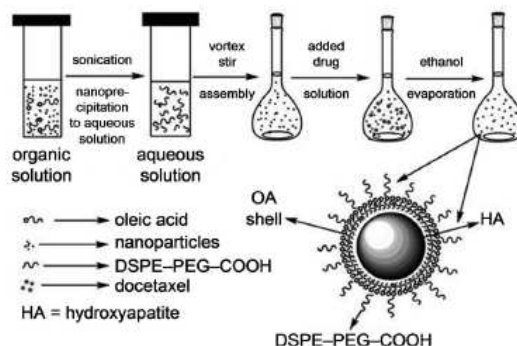


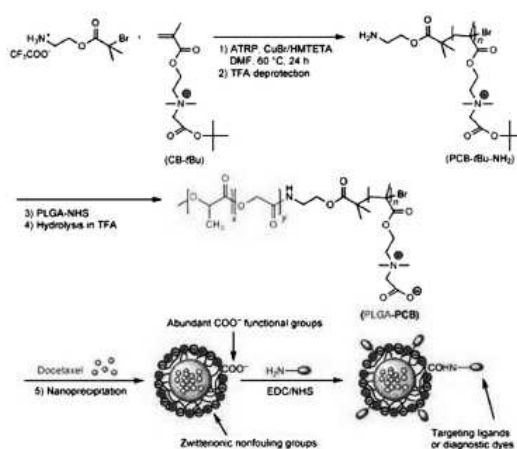
Figure 3. A) Antitumor activity and B) body weight change in HT1080-bearing nude mice treated with various formulations as indicated. Data represent the mean \pm SD ($n=6$). Dtxl: docetaxel; PM-Dtxl: PEG-b-PLA with docetaxel; NGR-PM-Dtxl: NGR-PEG-b-PLA with docetaxel. Reprinted with permission from ref. [65], Copyright 2009 Elsevier.

1.2. Other polymers

Besides PEG, other polymers have also been used as nanocarriers of anticancer drugs. For instance, poly(lactic acid-co-glycolic acid) (PLGA), a biocompatible, bioabsorbable polymer, shows promise in medical applications and can easily be tailored to vary release and degradation.⁵⁶⁰ Another example is *N*-(2-hydroxypropyl)methacrylamide (HPMA) copolymer, which, due to its hydrophobicity and slow hydrolysis in aqueous media, has been used to encapsulate drugs and control release.⁵⁴¹ In recent reports, PLGA and HPMA were described as two efficient nanocarriers of docetaxel.^{53,541} Cao et al. designed and developed PLGA-b-poly(carboxybetaine) (PLGA-b-PCB) copolymer that self-assembles into NPs with the hydrophobic PLGA core and a PCB shell. These NPs could be used for the loading of docetaxel; however, the efficiency of these docetaxel formulations for *in vitro* and *in vivo* testing still needs to be assessed (see Scheme 5).⁵³¹ HPMA has been used for docetaxel delivery by Ulbrich and colleagues, who described the synthesis and physicochemical characteristics of the biological activity of polymer prodrugs based on a docetaxel derivative (docetaxel-



Scheme 4. The formulation of nanoparticles and the process for drug loading. Reprinted with permission from ref. [66], Copyright 2010 Elsevier.



Scheme 5. Synthesis of PLGA-PCB copolymers, formation of PLGA-PCB/docetaxel NPs, and post-functionalization of NPs with targeting ligands or diagnostic dyes (TFA: trifluoroacetic acid; HMTETA: 1,1,4,7,10,10-hexamethyltriethylenetetramine; ATRP: atom-transfer radical polymerization). Reprinted with permission from ref. [53], Copyright 2010 Wiley-VCH.

LEV). The latter was acylated with levulinic acid and conjugated with a water-soluble HPMA drug carrier. The formulation is shown in Figure 4A.⁵⁴¹ The ensuing *in vivo* test demonstrated that the conjugates are relatively stable in blood (pH 7.4) and that the active drug is released under mildly acidic conditions (pH 5) reflecting the lysosomal environments in cells. This formulation of docetaxel indicated the high activity in treating EL4 T-cell lymphoma, and was devoid of side toxicity (see Figure 4B). Sanna et al. reported biodegradable block-copolymers, poly(lactide-co-caprolactone) (PLA-PCL) and poly(lactic acid-co-glycolic acid)-block-poly(glycolide) (PLGA-PCL) for the formulation of docetaxel-loaded NPs and compared them with PLA- and PLGA-NPs. These vectors were prepared by nanoprecipitation using Pluronic F-127 as surfactant. Cytotoxicity studies demonstrated the advantages of the docetaxel-loaded PLGA-PCL NPs over pure docetaxel in both a time- and concentra-

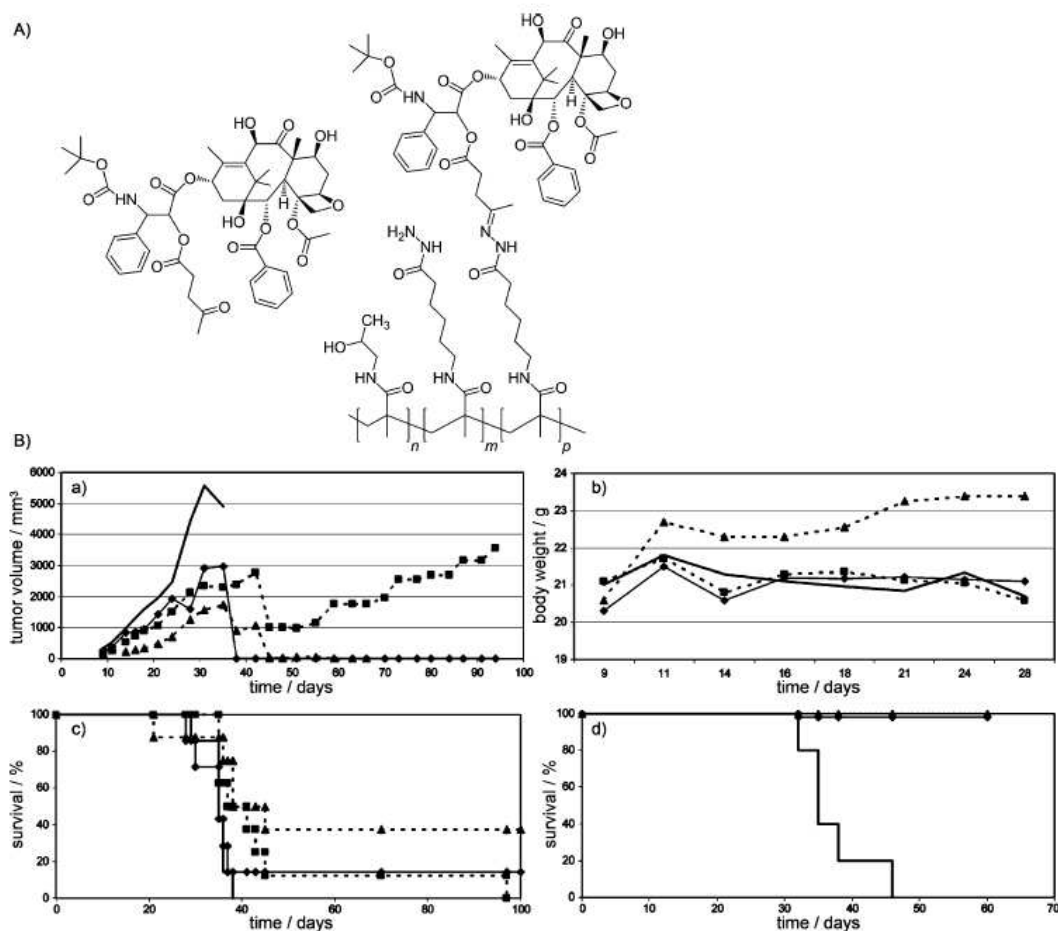


Figure 4. A) Structure of docetaxel derivative (docetaxel-LEV) (left) and polymer conjugate with docetaxel derivative HMPA-LEV-docetaxel (right). B) Antitumor efficacy, acute toxicity, and survival after re-transplantation of docetaxel-, docetaxel-LEV- and HMPA-LEV-docetaxel-treated EL4 lymphoma-bearing C57BL/6 mice. C57BL/6 mice were transplanted subcutaneously with 1×10^5 EL4 cells and treated with (◆—) Dtxl ($2 \times 20 \text{ mg kg}^{-1}$), (■—) Dtxl-LEV ($2 \times 20 \text{ mg kg}^{-1}$), (▲—) HMPA-LEV-Dtxl ($2 \times 20 \text{ (mg Dtxl equiv) kg}^{-1}$), or (—) HMPA-LEV-Dtxl ($2 \times 40 \text{ (mg Dtxl equiv) kg}^{-1}$), intravenous drug administration on days 8 and 12. Control mice were left untreated. Tumor growth (a), body weight (b) [(—) Dtxl ($2 \times 20 \text{ mg kg}^{-1}$), naive mice; (s) solvent 0.2 mL EtOH + Cremophor/PBS, naive mice], and overall survival (c) were monitored. Surviving mice (70 days) were re-transplanted with 1×10^5 EL4 cells and left untreated; survival time (d) was monitored. Reprinted with permission from ref. [54], Copyright 2010 American Chemical Society.

tion-dependent manner. In particular, an increase of 20% of PC3 growth inhibition was determined for PLGA-PCL NPs with respect to free drug after 72 h incubation and at all tested docetaxel concentrations.¹⁴⁴

DeSimone's research group reported the generation of engineered PLGA by a process consisting of particle replication in non-wetting templates that allowed the fabrication of particles of almost any shape and size independent of process parameters. These sizes and shapes could be used to affect cell uptake, biodistribution, and flow characteristics. Compared with other present formulations listed in Table 2, these particles had efficient loadings of docetaxel (up to 40%), and high encapsulation efficiencies (> 90%).¹⁵⁹ Very recently, Ernsting

et al.¹⁶⁰ developed a polymer conjugate (Cellax) composed of acetylated carboxymethylcellulose (CMC), docetaxel, and PEG (the formulation is shown in Figure 5A). Relative to Taxotere, this formulation exhibited a 38.6-fold greater area under the curve (AUC), and significantly lower clearance (2.5%) in pharmacokinetics. Furthermore, it can decrease nonspecific distribution of docetaxel to the heart, lung, and kidney by 48, 90, and 90%, respectively (see Figure 5B), relative to Taxotere. The tumor uptake of this formulation was 5.5-fold greater than that of Taxotere and it exhibited enhanced efficacy in metastatic mouse tumor models. These results demonstrated that this formulation improves the pharmacokinetics, biodistribution, and efficacy of docetaxel over Taxotere.

Fabrication method	Matrix	Theoretical loading [%]	Encapsulation efficiency [%]	Citation in ref. [55]
emulsion	PLGA	0.5–1	17–23	[24]
	PLA	0.5–1	11–22	[24]
	PLGA-mPEG	2	77–83	[25]
	PLGA and PLGA-mPEG	2	38–85	[26]
	PVP-b-PLGA	4	>95	[27]
	PLGA-mPEG	6	26	[26]
	PLGA-lecithin-PEG	10	62	[28]
	PLGA	11	70	[15]
nanoprecipitation	PLGA-PEG	10–15	21–51	[29]
	PEG-b-PLA	12	98	[30]
ultrasonication	NGA-PLA-PEG	5–15	95–98	[31]

Data collected from ref. [55].

2. Dendrimers as docetaxel nanocarriers

Since the mid-1990s, the biomedical applications of dendrimers have become increasingly promising.⁵⁷¹ As nanocarriers, dendrimers have been designed to improve the aqueous solubility, pharmacodynamics, pharmacokinetics (circulation time, organ uptake, and tumor accumulation), and bioavailability of

drugs both in vitro and in vivo. As described in a broad review in 2010,⁵⁷⁴¹ the leading principles for the use of dendrimers as delivery vehicles involve: 1) the charge of the terminal groups, which must be neutral or negative to avoid or minimize toxicity (or should be largely masked if cationic), 2) the design of the molecular architecture to optimize pharmacokinetics, 3) PEGylation for water solubility and biodistribution, 4) the choice between dendritic encapsulation and covalent attachment to the branches, and 5) the use of targeting groups (folic acid, peptides, monoclonal antibodies, and glycosides) that bind specifically to the receptor targets overexpressed on cancer cells. A recent report has concerned docetaxel delivery by functionalizing the dendrimer with cyclodextrins as nanocarriers and glycoclusters for optimal lectin binding.¹²⁴¹ In this case, the glycodendrimer–cyclodextrin conjugates for docetaxel delivery produced high drug solubility, and it was shown to be very efficient for docetaxel delivery (Figure 6). Moreover, this system suggests the possibility of exploiting guest-promoted clustering of multivalent carriers that might actually represent a new approach in active drug targeting.

3. Oligomers as docetaxel nanocarriers

Chitosan^{69–761} and cyclodextrin^{77–831} are two oligomers typically used for drug delivery. Chitosan is a linear polysaccharide composed of randomly distributed β -(1 \rightarrow 4)-linked D-glucosamine (deacetylated unit) and N-acetyl-D-glucosamine (acetylated

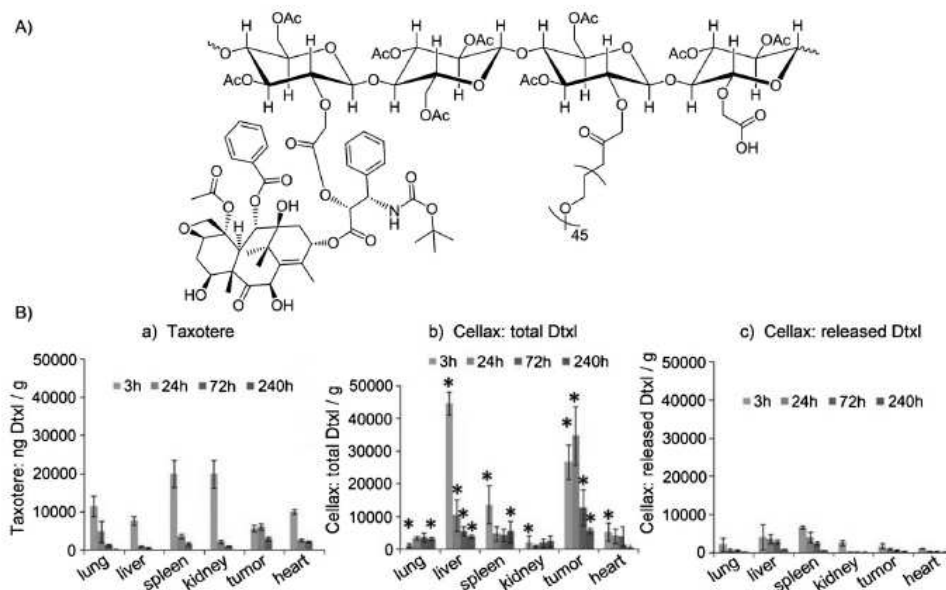


Figure 5. A) Structure of the Cellax polymer conjugate. This structure is a representation of the docetaxel, PEG, and free carboxylic acid elements distributed throughout the polymer chain. B) Biodistribution of docetaxel (Dtxl) delivered by Taxotere and Cellax. Cellax and Taxotere were administered intravenously at 40 (mg docetaxel) kg⁻¹ into EMT-6 tumor-bearing BALB/c mice, and the released and total docetaxel in the tissues were extracted and measured by LC-MS. Data represent the mean \pm SE ($n=3$); the differences in total docetaxel content between Taxotere- and Cellax-treated tissues were analyzed for significance ($*p < 0.05$, indicated in panel b). Reprinted with permission from ref. [56], Copyright 2012 Elsevier.

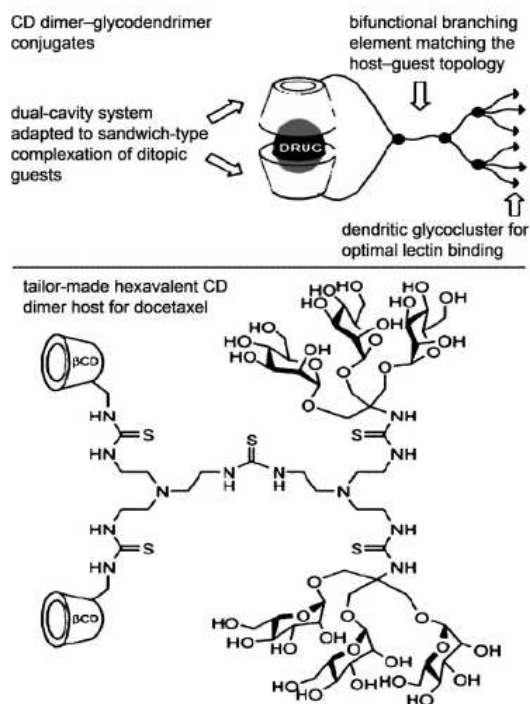


Figure 6. General architecture of CD dimer-glycodendrimer conjugates and chemical structure proposed as docetaxel carrier. Reprinted with permission from ref. [24], Copyright 2004 American Chemical Society.

unit). It is widely used for drug delivery and biomedical applications as a bioactive macromolecule. In addition, the presence of a primary amine at the C2 position allows specific modifications on the repeat unit.^[84] Cyclodextrins are candidates for drug delivery because of their ability to alter the physical, chemical, and biological properties of guest molecules through the formation of inclusion complexes with the widely used natural α , β , and γ -cyclodextrins that contain six, seven, and eight D-glucopyranose residues, respectively. Each cyclodextrin has its own ability to form inclusion complexes with specific guests, and among them β -cyclodextrin is the most widely used in anticancer drug delivery because of its fitting cavity (the cavity of α -cyclodextrin is too small and that of γ -cyclodextrin is too large) for anticancer drug molecules.^[85]

3.1. Chitosan

A key property of chitosan for drug delivery is its positive charge formed under acidic conditions upon protonation of its free amino groups. The lack of a positive charge means that chitosan is insoluble in neutral or basic environments. On the other hand, in acidic environments, protonation of the amino groups leads to increased solubility, with implications that are essential for biomedical applications. Chitosan maintains its

structure in a neutral environment, but becomes soluble and degrades under acidic conditions. This means that it is stable in the human bloodstream and can release drugs in tumor cells, given the acidic pH of the latter.^[86]

Chitosan is currently used as a popular nanocarrier for docetaxel delivery.^[86,87] For instance, the docetaxel prodrug conjugated to low-molecular-weight chitosan (LMWC) has much lower sub-acute toxicity in body weight loss and hematological toxicity than free docetaxel without conjugation (see Figure 7).^[87] Meanwhile, *in vivo* testing showed that the oral

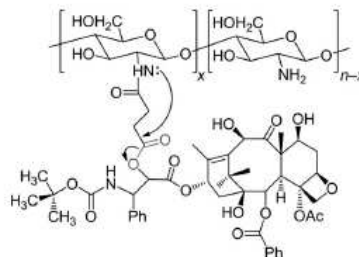


Figure 7. Structure of LMWC-docetaxel conjugate in which curved arrows illustrate the cleavage mechanism of the succinate linker to liberate the parent docetaxel. Reprinted with permission from ref. [87], Copyright 2009 Elsevier.

bioavailability obtained from this formulation is the highest reported to date. A comparison of bioavailability data for LMWC-docetaxel and free docetaxel is listed in Table 3. In addition, modified chitosan has also been used to efficiently en-

Parameter	LMWC-Docetaxel		Docetaxel	
	5 mg kg ⁻¹	10 mg kg ⁻¹	5 mg kg ⁻¹	10 mg kg ⁻¹
C_{max} [$\mu\text{g mL}^{-1}$]	0.82	2.08	66.57	125.58
t_{max} [min]	240.00	240.00	1.00	1.00
$t_{1/2}$ [min]	202.20	489.60	35.40	33.00
$AUC_{0-\infty}$ [h mL ⁻¹]	29.02	43.20	4.69	11.34

[a] Data collected from ref. [87].

capsulate docetaxel. Kim's research group reported a special drug-delivery system consisting of docetaxel conjugated glycol chitosan, modified by 5 β -cholanolic acid.^[88] In this scheme, docetaxel was mixed with hydrophobically modified glycol chitosan (HGC) conjugates in an organic solvent, and the mixture was dialyzed to produce nano-sized drug carriers in aqueous conditions to form self-assembled docetaxel-HGC NPs (see Figure 8). These docetaxel-HGC NPs exhibited high drug loading efficiency of docetaxel and slow drug release in *in vitro* tests.

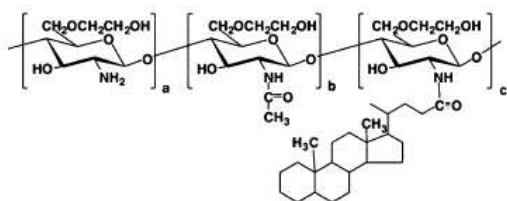


Figure 8. Structure of a hydrophobically modified glycol chitosan (HGC) conjugate by coupling of glycol chitosan with 5 β -cholanolic acid. Reprinted with permission from ref. [88], Copyright 2008 Elsevier.

3.2. Cyclodextrin

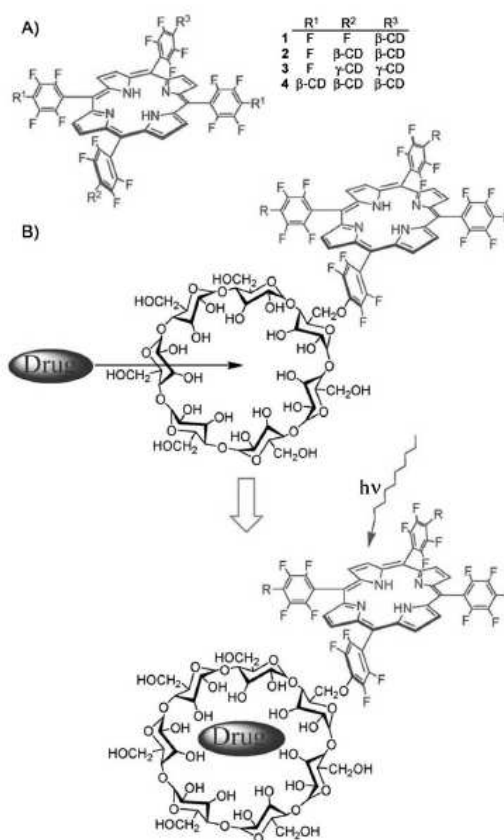
Due to the hydrophobic cavity and hydrophilic surface^[89] of cyclodextrin, docetaxel can be encapsulated into its hydrophobic cavity to obtain good solubility by the hydrophilic surface. Thus, it can potentially transport hydrophobic drugs. Králová et al.^[90] conjugated docetaxel to a porphyrinated cyclodextrin (Scheme 6). In vitro studies using mouse mammary 4T1 carcinoma cells indicated that the porphyrin receptor system combined efficient binding of the selected drug to the cyclodextrin cavity and photosensitizing properties of the porphyrin moiety with high accumulation of the whole complex in cancer tissues. The most common pharmaceutical application of cyclodextrins is to enhance the solubility, stability, and bioavailability of drug molecules. However, natural cyclodextrins have relatively low solubility, both in water and organic solvents, which limits their use in pharmaceutical formulations. Recently, various kinds of cyclodextrin derivatives have been prepared to extend the physicochemical properties and inclusion capacity of natural cyclodextrins as novel drug carriers of docetaxel. Fox example, Grosse et al. reported the effect of methyl- β -cyclodextrin (MEBCD) on the antitumor activity of docetaxel. The authors showed that MEBCD was able to significantly increase the cytotoxic activity of docetaxel in three different cell lines.^[91] Quaglia et al. investigated the application of heptakis-(2-*O*-oligo(ethyleneoxide)-6-hexadecylthio-)- β -CD (SC16OH) as a docetaxel nanocarrier and evaluated its potential treatment of solid tumors.^[92]

4. Inorganic NPs as docetaxel nanocarriers

NPs are generally defined as materials with three dimensions between 1 and 100 nm. Due to the specific physicochemical properties of the NPs themselves as well as the identity of the functional molecules added to their surfaces, they easily enter and traverse tissues, cells, and organelles. Thus, in the last decades nanotechnology and nanofabrication have significantly impacted biomedicine, especially in the field of drug delivery.^[93]

4.1. Gold nanoparticles (AuNPs)

Among all the types of inorganic NPs, AuNPs, first rationally synthesized and studied in 1857 by Faraday,^[94] are among the



Scheme 6. A) Prepared and tested porphyrin-CD conjugates. B) Schematic representation of the formation of a supramolecular carrier-drug complex with dual therapeutic function. Reprinted with permission from ref. [90], Copyright 2010 American Chemical Society.

most widely used NPs for drug delivery and other biological applications. This popularity is due to their nontoxic and biocompatible properties, their size- and shape-controlled synthesis, the ease of their surface modification with functional thiolate ligands, and their extremely rich and versatile optical properties related to their surface plasmon band (SPB). The latter is used for both diagnosis and therapy. AuNPs are often functionalized with PEG, which brings about the EPR effect^[95–98] that serves the vectorization strategy.^[98] As anticancer drug carriers, AuNPs have also been modified by thiolate or amine ligands at their periphery, and then used to encapsulate anticancer drugs. The anticancer drug can be linked to AuNPs by a covalent bond to become a prodrug, or it can be encapsulated by appropriate ligands near the surface of AuNPs with noncovalent bonds incorporating drugs into the monolayer.^[99–101] For instance, Rotello and co-workers reported the fabrication of biocompatible AuNPs to deliver drugs to cancer cells via their incorporation into the monolayer.^[98] The 2.5-nm-core AuNPs were functionalized with a hydrophobic alkanethiol interior

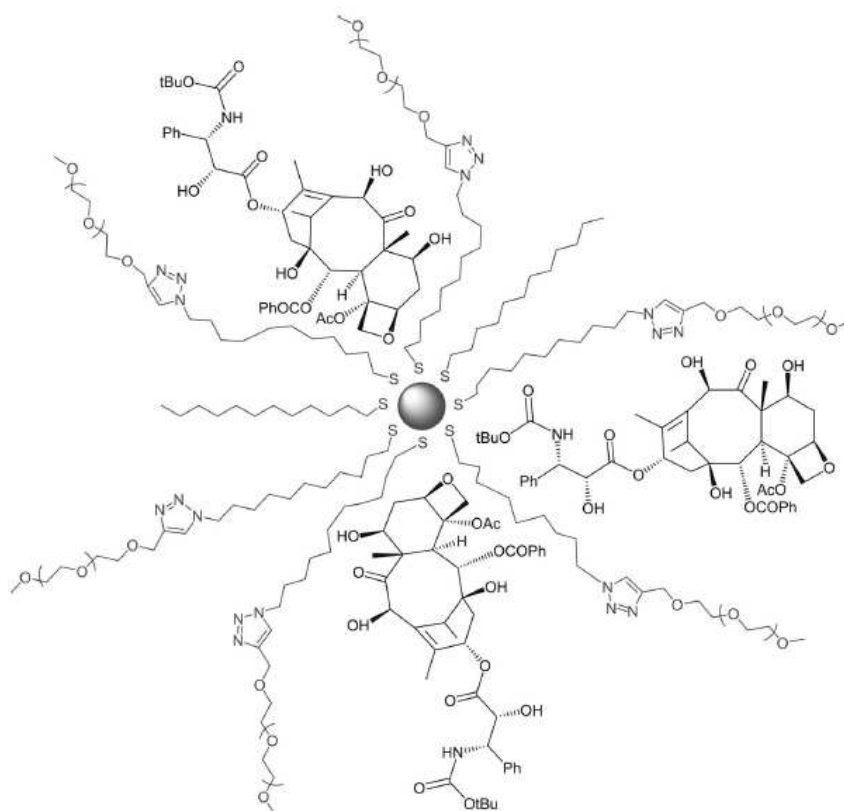


Figure 9. Encapsulation of docetaxel in gold nanoparticles considerably increases its solubility in water.

that encapsulated the drugs and with a tetra(ethylene glycol) (TEG) hydrophilic shell. The ligands possessed zwitterionic head groups that efficiently loaded the drugs.

Although researches have considered applications of AuNPs to anticancer drug delivery, only one report has appeared on AuNPs as drug carriers for docetaxel (Figure 9). Indeed, the PEG-functionalized AuNPs were shown to highly increase the solubility of docetaxel. Vectorization of PEGylated AuNP-encapsulated docetaxel was probed *in vitro* toward human colon carcinoma (HCT15) and human breast cancer (MCF7) cells. AuNPs alone presented no cytotoxicity toward either MCF7 or HCT15 adenocarcinoma cells. The AuNP-loaded docetaxel was 2.5-fold more efficient than Taxotere against MCF7 cells, and the IC_{50} value of AuNP-docetaxel in HCT15 cells was lower than that of Taxotere.^[102]

4.2. Silicone nanorattles

Silicone nanorattles are mesoporous silicone nanomaterials (MSNs) with hollow interiors. Because of their special nanostructure, MSNs have unique properties including large specific surface area and pore volume, tailored mesoporous structure,

high chemical and mechanical stability, and favorable biocompatibility. These properties impart MSNs with a prospective application as drug-delivery systems.^[103,104] Functionalized MSNs have already been used as robust drug carriers for on-demand drug release, co-delivery of two kinds of therapeutic agent, and encapsulation of hydrophobic anticancer drugs.^[105–110]

A few recent reports have appeared on MSNs for docetaxel encapsulation. For example, Li et al. and Chen et al. synthesized PEGylated silica nanorattles^[28,111] with a diameter of 125 nm, and the hydrophobic docetaxel was loaded into these nanorattles for liver cancer therapy.^[28] In Hep-G2 human liver cancer cells, the half-maximal inhibitory concentration (IC_{50}) of silica nanorattle-encapsulated docetaxel (SN-PEG-docetaxel) was much lower than that of free docetaxel, and the *in vivo* toxicity assessment also provided satisfactory results. It was shown that SN-PEG-docetaxel has low toxicity and high therapeutic efficacy (see Figure 10).

5. Liposomes as docetaxel nanocarriers

Liposomes, supramolecular assemblies of amphiphilic lipids, are well-established and versatile platforms for diverse biomed-

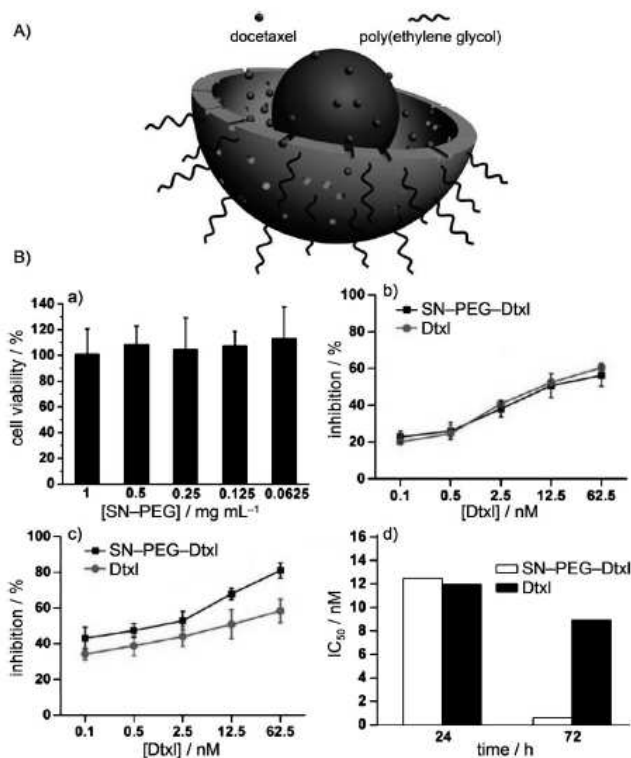


Figure 10. A) Diagram of the drug-delivery system based on silica nanorattles. B) Cytotoxicity of SN-PEG, SN-PEG-Dtxl, and Dtxl on Hep-G2 cells by MTT assays: a) Cell viability with concentrations of SN-PEG from 0.0625 to 1 mg mL⁻¹ for 72 h; inhibition rate of Dtxl and SN-PEG-Dtxl (Dtxl concentrations indicated) toward Hep-G2 cells for b) 24 and c) 72 h; d) corresponding IC₅₀ value for 24 and 72 h. Reprinted with permission from ref. [28], Copyright 2010 American Chemical Society.

ical applications, including drug delivery, biosensing, and catalysis.^[112–118] The first example of cell-specific targeting using ligand-conjugated liposomes was described in 1980, and thereafter a great number of targeted NPs were proposed and developed for drug delivery.^[119] Liposomes are widely used as drug-delivery vehicles because of their favorable safety profile, ease of surface modification, and long systemic half-life that can reach days after being surface modified with hydrophilic polymers such as PEG.^[120,121] Several liposomal drug formulations have been approved for clinical use, including Doxil (doxorubicin liposomes, first approved in 1995), AmBisome (amphotericin B liposomes), DaunoXome (daunorubicin liposomes), DepoCyt (cytarabine liposomes), DepoDur (morphine liposomes), and Visudyne (verteporfin liposomes).^[121–123] Limitations of liposomal drug delivery, however, include insufficient drug loading, fast drug release, and instability in storage.^[124]

Recently, efforts to study drug delivery with liposomes have increased. For instance, Zhang et al.^[120] reported the engineering of a novel lipid polymer hybrid NP as a robust drug-delivery platform. The NP comprises three distinct functional components: 1) a hydrophobic polymeric core in which drugs of

low water solubility can be encapsulated, 2) a hydrophilic polymeric shell with anti-biofouling properties to enhance NP stability and systemic half-life, and 3) a lipid monolayer at the interface between the core and the shell that acts as a molecular fence to promote drug retention inside the polymeric core, thereby enhancing drug encapsulation efficiency, increasing drug loading yield, and controlling drug release.

Due to all the advantages indicated above, many researchers have considered liposomes as docetaxel nanocarriers. A model of the interactions between docetaxel and model lipid membranes was described in 2008 by Fernández-Botello.^[125] Liposomes are used as nanocarriers together with targeting agents. For instance, folate as a targeting agent combined with liposome for docetaxel delivery provided good results for drug release and selectivity.^[126,127] Another example is the research carried out by Li's group, in which the authors designed a novel targeted nanoassembly loaded with docetaxel. They directly conjugated the nanocarrier with epidermal growth factor (EGF) as ligand

that was the targeting agent for epidermal growth factor receptor (EGFR) overexpressed on breast cancer cells (see Figure 11 A). Compared with nanoassemblies without targeting agent (NNA) or Taxotere, nanoassemblies with targeting agent (TNA) prevent docetaxel from rapid uptake by the mononuclear phagocyte system and increase their circulatory half-life (see Figure 11 Ba). Moreover, the TNAs also exhibited a bias to the tumor, with higher drug accumulation than other formulations in the *in vivo* test (see Figure 11 Bb, Bc).^[128]

Since 2001, phospholipids have been used as effective emulsifiers. They stay between the oil/water interface to lower the interfacial tension and thus facilitate the formulation of colloidal NPs. They proved to be much more efficient emulsifiers than the traditional chemical emulsifiers such as polyvinyl alcohol, and those of shorter saturated chains were more appropriate for NP formulation.^[129] The end functional group of phospholipids can be used to facilitate conjugation of targeting ligands (such as antibodies). For instance, the carboxylic group can be conjugated to the active primary amine of phosphoethanolamine or amino-PEG.^[16,37–39,130,131] A docetaxel-loaded intravenous lipid emulsion without Tween 80, produced by high-

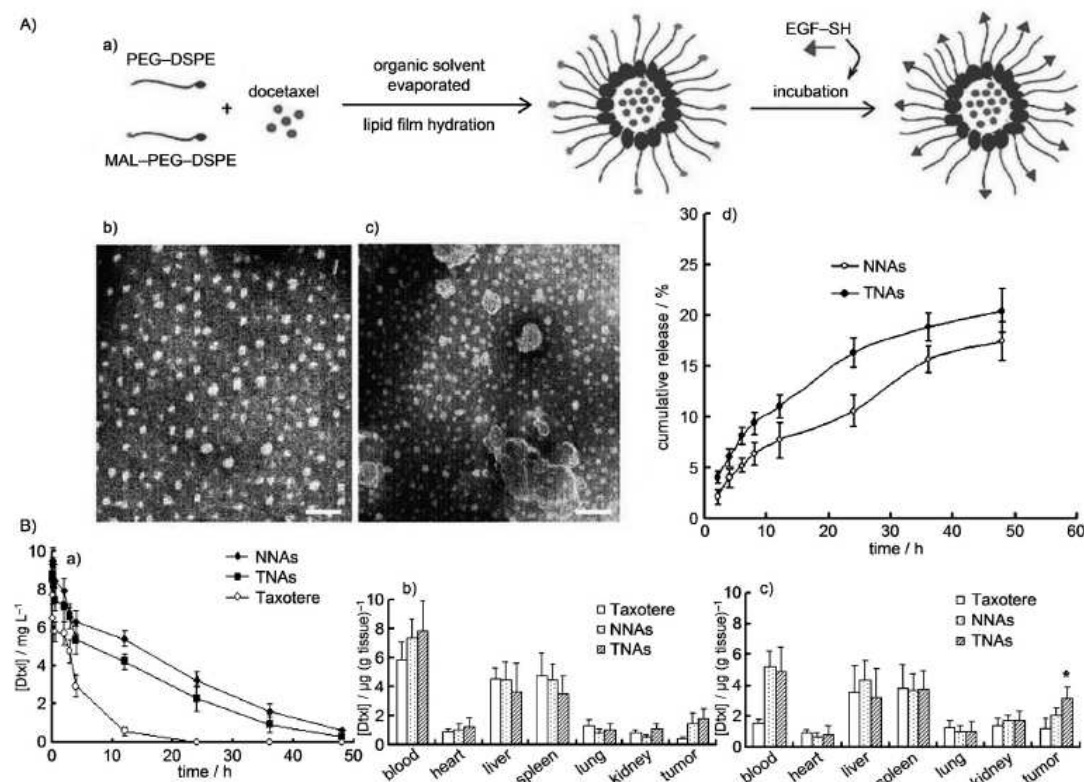


Figure 11. A) The physicochemical characteristics of nanoassemblies. a) Schematic representation of the strategy of developing targeted nanoassembly: Dis-tearoylphosphatidylethanolamine-*N*-poly(ethylene glycol)₂₀₀₀ and maleimide-derivatized PEG-DSPE were first self-assembled into nanoassemblies encapsulating docetaxel through a lipid film hydration method. The thiol-functionalized EGF was then conjugated with maleimide onto the surface of the nanoassemblies. Shown directly beneath are TEM images of b) TNAs and c) NNAs (scale bars = 100 nm). d) In vitro drug release profiles of NNAs and TNAs in pH 7.4 HBS buffer containing FBS (10% w/v). Data represent the mean \pm SEM from three independent experiments (NNAs: docetaxel-loaded nanoassemblies without EGF; TNAs: docetaxel-loaded targeted nanoassemblies with EGF). B) Pharmacokinetics and biodistribution of docetaxel in Taxotere, NNAs, or TNAs. a) Blood clearance curves of docetaxel in Taxotere, NNAs, or TNAs in healthy Sprague-Dawley rats; data represent the mean \pm SEM ($n=6$). Graphs to the right show tissue distributions of docetaxel in BALB/c mice with breast tumor nodules 9–10 mm in diameter at b) 2 and c) 12 h; data represent the mean \pm SEM ($n=6$), * $p < 0.05$ compared with the NNA group. Reprinted with permission from ref. [128], Copyright 2008 American Chemical Society.

pressure homogenization, was shown to be stable following autoclaving at 121 °C for 10 min and remained stable during a 12-month storage period at 6 ± 2 °C. The results of pharmacokinetics in rats and beagle dogs, tissue distribution, antitumor activity, safety tests, and toxicity strongly supported the feasibility of using docetaxel lipid emulsion for clinical applications owing to its biological equivalence with Taxotere, and showed that it is similar to Taxotere with regard to tissue distribution, antitumor activities, and safety, but less toxic than Taxotere.^[132]

B. Targeting agents for docetaxel delivery

As mentioned in the introduction, anticancer drug-delivery systems are usually composed of a nanocarrier and a targeting

agent. In this section, we briefly discuss and review targeting agents for potential use in anticancer drug delivery.

There are two types of targeting in nanomedicine: passive and active. Passive targeting proceeds via the EPR effect that was first discovered by Matsumura and Maeda.^[133] Some of the nanocarriers such as AuNPs can take advantage of the EPR effect. Taken alone, this effect may disclose limitations to achieving specific delivery of drugs to cancer cells, because the targeting driving force might be insufficient. Despite its passive and nonselective nature, however, this technique is still a major strategy for improving the delivery of nanomedicines to tumor sites.^[134] In particular, it is used as a complement to achieve targeting. Below, we focus on the active targeting agents in drug-delivery systems. Active-targeting approaches based on ligand modification exploit specific receptors that are overexpressed on the surface of tumor cells relative to normal

cells.^[21,38,135,136] The targeting agents in drug-delivery systems play two roles: 1) some of the targeting agents themselves play the role of anticancer drug, which can associate with tumors and prevent tumor growth; 2) they also bind small-molecule anticancer drugs and thus facilitate drug-mediate cancer cell death.

In this section, we concentrate on the second role of targeting agents, that is, we review their role as docetaxel delivery systems, such as monoclonal antibodies, peptides, folate, hyaluronic acid, fatty acid, and transferrin. The targeting agents are used together with a nanocarrier.

1. Monoclonal antibodies

Monoclonal antibodies are among the most well-known targeting agents, and they have been used with high selectivity. In research reported by Ojima et al., monoclonal antibodies were assayed against non-benign lung cancer cell lines and breast cancer cell lines, both as the nanocarrier and targeting agent for docetaxel and other anticancer drugs. The results were very promising in producing potential chemotherapeutic agents with few side effects.^[40] In an alternative strategy, a monoclonal antibody has been covalently attached to a liposome, and the resulting nanocarrier of docetaxel is discussed above in section A.5.^[128]

Targeting the EGFR pathway is an important approach for a variety of tumors using a variety of monoclonal antibodies.^[41] The EGFR is involved in malignant transformation and tumor growth through the inhibition of apoptosis, cellular proliferation, promotion of angiogenesis, and metastasis. It is also abnormally activated in many types of epithelial tumors and this typically correlates with aggressive tumor growth. Thus, in this section we concentrate on EGF, which is an efficient targeting ligand in cancer therapy for targeting EGFR-expressing tumors.^[41–44] EGFR-mediated drug delivery provides several advantages in cancer therapy such as enhanced specific cellular uptake and tumor cell penetration, maximal accumulation and penetration into tumor tissue via anti-EGFR antibodies, and decreased toxicity toward normal cells.^[41] The combination of docetaxel and anti-EGFR antibodies was proven to be efficient for gastric cancer,^[41] breast cancer,^[42] and ovarian cancer.^[43] Furthermore, some of the EGF antibodies are already in clinical use with docetaxel, and we discuss these applications below in section C.

Besides the simple combination of docetaxel and monoclonal antibodies, docetaxel and monoclonal antibodies also form docetaxel delivery systems as shown in Figure 1. For example, an antibody-modified docetaxel-loaded targeted nanostructured lipid carrier (tNLC) was designed. This formulation was used for *in vitro* and *in vivo* tests. It specifically enhanced cellular uptake and penetration into tumor cells, and maximally accumulated and penetrated into tumor sites via an anti-VEGFR-2 antibody (see Figure 12).^[44]

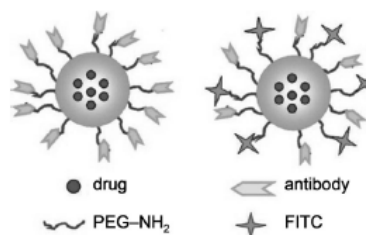


Figure 12. Schematic representation of antibody-labeled and antibody/FITC-co-labeled nanostructured lipid carriers (FITC = fluorescein isothiocyanate). Reprinted with permission from ref. [44], Copyright 2011 American Chemical Society.

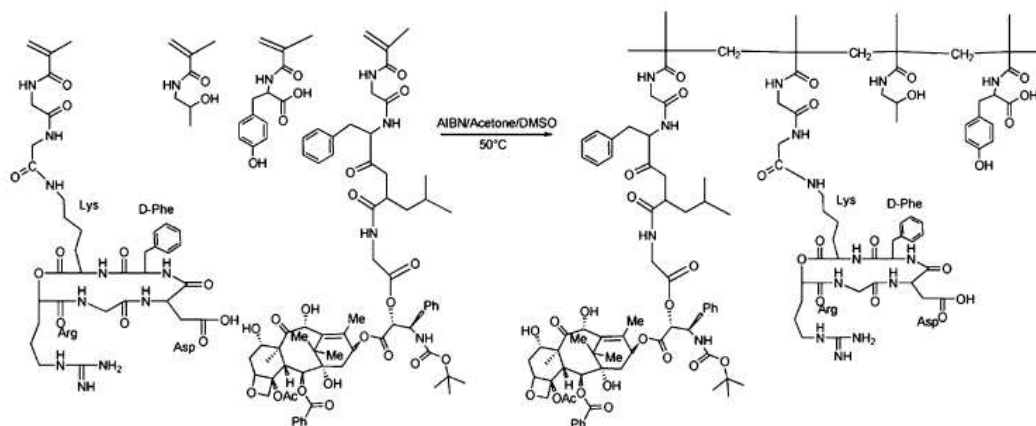
2. Peptides

Peptidic targeting agents such as vascular endothelial growth factor (VEGF), matrix metalloproteases (MMPs), and EGF have been identified for selective localization in tumor endothelial cells. Cancer cells were found to have a particular affinity for these peptides, which can therefore be used as efficient targeting agents for tumors.

For instance, the NGR peptide (Asn-Gly-Arg) showed good recognition ability as a targeting agent when conjugated to the nanocarrier PEG for delivering docetaxel to CD13-overexpressing tumors.^[137] The sequence Arg-Gly-Asp (RGD) is a selective high-affinity $\alpha_v\beta_3$ ligand. The conformationally restrained cyclic RGD binds $\alpha_v\beta_3$ with up to 200-fold higher affinity than linear peptides.^[138] The $\alpha_v\beta_3$ integrin-targeting conjugate HPMA copolymer–docetaxel–RGDfK of hydrodynamic diameter 3.0 nm resulted in a 20-fold increase in activity of conjugates over free docetaxel (Scheme 7).^[10] Moreover, RGD peptides conjugated to humanized antibodies,^[139] liposomes,^[140] and PEG^[141] improved biodistribution and increased accumulation in tumors.

3. Folate

Another current targeting agent is folate, a high-affinity ligand for folate receptors, which are expressed in various cancer cell types. Folate has been used for the construction of folate-receptor-mediated delivery systems. In a recent report, folate was used in connection with a lipid–polymer NP platform to demonstrate the potential of molecularly targeted NPs as a promising new class of radiosensitizers. The folate-targeted nanoparticle formulation of docetaxel is an effective radiosensitizer in folate-receptor-overexpressing head and neck tumor cells. The time of irradiation can be critical in achieving maximal efficacy with this nanoparticle platform. (see Figure 13 and Figure 14).^[127] Another example from Feng's research group^[142] is provided by folic acid targeting lipid shells and polymer-core nanoparticles (TLPNPs), which indicated almost full drug release ability (cumulative release nearly 90% after seven days), high cellular uptake efficiency, and decreased cytotoxicity (93% more effective than Taxotere).



Scheme 7. Synthesis and resulting structure of HPMA copolymer-RGDfK-docetaxel conjugates (select copolymers contained the monocyclized RGDfK peptide moiety for targeting docetaxel to $\alpha_v\beta_3$ integrins). Reprinted with permission from ref. [10], Copyright 2011 American Chemical Society.

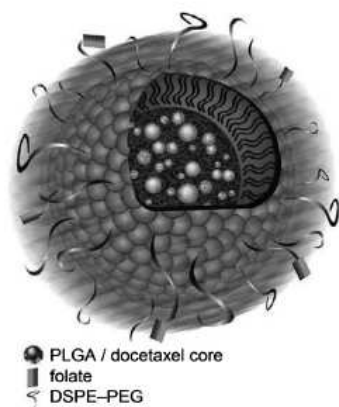


Figure 13. Depiction of nanoparticle. Reprinted with permission from ref. [127], Copyright 2011 American Chemical Society.

4. Hyaluronic acid

Hyaluronic acid (HA) is a common biocompatible and biodegradable natural substance that is composed of repeating disaccharide units of glucuronic acid and *N*-acetylglucosamine; it has seen frequent use in surgical applications for its viscoelastic properties. It is known to bind cell-surface receptors such as CD44, HAS2, and Hyal-2, which are overexpressed in several types of cancer.^[143–145] Moreover, HA offers great potential with demonstrations of good aqueous solubility and increased half-life in the body with lower toxicity. This suggests that HA would be an excellent targeting agent for the delivery of cytotoxic drugs to tumor sites. Kim and colleagues conjugated amphiphilic HA with ceramide (CE, see Scheme 8) to develop self-assembled NPs with docetaxel and Pluronic 85 (a copolymer surfactant from BASF).^[146] The *in vivo* tumor targeting efficiency of this formulation was evaluated in the MCF7/ADR tumor-

bearing mouse model by a noninvasive fluorescence imaging system. It showed a high targeting ability for CD44 receptors with an EPR effect. Thus it appears that this formulation might be useful as an anticancer drug-delivery system for CD44-over-expressing tumors.

5. Fatty acids

Fatty acids, especially polyunsaturated fatty acids (PUFAs), which are a component of vegetable oils, cold-water fish, and meat, are another group of cancer-cell targeting agents under current exploration. PUFAs are taken up more rapidly by tumor cells than by normal cells, as the higher proliferation of tumor cells requires more energy and consumes more PUFAs.^[46, 47]

The ω -6-polyunsaturated fatty acid γ -linolenic acid (GLA) garnered recent interest as a new anticancer agent, as it possesses effective tumoricidal properties while not inducing damage to normal cells or creating harmful systemic side effects. For example, Menendez et al. added GLA concurrently with docetaxel. The synergistic cytotoxicity was then observed toward estrogen-dependent MCF7 and estrogen-independent MDA-MB-231 human mammary carcinoma cell lines and additive cytotoxicity toward the estrogen-independent SK-BR3 human mammary carcinoma line.^[147] This indicated that GLA could enhance the cytotoxicity of docetaxel in human breast carcinoma cells.

6. Transferrin

Transferrin (Tf) is a homodimeric membrane protein composed of 90 kDa glycosylated subunits linked by two disulfide bonds. Due to the increased number of Tf receptors on various tumors such as lung adenocarcinoma, breast cancer, and brain cancers relative to normal cells, Tf holds significant potential as an efficient targeting agent for cancer therapeutics.^[148] It has been used in human clinical trials with adriamycin, cisplatin,

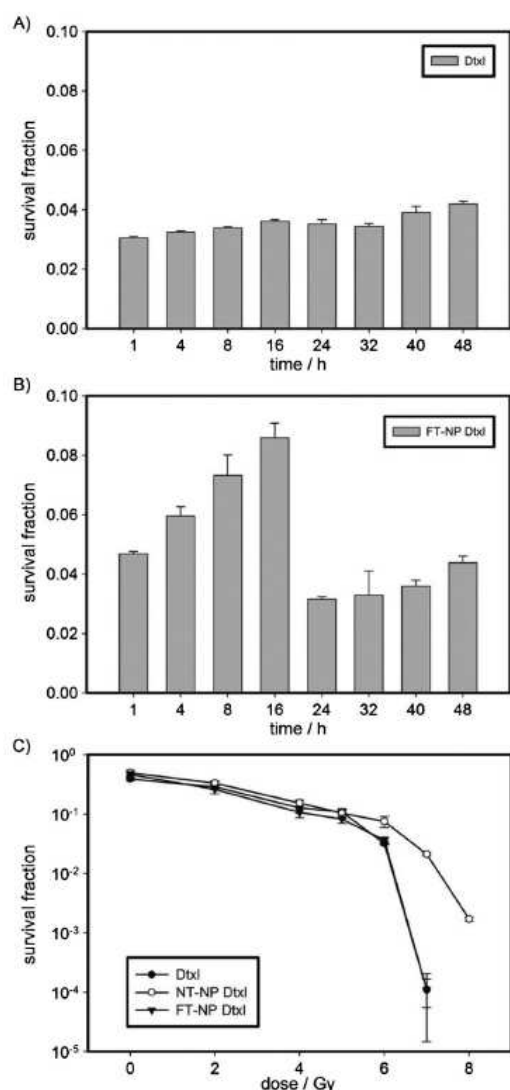


Figure 14. The timing of irradiation alters the efficacy of FT-NP Dtxl in vitro: Graphs of surviving fraction from clonogenic survival assays of KB cells treated with A) Dtxl or B) FT-NP Dtxl irradiated (4 Gy) at the indicated times. C) Clonogenic survival assay of KB cells treated with Dtxl, NT-NP Dtxl, or FT-NP Dtxl and the indicated radiation dose 24 h post-treatment. Error bars correspond to standard deviations of repeated measurements (two separate runs, three samples per time point). NT-NP: non-targeting NP; Dtxl: docetaxel. Reprinted with permission from ref. [127], Copyright 2011 American Chemical Society.

and doxorubicin,^[149–151] enhancing the efficacy and decreasing the side effects of anticancer drugs.

A recent publication reported Tf as targeting agent conjugated with docetaxel.^[152] A NP system for targeted drug delivery across the blood–brain barrier (BBB) consisted of Tf-conju-

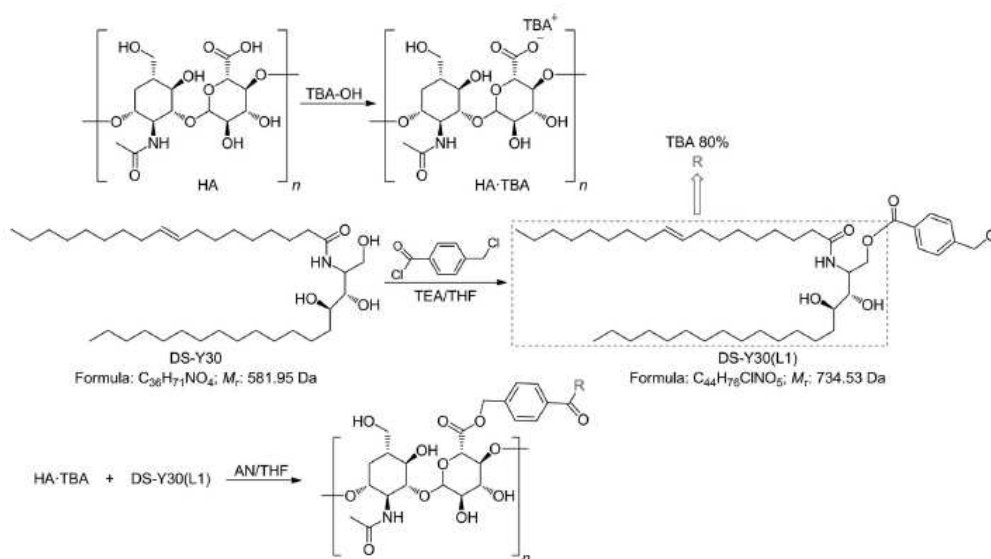
gated NPs of poly(lactide)-D- α -tocopheryl poly(ethylene glycol) succinate (PLA-TPGS) diblock copolymer. Cellular uptake and cytotoxicity of the Tf-conjugated PLA-TPGS NP formulation of docetaxel as a model drug were investigated in close comparison with those for the PLGA NP formulation, the bare PLA-TPGS NP formulation, as well as with Taxotere. The results showed that the Tf-conjugated PLA-TPGS NP formulation has significant advantages over the other two NP formulations and the original therapeutic agents. Moreover, IC_{50} data showed that the Tf-conjugated PLA-TPGS NP formulation of docetaxel could be 23, 17, and 229% more efficient than the PLGA NPs, the PLA-TPGS NPs, and Taxotere after treatment for 24 h, respectively. Finally, investigation of their preliminary ex vivo biodistribution demonstrated that the Tf-conjugated PLA-TPGS NP formulation is able to deliver imaging and therapeutic agents across the BBB.

C. Docetaxel in clinical use

1. Two formulations of docetaxel in clinical use

Besides the in vitro and in vivo tests, docetaxel has already been in applied clinical use for a long period. To the best of our knowledge, there are currently two formulations of docetaxel. The first clinical formulation is in water-soluble Polysorbate 80, also named Tween 80, E433, or Alkest TW 80, a nonionic surfactant and emulsifier derived from polyethoxylated sorbitan and oleic acid (polyoxyethylene (20) sorbitan monooleate) that includes hydrophilic polyoxyethylene groups. The trade name of the clinical formulation of docetaxel in Polysorbate 80 is Taxotere. Clinical trials have demonstrated that Taxotere could effectively decrease prostate-specific antigen (PSA) levels and improve symptoms, and even the survival rate in HRPC patients. However, the adverse effects of docetaxel treatment as Taxotere include hypersensitivity reactions, bone marrow suppression, cutaneous reactions, fluid retention, peripheral neuropathy, alopecia, cardiac disorders, and fatigue.^[12] The ethanol/Tween 80 solvent required in the formulation to increase the docetaxel solubility is at least partly responsible for the hypersensitivity reaction, decreased uptake by tumor tissue and increased exposure to other body compartments.^[13,14] Therefore, alternative formulations that circumvent these problems and selectively vectorize docetaxel to the cancer cells are needed.

The new docetaxel formulation known as BIND-014 was reported in 2010.^[48] BIND-014 is a polymeric NP that contains both a nanocarrier and a targeting agent. BIND-014 is targeted to prostate-specific membrane antigen (PSMA), a cell-surface antigen abundantly expressed on the surface of cancer cells and on new blood vessels that feed a wide array of solid tumors. BIND-014 carries docetaxel within a matrix of phosphatidylcholine (PC) covered with a coating of PEG, and ligands targeted to PSMA are embedded on the surface of the PEG coating. BIND-014 allows gradual release of docetaxel upon degradation of the PC, and the PEG encapsulation allows evasion of the body's immune response. In preclinical cancer models, BIND-014 was shown to deliver up to 20-fold more do-



Scheme 8. Synthesis of HA-CE conjugation. Reprinted with permission from ref. [146], Copyright 2011 Elsevier.

docetaxel to tumors than an equivalent dose of Taxotere.^[48] At the beginning of 2011, the phase I study of BIND-014 involved an ascending, intravenous dose design to assess the safety, tolerability, and pharmacokinetics of BIND-014 in approximately 30 cancer patients. The primary objective of the study is to determine the maximum tolerated dose of BIND-014, to assess preliminary evidence of antitumor activity, and to assess pharmacokinetic profile in cancer patients.

2. Combination of docetaxel in clinical use

Most cancer chemotherapies employ a combination of drugs. For combination treatments, it is important to assess any interactions between two or more anticancer agents in clinical use. In this section we review some of the recent literature concerning clinical combinations involving docetaxel. Docetaxel was combined with other chemotherapeutic anticancer drugs such as doxorubicin,^[153] carboplatin,^[154] and capecitabine,^[156] or other monoclonal antibodies such as trastuzumab,^[153] cetuximab,^[154] and bevacizumab^[155] to treat various types of cancers. The combinations were more efficient than the simple anticancer drugs. For example, Belani et al. reported the method of cetuximab in combination with carboplatin and docetaxel for patients with metastatic or advanced-stage non-small-cell lung cancer in a phase III study. The results indicated that the novel combination of cetuximab with docetaxel and carboplatin results in modest anticancer activity for patients with advanced cases and has an acceptable toxicity profile.^[154] In addition, the phase II and III clinical data for the capecitabine/docetaxel combination against metastatic breast cancer showed a synergistic effect compared with the simple additive effects of single-agent treatments.^[156] The clinical use of combinations

thus proves the increased efficacy of efficient drug-delivery systems for docetaxel (as with other drugs) that contain multiple drugs with targeting agents in cancer therapy.

Conclusions and Outlook

Docetaxel, as with any other anticancer drug or potential anticancer agent, is not fully devoid of side effects due to nonselective toxicity. As reviewed herein, significant efforts and improvements in docetaxel delivery for cancer therapy have taken place over the past decade. The main purpose of using various nanocarriers and targeting agents is to provide docetaxel with sufficient aqueous solubility, stability, and selectivity for tumors.

However, each nanocarrier for docetaxel delivery mentioned herein has its advantages and disadvantages. For example, PEGs have good water solubility and biocompatibility, but for use as nanocarriers, they must be functionalized with hydrophobic groups for encapsulating docetaxel. Due to their relatively small size, PEGs can easily release their drug cargo in the bloodstream before target cancer cells are reached. Another drawback involves chitosan. Although it is readily soluble under acidic conditions, it has poor solubility in basic environments, and this limits its capacity to transport anticancer drugs to tumor tissues throughout the body (thus, other modifications of the chitosan molecule would be required). A final example involves silicone NPs.^[157] The polydispersity and amorphous nature of mesoporous silica poses a major challenge in understanding and controlling the mass-transport properties at the nanometer level that are keys to drug delivery and controlled release in biological systems. Among all the current nanocarriers for docetaxel, AuNPs have not yet been the sub-

ject of many reports despite their functional flexibility. They present numerous advantages for docetaxel delivery: their lack of toxicity, biocompatibility, bioactivity, size-controlled synthesis, surface plasmon band, passive targeting, and EPR effect.^[148, 158–165] In particular, AuNPs are easy to functionalize at the surface by using thiolate ligands. Thus, they could be considered a platform for drug delivery upon functionalization with hydrophilic thiolated PEG ligands and other specific ligands linking docetaxel, active targeting agents, or other nanocarriers. At this point, no toxicity has been disclosed for non-cancer cells, and any toxicity will be due to certain (e.g., cationic) ligands. Thus PEGylated AuNPs are of particular interest. Finally, dendrimer design,^[166, 167] eventually combined with AuNPs, holds great promise thanks to powerful capacities in functionalization and encapsulation. For clinical applications, all these macromolecules will have to face the problems of polydispersity and reproducibility in commercial sources.

In conclusion, docetaxel has been extensively used alone or in combination with other anticancer drugs against various types of cancer as its Taxotere formulation during the last decade, and its clinical uses have been extensively reviewed. However, only a small fraction of docetaxel administered in this formulation reaches cancer cells, and this causes dramatic side effects and sets a limit on dosing. Consequently, intense research over the last few years has been directed toward docetaxel vectorization using a carrier connected to a targeting agent. Many studies carried out *in vitro* and *in vivo* show advantages and considerable increase in docetaxel delivery using this strategy, which has been reviewed here. The most favorable results have been obtained with some biocompatible polymers as carriers and antibodies as targeting agents, but thorough research projects are also being conducted in many other directions. Despite the current enthusiasm emanating from these publications, promises must await clinical trials of such formulations. Some of these approaches with liposomes,^[168] cyclodextrins,^[169] mixed micelles,^[170] sub-micron emulsions,^[171] and NPs^[172] have so far revealed clinical difficulties due to low entrapment efficiency, complicated preparation procedures, and low physicochemical stability in long-term storage. The only formulation that has reached phase I clinical trials (in 2010) is BIND-014, which carries docetaxel within a matrix of PC covered with a coating of PEG, and ligands targeted to PSMA that are embedded on the surface of the PEG coating. It is believed that further work should be conducted on the fundamental aspects, soon reaching clinical administration with the hope of improvement over the current Taxotere formulation. Indeed, considerable progress in vectorization nanotechnology now allows the combination of diagnosis and therapy through co-called “theranostic”^[161, 173–175] (and also eventually bypassing tumor resistance in “quadrugnostic”^[176]) approaches in a single multifunctional vector, such as gold nanoparticles, as briefly discussed above.^[154–161]

Abbreviations

AuNP: gold nanoparticle
 BBB: blood-brain barrier

CD13: cluster of differentiation 13 glycoprotein
 DSPE: 1,2-distearoyl-*sn*-glycero-3-phosphoethanolamine
 EGF: epidermal growth factor
 EGFR: epidermal growth factor receptor
 EPR: enhanced permeability and retention
 HCT15: human colon carcinoma
 HGC: hydrophobically modified glycol chitosan
 HMPA: *N*-(2-hydroxypropyl)methacrylamide
 MCF7: human breast cancer
 MDA-MB-231: human mammary carcinoma
 MEBCD: methyl- β -cyclodextrin
 MMP: matrix metalloproteinase
 NGR: Asn-Gly-Arg
 NP: nanoparticle
 PBCA: PEGylated poly(*n*-butylcyanoacrylate)
 PEG: poly(ethylene glycol)
 PEG-b-PCL: poly(ethylene glycol)-block-poly(ϵ -caprolactone)
 PEG-b-PLA: poly(ethylene glycol)-block-poly(D,L-lactic acid)
 PEO: poly(ethylene oxide)
 PLA: poly(D,L-lactic acid)
 PLGA: poly(lactic acid-co-glycolic acid)
 PLGA-b-PCB: poly(lactic acid-co-glycolic acid)-block-poly(carboxybetaine)
 PLA-TPGS: poly(lactide)-D- α -tocopheryl poly(ethylene glycol) succinate
 PUFAs: polyunsaturated fatty acids
 RGD: Arg-Gly-Asp
 SC16OH: heptakis-(2-*O*-oligo(ethyleneoxide)-6-hexadecylthio)- β -cyclodextrin
 SPB: surface plasmon band
 TEG: tetra(ethylene glycol)
 Tf: transferrin
 VEGFR: vascular endothelial growth factor receptor

Acknowledgements

Financial support for the China Scholarship Council (CSC) from the People's Republic of China (PhD grant to P.Z.), Université Bordeaux 1, Centre National de la Recherche Scientifique (CNRS), and Agence Nationale de la Recherche (ANR) is acknowledged.

Keywords: cancer · dendrimers · docetaxel · drug-delivery systems · gold nanoparticles

[1] a) ACS Cancer Facts & Figures, American Cancer Society, 2010; <http://www.cancer.org/Research/CancerFactsFigures/CancerFactsFigures/cancer-facts-and-figures-2010> (accessed March 29, 2012); b) S. Elad, Y. Zadik, I. Hewson, A. Hovan, M. E. P. Correa, R. Logan, L. S. Elting, F. K. L. Spijkervet, M. T. Brennan, *Support Care Cancer* **2010**, *18*, 993–1006; c) U. Rüther, C. Nunnensiek, H. J. Schmoll, *Secondary Neoplasias Following Chemotherapy, Radiotherapy, and Immunosuppression, Contributions to Oncology, Vol. 55* (Beiträge zur Onkologie), Karger, Freiburg/Basel, **2000** [ISBN 380557116X]; d) C. Dubernet, *Bull. Cancer* **2011**, *98*, 1363–1371.

- [2] E. Espinosa, P. Zamora, F. Jaime, B. Manuel, *Cancer Treat. Rev.* **2003**, *29*, 515–523.
- [3] J. N. Denis, A. E. Greene, D. Guénard, F. Guéritte-Voegelein, L. Mangatal, P. Potier, *J. Am. Chem. Soc.* **1988**, *110*, 5917–5919.
- [4] F. Lavelle, F. Guéritte-Voegelein, D. Guénard, *Bull. Cancer* **1993**, *80*, 326–338.
- [5] K. C. Nicolaou, R. K. Guy, P. Potier, *Sci. Am.* **1996**, *274*, 94–98.
- [6] Y. F. Wang, Q. W. Shi, M. Dong, H. Kiyota, Y. C. Gu, B. Cong, *Chem. Rev.* **2011**, *111*, 7652–7709.
- [7] F. Guéritte-Voegelein, D. Guénard, F. Lavelle, M. T. Le Giff, L. Mangatal, P. Potier, *J. Med. Chem.* **1991**, *34*, 992–998.
- [8] a) D. Guénard, F. Guéritte-Voegelein, P. Potier, *Acc. Chem. Res.* **1993**, *26*, 160–167; b) H. Lataste, V. Senilh, M. Wright, D. Guénard, P. Potier, *Proc. Natl. Acad. Sci. USA* **1984**, *81*, 4090–4094.
- [9] a) M. Montana, C. Ducros, P. Verhaeghe, T. Terme, P. Vanelle, P. Rathelot, *J. Chemother.* **2011**, *23*, 59–66; b) F. Petrelli, K. Borgonovo, S. Barni, *Expert Opin. Pharmacother.* **2010**, *11*, 1413–1432; c) E. Miele, G. P. Spinelli, F. Tomao, S. Tomao, *Int. J. Nanomed.* **2009**, *4*, 99–105.
- [10] A. Ray, N. Larson, D. B. Pike, M. Grüner, S. Naik, H. Bauer, A. Malugin, K. Greish, H. Ghandehari, *Mol. Pharmaceutics* **2011**, *8*, 1090–1099.
- [11] a) I. Youm, X. Y. Yang, J. B. Murovichick, B. B. Youan, *Nanoscale Res. Lett.* **2011**, *6*, 630; b) A. Inal, M. A. Kaplan, M. Kucukoner, A. Isikdogan, *Neoplasma* **2012**, *59*, 233–236; c) T. Narita, A. Suzuki, E. Hashizume, M. Yajima, *Gan To Kagaku Ryoho* **2012**, *39*, 119–122; d) B. Sorbe, M. Grafund, G. Horvath, M. Swahn, K. Boman, R. Bangshoj, M. Lood, H. Malmstrom, *Int. J. Gynecol. Cancer* **2012**, *22*, 47–53; e) Z. Mu, C. M. Ma, X. Chen, D. Cvetkovic, A. Pollack, L. Chen, *Phys. Med. Biol.* **2012**, *57*, 535–545; f) D. Y. Kim, D. H. Lee, S. J. Jang, S. W. Kim, C. Suh, J. S. Lee, *Cancer Res. Treat.* **2011**, *43*, 212–216; g) S. Clarke, L. Rivory, *Clin. Pharmacokin.* **1999**, *36*, 99–114.
- [12] D. P. Petrylak, *Rev. Urol.* **2006**, *8*, 548–555.
- [13] L. van Zuylen, J. Verweij, A. Sparreboom, *Invest. New Drugs* **2001**, *19*, 125–141.
- [14] V. Sanna, A. M. Roggio, A. M. Posadino, A. Cossu, S. Marceddu, A. Mariani, V. Alzari, S. Uzzau, G. Pintus, M. Sechi, *Nanoscale Res. Lett.* **2011**, *6*, 260.
- [15] K. A. Lyseng-Williamson, C. Fenton, *Drugs* **2005**, *65*, 2513–2531.
- [16] G. Thota, *Bioorg. Med. Chem.* **2007**, *15*, 3597–3623.
- [17] A. Inno, M. Basso, M. A. Cassano, C. Barone, *Clin. Med. Insights Therapeutics* **2010**, 663–680.
- [18] J. Crown, M. O'Leary, W. S. Ooi, *Oncologist* **2004**, *9*, 24–32.
- [19] D. Peer, J. M. Karp, S. Hong, O. C. Farokhzad, R. Marglit, R. Langer, *Nat. Nanotechnol.* **2007**, *2*, 751–760.
- [20] C. Mohanty, M. Das, J. R. Kanwar, S. K. Sahoo, *Curr. Drug. Delivery* **2011**, *8*, 45–56.
- [21] J. D. Byrne, T. Betancourt, L. Brannon-Peppas, *Adv. Drug Delivery Rev.* **2008**, *60*, 1615–1626.
- [22] B. Haley, E. Frenkel, *Urol. Oncol.* **2008**, *26*, 57–64.
- [23] L. E. Euliss, J. A. DuPont, S. Gratton, J. DeSimone, *Chem. Soc. Rev.* **2006**, *35*, 1095–1104.
- [24] J. M. Benito, M. Gomez-García, C. Ortiz-Mellet, I. Baussanne, J. Defaye, J. M. Garcia-Fernandez, *J. Am. Chem. Soc.* **2004**, *126*, 10355–10363.
- [25] U. Boas, P. M. H. Heegaard, *Chem. Soc. Rev.* **2004**, *33*, 43–63.
- [26] S. Svenson, A. S. Chauhan, *Nanomedicine* **2008**, *3*, 679–702.
- [27] X. C. Yang, B. Samanta, S. S. Agasti, Y. Jeong, Z. Zhu, S. Rana, O. R. Miranda, V. M. Rotello, *Angew. Chem.* **2011**, *123*, 497–501; *Angew. Chem. Int. Ed.* **2011**, *50*, 477–481.
- [28] L. Li, F. Tang, H. Liu, T. Liu, N. Hao, D. Chen, X. Teng, J. He, *ACS Nano* **2010**, *4*, 6874–6882.
- [29] P. Jain, I. H. El-Sayed, M. A. El-Sayed, *Nano Today* **2007**, *2*, 18–29.
- [30] A. S. Mikhail, C. Allen, *Biomacromolecules* **2010**, *11*, 1273–1280.
- [31] S. S. Feng, L. Mei, P. Anitha, C. W. Gan, W. Zhou, *Biomaterials* **2009**, *30*, 3297–3306.
- [32] R. M. Straubinger, S. V. Balasubramanian, *Methods Enzymol.* **2005**, *391*, 97–117.
- [33] A. L. Klibanov, K. Maruyama, V. P. Torchilin, L. Huang, *FEBS Lett.* **1990**, *268*, 235–237.
- [34] V. Maria, T. Daniel, T. Dolores, V. Anxo, F. Dominguez, J. A. Maria, *Biomacromolecules* **2008**, *9*, 2186–2193.
- [35] H. Adachi, T. Irie, K. Uekama, T. Manako, T. Yano, M. Saita, *Eur. J. Pharm. Sci.* **1993**, *1*, 117–123.
- [36] C. K. Osborne, *Breast Cancer Res. Treat.* **1998**, *51*, 227–238.
- [37] B. Yu, H. C. Tai, W. Xue, L. J. Lee, R. J. Lee, *Mol. Membr. Biol.* **2010**, *27*, 286–298.
- [38] U. Kedar, P. Phutane, S. Shidhaye, V. Kadam, *Nanomedicine* **2010**, *6*, 714–729.
- [39] X. L. Wang, R. Xu, Z. R. Lu, *J. Controlled Release* **2009**, *134*, 207–13.
- [40] I. Ojima, X. Geng, X. Wu, C. Qu, C. P. Borella, H. Xie, S. D. Wilhelm, B. A. Leece, L. M. Bartle, V. S. Goldmacher, R. V. Chari, *J. Med. Chem.* **2002**, *45*, 5620–5623.
- [41] B. Hotz, U. Keilholz, A. Fusi, H. J. Buhr, H. G. Hotz, *Gastric Cancer* **2011**, DOI: 10.1007/s10120-011-0102-9.
- [42] a) J. L. Merlin, M. B. Heyob, N. Bachmann, *Ann. Oncol.* **2002**, *13*, 1743–1748; b) X. Huang, M. Bennett, P. E. Thorpe, *Cancer Res.* **2005**, *65*, 4408–4416.
- [43] L. Wang, H. Chen, F. Liu, M. C. Madigan, C. A. Power, J. Hao, K. I. Patterson, M. H. Pourgholami, P. M. O'Brien, A. C. Perkins, Y. Li, *Cancer Lett.* **2011**, *300*, 122–133.
- [44] D. Liu, F. Liu, Z. Liu, L. Wang, N. Zhang, *Mol. Pharmaceutics* **2011**, *8*, 2291–2301.
- [45] I. Ojima, S. Lin, T. Wang, *Curr. Med. Chem.* **1999**, *6*, 927–954.
- [46] L. A. Sauer, W. O. Nagel, R. T. Dauchy, L. A. Miceli, J. E. Ausin, *Cancer Res.* **1986**, *46*, 3469–3475.
- [47] a) L. A. Sauer, J. W. Stayman, R. T. Dauchy, *Cancer Res.* **1982**, *42*, 4090–4097; b) H. Bartsch, J. Nair, R. W. Owen, *Carcinogenesis* **1999**, *20*, 2209–2218.
- [48] R. F. Service, *Science* **2010**, *330*, 314–315.
- [49] H. Ringsdorf, *J. Polym. Sci. Polym. Symp.* **1975**, *51*, 135–153.
- [50] H. Ringsdorf, H. B. Schlarb, J. Venzmer, *Angew. Chem.* **1988**, *100*, 117–162; *Angew. Chem. Int. Ed. Engl.* **1988**, *27*, 113–158.
- [51] R. Langer, *Acc. Chem. Res.* **1993**, *26*, 537–542.
- [52] H. C. Shin, A. W. Alani, D. A. Rao, N. C. Rockich, G. S. Kwon, *J. Controlled Release* **2009**, *140*, 294–300.
- [53] Z. Cao, Q. Yu, H. Xue, G. Cheng, S. Jiang, *Angew. Chem.* **2010**, *122*, 3859–3864; *Angew. Chem. Int. Ed.* **2010**, *49*, 3771–3776.
- [54] T. Etrych, M. Sirova, L. Starovoytova, B. Rihova, K. Ulbrich, *Mol. Pharmaceutics* **2010**, *7*, 1015–1026.
- [55] E. M. Enlow, J. C. Luft, M. E. Napier, J. M. DeSimone, *Nano Lett.* **2011**, *11*, 808–813.
- [56] M. J. Ernting, W. Tang, N. W. MacCallum, S. D. Li, *Biomaterials* **2012**, *33*, 1445–1454.
- [57] a) T. M. Allen, P. R. Cullis, *Science* **2004**, *303*, 1818–1822; b) U. Boas, J. B. Christensen, *Dendrimers in Medicine and Biotechnology*, Royal Chemical Society Publishing, Cambridge, **2006**; c) *Dendrimers in Medicine* (Eds.: B. Klajnert, M. Bryszewska), Nova Science Publishers, New York, **2007**; d) D. Astruc, E. Boisselier, C. Ornelas, *Chem. Rev.* **2010**, *110*, 1857–1959.
- [58] K. E. Uhrich, S. M. Cannizzaro, R. S. Langer, K. M. Shakesheff, *Chem. Rev.* **1999**, *99*, 3181–3198.
- [59] D. D. Lasic, F. J. Martin, A. Gabizon, S. K. Huang, D. Papahadjopoulos, *Biochim. Biophys. Acta.* **1991**, *1070*, 187–192.
- [60] B. G. Muller, T. Kissel, *Pharm. Pharmacol. Lett.* **1993**, *3*, 67.
- [61] V. Omelyanenko, P. Kopeckova, C. Gentry, J. Kopecek, *J. Controlled Release* **1998**, *53*, 25–37.
- [62] S. N. Pang, *J. Am. Coll. Toxicol.* **1993**, *12*, 429.
- [63] V. P. Torchilin, *J. Controlled Release* **2001**, *73*, 137–172.
- [64] C. Allen, D. Maysinger, A. Eisenberg, *Coll. Surf. B* **1999**, *16*, 1–35.
- [65] X. Wang, Y. Wang, X. Chen, J. Wang, X. Zhang, Q. Zhang, *J. Controlled Release* **2009**, *139*, 56–62.
- [66] Y. Luo, Y. Ling, W. Guo, J. Pang, W. Liu, Y. Fang, X. Wen, K. Wei, G. Xin, *J. Controlled Release* **2010**, *147*, 278–288.
- [67] K. R. Chaudhari, M. Ukawala, A. S. Manjappa, A. Kumar, P. K. Mundada, A. K. Mishra, R. Mathur, J. Mönkkönen, R. S. R. Murthy, *Pharm. Res.* **2012**, *29*, 53–68.
- [68] J. M. Anderson, M. S. Shive, *Adv. Drug Delivery Rev.* **1997**, *28*, 5–24.
- [69] L. Ilium, *Pharm. Res.* **1998**, *15*, 1326–1331.
- [70] M. Thanou, J. C. Verhoef, H. E. Junginger, *Adv. Drug Delivery Rev.* **2001**, *50*, 591–5101.
- [71] S. Şenel, S. J. McClure, *Adv. Drug Delivery Rev.* **2004**, *56*, 1467–1480.
- [72] W. Cui, X. Lu, K. Cui, J. Wu, Y. Wei, Q. Lu, *Langmuir* **2011**, *27*, 8384–8390.

- [73] G. B. Jiang, D. Quan, K. Liao, H. Wang, *Mol. Pharmaceutics* **2006**, *3*, 152–160.
- [74] R. Zarzycki, G. Rogacki, Z. Modrzejewska, K. Nawrotek, *Ind. Eng. Chem. Res.* **2011**, *50*, 5866–5872.
- [75] H. Wang, M. Roman, *Biomacromolecules* **2011**, *12*, 1585–1593.
- [76] T. Kean, M. Thanou, *Adv. Drug Delivery Rev.* **2010**, *62*, 3–11.
- [77] K. Uekama, *Chem. Pharm. Bull.* **2004**, *52*, 900–915.
- [78] T. Cserhádi, J. Hollo, *Int. J. Pharm.* **1994**, *108*, 69–75.
- [79] G. C. Ceschel, P. C. Mora, S. L. Borgia, P. Maffei, C. Ronchi, *J. Pharm. Sci.* **2002**, *91*, 2399–2407.
- [80] Y. Miyamoto, M. Nakahara, K. Motoyama, T. Ishiguro, Y. Oda, I. Okamoto, A. Yagi, H. Nishimura, F. Hirayama, K. Uekama, H. Arima, *Int. J. Pharm.* **2011**, *413*, 63–72.
- [81] N. Ono, Y. Miyamoto, T. Ishiguro, K. Motoyama, F. Hirayama, D. Iohara, H. Seo, S. Tsuruta, H. Arima, K. Uekama, *J. Pharm. Sci.* **2011**, *100*, 1935–1943.
- [82] K. Motoyama, Y. Nakashima, Y. Aramaki, F. Hirayama, K. Uekama, H. Arima, *J. Drug Delivery* **2011**, *2011*, 1–13.
- [83] T. Higashi, F. Hirayama, H. Arima, K. Uekama, *Bioorg. Med. Chem. Lett.* **2007**, *17*, 1871–1874.
- [84] R. Auzély-Velty, M. Rinaudo, *Macromolecules* **2001**, *34*, 3574–3580.
- [85] K. Uekama, F. Hirayama, T. Irie, *Chem. Rev.* **1998**, *98*, 2045–2076.
- [86] E. Lee, J. Lee, I. H. Lee, M. Yu, H. Kim, S. Y. Chae, S. Jon, *J. Med. Chem.* **2008**, *51*, 6442–6449.
- [87] E. Lee, H. Kim, I. H. Lee, S. Jon, *J. Controlled Release* **2009**, *140*, 79–85.
- [88] H. Y. Hwang, I. S. Kim, I. C. Kwon, Y. H. Kim, *J. Controlled Release* **2008**, *128*, 23–31.
- [89] T. Loftsson, M. Masson, *Int. J. Pharm.* **2001**, *225*, 15–30.
- [90] J. Králová, Z. Kejřík, T. Briza, P. Poucková, A. Kral, P. Martasek, V. Kral, *J. Med. Chem.* **2010**, *53*, 128–138.
- [91] P. Y. Grosse, F. Bressolle, F. Pinguet, *Eur. J. Cancer* **1998**, *34*, 168–174.
- [92] F. Quaglia, L. Ostacolo, A. Mazzaglia, V. Villari, D. Zaccaria, M. T. Sciortino, *Biomaterials* **2009**, *30*, 374–382.
- [93] I. Brigger, C. Dubernet, P. Couvreur, *Adv. Drug Delivery Rev.* **2002**, *54*, 631–651.
- [94] M. Faraday, *Philos. Trans.* **1857**, *147*, 145–181.
- [95] M.-C. Daniel, D. Astruc, *Chem. Rev.* **2004**, *104*, 293–346.
- [96] M. Tsoli, H. Kuhn, H. Brandau, H. Esche, G. Schmid, *Small* **2005**, *1*, 841–844.
- [97] R. Bhattacharya, P. Mukherjee, *Adv. Drug Delivery Rev.* **2008**, *60*, 1289–1306.
- [98] B. Duncan, C. Kim, V. M. Rotello, *J. Controlled Release* **2010**, *148*, 122–127.
- [99] J. C. Love, L. A. Estroff, J. K. Kriebel, R. G. Nuzzo, G. M. Whitesides, *Chem. Rev.* **2005**, *105*, 1103–1170.
- [100] B. Asadishad, M. Vossoughi, I. Alamzadeh, *Biotechnol. Lett.* **2010**, *32*, 649–654.
- [101] C. Park, H. Youn, H. Kim, T. Noh, Y. H. Kook, E. X. Oh, H. J. Park, C. Kim, *J. Mater. Chem.* **2009**, *19*, 2310–2315.
- [102] A. Francois, A. Larocque, N. Pinaud, L. Salmon, J. Ruiz, J. Robert, D. Astruc, *ChemMedChem* **2011**, *6*, 2003–2008.
- [103] A. Nan, X. Bai, S. J. Son, S. B. Lee, H. Ghandehari, *Nano Lett.* **2008**, *8*, 2150–2154.
- [104] Y. Piao, A. Bums, J. Kim, U. Wiesner, T. Hyeon, *Adv. Funct. Mater.* **2008**, *18*, 3745–3758.
- [105] N. K. Mal, M. Fujiwara, Y. Tanaka, *Nature* **2003**, *421*, 350–353.
- [106] F. Torney, B. G. Trewyn, V. S. Lin, K. Wang, *Nat. Nanotechnol.* **2007**, *2*, 295–300.
- [107] C. Y. Lai, B. G. Trewyn, D. M. Jeftinija, K. Jeftinija, S. Xu, S. Jeftinija, V. S. Lin, *J. Am. Chem. Soc.* **2003**, *125*, 4451–4459.
- [108] J. Lu, M. Liong, J. L. Zink, F. Tamanoi, *Small* **2007**, *3*, 1341–1346.
- [109] A. M. Chen, M. Zhang, D. Wei, D. Stueber, O. Taratula, T. Minko, H. He, *Small* **2009**, *5*, 2673–2677.
- [110] J. M. Rosenholm, E. Peuhu, J. E. Eriksson, C. Sahlgren, M. Linden, *Nano Lett.* **2009**, *9*, 3308–3311.
- [111] D. Chen, L. Li, F. Tang, S. Qi, *Adv. Mater.* **2009**, *21*, 3804–3807.
- [112] F. Y. Huang, W. L. Wei, Y. N. Li, G. H. Tan, H. F. Dai, J. L. Guo, H. Wang, Y. H. Huang, H. G. Zhao, S. L. Zhou, L. Li, Y. Y. Lin, *Eur. J. Cancer* **2012**, DOI: 10.1016/j.ejca.2011.12.018.
- [113] Y. Komizu, H. Ueoka, R. Ueoka, *Biochem. Biophys. Res. Commun.* **2012**, *418*, 81–86.
- [114] C. Li, J. Shen, X. Wei, C. Xie, W. Lu, *J. Drug Targeting* **2012**, *20*, 264–271.
- [115] H. Choi, S. I. Choi, G. S. Lee, D. J. Ahn, *J. Nanosci. Nanotechnol.* **2011**, *11*, 6203–6207.
- [116] J. T. Connelly, S. Kondapalli, M. Skoupi, J. S. Parker, B. J. Kirby, A. J. Baumner, *Anal. Bioanal. Chem.* **2012**, *402*, 315–323.
- [117] J. W. Choi, J. S. Lee, S. W. Kim, C. O. Yun, *Adv. Drug Deliv. Rev.* **2012**, DOI: 10.1016/j.addr.2011.12.011.
- [118] L. Hosta-Rigau, R. Chandrawati, E. Saveriades, P. D. Odermatt, A. Postma, F. Ercole, K. Breheny, K. L. Wark, B. Stadler, F. Caruso, *Biomacromolecules* **2010**, *11*, 3548–3555.
- [119] O. C. Farokhzad, R. Langer, *ACS Nano* **2009**, *3*, 16–20.
- [120] L. Zhang, J. M. Chan, F. X. Gu, J. W. Rhee, A. Z. Wang, A. F. Radovic-Moreno, F. Alexis, R. Langer, O. C. Farokhzad, *ACS Nano* **2008**, *2*, 1696–1702.
- [121] V. P. Torchilin, *Nat. Rev. Drug Discovery* **2005**, *4*, 145–160.
- [122] Phase II clinical trial of PEGylated liposomal doxorubicin (Doxil) in sarcoma: K. M. Skubitz, *Cancer Invest.* **2003**, *21*, 167–176.
- [123] L. Zhang, F. X. Gu, J. M. Chan, A. Z. Wang, R. S. Langer, O. C. Farokhzad, *Clin. Pharmacol. Ther.* **2008**, *83*, 761–769.
- [124] S. Rai, R. Paliwal, P. N. Gupta, K. Khatri, A. K. Goyal, B. Vaidya, *Curr. Nanosci.* **2008**, *4*, 30–44.
- [125] A. Fernández-Botello, F. Comelles, M. A. Alsina, P. Cea, F. Reig, *J. Phys. Chem. B* **2008**, *112*, 13834–13841.
- [126] G. Zhai, J. Wu, G. Xiang, W. Mao, B. Yu, H. Li, L. Piao, L. J. Lee, R. J. Lee, *J. Nanosci. Nanotechnol.* **2009**, *9*, 2155–2161.
- [127] M. E. Werner, J. A. Copp, S. Karve, N. D. Cummings, R. Sukumar, R. C. Li, M. E. Napier, R. C. Chen, A. D. Cox, A. Z. Wang, *ACS Nano* **2011**, *5*, 8990–8998.
- [128] Y. Gao, L. Chen, W. Gu, Y. Xi, L. Lin, Y. Li, *Mol. Pharmaceutics* **2008**, *5*, 1044–1054.
- [129] S. S. Feng, G. F. Huang, *J. Controlled Release* **2001**, *71*, 53–69.
- [130] T. Yang, M. K. Choi, F. D. Cui, S. J. Lee, S. J. Chung, C. K. Shim, *Pharm. Res.* **2007**, *24*, 2402–2411.
- [131] N. Debotton, M. Parnes, J. Kadouche, S. Benita, *J. Controlled Release* **2008**, *127*, 219–30.
- [132] M. Zhao, M. Su, X. Lin, Y. Luo, H. He, C. Cai, X. Tang, *Pharm. Res.* **2010**, *27*, 1687–1702.
- [133] Y. Matsumura, H. Maeda, *Cancer Res.* **1986**, *46*, 6387–6392.
- [134] S. E. Gratton, P. A. Ropp, P. D. Pohlhaus, J. C. Luft, V. J. Madden, M. E. Napier, J. M. Desimone, *Proc. Natl. Acad. Sci. USA* **2008**, *105*, 11613–11618.
- [135] M. Ferrari, *Nat. Rev. Cancer* **2005**, *5*, 161–171.
- [136] R. Misra, S. Acharya, F. Dilnawaz, S. K. Sahoo, *Nanomedicine* **2009**, *4*, 519–530.
- [137] R. Pasqualini, E. Koivunen, E. Ruoslahti, *Nat. Biotechnol.* **1997**, *15*, 542–546.
- [138] E. Koivunen, B. Wang, E. Ruoslahti, *Biotechnology* **1995**, *13*, 265–270.
- [139] A. J. Schraa, R. J. Kok, H. E. Moorlag, E. J. Bos, J. H. Proost, D. K. Meijer, L. F. de Leij, G. Molema, *Int. J. Cancer* **2002**, *102*, 469–475.
- [140] P. K. Dubey, V. Mishra, S. Jain, S. Mahor, S. P. Vyas, *J. Drug Targeting* **2004**, *12*, 257–264.
- [141] X. Chen, R. Park, A. H. Shahinian, J. R. Bading, P. S. Conti, *Nucl. Med. Biol.* **2004**, *31*, 11–19.
- [142] Y. Liu, K. Li, J. Pan, B. Liu, S. S. Feng, *Biomaterials* **2010**, *31*, 330–338.
- [143] L. Udabage, G. R. Browlee, S. K. Nilsson, T. J. Brown, *Exp. Cell Res.* **2005**, *310*, 205–217.
- [144] M. Serra, R. M. Rabanal, L. Miquel, C. Domenzain, A. Bassols, *J. Comp. Pathol.* **2004**, *130*, 171–180.
- [145] W. Hyung, H. Ko, J. Park, *Biotechnol. Bioeng.* **2008**, *99*, 442–54.
- [146] H. J. Cho, H. Y. Yoon, H. Koo, S. K. Ko, J. S. Shim, J. H. Lee, K. Kim, I. C. Kwon, D. K. Kim, *Biomaterials* **2011**, *32*, 7181–7190.
- [147] J. A. Menendez, S. Ropero, R. Lupu, R. Colomer, *Oncol. Rep.* **2004**, *11*, 1241–1252.
- [148] M. Singh, *Curr. Pharm. Des.* **1999**, *5*, 443–451.
- [149] W. P. Faulk, C. G. Taylor, C. J. Yeh, J. A. McIntyre, *Mol. Biother.* **1990**, *2*, 57–60.
- [150] J. F. Head, F. Wang, R. L. Elliott, *Adv. Enzyme Regul.* **1997**, *37*, 147–169.
- [151] M. Chidambaram, R. Manavalan, K. Kathiresan, *J. Pharm. Pharm. Sci.* **2011**, *14*, 67–77.
- [152] C. W. Gan, S. S. Feng, *Biomaterials* **2010**, *31*, 7748–7757.

- [153] A. Anton, A. Ruiz, M. A. Seguí, L. Calvo, M. Munoz, J. Lao, F. Sancho, L. Fernandez, *Ann. Oncol.* **2009**, *20*, 454–459.
- [154] C. P. Belani, M. T. Schreeder, R. G. Steis, R. A. Guidice, T. A. Marsland, E. H. Butler, S. S. Ramalingam, *Cancer* **2008**, *113*, 2512–2517.
- [155] R. S. Herbst, V. J. O'Neill, L. Fehrenbacher, C. P. Belani, P. D. Bonomi, L. Hart, O. Melnyk, D. Ramies, M. Lin, A. Sandler, *J. Clin. Oncol.* **2007**, *25*, 4743–4750.
- [156] N. Frances, L. Claret, R. Bruno, A. Iliadis, *Cancer Chemother. Pharm.* **2011**, *68*, 1413–1419.
- [157] I. I. Slowing, J. L. Vivero-Escoto, C. W. Wu, V. S. Lin, *Adv. Drug Delivery Rev.* **2008**, *60*, 1278–1288.
- [158] U. Dreshler, B. Erdogan, V. M. Rotello, *Chem. Eur. J.* **2004**, *10*, 5570–5579.
- [159] C. J. Murphy, A. M. Golet, J. W. Stone, P. N. Sisco, A. M. Alkilany, E. C. Goldsmith, S. C. Baxter, *Acc. Chem. Res.* **2008**, *41*, 1721–1730.
- [160] S. Lal, S. E. Clare, N. J. Halas, *Acc. Chem. Res.* **2008**, *41*, 1842–1851.
- [161] P. K. Jain, I. H. El-Sayed, M. A. El-Sayed, *Nano Today* **2007**, *2*, 18–29.
- [162] G. F. Paciotti, D. G. I. Kinston, L. Tamarkin, *Drug Dev. Res.* **2006**, *67*, 47–54.
- [163] E. Boisselier, D. Astruc, *Chem. Soc. Rev.* **2009**, *38*, 1759–1782.
- [164] A. Llevot, D. Astruc, *Chem. Soc. Rev.* **2012**, *41*, 242–257.
- [165] R. Bardhan, S. Lal, A. Joshi, N. J. Halas, *Acc. Chem. Res.* **2011**, *44*, 936–946.
- [166] D. Astruc, *C. R. Acad. Sci. Ser. IIb* **1996**, *322*, 757–766.
- [167] *Dendrimer-Based Nanomedicine* (Eds.: I. J. Majoros, J. R. Baker, Jr.), Pan Stanford Publishing, Stanford, **2008**.
- [168] M. L. Immordino, P. Brusa, S. Arpicco, B. Stella, F. Dosio, L. Cattel, *J. Controlled Release* **2003**, *91*, 417–429.
- [169] N. H. Kim, J. Y. Lee, J. S. Kim, N. K. Lee, W. J. Jang, J. G. Oh, J. Y. Lee, W. S. Kim, J.-H. Sung, K. A. Um, (SK Chemicals Co., Ltd.), "Stable Pharmaceutical Composition Containing Docetaxel and a Method of Manufacturing the Same", WO2007136219, KR, **2007**.
- [170] B. Liu, M. Yang, R. Li, Y. Ding, X. Qian, L. Yu, *Eur. J. Pharm. Biopharm.* **2008**, *69*, 527–534.
- [171] K. Gao, J. Sun, K. Liu, X. Liu, Z. He, *Drug Dev. Ind. Pharm.* **2008**, *34*, 1227–1237.
- [172] T. Musumeci, C. A. Ventura, I. Giannone, B. Ruozi, L. Montenegro, R. Pignatello, *Int. J. Pharm.* **2006**, *325*, 172–179.
- [173] F. M. Kievit, M. Zhang, *Adv. Mater.* **2011**, *23*, H217–H247.
- [174] Y. Matsumura, *Adv. Drug Delivery Rev.* **2011**, *63*, 184–192.
- [175] M. P. Melancon, M. Zhou, C. Li, *Acc. Chem. Res.* **2011**, *44*, 947–956.
- [176] A. Shapira, Y. D. Livney, *Drug Resist. Updates* **2011**, *14*, 150–153.

Received: January 26, 2012

Revised: March 16, 2012

Published online on ■■■ ■■, 0000

Chapter 2
The improvement of Functionalization of AuNPs
by “Click” Chemistry

2.1 Introduction

The copper-catalyzed alkyne-azide Huisgen-type cycloaddition, (click reaction) has considerable impact on organic, bio-organic, medicinal and materials chemistry. The case of the functionalization of AuNPs using click chemistry is especially dramatic as shown by various reports that have produced clicked AuNP in remarkably low yields.

In previous work of our group, it was shown possible to functionalize AuNP by click reaction using the Sharpless catalyst, but this “catalyst” had to be used in stoichiometric amount. Since then, we have even found that with some substrates up to 400% of CuSO₄ + sodium ascorbate is necessary for click functionalization of AuNP, which is especially damaging when the AuNP are functionalized for biomedical use because of the toxicity of copper salts.

The catalyst [Cu(hexabenzyl)Tren]Br was first prepared and probed in molecular chemistry including dendrimers by Liyuang Liang, a former PhD students in our group (2008-2011), and published a full paper concerning this catalyst (Adv. Syn. Catal. 2011). In this previous report, this catalyst was considered to be very efficient with various “click” reactions. Thus, in this chapter, we probed and reported here the use of this catalyst that is remarkably efficient in truly catalytic amounts under ambient conditions with a variety of alkyne substrates for the functionalization of azido-terminated AuNP that are an especially difficult case with AuNP functionalization..

2.2 Click Functionalization of Gold Nanoparticles Using the very Efficient Datalyst Copper (I) (Hexabenzyl) tris (2-aminoethyl)- amine Bromide

Click Functionalization of Gold Nanoparticles Using the Very Efficient Catalyst Copper(I) (Hexabenzyl)tris(2-aminoethyl)-amine Bromide

Pengxiang Zhao,^a Maxime Grillaud,^a Lionel Salmon,^b Jaime Ruiz,^a and Didier Astruc^{a,*}

^a ISM, UMR CNRS N° 5255, Univ. Bordeaux, 33405 Talence Cedex, France

Fax: (+33)-5-4000-6994; e-mail: d.astruc@ism.u-bordeaux1.fr

^b Laboratoire de Chimie de Coordination, UPR CNRS N° 8241, 205 Route de Narbonne, 31077 Toulouse Cedex 04, France

Received: November 4, 2011; Published online: ■ ■ ■, 0000

Supporting information for this article is available on the WWW under <http://dx.doi.org/10.1002/adsc.201100865>.

Abstract: Whereas previous “click” functionalization (Huisgen-type copper-catalyzed alkyne-azide cycloaddition, CuAAC) of various gold nanoparticles (AuNP) had systematically proven to be very difficult, tedious, providing low yields with the use of high amounts of copper sulfate+sodium ascorbate – the classic Sharpless catalyst, the new catalyst copper(I) (hexabenzyl)tris(2-aminoethyl)amine bromide, $[\text{Cu}(\text{I})(\text{Hexabenzyl})\text{Tren}]\text{Br}$ is shown here to be very efficient for the introduction of a large variety of organic, organometallic, dendronic and polymeric molecular fragments of various sizes, topologies and

hydrophilicities. Indeed, 0.1–0.15 equiv. of this catalyst in toluene was used in each reaction under ambient conditions for 8 to 48 h with good yields without AuNP aggregation. The new functional AuNP have been characterized by ¹H NMR, IR and UV-vis. (plasmon band) spectroscopy, cyclic voltammetry (CV), dynamic light scattering (DLS) and transmission electron microscopy (TEM).

Keywords: alkynes; azides; click chemistry; copper catalysts; dendrimers; gold nanoparticles; polymers

Introduction

Click chemistry,^[1] especially the copper-catalyzed alkyne-azide Huisgen-type cycloaddition, CuAAC,^[2] has appeared as one of the most currently used methods allowing one to bring two molecular fragments together, and is having considerable impact on organic, bio-organic, medicinal and materials chemistry.^[3] The simplicity and availability of copper sulfate and sodium ascorbate,^[2a] the most currently used catalyst that allows the performance of click chemistry in aqueous solvents, have rendered this method very popular in the last decade.^[3] A problem arising with this catalyst in molecular chemistry, however, was the low reaction rates under ambient conditions, which was a drawback for biomedical use. This problem appeared to be even more damaging for the synthesis of click dendrimers, because, in our hands, the Sharpless Cu(I) “catalyst” remained trapped inside the multiple 1,2,3-triazolyl-dendrimer branches when the dendrimers^[4] were constructed with Newkome’s 1→3 connec-

tivity.^[5] Thus, it appeared necessary to design a click catalyst in which the Cu(I) species would be protected by a polydentate nitrogen ligand that would also accelerate the reaction.^[6,7] Therefore, we have recently investigated the synthesis and use of soluble Cu(I)-Tren complexes with Tren = tris-(2-aminoethyl)amine.^[8] The parent Tren ligand $\text{N}(\text{CH}_2\text{CH}_2\text{NH}_2)_3$ is commercial and inexpensive, and hexasubstituted Tren derivatives are easily obtained by reactions of $\text{N}(\text{CH}_2\text{CH}_2\text{NH}_2)_3$ with alkyl iodides or benzyl bromide.^[9] A Tren complex, $\text{Cu}(\text{I})(\text{HexamethylTren})\text{Br}$, was first used for click chemistry by the group of Matyjaszewski who showed that it reacted 50 times faster than CuBr .^[6] Given the insolubility of this complex, we recently reported and used the new complex $[\text{Cu}(\text{I})(\text{Hexabenzyl})\text{Tren}]\text{Br}$ that is soluble in toluene and disclosed excellent efficiency for click catalysis, including for the click synthesis of dendrimers.^[10]

The case of the functionalization of gold nanoparticles (AuNP) using click chemistry is especially dra-



Click Functionalization of Gold Nanoparticles Using the Very Efficient Catalyst Copper(I) (Hexabenzyl)tris(2-aminoethyl)-amine Bromide

Pengxiang Zhao,^a Maxime Grillaud,^a Lionel Salmon,^b Jaime Ruiz,^a and Didier Astruc^{a,*}

^a ISM, UMR CNRS N° 5255, Univ. Bordeaux, 33405 Talence Cedex, France

Fax: (+33)-5-4000-6994; e-mail: d.astruc@ism.u-bordeaux1.fr

^b Laboratoire de Chimie de Coordination, UPR CNRS N° 8241, 205 Route de Narbonne, 31077 Toulouse Cedex 04, France

Received: November 4, 2011; Published online: ■ ■ ■, 0000

Supporting information for this article is available on the WWW under <http://dx.doi.org/10.1002/adsc.201100865>.

Abstract: Whereas previous “click” functionalization (Huisgen-type copper-catalyzed alkyne-azide cycloaddition, CuAAC) of various gold nanoparticles (AuNP) had systematically proven to be very difficult, tedious, providing low yields with the use of high amounts of copper sulfate+sodium ascorbate – the classic Sharpless catalyst, the new catalyst copper(I) (hexabenzyl)tris(2-aminoethyl)amine bromide, [[Cu(I)(Hexabenzyl)Tren]Br] is shown here to be very efficient for the introduction of a large variety of organic, organometallic, dendronic and polymeric molecular fragments of various sizes, topologies and

hydrophilicities. Indeed, 0.1–0.15 equiv. of this catalyst in toluene was used in each reaction under ambient conditions for 8 to 48 h with good yields without AuNP aggregation. The new functional AuNP have been characterized by ¹H NMR, IR and UV-vis. (plasmon band) spectroscopy, cyclic voltammetry (CV), dynamic light scattering (DLS) and transmission electron microscopy (TEM).

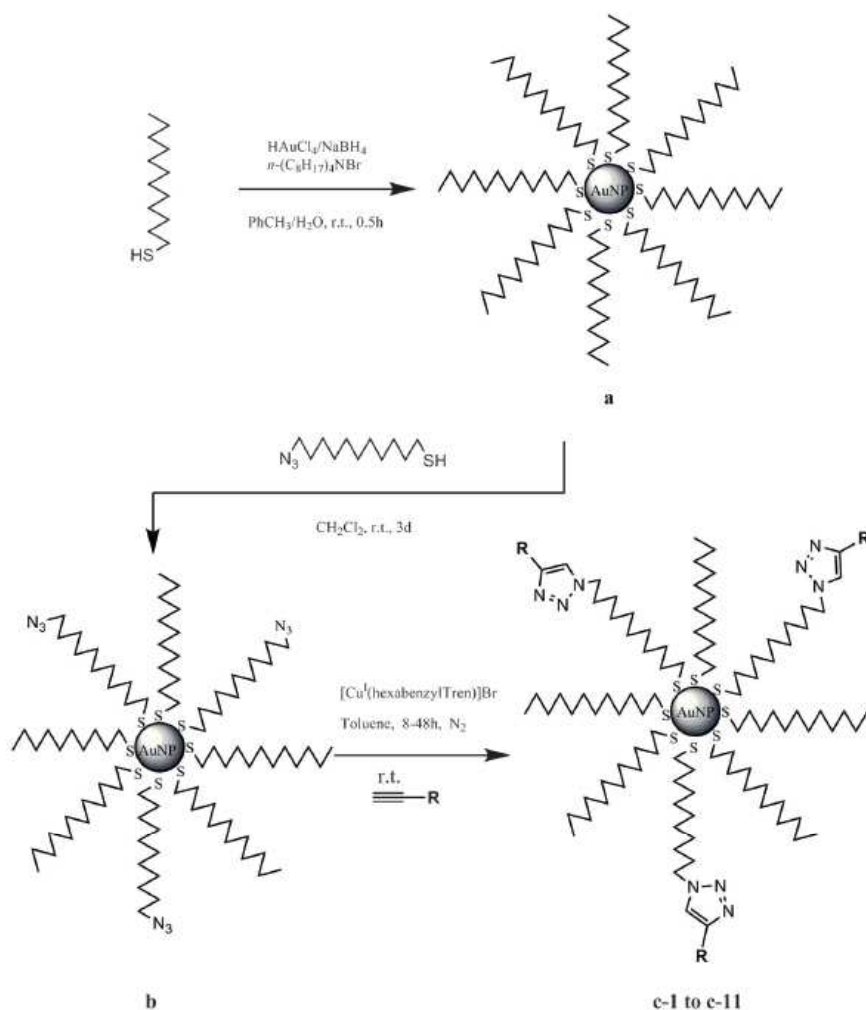
Keywords: alkynes; azides; click chemistry; copper catalysts; dendrimers; gold nanoparticles; polymers

Introduction

Click chemistry,^[1] especially the copper-catalyzed alkyne-azide Huisgen-type cycloaddition, CuAAC,^[2] has appeared as one of the most currently used methods allowing one to bring two molecular fragments together, and is having considerable impact on organic, bio-organic, medicinal and materials chemistry.^[3] The simplicity and availability of copper sulfate and sodium ascorbate,^[2a] the most currently used catalyst that allows the performance of click chemistry in aqueous solvents, have rendered this method very popular in the last decade.^[3] A problem arising with this catalyst in molecular chemistry, however, was the low reaction rates under ambient conditions, which was a drawback for biomedical use. This problem appeared to be even more damaging for the synthesis of click dendrimers, because, in our hands, the Sharpless Cu(I) “catalyst” remained trapped inside the multiple 1,2,3-triazolyl-dendrimer branches when the dendrimers^[4] were constructed with Newkome’s 1→3 connec-

tivity.^[5] Thus, it appeared necessary to design a click catalyst in which the Cu(I) species would be protected by a polydentate nitrogen ligand that would also accelerate the reaction.^[6,7] Therefore, we have recently investigated the synthesis and use of soluble Cu(I)-Tren complexes with Tren = tris-(2-aminoethyl)amine.^[8] The parent Tren ligand N(CH₂CH₂NH₂)₃ is commercial and inexpensive, and hexasubstituted Tren derivatives are easily obtained by reactions of N(CH₂CH₂NH₂)₃ with alkyl iodides or benzyl bromide.^[9] A Tren complex, Cu(I)(Hexamethyl)Tren]Br, was first used for click chemistry by the group of Matyjaszewski who showed that it reacted 50 times faster than CuBr.^[6] Given the insolubility of this complex, we recently reported and used the new complex [Cu(I)(Hexabenzyl)Tren]Br that is soluble in toluene and disclosed excellent efficiency for click catalysis, including for the click synthesis of dendrimers.^[10]

The case of the functionalization of gold nanoparticles (AuNP) using click chemistry is especially dra-



Scheme 1. Synthetic Scheme for the functionalization of AuNP using click reactions with the catalyst [Cu(I)(Hexabenzyl)-Tren]Br. The numbering of the AuNP **c-n** corresponds to those of the alkynes **n** (for instance **c-1** is the AuNP clicked with phenylacetylene, **1**, etc.).

matic as shown by various reports that have produced clicked AuNP in remarkably low yields. Brust's group introduced 2500 azide-functionalized thiolate ligands onto AuNP of 12 nm diameter and 7 lipase groups by click chemistry using excess lipase, which corresponded to 0.3% of clicked azido groups.^[11] William's group substituted 52% of the alkylthiolate ligands by reaction with bromoundecanethiols, and the substitution of the bromide by azide was achieved in 92% yield. The subsequent click reactions with several terminal alkynes (in excess) that were activated by a carbonyl linkage (*vide infra*) produced triazole rings with conversions mostly between 1 and 22% yield of 1,2,3-tri-

azole formation in various solvents (54% was obtained in one specific case).^[12] Simon's group assembled AuNP on DNA templates *via* click chemistry using a 1000-fold excess of AuNP.^[13] These repeatedly low yields showed that difficulties are encountered in the application of click chemistry to the functionalization of AuNP. They were attributed to the lack of reactivity due to solubility problems and to decomposition or aggregation of the Cu(I) catalysts,^[12] but they dramatically contrast with the exceedingly easy click reactions that are well known in organic synthesis to proceed under very mild conditions and that have made these click reactions so popular.^[2,3] Limapichat

field with applications in optics, biology, nanomedicine and catalysis.^[16] Recently, it was shown possible to functionalize AuNP by click reaction using the Sharpless catalyst, but this “catalyst” had to be used in a stoichiometric amount.^[17] Since then, we have even found that with some substrates up to 400% of CuSO₄+sodium ascorbate is necessary for click functionalization of AuNP, which is especially damaging when the AuNP are functionalized for biomedical use^[18] because of the toxicity of copper salts. We have now probed and report here the use of the catalyst [Cu(Hexabenzyl)Tren]Br that is remarkably efficient in truly catalytic amounts under ambient conditions with a variety of alkyne substrates for the functionalization of azido-terminated AuNP.

Results and Discussion

Prefunctionalization of AuNP with Azido-Terminated Thiolate Ligands

Scheme 1 indicates the general route to the functionalization of AuNPs. First, the undecylthiolate-AuNP were synthesized by the Brust–Schiffrin method^[19] and characterized *inter alia* by the UV-vis. spectroscopy disclosing, as expected, the plasmon band at 520 nm. In former work, at this stage we had conducted ligand exchange of undecylthiolate by bromoundecylthiolate ligands^[20] followed by nucleophilic substitution of bromide by azido group on the functional AuNP, but in the present study the azidoundecylthiolate ligand was advantageously used directly in ligand-exchange reaction.^[15] Thus the ligand-substitution reaction of alkylthiolate ligands by azidoundecanethiol^[14,20] provided the mixed undecathiolate-azidoundecanethiolate-AuNP (AuNP **b**) in which the proportion of azidoundecanethiolate ligands was determined by integration of the ¹H NMR signals (see the Supporting Information) and was found to be 40 ± 5%. The azido termini were then functionalized by catalyzed click reaction with various terminal alkynes using 10–15 mol% of the complex [Cu(I)(Hexabenzyl)Tren]Br as the catalyst (Figure 1).

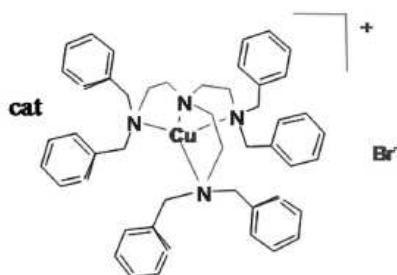


Figure 1. The catalyst [Cu(I)(Hexabenzyl)Tren]Br.

Functionalization of AuNP by Click Chemistry using the Catalyst [Cu(I)(Hexabenzyl)Tren]Br

A large variety of alkynes were used from commercial sources or prepared according to literature procedures (see the Supporting Information) including organic,^[17] organometallic^[21] and dendronic^[17,22] alkynes. In the presence of the catalyst [Cu(I)(Hexabenzyl)Tren]Br (10% catalyst for the synthesis of **c-1-c-10**; 15% catalyst for the synthesis of **c-11**), the click reactions were conducted in 8–48 h in toluene under ambient conditions, and provided isolated yields between 41% and 91% depending on the alkyne substrate. This procedure is very simple, because the catalyst and the excess alkyne are completely removed by washing the AuNP products with methanol and ether in which they are not soluble and do not aggregate.

Confirmation of Triazole Ring Formation in Click Chemistry

It is well known that, in ¹H NMR, the Knight effect perturbs the observation of signals all the more so when the atoms are closer to the AuNP surface.^[16] Thus, as compared with the free ligands, the ¹H NMR spectra of the thiolate ligands of the AuNP are much broader, and the NMR signals of the H atoms that are close to the gold surface cannot be observed. Nevertheless, the signals of the terminal groups can be readily observed, even if they are larger than in the free ligands (see the Supporting Information). Figure 2 shows an example of ¹H NMR spectrum change of the AuNP upon click reaction, in particular with the disappearance of the signal of the terminal CH₂N₃ groups of the AuNP ligands at 3.25 ppm vs.

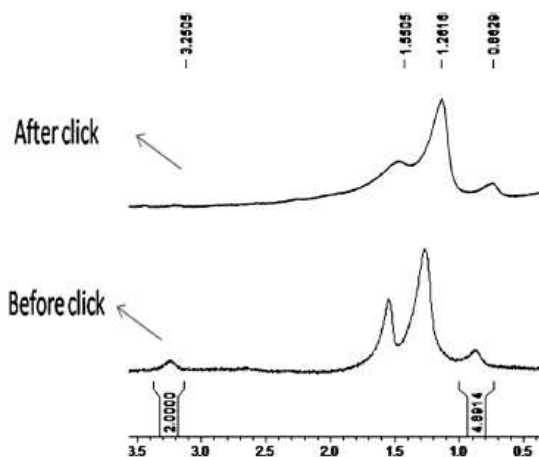


Figure 2. ¹H NMR spectra of AuNP before (AuNP **b**) and after (AuNP **c-5**) click reaction.

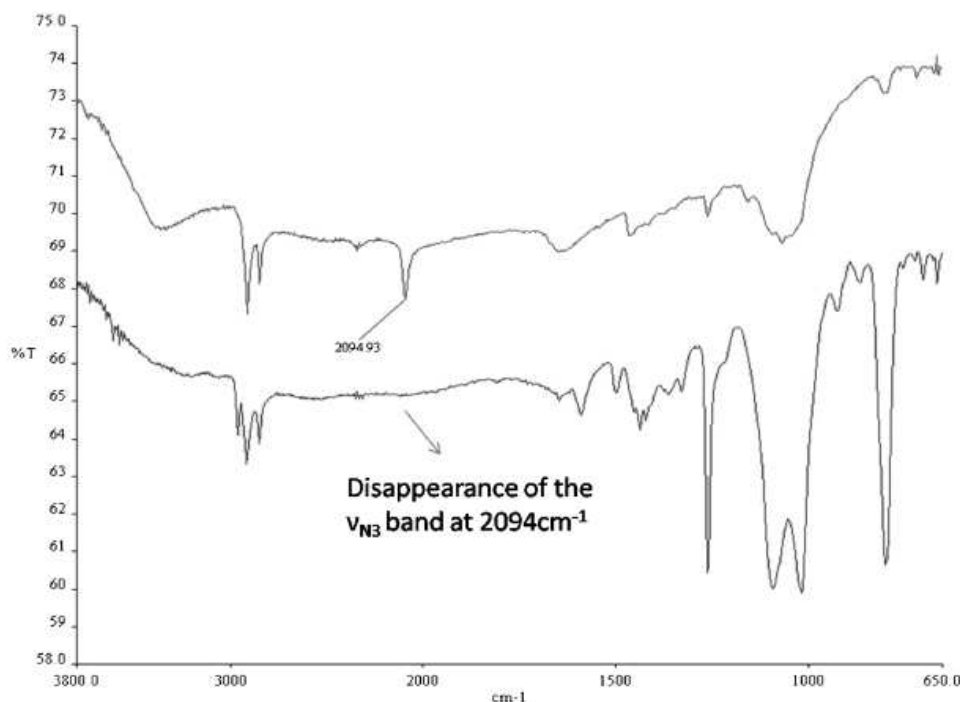


Figure 3. The IR spectra before (AuNP **b**) and after click reaction (AuNP **c-10**).

TMS in CDCl_3 . Also, sometimes, the weak signal of the single triazole proton near 7.5 ppm could be observed (see the Supporting Information). Figure 3 shows an example of infrared spectrum change upon click reaction, in particular with the disappearance of the ν_{N_3} band at 2094 cm^{-1} that was an excellent criterion of the completion of all the click reactions.

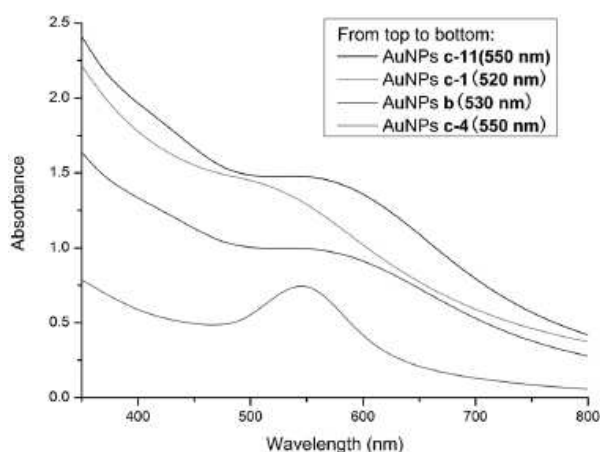


Figure 4. Plasmon band of AuNP recorded in the UV-vis spectra.

The Plasmon Band of the AuNPs: Red Shift and Increase of Extinction Coefficient

Figure 4 shows the plasmon band of four distinct AuNPs observed in their UV-vis spectra. Before the click reaction, the plasmon band of the AuNP **b** is located at 520 nm. After the click functionalization, the plasmon band has undergone a red shift; in particular the plasmon bands of **c-4** and **c-11** are shifted from 520 nm to 550 nm, respectively. Compared with the AuNP **b**, the extinction coefficient ϵ (Table 1) is also significantly increased upon click reaction. It is well known that the plasmon band of AuNP is very sensitive to various parameters such as the AuNP size, interparticle distance and refraction index of the surrounding medium.^[14] In the present case, considerable structural change occurs upon click functionalization, and the variation of the plasmon band strongly depends on this structural change that eventually influences one or several of these parameters. The plasmon band variations can also be compared to the transmission electron microscopy (TEM, Table 1) data concerning potential core-size increase (*vide infra*).

Table 1. Characteristics of the click-functionalized AuNP.

AuNP	Yield [%] ^[a]	Plasmon band: λ [nm]	Plasmon band: ϵ [M ⁻¹ cm ⁻¹]	Molecular weight [Dalton]	AuNP core (TEM [nm]) ^[b]	AuNP ^[c] diameter (DLS [nm])	PDI (DLS)	$E_{1/2}$ [V]
AuNP a	49	520						
AuNP b	89	520	2.8×10^5	1.34×10^5	2.7	24.1 ^[c]	0.390	
AuNP c-1	48	530	3.5×10^5	1.40×10^5		22.3 ^[c]	0.190	
AuNP c-2	41	530	3.9×10^5	1.45×10^5		19.6 ^[c]	0.158	0.71
AuNP c-3	78	530	3.1×10^5	1.45×10^5		28.5 ^[c]	0.383	
AuNP c-4	89	550	6.2×10^5	2.20×10^5	3.1	10.3 ^[d]	0.297	
AuNP c-5	52	540	2.9×10^5	1.38×10^5		24.6 ^[c]	0.320	
AuNP c-6	91	550	5.5×10^5	1.72×10^5		10.6 ^[c]	0.158	
AuNP c-7	88	550	5.1×10^5	1.80×10^5		10.2 ^[c]	0.138	
AuNP c-8	57	540	3.7×10^5	1.40×10^5		23.4 ^[c]	0.267	
AuNP c-9	47	530	3.2×10^5	1.52×10^5		25.0 ^[d]	0.323	
AuNP c-10	69	530	3.9×10^5	1.45×10^5		27.1 ^[c]	0.391	
AuNP c-11	75	550	4.5×10^5	1.85×10^5	2.9	23.3 ^[c]	0.241	0.54

^[a] Isolated yields.^[b] ± 0.3 nm.^[c] ± 3 nm.^[d] ± 1 nm.^[e] ± 0.05 V (vs. decamethylferrocene as the internal reference, [(*n*-Bu)₄N][PF₆] 0.1 M; CH₂Cl₂; 25 °C; 0.1 V s⁻¹).

AuNP Diameter

Figure 5 (a–c) shows the TEM images and histograms that were recorded before and after click functionalization for **c-4** and **c-11**. The diameter of the AuNP increased from 2.7 nm for **b** to 3.1 nm for **c-4** after click functionalization and to 2.9 nm for **c-11**. Thus, a slight size increase is observed, but it is hardly significant. It might eventually indicate a minute Ostwald ripening^[14a] that could at least partly explain the red shift and intensity enhancement of the plasmon band. The number of atoms and the molecular weight of each AuNP can be calculated from the core size determined by TEM (see the Supporting Information).^[15] For instance, the AuNP **b** contains 577 ± 20 gold atoms (note that Schmid's magic number with five gold atom layers is 561)^[15a,b] and the molecular weight is 1.34×10^5 Dalton.

Dynamic diameters of the AuNP: Dynamic Light Scattering

The size of the AuNP obtained from dynamic light scattering (DLS) measurements was determined in CH₂Cl₂, and can be compared with the core size investigated by TEM. The DLS measurements (Table 1) indicate much larger hydrodynamic diameters than core diameters, because they take into account the ligand bulk and also eventually the solvent molecules that would be weakly linked to the ligand termini. Baughman's group^[23] and Rinaldi's group^[24] both made similar observations when using DLS to characterize AuNP, and they attributed these results to the metallic nature of AuNP contributing to the intensity increase of scattered light and to possible aggregation of AuNP. In the present measurements of the dynamic diameter of AuNP by DLS, no significant growth of AuNP was disclosed upon click functionalization. The dynamic diameters of **c-4**, **c-6** and **c-7** are only about 10 nm which, however, is much smaller than the other

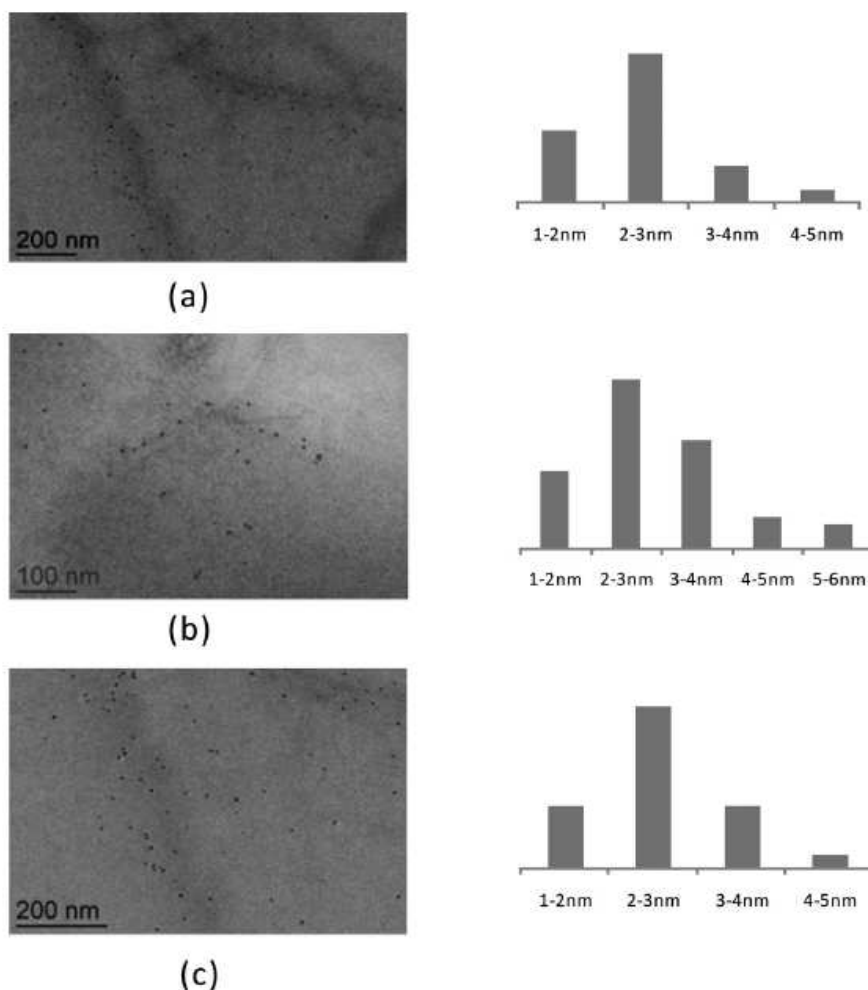


Figure 5. (a) TEM of AuNP **c-1**; (b) TEM of the AuNP **c-4**; (c) TEM of AuNP **c-11**.

click-functionalized AuNP. This might be taken into account by the model in Figure 6. As shown, the AuNP containing small molecular fragments at their periphery might “aggregate”, thus the diameter measured by DLS might contain several nanoparticles (Figure 6, a). On the other hand, for AuNP with large molecular or polymer fragments at the periphery such as in **c-4**, **c-6** and **c-7**, the diameter measured by DLS might only contain two or three nanoparticles (Figure 6, b).

Cyclic Voltammetry of AuNP Containing Redox-Active Thiolate Ligands

For AuNP containing redox-active ligands, **c-2**, and **c-11**, cyclic voltammetry (CV) confirms again their functionalization.^[14,22] For instance, Figure 7 shows the CV of **c-11** that contains dendrons with ferrocenyl ter-

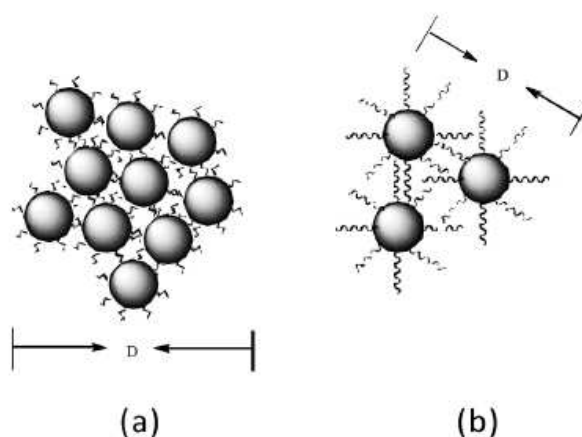


Figure 6. Model of the dynamic diameter measurement by DLS. (a) Clicked AuNP with small molecular fragments at the periphery; (b) clicked AuNP with large molecular fragments at the periphery.

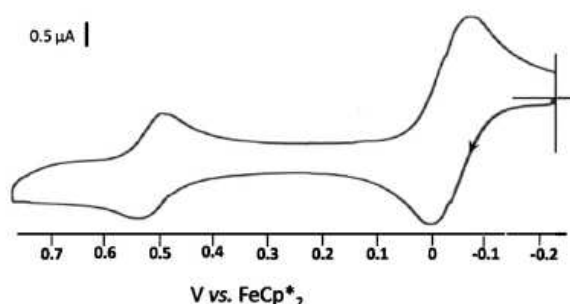


Figure 7. Cyclic voltammetry of **c-11**. $E_{1/2}=0.54$ V; $\Delta E_p=0.06$ V. Electrolyte: $[(n\text{-Bu})_4\text{N}][\text{PF}_6]$ 0.1M; working and counter electrodes: Pt; reference electrode: Ag; solvent CH_2Cl_2 ; scan rate: 0.1 V s^{-1} ; internal reference: decamethylferrocene (CV wave on the right size at 0 V).

mini introduced in the click reaction, whereby decamethylferrocene is the internal reference.^[25] In this case, $E_{1/2}=0.54$ V, which confirms the attachment of ferrocenylated dendrons in the AuNP. The difference in peak potentials for the forward and reverse scans ($\Delta E_p=0.06$ V) is not significantly different from 58 mV at 20 °C that corresponds to a reversible heterogeneous electron transfer, although the slightly broadened wave probably results from a small electrostatic effect among the three close redox sites.^[26]

Conclusions

The present study shows that the new catalyst $[\text{Cu}(\text{I})(\text{Hexabenzyl})\text{Tren}]\text{Br}$ now offers the first truly catalytic click reaction for the functionalization of AuNP with a large variety of organic, organometallic, dendronic, and polymeric alkynes of various sizes, topologies and hydrophilicities that do not include electron-deficient alkynes. It should be recalled that the Huisgen reactions of electron-deficient alkynes proceed under ambient conditions in water without catalyst, although the selectivity is not as good as with a Cu(I) catalyst.^[27] The Huisgen reaction without catalyst is also possible with electron-rich alkynes, but it requires temperatures of the order of 100 °C.^[3k,r,28] This new experimental procedure under ambient conditions with electron-rich alkynes that are quite bulky and complex molecules can be easily monitored using classical spectroscopic tools (^1H NMR, IR, and UV-vis). It does not lead to AuNP aggregation and involves an easy purification of the clicked AuNP upon only washing with methanol and ether. The successful click functionalization with polyethylene glycol and dendronic PEGs in quasi-quantitative yields should be of practical interest for biomedical applications^[29] in view of the enhanced permeation effect of PEGs in cancer diagnostic and therapy.^[30] This new synthetic

method should thus push forward the utilizations and applications of AuNP.^[15]

Experimental Section

General Data

All solvents and chemicals were used as received. ^1H NMR spectra were recorded at 25 °C with a Bruker 300 (300 MHz) spectrometer. All the chemical shifts are reported in parts per million (δ , ppm) with reference to Me_4Si for the ^1H and ^{13}C NMR spectra. The DLS measurements were made using a Malvern Zetasizer 3000 HSA instrument at 25 °C at an angle of 90°. The infrared (IR) spectra were recorded on an ATI Mattson Genesis series FT-IR spectrophotometer. UV-vis absorption spectra were measured with a Perkin-Elmer Lambda 19 UV-vis spectrometer. Electrochemical measurements were recorded on a PAR 273 potentiostat under a nitrogen atmosphere.

Synthesis of Undecanethiolate-AuNP (a)

Undecanethiolate-AuNP was obtained by the traditional Schiffrin–Brust method. Briefly, an aqueous solution of hydrogen tetrachloroaurate (30 mL, 30 mmol dm^{-3} , 0.9 mmol) was mixed with the toluene solution of tetra(octylammonium)bromide (40 mL, 100 mmol dm^{-3} , 4 mmol). The two-phase mixture was vigorously stirred until all the hydrogen tetrachloroaurate was transferred into the organic layer, and undecanethiol (0.8 mmol) was then added to the organic phase. A freshly-prepared solution of sodium borohydride (25 mL, 0.4 mol dm^{-3} , 10 mmol) was slowly added with vigorous stirring. After further stirring for 0.5 hour, the organic phase was separated and dried over sodium sulfate, then evaporated using a rotary evaporator and washed three times with ethanol; yield: 49%. ^1H NMR (CDCl_3 , 300 MHz): $\delta=1.24$ (22 H, CH_2 of undecyl chain), 0.88 (3 H, CH_3); UV-vis: plasmon band at 520 nm.

Synthesis of AuNP (b)

Undecanethiolate-AuNP (160 mg) was dissolved in CH_2Cl_2 , and azidoundecanethiol (200 mg) was added to the solution. After stirring for 3 days under N_2 at room temperature, the solvent was evaporated, and the AuNP were washed with ethanol and methanol in order to remove the excess thiol; yield: 89%. ^1H NMR (CDCl_3 , 300 MHz): $\delta=3.25$ (2 H, $\text{CH}_2\text{-N}_3$), 1.26 (22 H, CH_2 of undecyl chain), 0.88 (3 H, CH_3); UV-vis: plasmon band at 520 nm; IR: ν_{N_3} band: 2094 cm^{-1} ; DLS (dynamic light scattering): 24.1 nm; TEM: 2.7 ± 0.3 nm.

General Procedure for the Click Reaction of Undecanethiolate-AuNP with Alkynes: Synthesis of the AuNP c-I–c-II

Azidoundecanethiolate-AuNP (20 mg, 0.01 mmol azide branch, 1 equiv.) and the alkyne (0.05 mmol, 5 equiv.) were dissolved in toluene, then the solution was flushed with N_2 . $[\text{Cu}(\text{I})(\text{Hexabenzyl})\text{Tren}]\text{Br}$ (0.001 mmol, 0.1 equiv.) was added, and the solution was allowed to stir overnight at 30 °C under N_2 . After removing toluene under vacuum, the

AuNP were washed with methanol and ether in order to remove the excess alkyne and the catalyst.

Synthesis of AuNP c-1: From phenylacetylene **1** (0.05 mmol, 5 equiv., 5 mg); yield: 10 mg (48%). $^1\text{H NMR}$ (CDCl_3 , 300 MHz): $\delta=7.81$ (2H, C-CH-phenyl) 7.77 (1H, CH of triazole) 4.36 (2H, triazole- CH_2), 1.24 (22H, CH_2 of undecyl chain), 0.84 (3H, CH_3); UV-vis: the plasmon band at 530 nm, $\epsilon=3.5\times 10^5\text{ M}^{-1}\text{ cm}^{-1}$; IR: disappearance of the ν_{N_3} band at 2094 cm^{-1} ; DLS: 22.3 nm.

Synthesis of AuNP c-2: From ferrocenylacetylene **2** (0.05 mmol, 5 equiv., 12 mg); yield: 12 mg (41%). $^1\text{H NMR}$ (CDCl_3 , 300 MHz): $\delta=4.48$ (2H, triazole- CH_2), 4.29 and 4.21 (9H, Cp), 1.28 (22H, CH_2 of undecyl chain), 0.90 (3H, CH_3); UV-vis: plasmon band at 530 nm, $\epsilon=3.9\times 10^5\text{ M}^{-1}\text{ cm}^{-1}$; IR: disappearance of the ν_{N_3} band at 2094 cm^{-1} ; DLS: 19.6 nm.

Synthesis of AuNP c-3: From the dendron **3** (0.05 mmol, 5 equiv., 13 mg); yield: 17 mg (78%). $^1\text{H NMR}$ (CDCl_3 , 300 MHz): $\delta=7.21$ and 6.94 (4H, CH aromatic), 5.57 (3H, CH of allyl), 5.01 (6H, CH_2 -CH-allyl), 4.68 (2H, triazole- CH_2 -O), 2.41 (6H, CH_2 of allyl), 1.25 (22H, CH_2 of undecyl chain), 0.88 (3H, CH_3); UV-vis: plasmon band at 530 nm, $\epsilon=3.1\times 10^5\text{ M}^{-1}\text{ cm}^{-1}$; IR: disappearance of the ν_{N_3} band at 2094 cm^{-1} ; DLS: 28.5 nm.

Synthesis of AuNP c-4: From alkynyl-PEG **4** (0.05 mmol, 5 equiv., 100 mg), reaction in THF/ H_2O (1:1). After removing THF under vacuum, the aqueous phase was filtered and dialyzed for 3 days, then extracted with CH_2Cl_2 three times, and dried over sodium sulfate. The solvent was then removed under vacuum; yield: 35 mg (89%). $^1\text{H NMR}$ (CDCl_3 , 300 MHz): $\delta=7.74$ (1H, CH of triazole) 4.16 (2H, triazole- CH_2), 3.60 (180H, $\text{OCH}_2\text{CH}_2\text{O}$), 3.34 (3H, CH_3O), 2.67 (4H, - CH_2 -S-S- CH_2 -), 1.24 (22H, CH_2 of undecyl chain), 0.84 (3H, CH_3); UV-vis: plasmon band at 550 nm, $\epsilon=6.2\times 10^5\text{ M}^{-1}\text{ cm}^{-1}$; IR: disappearance of the ν_{N_3} band at 2094 cm^{-1} ; DLS: 10.3 nm; TEM: 3.1 ± 0.3 nm.

Synthesis of AuNP c-5: From propionic acid **5** (0.05 mmol, 5 equiv., 4 mg). The procedure described above for **c-1** was used; yield: 11 mg (52%). $^1\text{H NMR}$ (CDCl_3 , 300 MHz): $\delta=7.41$ (1H, CH of triazole) 3.75 (2H, triazole- CH_2), 1.30 (22H, CH_2 of undecyl chain), 0.92 (3H, CH_3); UV-vis: plasmon band at 540 nm, $\epsilon=2.9\times 10^5\text{ M}^{-1}\text{ cm}^{-1}$; IR: disappearance of the ν_{N_3} band at 2094 cm^{-1} ; DLS: 24.6 nm.

Synthesis of AuNP c-6: From **6** (0.05 mmol, 5 equiv., 30 mg). The procedure described above for **c-1** was used; yield: 23 mg (91%). $^1\text{H NMR}$ (CDCl_3 , 300 MHz): $\delta=7.29$ (1H, CH of triazole) 6.59 (2H, CH-arom), 4.49 (2H, triazole- CH_2 -O), 4.15 (8H, OCH_2 -arom and arom- OCH_2CH_2), 3.64 and 3.58 (30H, - $\text{OCH}_2\text{CH}_2\text{O}$ -), 3.37 (3H, CH_3O), 1.25 (22H, CH_2 of undecyl chain), 0.87 (3H, CH_3); UV-vis: plasmon band at 550 nm, $\epsilon=5.5\times 10^5\text{ M}^{-1}\text{ cm}^{-1}$; IR: disappearance of the ν_{N_3} band at 2094 cm^{-1} ; DLS: 10.9 nm.

Synthesis of AuNP c-7: From **7** (0.05 mmol, 5 equiv., 40 mg). The procedure described above for **c-1** was used; yield: 24 mg (88%). $^1\text{H NMR}$ (CDCl_3 , 300 MHz): $\delta=7.57$ (1H, CH of triazole) 6.77 (2H, CH-arom), 4.90 (2H, triazole- CH_2 - CH_2), 4.15 (8H, OCH_2 -arom and arom- OCH_2CH_2), 3.66 and 3.55 (48H, $\text{OCH}_2\text{CH}_2\text{O}$), 3.37 (3H, CH_3O), 1.25 (22H, CH_2 of undecyl chain), 0.88 (3H, CH_3); UV-vis: plasmon band at 550 nm, $\epsilon=5.1\times 10^5\text{ M}^{-1}\text{ cm}^{-1}$; IR: disappearance of the ν_{N_3} band at 2094 cm^{-1} ; DLS: 10.2 nm.

Synthesis of AuNP c-8: From ethynylcobalticinium hexafluorophosphate **8** (0.05 mmol, 5 equiv., 6 mg). The procedure described above for **c-1** was used; yield: 12 mg (57%). $^1\text{H NMR}$ (CDCl_3 , 300 MHz): $\delta=7.51$ (1H, CH of triazole), 5.87, 5.77 and 5.28 (9H, Cp), 1.25 (22H, CH_2 of undecyl chain), 0.89 (3H, CH_3); UV-vis: plasmon band at 540 nm, $\epsilon=3.7\times 10^5\text{ M}^{-1}\text{ cm}^{-1}$; IR: disappearance of the ν_{N_3} band at 2094 cm^{-1} ; DLS: 23.4 nm.

Synthesis of AuNP c-9: From the iron complex **9** (0.05 mmol, 5 equiv., 19 mg). The procedure described above for **c-1** was used; yield: 11 mg (47%). $^1\text{H NMR}$ (CD_3CN , 300 MHz): $\delta=7.61$ (1H, - NHCO -), 7.45 (1H, CH of triazole), 4.97 and 4.70 (5H, Cp), 4.15 (2H, - CONH-CH_2 -), 2.40 (15H, CH_2 -Cp), 2.13, 1.28 (22H, CH_2 of undecyl chain), 0.89 (3H, CH_3); UV-vis: plasmon band at 530 nm, $\epsilon=3.2\times 10^5\text{ M}^{-1}\text{ cm}^{-1}$; IR: disappearance of the ν_{N_3} band at 2094 cm^{-1} ; DLS: 25.0 nm.

Synthesis of AuNP c-10: From the dendron **10** (0.05 mmol, 5 equiv., 26 mg). The procedure described above for **c-1** was used; yield: 17 mg (69%). $^1\text{H NMR}$ (CDCl_3 , 300 MHz): $\delta=6.94$ (2H, CH aromatic), 6.03 (3H, CH of allyl), 5.01 (6H, CH_2 -CH-allyl), 4.51 (8H, OCH_2 -arom and arom- OCH_2CH_2), 4.15 (2H, triazole- CH_2 -O), 2.41 (6H, CH_2 of allyl), 1.21 (22H, CH_2 of undecyl chain), 0.92 (3H, CH_3); UV-vis: plasmon band at 530 nm, $\epsilon=3.9\times 10^5\text{ M}^{-1}\text{ cm}^{-1}$; IR: disappearance of the ν_{N_3} band at 2094 cm^{-1} ; DLS: 27.1 nm.

Synthesis of AuNP c-11: From the dendron **11** (0.05 mmol, 5 equiv., 55 mg). The procedure described above for **c-1** was used; yield: 23 mg (75%). $^1\text{H NMR}$ (CDCl_3 , 300 MHz): $\delta=7.21$ and 6.91 (12H, CH-arom), 4.33 and 4.07 (27H, Cp), 4.10 (2H, triazole- CH_2), 1.89 (6H, - $\text{CH}_2\text{CH}_2\text{CH}_2\text{Si}$ -), 1.31 (22H, CH_2 of undecyl chain), 1.09 (6H, - $\text{CH}_2\text{CH}_2\text{CH}_2\text{Si}$ -), 0.91 (3H, CH_3), 0.64 (6H, - $\text{CH}_2\text{CH}_2\text{Si}$ -), 0.19 (18H, CH_2 -Si- CH_3); UV-vis: plasmon band at 550 nm, $\epsilon=4.5\times 10^5\text{ M}^{-1}\text{ cm}^{-1}$; IR: disappearance of the ν_{N_3} band at 2094 cm^{-1} ; DLS: 23.3 nm; TEM: 2.9 ± 0.3 nm.

Supporting Information

All spectra with data ($^1\text{H NMR}$, UV-vis, and infrared), TEM with histograms and DLS data of AuNP and CV of AuNPs containing redox-active ligands are available in the Supporting Information.

Acknowledgements

Financial support from the China Scholarship Council (CSC) from the People's Republic of China (Ph. D. grant to PZ), the Université Bordeaux I, the Centre National de la Recherche Scientifique (CNRS) and the Agence Nationale de la Recherche (ANR) is gratefully acknowledged.

References


- [1] H. C. Kolb, M. G. Finn, K. B. Sharpless, *Angew. Chem.* **2001**, *113*, 2056–2075; *Angew. Chem. Int. Ed.* **2001**, *40*, 2004–2021.

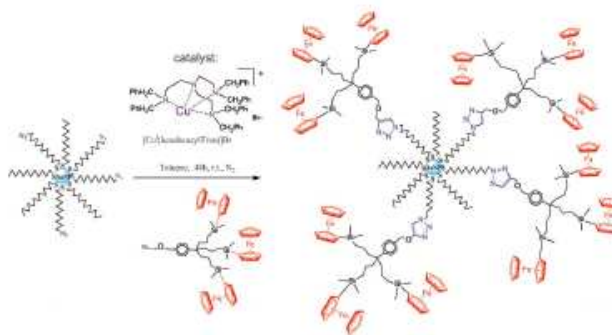
- [2] a) V. V. Rostovtsev, L. G. Green, V. V. Fokin, K. B. Sharpless, *Angew. Chem.* **2002**, *114*, 2708–2711; *Angew. Chem. Int. Ed.* **2002**, *41*, 2596–2599; b) C. W. Tornøe, C. Christensen, M. Meldal, *J. Org. Chem.* **2002**, *67*, 3057–3064.
- [3] a) V. D. Bock, H. Hiemstra, J. H. van Maarseveen, *Eur. J. Org. Chem.* **2006**, 51–68; b) W. H. Binder, R. Sachsenhofer, *Macromol. Rapid Commun.* **2007**, *28*, 15–54; c) D. Fournier, R. Hoogenboom, U. S. Schubert, *Chem. Soc. Rev.* **2007**, *36*, 1369–1380; d) M. Meldal, C. W. Tornøe, *Chem. Rev.* **2008**, *108*, 2952–3015; e) J. F. Lutz, Z. Zarafshani, *Adv. Drug Delivery Rev.* **2008**, *60*, 958–970; f) J. F. Lutz, H. G. Börner, *Prog. Polym. Sci.* **2008**, *33*, 1–39; g) B. Droumaguet, K. Velonia, *Macromol. Rapid Commun.* **2008**, *29*, 1073–1089; h) G. Franc, A. Kakkar, *Chem. Commun.* **2008**, 5267–5276; i) W. H. Binder, R. Zirbs, *Encyclopedia of Polymer Science and Technology*, Wiley, New York, **2009**; j) H. R. Marsden, A. Kros, *Macromol. Biosci.* **2009**, *9*, 939–951; k) J. E. Hein, V. V. Fokin, *Chem. Soc. Rev.* **2010**, *39*, 1302–1315; l) P. L. Golas, K. Matyjaszewski, *Chem. Soc. Rev.* **2010**, *39*, 1338–1354; m) B. S. Sumerlin, A. P. Vogt, *Macromolecules* **2010**, *43*, 1–13; n) U. Mansfeld, C. Pietsch, R. Hoogenboom, C. R. Becer, U. S. Schubert, *Polym. Chem.* **2010**, *1*, 1560–1598; o) H. Struthers, T. L. Mindt, R. Schibli, *Dalton Trans.* **2010**, *39*, 675–696; p) M. D. Best, *Biochemistry* **2009**, *48*, 6571–6584; q) D. G. Mullen, D. Q. McNerny, A. Desai, X. Cheng, S. C. DiMaggio, A. Kotlyar, Y. Zhong, S. Qin, C. V. Kelly, T. P. Thomas, I. Majoros, B. G. Orr, J. R. Baker, M. M. B. Holl, *Bioconjugate Chem.* **2011**, *22*, 679–689; r) L. Liang, D. Astruc, *Coord. Chem. Rev.* **2011**, *255*, 2933–2945.
- [4] a) C. Ornelas, J. Ruiz, E. Cloutet, S. Alves, D. Astruc, *Angew. Chem.* **2007**, *119*, 890–895; *Angew. Chem. Int. Ed.* **2007**, *46*, 872–877; b) R. Djeda, A. Rapakousiou, L. Liang, N. Guidolin, J. Ruiz, D. Astruc, *Angew. Chem.* **2010**, *122*, 8328–8332; *Angew. Chem. Int. Ed.* **2010**, *49*, 8152–8156.
- [5] a) G. R. Newkome, Z. Yao, G. R. Baker, V. K. Gupta, *J. Org. Chem.* **1985**, *50*, 2003–2004; b) G. R. Newkome, C. Shreiner, *Chem. Rev.* **2010**, *110*, 6338–6442.
- [6] a) P. L. Golas, N. V. Tsarevsky, B. S. Sumerlin, K. Matyjaszewski, *Macromolecules* **2006**, *39*, 6451–6457; b) P. L. Golas, N. V. S. Tsarevsky, K. Matyjaszewski, *Macromol. Rapid Commun.* **2008**, *29*, 1167–1171.
- [7] a) V. O. Rodionov, V. I. Presolski, S. Gardiner, Y. H. Lim, M. G. Finn, *J. Am. Chem. Soc.* **2007**, *129*, 12696–12704; b) V. O. Rodionov, V. I. Presolski, D. D. Diaz, V. V. Fokin, M. G. Finn, *J. Am. Chem. Soc.* **2007**, *129*, 12705–12712.
- [8] N. Candelon, D. Lastécouères, A. K. Diallo, J. Ruiz, D. Astruc, J.-M. Vincent, *Chem. Commun.* **2008**, 741–743.
- [9] a) R. Morassi, L. Sacconi, *Inorg. Synth.* **1976**, *16*, 174–180; b) G. Andereg, *Inorg. Chim. Acta* **1986**, *111*, 25–30; c) L. A. Carpino, D. Sadat-Aalae, M. Bayermann, *J. Org. Chem.* **1990**, *55*, 1673–1675; d) D. Chen, A. E. Martell, *Tetrahedron* **1991**, *47*, 6895–6902; e) V. Percec, A. V. Popov, E. Ramirez-Castillo, O. Weichold, *Polym. Chem.* **2003**, *41*, 3283–3299; f) G. Barré, D. Taton, D. Lastécouère, J.-M. Vincent, *J. Am. Chem. Soc.* **2004**, *126*, 7764–7765.
- [10] L. Liang, J. Ruiz, D. Astruc, *Adv. Synth. Catal.* **2011**, *353*, 3434–3450.
- [11] J. L. Brennan, N. S. Hatzakis, T. R. Tikhudo, N. Dirvianskyte, V. Razumas, S. Patkar, J. Vind, A. Svendsen, R. J. M. Nolte, A. E. Rowan, M. Brust, *Bioconjugate Chem.* **2006**, *17*, 1373–1375.
- [12] a) D. A. Fleming, C. J. Thode, M. E. Williams, *Chem. Mater.* **2006**, *18*, 2327–2334; b) C. J. Thode, M. E. Williams, *J. Colloid Interface Sci.* **2008**, *320*, 346–352.
- [13] M. Fischler, A. Sologubenko, J. Mayer, G. Clever, G. Burley, J. Gierlich, T. Carell, U. Simon, *Chem. Commun.* **2008**, 169–171.
- [14] W. Limapichat, A. Basu, *J. Colloid Interface Sci.* **2008**, *318*, 140–144.
- [15] a) W. J. Sommer, M. Weck, *Langmuir* **2007**, *23*, 11991–11995; b) W. Ostwald, *Lehrbuch der Allgemeinen Chemie*, **1896**, Vol. 2, Part 1, Leipzig; c) M. Kahlweit *Advan. Coll. Interf. Sci.* **1975**, *5*, 1–35.
- [16] a) G. Schmid, M. Bäuml, M. Geerskens, I. Heim, C. Osemann, T. Sawitowski, *Chem. Soc. Rev.* **1999**, *28*, 179–185; b) M.-C. Daniel, D. Astruc, *Chem. Rev.* **2004**, *104*, 293–346; c) V. R. Reddy, *Synlett* **2006**, 1791–1792; d) J. K. Ling, M. Maier, B. Okenve, V. Kotaidis, H. Ballot, A. Plech, *J. Phys. Chem. B* **2006**, *110*, 15700–15707; e) B. K. Pong, H. I. Elim, J. Chong, W. Ji, B. L. Trout, J. Y. Lee, *J. Phys. Chem. C* **2007**, *111*, 6281–6287; f) J. D. Gibson, B. P. Khanal, E. R. Zubarev, *J. Am. Chem. Soc.* **2007**, *129*, 11653–11661; g) S. D. Perrault, W. C. W. Chan, *J. Am. Chem. Soc.* **2009**, *131*, 17042–17043.
- [17] E. Boisselier, L. Salmon, J. Ruiz, D. Astruc, *Chem. Commun.* **2008**, 5788–5790.
- [18] A. François, A. Laroche, N. Pinaud, L. Salmon, J. Ruiz, J. Robert, D. Astruc, *ChemMedChem* **2011**, *6*, 2003–2006.
- [19] M. Brust, M. Walker, D. Bethell, D. J. Schiffrin, R. Whyman, *J. Chem. Soc. Chem. Commun.* **1994**, 801–802.
- [20] a) A. C. Templeton, W. P. Wuelfing, R. W. Murray, *Acc. Chem. Res.* **2000**, *33*, 27–36; b) R. M. Crooks, M. Zhao, L. Sun, V. Chechik, L. K. Yeung, *Acc. Chem. Res.* **2001**, *34*, 181–190; c) Q. Dai, J. G. Worden, J. Trullinger, Q. Huo, *J. Am. Chem. Soc.* **2005**, *127*, 8008–8009; d) H. Duan, M. Kuang, G. Zhang, D. G. Kurth, H. Mohwald, *Langmuir* **2005**, *21*, 11495–11499; e) S. Nuss, H. Bottcher, H. Wurm, M. L. Hallensleben, *Angew. Chem.* **2001**, *113*, 4137–4139; *Angew. Chem. Int. Ed.* **2001**, *40*, 4016–4018.
- [21] a) M. Lacoste, F. Varret, L. Toupet, D. Astruc, *J. Am. Chem. Soc.* **1987**, *109*, 6504–6506; b) M.-H. Desbois, D. Astruc, J. Guillin, F. Varret, A. X. Trautwein, G. Ville-neuve, *J. Am. Chem. Soc.* **1989**, *111*, 5800–5809; c) M. Wildchek, C. Rieker, P. Jaitner, H. Schottenberger, K. E. J. Schwarzans, *J. Organomet. Chem.* **1990**, *396*, 355–361; d) R. Djeda, C. Ornelas, J. Ruiz, D. Astruc, *Inorg. Chem.* **2010**, *49*, 6085–6101; e) A. K. Diallo, S. Manuel, E. Monflier, J. Ruiz, D. Astruc, *Tetrahedron Lett.* **2010**, *51*, 4617–4619.
- [22] a) M.-C. Daniel, J. Ruiz, S. Nlate, J.-C. Blais, D. Astruc, *J. Am. Chem. Soc.* **2003**, *125*, 2617–2628; b) A. K. Diallo, E. Boisselier, L. Liang, J. Ruiz, D. Astruc, *Chem. Eur. J.* **2010**, *16*, 11832–11835.

- [23] J. Wilcoxon, R. Williamson, R. Baughman, *J. Chem. Phys.* **1993**, *98*, 9933–9950.
- [24] A. P. Herrera, O. Resto, J. G. Briano, C. Rinaldi, *Nanotechnology* **2005**, *16*, S618–S625.
- [25] a) N. Connelly, W. E. Geiger, *Chem. Rev.* **1996**, *96*, 877–910; b) J. Ruiz, D. Astruc, *C. R. Acad. Sci. Paris, t. 1, Sér. II c*, **1998**, 21–27.
- [26] A. J. Bard, L. R. Faulkner, *Electrochemical Methods: Fundamentals and Applications*, 2nd edn., John Wiley & Sons, New York, **2001**.
- [27] Z. Li, T. S. Seo, J. Ju, *Tetrahedron Lett.* **2004**, *45*, 3143.
- [28] R. Huisgen, *Angew. Chem.* **1963**, *75*, 604–637; *Angew. Chem. Int. Ed. Engl.* **1963**, *2*, 565–570.
- [29] a) D. Astruc, *C. R. Acad. Sci. Sér. II b*, **1996**, 322, 757–766; b) R. Haag, *Angew. Chem.* **2004**, *116*, 280–284; *Angew. Chem. Int. Ed.* **2004**, *43*, 278–282; c) E. Boisselier, D. Astruc, *Chem. Soc. Rev.* **2009**, *38*, 1759–1782.
- [30] a) Y. Matsumura, H. Maeda, *Cancer Res.*, **1986**, *46*, 6387–6392; b) S. H. Jang, M. G. Wientjes, D. Lu, *Pharm. Res.* **2003**, *20*, 1337–1350; c) C. Lee, J. A. McKay, J. M. J. Fréchet, F. C. Szoda, *Nature Biotechnol.* **2005**, *23*, 1517–1526; d) R. T. Poon, N. Borys, *Expert Opin. Pharmacother.* **2009**, *10*, 333–343.

12 Click Functionalization of Gold Nanoparticles Using the Very Efficient Catalyst Copper(I) (Hexabenzyl)tris(2-aminoethyl)-amine Bromide

Adv. Synth. Catal. **2012**, *354*, 1–12

 Pengxiang Zhao, Maxime Grillaud, Lionel Salmon, Jaime Ruiz, Didier Astruc*



The support information of this paper is available on the internet.

<http://onlinelibrary.wiley.com/doi/10.1002/adsc.201100865/pdf> (if

needed)



Chapter 3
Biomedical Applications of Gold Nanoparticles

3.1 Introduction

This chapter is composed of two sections. Both of them concern the biocompatible AuNPs containing PEG ligands, and their applications on biology.

The first section deals with the encapsulation of docetaxel by PEG functionalized AuNPs for potential applications to cancer therapy. This involves the collaboration work with Dr Gillian Barratt's group at the Faculté de Pharmacie of the Université Paris Sud in Châtenay-Malabry. The novel drug delivery system (DDS) in the present of AuNPs and the covalent linked targeting agent folic acid was prepared in Bordeaux, and the biotests were carried out in Châtenay-Malabry with the collaboration of Prof Gillian Barratt's group with the help of Rachel Oliveira.

The second section demonstrates the encapsulation of water soluble vitamins (B3, B6, B9 and C) by thiolate-mPEG protected AuNPs. The vitamins could be encapsulated into hydrophobic core of AuNPs by the mPEG ligand. Due to the biocompatibility of PEG, the PEG capped AuNPs with encapsulated vitamins have potential applications in the hydrophobic part of human bodies.

3.2 Gold Nanoparticles on Docetaxel Drug Delivery Systems.

Folate-functionalized Gold Nanoparticles for Anti-cancer Docetaxel Delivery

Abstract

In this study, a novel drug delivery system for docetaxel was prepared. Firstly, the PEG and mPEG-coated AuNPs were synthesized, followed by covalent functionalization with folic acid at the PEG termini. This structure of this system was confirmed by ¹H NMR, TEM, UV-vis spectroscopy and Dynamic Light Scattering (DLS). Tests in cell culture using AuNPs with encapsulated docetaxel were carried out to evaluate the efficiency of this drug delivery system.

Key words: gold nanoparticles, docetaxel, folic acid, drug delivery system

Introduction

Drug carriers are attracting increasing interest in nanomedicine, especially for cancer treatment.¹⁻⁴ In particular, liposomes,⁵ polymer nanoparticles,⁶ nanocapsules,⁷ silica

nanorattles⁸ and dendrimers^{9,10} have been widely investigated. Among nano-sized carriers, gold nanoparticles¹² are a very attractive non-toxic family that provide theranostic (combined diagnostic and therapeutic) functions.¹³⁻¹⁹

Docetaxel²⁰⁻²⁵ is, together with paclitaxel, one of the most powerful anticancer drugs in the taxane family. Compared with other currently used anticancer drugs, it has a broad spectrum of activity against a variety of tumors. Despite successful performances by docetaxel against several kinds of tumors,²⁶⁻³⁴ there are still severe limitations such as its poor aqueous solubility (normally at the level of $\mu\text{g/ml}$) and its systematic toxicity.^{25,32,33}

In a previous study of our group using “passive” targeting of docetaxel, PEG-functionalized AuNPs were shown to greatly increase the solubility of docetaxel. Delivery of PEGylated AuNP-encapsulated docetaxel was studied *in vitro* with human colon carcinoma (HCT15) and human breast cancer (MCF7) cells. AuNPs alone presented no cytotoxicity towards either MCF7 or HCT15 adenocarcinoma cells. The AuNP-loaded docetaxel was 2.5-fold more efficient than docetaxel against MCF7 cells, and the IC_{50} of AuNP-docetaxel in HCT15 cells was lower than that of docetaxel.¹⁴

In the present article, we describe a new drug delivery system (DDS) involving “active” targeting with PEG-coated AuNPs with covalently bound folate at the termini, encapsulating docetaxel by non covalent supramolecular interactions. In this system, folate is the active targeting agent, while the AuNPs played a role of nanocarrier for docetaxel delivery. To our knowledge, it is the first time that folate has been covalently bound to AuNP for docetaxel delivery. The efficiency of this system was investigated by an *in-vitro* study.

Results and discussion

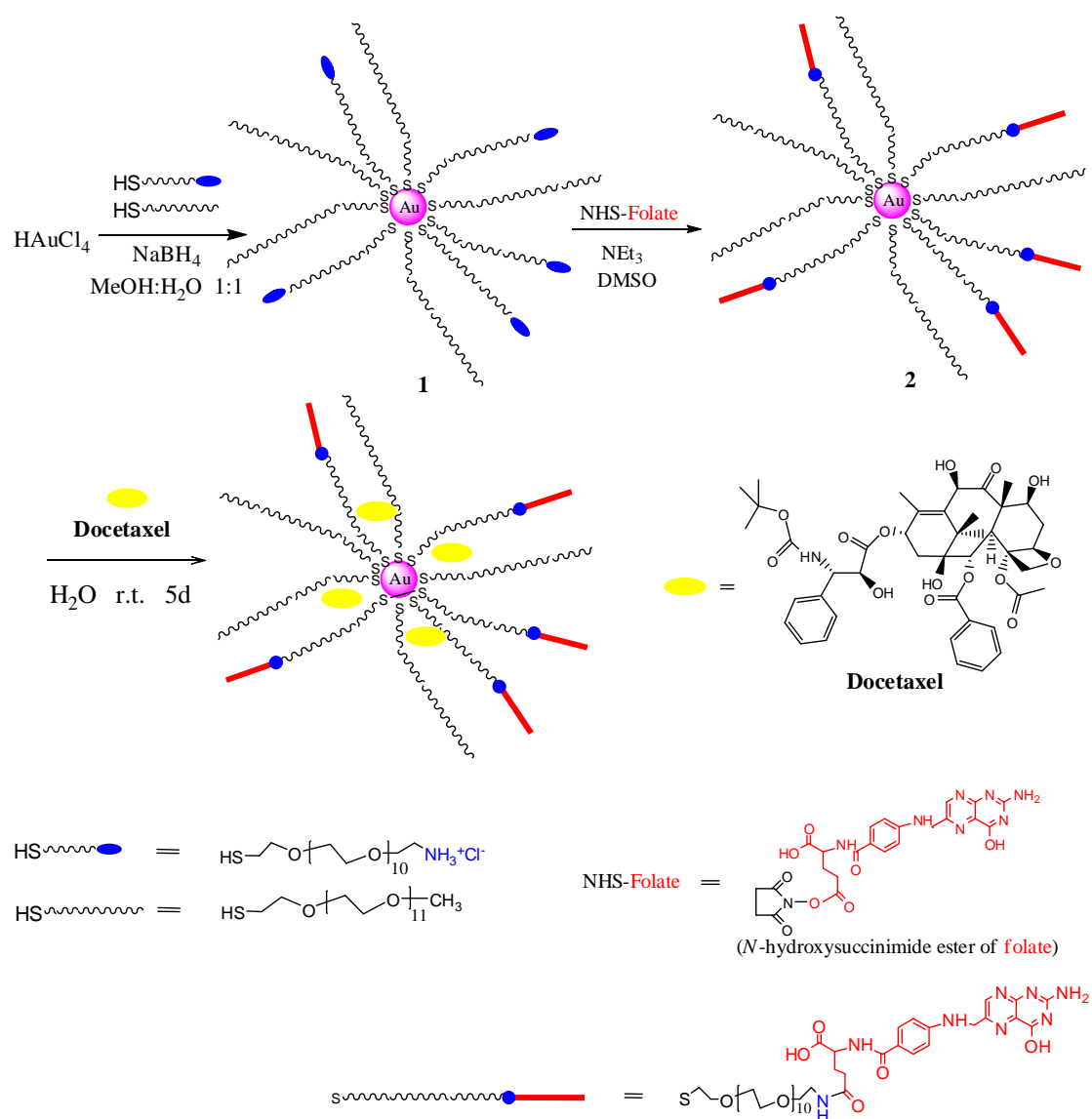
Synthesis and characterization of AuNPs

As shown in Scheme 1, the AuNP **1** was synthesized by modified Brust method³⁵, (see experimental section). From the ^1H NMR spectrum of AuNP **1** (see SI), it can be seen that the AuNP surface was capped by 50% HS-mPEG and 50% HS-PEG-NH₂ · HCl. This indicated that 50% of capped ligand on AuNP **1** could be functionalized by NHS-folate through the coupling reaction, leading to AuNPs with folate functionalization at the periphery (AuNP **2**).

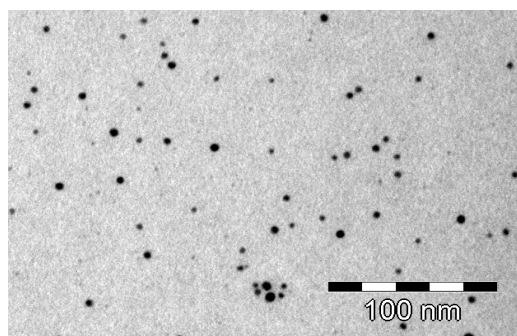
The folate functionalization at the termini of AuNP **2** is confirmed by the ^1H NMR spectrum (SI). The size of the AuNPs, determined by transmission electron microscopy (TEM) is 4 ± 0.5 nm (Figure 2) with a classic satisfactory dispersity. The plasmon band is observed at 530 nm (Figure 3) which also confirms that the size of the AuNPs is larger than 3 nm.

The AuNPs **2** were used to encapsulate the docetaxel for the following *in vitro* study. The encapsulation procedure is described in the experimental section. Here numerous weak hydrogen bonds form between the OH and NH group of docetaxel (Scheme 1) and the numerous oxygen atoms of the PEG polymer. These weak but numerous

hydrogen bonds allow to use the PEGs as a molecular solvent encapsulating docetaxel molecules in water for its solubilization in water.



Scheme 1. The synthesis route of AuNPs and the encapsulation of docetaxel.



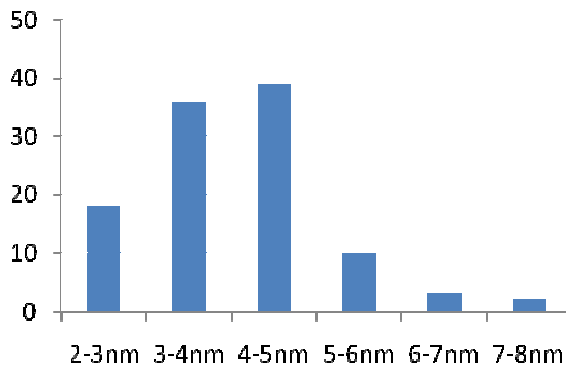


Figure 2 The size and size distribution of AuNP 2 by TEM.

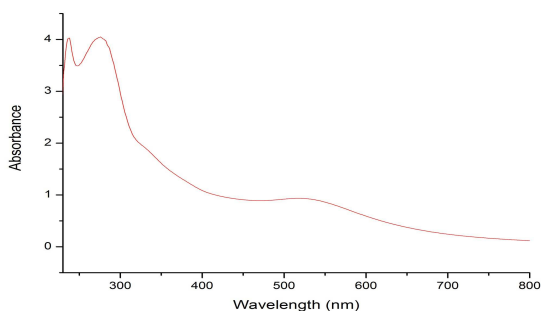


Figure 3 The plasmon band absorption spectrum of AuNP 2.

Evaluation of AuNP 2 on HUVEC cells

In order to test the biocompatibility of AuNPs, the MTT assay on HUVEC cells was used after incubation with AuNP 2. As shown in Figure 4, the HUVEC cells cultured with FA-Au NPs with various concentration had similar viability to the untreated control group ($p > 0.05$). These results show that FA-Au NPs have good biocompatibility and no toxicity to HUVEC cells.

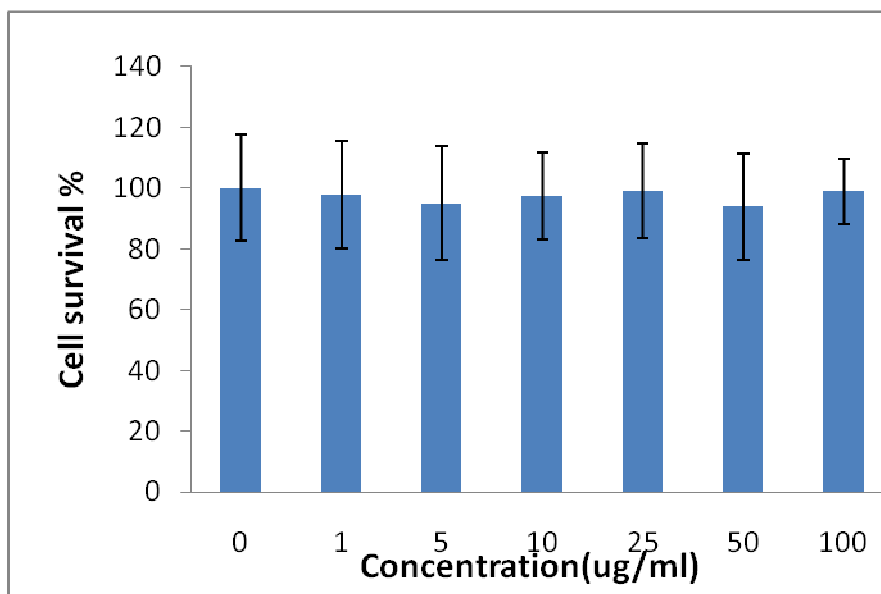


Figure 4 Viability of HUVEC cells in presence of AuNPs 2, estimated by the MTT test.

***In vitro* cytotoxicity of AuNPs with encapsulated docetaxel towards LnCap prostate cancer cells**

Figure 5 shows that a 48-h of treatment with the Au / DOC nanoparticles caused a small decrease in cell viability at most concentrations. On the other hand, free DOC did not affect cell viability at 48 h. However the dose-effect was more prominent after 6 days of treatment. In this case, the Au/DOC showed a similar effect to free DOC. Unloaded AuNPs had no effect on cell viability at either time-point (data not shown). These results were confirmed by observation with an optical microscope.

The morphology of the cells was observed after 6 days of treatment using an optical microscope (Leitz Diaplan) at 100X magnification. Typical photomicrographs are shown in Figure 6, which indicated much fewer cells after 6 days of treatment with DOC or Au/DOC compared with control cells or cells treated with unloaded nanoparticles.

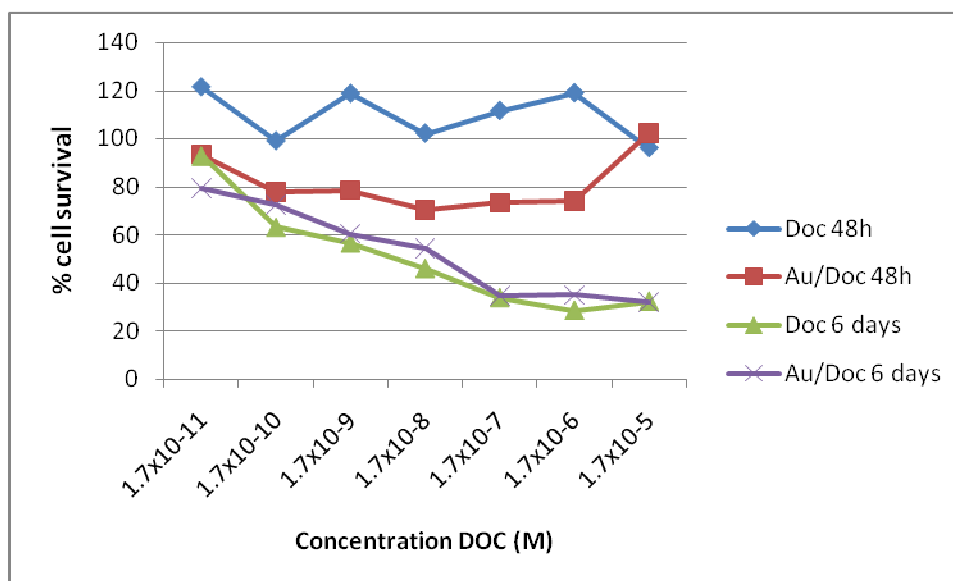


Figure 5 Percentage of cell survival in contact with DOC and Au/DOC after 48h and 6 days. (Test was carried out in Châtenay-Malabry by Rachel Oliveira.)

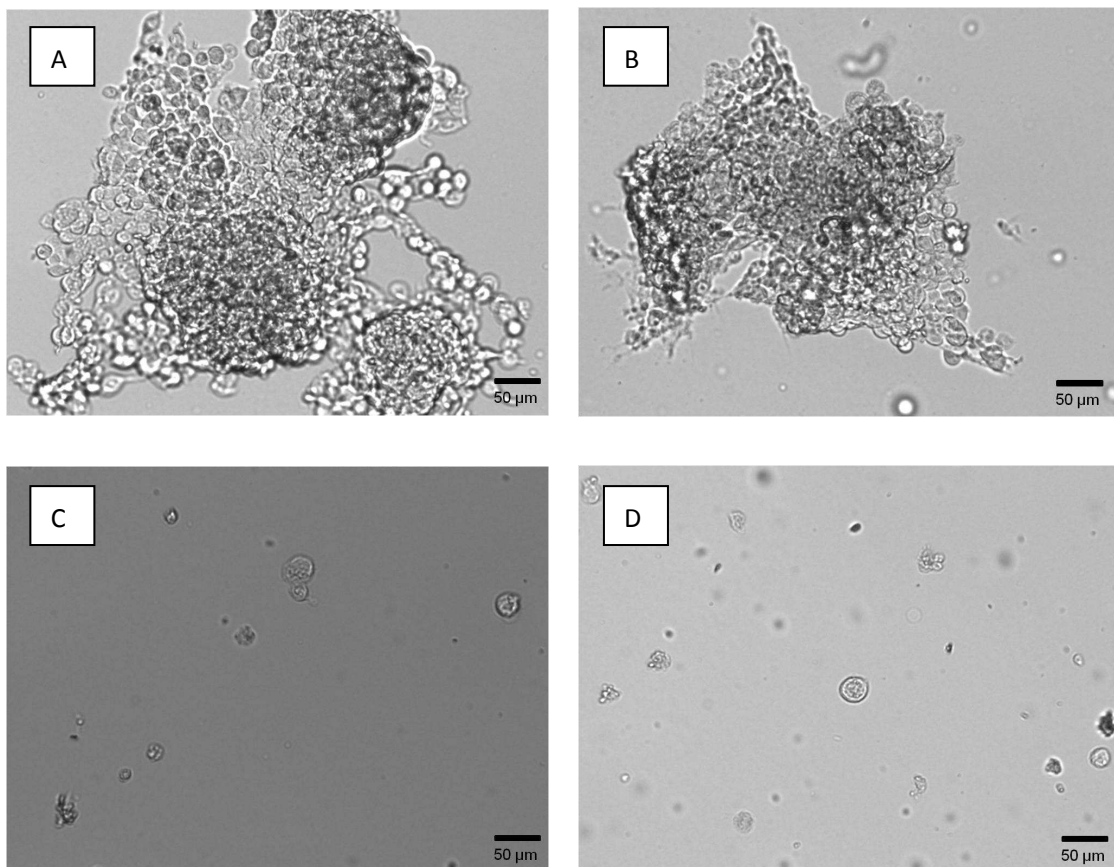


Figure 6 Optical microscopy images of LnCap cells after 6 days: (A) control without treatment; (B) cells with Au; (C) cells with DOC 1.7×10^{-5} M; (D) cells with Au/Doc 1.7×10^{-5} M. The bar represents 50 μm . (Test was carried out in Châtenay-Malabry by Rachel Oliveira.)

Conclusions and outlook

In this study, AuNPs have been functionalized with PEG₂₀₀₀ by “click” chemistry in order to encapsulate docetaxel by supramolecular interactions for further *in vitro* and *in vivo* study. The PEG-protected AuNPs with folate functionalization show an excellent biocompatibility. These AuNPs used for docetaxel delivery indicate an efficient anticancer property for prostate cancer cells in an *in-vitro* test. In future work, *in vivo* evaluation of this DDS will be needed. Also, we envisage to prepare the AuNPs with longer PEG (i.e. PEG₂₀₀₀ or PEG₅₀₀₀) as the stabilizer, and compare the different anticancer properties of AuNPs protected with longer PEG chains with those bearing shorter PEG chains.

Experimental section

General Data.

All solvents and chemicals were used as received. ^1H NMR spectra were recorded at 25°C with a Bruker 300 (300 MHz) spectrometer. All the chemical shifts are reported in parts per million (δ , ppm) with reference to Me₄Si for the ^1H and ^{13}C NMR spectra.

The DLS measurements were made using a Malvern Zetasizer 3000 HSA instrument at 25°C at an angle of 90°. The infrared (IR) spectra were recorded on an ATI Mattson Genesis series FT-IR spectrophotometer. UV-vis. absorption spectra were measured with Perkin-Elmer Lambda 19 UV-vis. spectrometer. The MTS reagent was purchased from Promega (Madison, USA). Cell culture reagents were from Lonza (Basel, Belgium). Docetaxel was purchased from Sigma-Aldrich (Illkirch, France) and DMSO from Carlo Erba (Milan, Italy).

Synthesis of HS-PEG-NH₂ • HCl

The molecular weight of PEG was 400. The synthesis route of HS-PEG-NH₂ • HCl was followed by the reference³⁶ ¹H NMR (CDCl₃, 300 MHz) 3.58 (40H, -CH₂CH₂O-), 3.17(2H, -CH₂NH₂HCl), 2.70 (2H, HSCH₂-).

Synthesis of HS-mPEG

The molecular weight of mPEG was 550. The synthesis route of HS-mPEG was followed by the reference.³⁷ ¹H NMR (CDCl₃, 300 MHz) 3.60(40H, -CH₂CH₂O-), 3.33(3H, -OCH₃), 2.68(2H, HSCH₂-).

Synthesis of Folate-NHS

The synthesis of folate-NHS proceeded as described by Zhang et al.³⁸ Briefly, Folic acid (1.0g, 2.3mmol) and triethylamine (5ml) were added into DMSO (30ml) and the mixture stirring at r.t. under nitrogen atmosphere until folic acid was completely dissolved. Then NHS (0.3g, 2.6mmol) and DCC (0.75g, 3.6mol) were added and the mixture was stirred overnight at 80°C under a nitrogen atmosphere. After filtration, the filtrate was poured into 300mL acetonitrile, and the yellow precipitate was washed twice with ethanol and diethyl ether, and the yellow powder was collected. Yield: 82%. ¹H NMR (DMSO-d₆, 300 MHz) 8.60 (1H, pyrazine ring), 7.61 (1H, arom ring), 6.97 (1H, -CH₂NH-arom ring), 6.63 (1H, arom ring), 4.64 (2H, -CH₂NH-arom ring), 2.82 (4H, -NOC-CH₂CH₂-CON-), 2.29(2H, -CH₂CH₂COO-), 1.99(2H, -CH₂CH₂CH₂COOH).

Synthesis of AuNPs 1

Thiolate-mPEG (Mw = 550; 55mg, 0.1mmol) and thiolate-PEG-NH₂HCl (Mw = 490 49mg, 0.1mmol) were dissolved into 10mL MeOH, and this solution added into a solution of HAuCl₄ (100mg) in 30mL (MeOH:H₂O 1:1). After stirring for 5 minutes, 1ml of a freshly prepared NaBH₄ (100mg) aqueous solution was added dropwise and with vigorously stirring for another 1h. Then, MeOH was evaporated under reduced pressure, and the water phase was salted into 30mL CH₂Cl₂ with a minimum amount of NaCl. The organic phase was separated and dried over Na₂SO₄. After evaporated of the solvent under vacuum, the crude product was dissolved in 30mL distilled water followed by dialysis. Yield: 45mg. ¹H NMR (CDCl₃, 300 MHz) 3.58 (40H, -CH₂CH₂O-), 3.33 (3H, -OCH₃), 3.17 (2H, -CH₂NH₂HCl), UV-vis: plasmon band at 530 nm. DLS: 57.6 nm. TEM: 4 ± 0.5 nm.

Synthesis of the AuNPs 2

20mg of AuNPs **1** from the above synthesis was dissolved into 4mL CH₂Cl₂, and 0.02mmol FA-NHS was dissolved into 4ml DMSO, 0.2mL triethylamine (TEA) was added into the mixture and stirred overnight at r.t.. After evaporating CH₂Cl₂ under vacuum, 50ml ether was poured into the solution, and then the precipitate was collected and dissolved into CH₂Cl₂, and filtered over paper. The filtrate was evaporated to obtain the product as 14mg of deep red crystals. ¹H NMR (DMSO-d₆, 300 MHz) 6.97 (1H, -CH₂NH-arom ring), 6.63 (1H, arom ring), 3.58 (40H, -CH₂CH₂O-), 3.33 (3H, -OCH₃), 2.29 (2H, -CH₂CH₂COO-), 1.99 (2H, -CH₂CH₂CH₂COOH). UV-vis: plasmon band at 530 nm. DLS: 50.4 nm. TEM: 4 ± 0.5 nm.

Encapsulation of docetaxel

A stock solution of docetaxel was carefully prepared with 5.92 mg of docetaxel (XP105 DeltaRange Analytical Balance - Mettler Toledo, (Zurich, Switzerland), dissolved in 0.2 mL of DMSO, followed by further dilution in distilled water. In order to encapsulate the drug, 1 mL of a suspension of AuNPs **2** at 10 mg/mL was added to 14.3 mL of a DOC solution of 0.28 mg/mL. All solutions were sterilized using a 0.2 μm cellulose acetate sterile syringe filter and handled in a sterile environment in order to prevent microbial contamination during the encapsulation period. The final mixture was stirred for 5 days during 30 °C and used directly to evaluate their cytotoxicity against human prostate cancer cells.

Evaluation of biocompatibility of AuNP 2

The toxicity of FA-Au NPs was evaluated by MTT assay, which was used to evaluate the viability of HUVEC cells after incubation with the FA-Au NPs.

In detail, the HUVEC cells were seeded to the 96-well culture plate, and incubated for 18h. Then, the cells were cultured with FA-Au NPs of various concentrations (1, 5, 10, 20, 50 and 100μg/ ml) for 24h. Cells without adding AuNPs were used as a control group (0μg/ ml). MTT reagents were added into each well and cultured for another 4h. Then the medium was removed, and the cells were lysed in DMSO. After formazan was dissolved, the absorbance at the wavelength of 540 nm was read. Relative cell survival was represented as a percentage of the control group. Five parallel samples were performed in each group.

Cytotoxicity evaluation

The human prostate cell line LnCap (ECACC Reference 89110211) was obtained from the Institut Bergonié, Bordeaux. Cells were routinely grown in RPMI-1640 medium supplemented with L-glutamine, 10% of fetal bovine serum and 5% penicillin-streptomycin. Cells were incubated at 37 °C in an atmosphere containing 5% CO₂ and passaged once a week. Cell viability was estimated using the Promega Cell Titer 96 Aqueous Non-Radioactive Cell Proliferation (MTS) assay.³⁹

The cells were seeded in 96-well plates (5000 cells in 50 μL per well). Free docetaxel (DOC), alone and AuNP loaded with docetaxel (Au/DOC) were suspended in culture

medium, serially diluted and added 96-well microtiter plates (50 μ L/well), 24h after seeding the cells. The plates were incubated for a further 48 h or 6 days. Ninety minutes prior to the end of each exposure period, the MTS reagent (20 μ L/ well) was added.

The absorbance of the formazan product was read with a 492 nm high-pass filter in a Multiskan MS microwell plate reader (Labsystem, city, country) Background absorbance due to the non-specific reaction between the test compounds and the MTS reagent was measured in wells without cells and was subtracted from the values measured in the presence of cells.⁴⁰ Cell viability was calculated as a percentage of the absorbance of untreated cells. Triplicate wells were used for each point. The low concentration of DMSO present in the samples of free docetaxel was tested alone and found to have no effect on cell viability.

Acknowledgement

Financial support from the China Scholarship Council (CSC) of the People's Republic of China (Ph. D. grants to PZ), the Université Bordeaux 1, the Centre National de la Recherche Scientifique (CNRS) and the Agence Nationale pour la Recherche (ANR) is gratefully acknowledged. Financial support from the Brazilian government, CAPES 04/CII-2008, Rede Nanobiotec-Brasil, 23038.019135/2009-63 is also acknowledged.

References

1. Peer, D., Karp, J. M., Hong, S., Farokhzad, O. C., Marglit, R., and Langer, R. (2007) Nanocarriers as an emerging platform for cancer therapy. *Nat. Nanotechnol.* 2, 751–760.
2. Mohanty, C., Das, M., Kanwar, J. R., and Sahoo, S. K. (2011) Receptor mediated tumor targeting: an emerging approach for cancer therapy. *Curr. Drug. Deliv.* 8, 45–56.
3. Euliss, L. E., DuPont, J. A., Gratton, S., and DeSimone, J. (2006) Imparting size, shape, and composition control of materials for nanomedicine. *Chem. Soc. Rev.* 35, 1095–1104.
4. C. Dubernet, *Bull Cancer* **2011**, 98, 1363-1371.
5. Torchilin, V. P. (2005) Recent advances with liposomes as pharmaceutical carriers. *Nat. Rev. Drug Discov.* 4, 145–160
6. Brigger, I., Dubernet, C., and Couvreur, P. (2002) Nanoparticles in cancer therapy and diagnosis. *Adv. Drug Deliv. Rev.* 54, 631–651.
7. Yang, X. C., Samanta, B., Agasti, S. S., Jeong, Y., Zhu, Z., Rana, S., Miranda, O. R., and Rotello, V. M. Drug delivery using nanoparticle-stabilized nanocapsules. (2011) *Angew. Chem. Int. Ed.* 123, 497–501.
8. Li, L., Tang, F., Liu, H., Liu, T., Hao, N., Chen, D., Teng, X., and He, J. (2010) *In vivo* delivery of silica nanorattle encapsulated docetaxel for liver cancer therapy with low toxicity and high efficacy. *ACS Nano.* 4, 6874–6882.
9. Svenson, S., and Chauhan, A. S. (2008) Dendrimers for enhanced drug solubilization. *Nanomedicine* 3, 679–702.
10. Astruc, D., Boisselier, E., and Ornelas, C. (2010) Dendrimers designed for functions: from physical, photophysical, and supramolecular properties to applications

in sensing, catalysis, molecular electronics, photonics, and nanomedicine. *Chem. Rev.* **110**, 1857–1959.

- 11.** Astruc, D. (1996) Research Avenues on Dendrimers Towards Molecular Biology: from Biomimeticism to Medicinal Engineering. *C. R. Acad. Sci.* **322**, *Série II b*, 757-766.
- 12.** Daniel, M. C, and Astruc, D. (2004) Gold nanoparticles: assembly, supramolecular chemistry, quantum-size-related properties, and applications toward biology, catalysis, and nanotechnology. *Chem. Rev.* **104**, 293–346.
- 13.** Duncan, B., Kim, C., and Rotello, V. M. (2010) Gold nanoparticle platforms as drug and biomacromolecule delivery systems. *J. Controlled Release* **148**, 122–127.
- 14.** Murphy, C. J., Golet, A. M., Stone, J. W., Sisco, P. N., Alkilany, A. M., Goldsmith, E. C., and Baxter, S. C. (2008) Gold nanoparticles in biology: beyond toxicity to cellular imaging. *Acc. Chem. Res.* **41**, 1721–1730.
- 15.** Lal, S., Clare, S. E., and Halas, N. J. (2008) Nanoshell-enabled photothermal cancer therapy: impending clinical impact. *Acc. Chem. Res.* **41**, 1842–1851.
- 16.** Jain, P. K., El-Sayed, I. H., and El-Sayed, M. A. (2007) Au nanoparticles target cancer. *Nanotoday* **2**, 18–29.
- 17.** Pasciotti, G. F., Kinston, D. G. I., and Tamarkin, L. (2006) Colloidal gold nanoparticles: a novel nanoparticle platform for developing multifunctional tumor-targeted drug delivery vectors. *Drug Dev. Res.* **67**, 47–54.
- 18.** Boisselier, E., and Astruc, D. (2009) Gold nanoparticles in nanomedicine: preparations, imaging, diagnostics, therapies and toxicity. *Chem. Soc. Rev.* **38**, 1759–1782.
- 19.** Llevot, A., and Astruc, D. (2011) Application of gold nanoparticles to the diagnostic and therapy of cancer. *Chem. Soc. Rev.* **Article ASAP**.
- 20.** F. Lavelle, F. Gueritte-Voegelein, D. Guénard, *Bull. Cancer* **1993**, **80**, 326–338.
- 21.** K. C. Nicolaou, R. K. Guy, P. Potier, *Sci. Am.* **1996**, **274**, 94–98;
- 22.** Y. F. Wang, Q. W. Shi, M. Dong, H. Kiyota, Y.C. Gu, B. Cong, *Chem. Rev.* **2012**, **ASAP**, DOI: 10.1021/cr100147u.
- 23.** F. Gueritte-Voegelin, D. Guénard, F. Lavelle, M.T. Le Giff, L. Mangatal, P. Potier, *J. Med. Chem.* **1991**, **34**, 992-998;
- 24.** a) D. Guénard, F. Guéritte-Voegelin, P. Potier, *Acc. Chem. Res.* **1993**, **26**, 160-167; b) H. Lataste, V. Senilh, M. Wright, D. Guénard, P. Potier, *Proc. Nat. Acad. Sci.* **1984**, **81**, 4090-4094.
- 25.** P. Zhao, D. Astruc, *ChemMedChem* (2012) DOI: 10.1002/cmdc.201200052.
- 26.** Fernandez-Botello, A., Comelles, F., Alsina, M. A., Cea, P., and Reig, F. (2008) A monolayer study on interactions of docetaxel with model lipid membranes. *J. Phys. Chem. B.* **112**, 13834–13841.
- 27.** Zhai, G., Wu, J., Xiang, G., Mao, W., Yu, B., Li, H., Piao, L., Lee, L. J., and Lee, R. J. (2009) Preparation, characterization and pharmacokinetics of folate receptor-targeted liposomes for docetaxel delivery. *J. Nanosci. Nanotechnol.* **9**, 2155–2161.
- 28.** Werner, M. E., Copp, J. A., Karve, S., Cummings, N. D., Sukumar, R., Li, C., Napier, M. E., Chen, R. C., Cox, A. D., and Wang, A. Z. (2011) Folate-targeted polymeric nanoparticle formulation of docetaxel is an effective molecularly targeted radiosensitizer with efficacy dependent on the timing of radiotherapy. *ACS Nano* **Article ASAP** DOI: 10.1021/nn203165z.
- 29.** Gao, Y., Chen, L., Gu, W., Xi, Y., Lin, L., and Li, Y. (2008) Targeted

nanoassembly loaded with docetaxel improves intracellular drug delivery and efficacy in murine breast cancer model. *Mol. Pharm.* 5, 1044–1054.

30. Cho, H. J., Yoon, H. Y., Koo, H., Ko, S. K., Shim, J. S., Lee, J. H., Kim, K., Kwon, I. C., and Kim, D. K. (2011) Self-assembled nanoparticles based on hyaluronic acid-ceramide (HA-CE) and Pluronic® for tumor-targeted delivery of docetaxel. *Biomaterials* 32, 7181-7190.

31. Menendez, J. A., Ropero, S., Lupu, R., and Colomer, R. (2004) Omega-6 polyunsaturated fatty acid gamma-linolenic acid (18:3n-6) enhances docetaxel (Taxotere) cytotoxicity in human breast carcinoma cells: Relationship to lipid peroxidation and HER-2/neu expression. *Oncol Rep.* 11, 1241-1252

32. A. Inno, M. Basso, M., A. Cassano, C. Barone, *Therapeutics* **2010**, 2, 663-680

33. G. Thota, *Bioorg. Med. Chem.* **2007**, 15, 3597–3623.

34. Francois, A., Laroche, A., Pinaud, N., Salmon, L., Ruiz, J., Robert, J., and Astruc, D. (2011) Encapsulation of docetaxel into PEGylated gold nanoparticles for vectorization to cancer cells. *Chem. Med. Chem.* 6, 2003-2008.

35. Brust, M. Walker, D. Bethell, D.J. Schiffrin, R. Whyman, *Chem. Commun.* **1994**, 801-802.

36. K. Yoshimoto, Y. Hoshino, T. Ishii, Y. Nagasaki, *Chem. Commun.* **2008**, 5369-5371.

37. M. Zheng, Z. Li, X. Huang, *Langmuir*, **2004**, 20, 4226-4235.

38. C. Zhang, S. Gao, W. Jiang, S. Lin, F. Du, Z. Li, W. Huang, *Biomaterials* **2010**, 31, 6075-6086.

39. G. Malich, B. Markovic, C. Winder. *Toxicology* **1997**, 124, 179-192.

40. A. Hayes, B. Markovic, *Cosmet. Toiletries.* **1999**, 12, 24-30.

Support Information

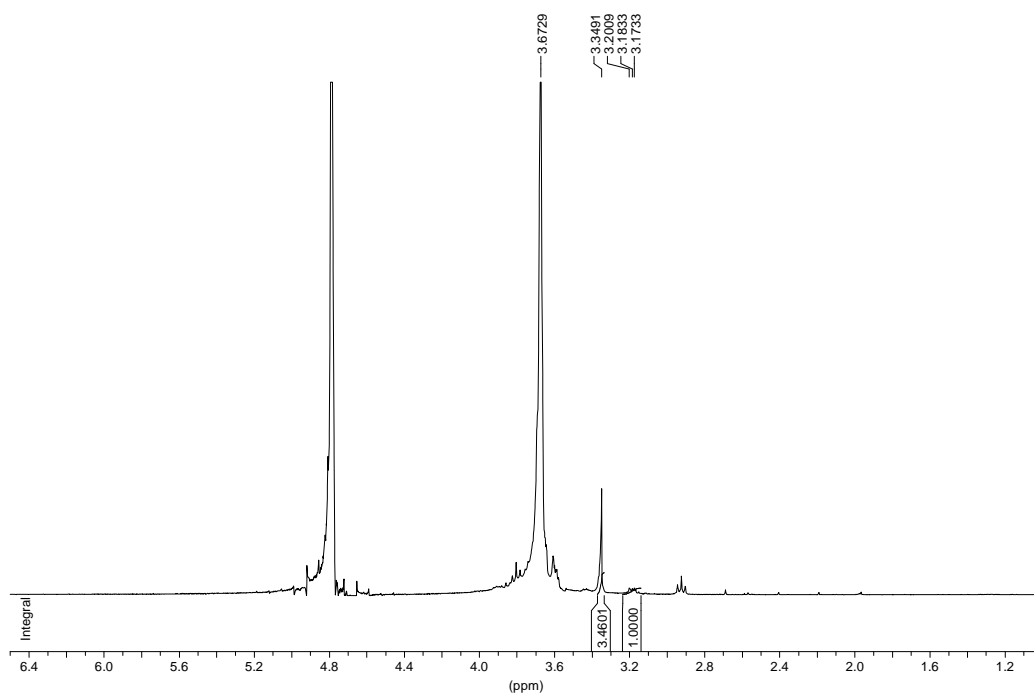
Folate-functionalized Gold Nanoparticles on Docetaxel Delivery System

Support information

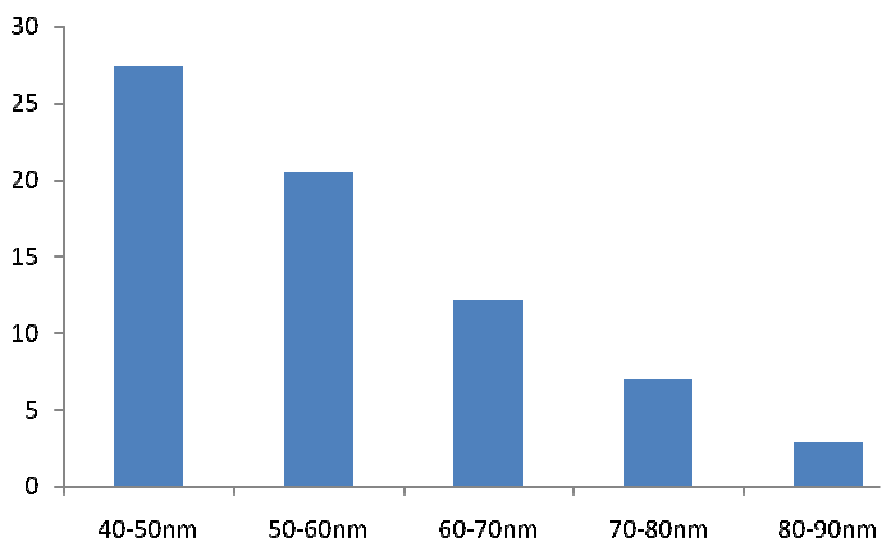
Characterization of AuNP 1	123
¹ H NMR of AuNP 1.....	123
DLS of AuNP 1.....	124
UV- vis of AuNP 1.....	124
TEM of AuNP 1.....	125
Characterization of AuNP 2	126
¹ H NMR of AuNP 2.....	126
DLS of AuNP 2.....	126

Characterization of AuNP 1

¹H NMR of AuNP 1

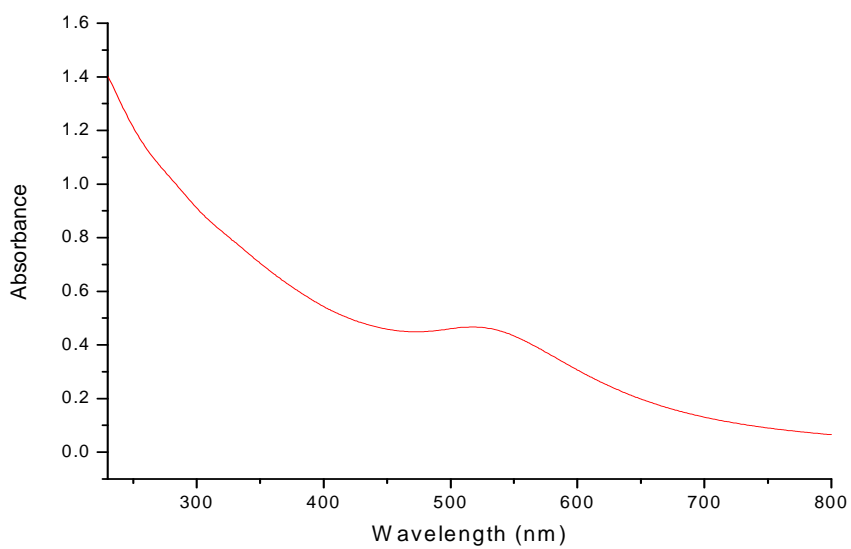


DLS of AuNP 1



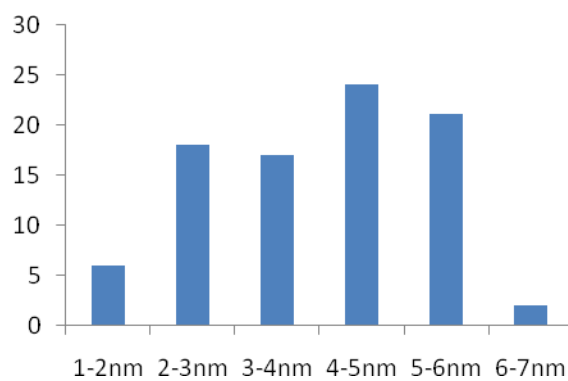
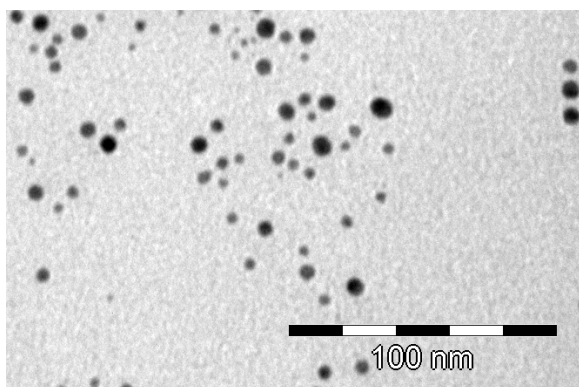
The average dynamic diameter of AuNPs was 57.4nm

UV- vis of AuNP 1



The plasmon band at 530 nm

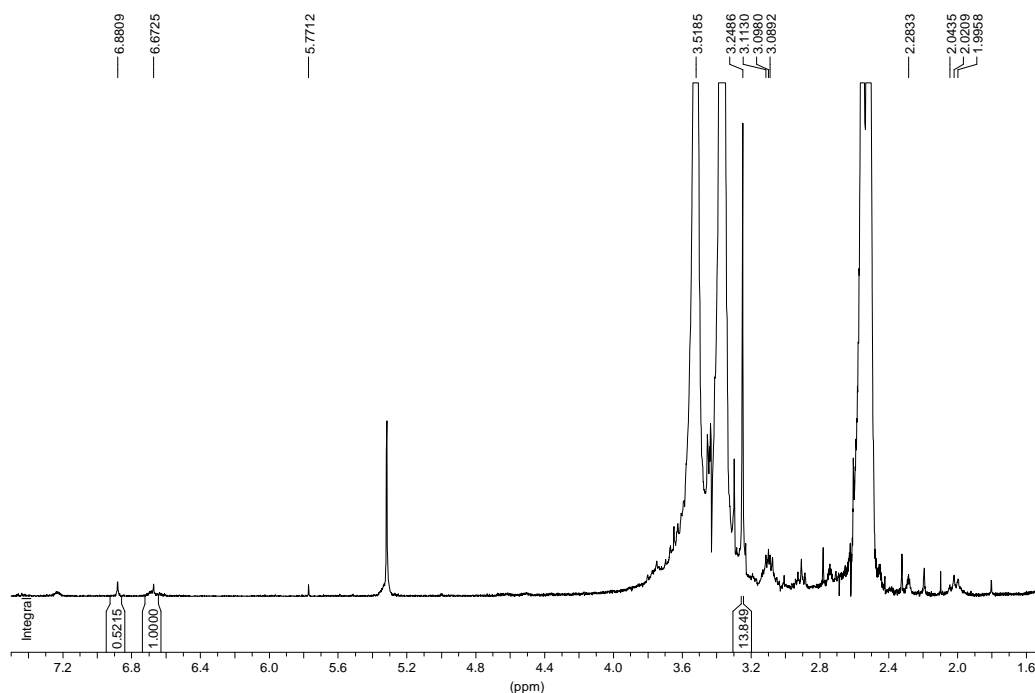
TEM of AuNP 1



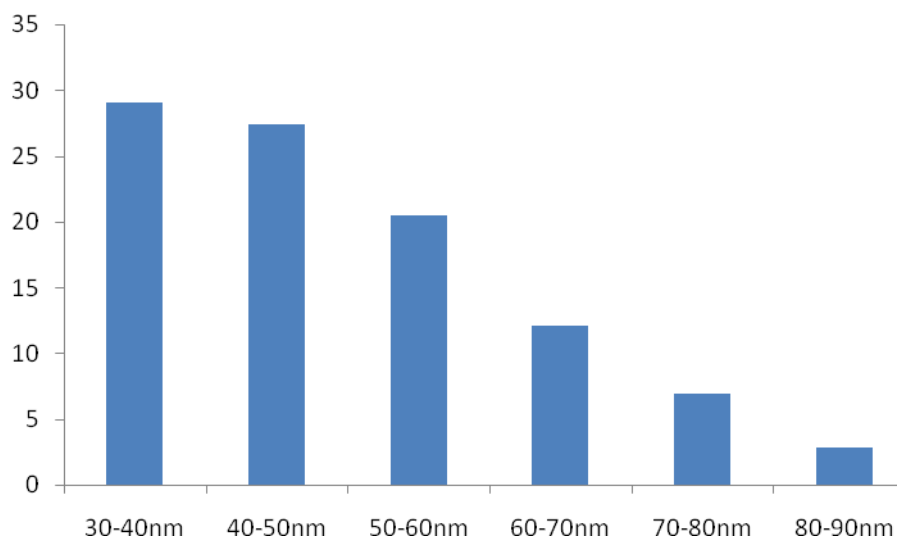
TEM: the average size of the AuNP was 3.5 ± 0.5 nm

Characterization of AuNP 2

¹H NMR of AuNP 2



DLS of AuNP 2



The average dynamic diameter of AuNPs was 50.6nm

3.3 Encapsulation of Water-soluble Vitamins by Gold Nanoparticles in Hydrophobic Media

1

Encapsulation of Water-soluble Vitamins by Gold Nanoparticles in Hydrophobic Media

Pengxiang Zhao,[§] Jaime Ruiz,[§] Lionel Salmon,[§] Didier Astruc^{§*}

[§]ISM, Univ. Bordeaux, 351 Cours de la Libération, 33405 Talence Cedex, France. E-mail: d.astruc@ism.u-bordeaux1.fr

[¶]Laboratoire de Chimie de Coordination, UPR CNRS N°8241, 205 Route de Narbonne, 31077 Toulouse Cedex, France

(Received <Month><Date>, <Year>; CL-<No>; E-mail: <insert corresponding e-mail address>)

Thiolate-mPEG ligand-protected gold nanoparticles (AuNPs) are shown to encapsulate the water-soluble vitamins C (ascorbic acid), B3 (nicotinic acid), B6 (pyridoxine) and B9 (folic acid) in a hydrophobic medium, i.e. between 1000 and 3000 vitamin molecule per 6-nm-coredAuNPs (overall size: 19.2 ± 2 nm) in dichloromethane solution.

Vitamins are organic compounds that are required as nutrients in tiny amounts by organisms. Many vitamins are soluble in aqueous solvents, which favors their facile assimilation, but are not soluble in hydrophobic media, which prevents their access to hydrophobic areas of the body.¹ This is the case for vitamin C, B3, B6 and B9 (Figure 1). Vitamin C (ascorbic acid, AA), is a well-known anti-oxidant that protects the body against oxidative stress and is an electron donor for eight different enzymes and a cofactor in several vital enzymatic reactions. It is involved in the synthesis of red blood cells, contributes to the immune system and to the defense against infections, favors the absorption of iron, and is required for the synthesis of skin collagen.² Vitamin B3 (nicotinic acid, NA), a precursor of NADH, NAD⁺, NADP⁺, and NADPH, plays essential metabolic roles in living cells and is involved in both DNA repair and the production of steroid hormones in the adrenal gland.³ Vitamin B6 (pyridoxine, PN), is an active factor and cofactor in many reactions of amino acid metabolism, including transamination, deamination, and decarboxylation.⁴ Vitamin B9 (folic acid, FA) is essential to the body inter alia for the synthesis, repair and methylation of DNA. It is especially important in aiding rapid cell division and growth, such as in infancy and pregnancy.⁵

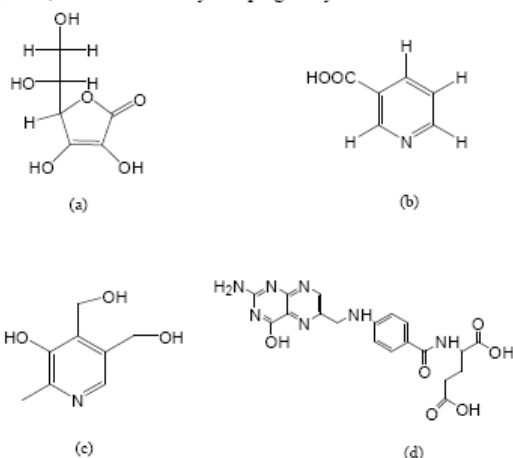
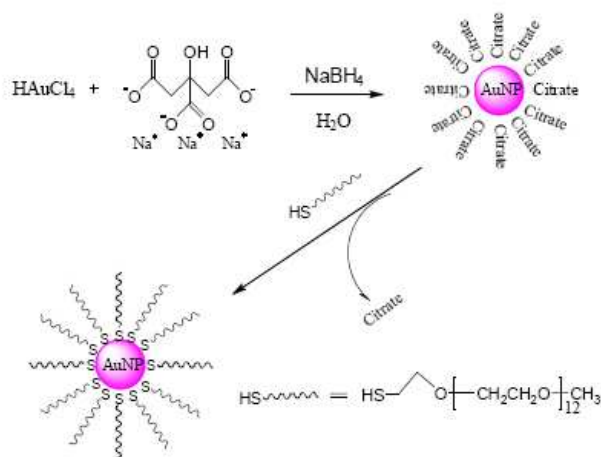


Figure 1. Structures of the water-soluble vitamins a) vitamin C (ascorbic acid, AA); b) vitamin B3 (nicotinic acid, NA); c) vitamin B6 (pyridoxine, PN); d) vitamin B9 (folic acid, FA).

Among the multiple investigations and uses of gold nanoparticles (AuNPs),⁶ those involved in nanomedicine benefit from the template effect that is increased by rather strong AuNP-thiolate ligand bonds.⁷ In addition, AuNPs are well known for their general lack of intrinsic toxicity contrasting with those of other nanoparticles and largely exploited in the fast expanding nanobiomedical field for imaging and therapy.⁷ In this context, the encapsulation or stabilization of gold nanoparticles (AuNPs) by PEG dendrimers is known.⁸

Here we report the encapsulation of water-soluble vitamins using PEGylated AuNPs¹⁰ for their solubilization in a hydrophobic solvent. The idea relevant to the micelles consists in using the amphiphilic properties of the poly ethylene glycol (PEG) termini that provide PEG-AuNP solubilization in dichloromethane and the PEG compatibility with water-soluble vitamins forcing the vitamins to remain in the PEG-AuNP interior in order to escape the hydrophobic solvent. For this purpose, we have designed AuNPs in such a way that they be soluble in dichloromethane. Thus, the AuNP ligands are polyethylene glycol (PEG)-thiolate that are accessible *via* the corresponding thiol. The PEGs present the advantage of being biocompatible, providing many biomedical and medicinal studies and uses. In particular, they are known for their enhanced permeation and retention effect (EPR), i.e. they tend to accumulate in tumor tissue much more than in normal tissues and therefore stimulate the production of blood vessels which induces the quick growth of tumor cells. This EPR effect is useful to target drug- and imagery-containing nanovectors towards cancer cells.⁹ The PEG ligands are also now shown to make possible the dissolution of all these vitamins in the “nanomolecular solvent” upon assembling the PEG-thiolate ligand around the AuNP template.

Thus, the PEG-thiolate-AuNPs¹⁰ were synthesized by mixing a solution of trisodium citrate and a solution of HAuCl₄ at room temperature (r.t.) followed by the addition of a freshly prepared NaBH₄ solution with vigorously stirring. After 10 min, a solution of 1-thiol mPEG¹¹ was also added, then the reaction medium was stirred for 1 day, and dialyzed for 2 days (Scheme 1).



Scheme 1. Synthetic route to PEG-thiolate-AuNPs.

The AuNPs were characterized by UV-vis. spectroscopy, showing an intense plasmon band at 520 nm, IR spectroscopy and dynamic light scattering (DLS) showing an overall AuNP size of 19.2 ± 2 nm (see the Supplementary Information). The size of the AuNP core obtained by TEM is 6.6 ± 0.5 nm (Figure 2), which corresponds, according to Leff's calculations,¹² to 639 thiolate mPEG ligands on the AuNP surface.

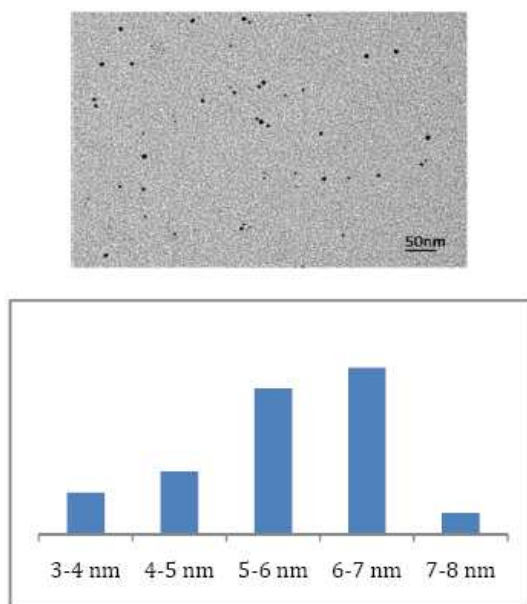


Figure 2. TEM of AuNPs. The average AuNP core size is 6.6 ± 0.5 nm.

Encapsulation of the vitamins C, B3, B6 and B9 was achieved upon progressive addition of the vitamins as powders to a stirred dichloromethane solution containing the AuNPs until the

vitamins became insoluble. For each vitamin, the amounts added were calculated *versus* each AuNP-thiolate-PEG ligand. The maximum amount of encapsulated vitamin was 4.5 ± 0.5 equiv. vitamin C or B3 *per* ligand, 2.5 ± 0.3 equiv. vitamin B6 *per* ligand, and 1.5 ± 0.2 equiv. vitamin B9 *per* ligand. The dichloromethane solutions of AuNP-thiolate-PEG that were saturated with vitamin, then filtered, were characterized in UV-vis. spectroscopy by a more or less important red shift of the plasmon band depending on the vitamin (Figure 3) and by the observation of the IR spectra of these four hydrophobic vitamins in addition to the AuNP absorptions (see the S. I.).

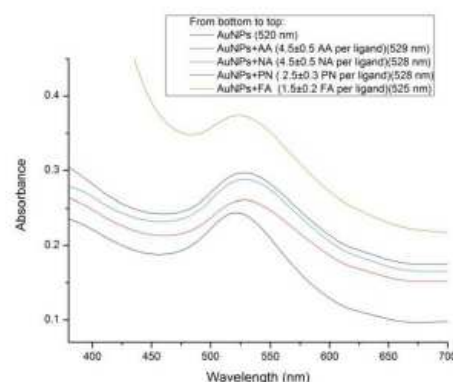


Figure 3. The plasmon band shifts of AuNPs upon encapsulation of vitamin C (AA), B3 (NA), B6 (PN) and B9 (FA).

In conclusion, very large amounts of water-soluble, hydrophilic vitamins that are not soluble in could be encapsulated in PEG-thiolate-AuNPs as demonstrated by solubilization of the four vitamins in dichloromethane in the presence of the PEG-thiolate-AuNPs. The impressive encapsulated amounts *per* AuNP in DCM are 2800 ± 400 molecules of vitamin C or B3, 1920 ± 200 molecules of vitamin B6 and 950 ± 100 molecules of vitamin B9.

Financial support from the China Scholarship Council (CSC) of the People's Republic of China (Ph. D. grants to Pengxiang Zhao), the Université de Bordeaux, the Centre National de la Recherche Scientifique (CNRS) and the Agence Nationale pour la Recherche (ANR) is gratefully acknowledged.

References and Notes

†Present address: ISM, UMR CNRS N° 5255, Univ. Bordeaux, 33405 Talence Cedex, France. Fax: 33 540 00 6995.
E-mail: d.astruc@ism.u-bordeaux1.fr

†Supplementary Information (SI) available: Synthesis of AuNPs, determination of the number of AuNP-thiolate-PEG ligands, encapsulation of vitamins by AuNPs, characterization of the AuNPs alone and AuNPs containing encapsulated vitamins (UV-vis., and IR spectra, and DLS).

- (a) D. A. Bender, *Nutritional chemistry of the vitamins*. Cambridge University Press, Cambridge, U. K., 2003; (b) G. F. Combs, *The vitamins: fundamental aspects in nutrition and health*, Elsevier, San Diego, 2008.
- (a) J. W. Harris, *Ascorbic acid: biochemistry and biomedical cell biology*. New York: Plenum Press, 1996; (b) S. Padayatty, A. Katz, Y. Wang, P. Eck, O. Kwon, J. Lee, S. Chen, C. Corpe, A. Dutta, S. Dutta, M. Levine, *J. Am. Coll. Nutr.* 2003, 22, 18; (c) Gropper SS,

-
- 3 Smith JL, Grodd JL, *Advanced nutrition and human metabolism* (4th ed.). Belmont, CA, USA: Thomson Wadsworth, 2004, pp. 260–275.
- 3 (a) M. Cox, A. L. Lehninger, D. R. Nelson, *Principles of biochemistry*, Worth Publishers, New York, 2000; (b) S. E. Wolverson, *Comprehensive Dermatologic Drug Therapy*, 2nd ed.; W. B. Saunders (Elsevier), Amsterdam, 2007.
- 4 D. B. McCormick, *Vitamin B₆ In: Present knowledge in Nutrition* (Bowman, B. A. and Russell, R. M., eds), 9th edition, vol.2, p.270. Washington, D.C.: International Life Sciences Institute, 2006.
- 5 T. R. Rawalpalli in *Kirk-Otmer Encyclopedia of chemical technology*, Vol25, Wiley, New York, 2001.
- 6 (a) M. Brust, M. Walker, D. Bethell, D. J. Schiffrin, R. Whyman, *Chem. Commun.*1994, 801; (b) C. A. Mirkin, R. L. Letsinger, J. J. Storhoff, *Nature*1996, 382, 607; (c) S. Link, M. A. El-Sayed, *J. Phys. Chem. B*1999, 103, 8410; (d) A. C. Templeton, M. P. Wuefing, R. W. Murray, *Acc. Chem. Res*2000, 33, 27; (e) M. Haruta, M. Date, *Appl. Catal. A General*2001, 222, 427; (f) C. M. Niemeyer, *Angew. Chem. Int. Ed*2001, 40, 4128; (g) Y. G. Sun, Y. N. Xia, *Science*2002, 298, 2171; (h) K. L. Kelly, E. Coronado, G. C. Schatz, *J. Phys. Chem. B*2003, 107, 668; (i) L. R. Hirsch, R. J. Stafford, S. R. Sershen, B. Rivera, R. E. Price, J. D. Hazle, N. J. Halas, J. L. West, *Proc. Natl. Acad. Sci.*2003, 100, 13549; (j) E. Katz, I. Willner, *Angew. Chem., Int. Ed*2004, 43, 6042; (k) M.-C. Daniel, D. Astruc, *Chem. Rev.* 2004, 104, 293; (l) C. J. Murphy, T. K. San, A. M. Gole, C. J. Orendorff, J. X. Gao, S. E. Hunyadi, T. Li, *J. Phys. Chem. B*2005, 19, 13857; (m) J.P. Juste, P. Santos, L.M. L. Marzan, P. Mulvaney, *Coord. Chem. Rev.*2005, 249, 1870; (n) L. Dykman, N. Khlebtsov, *Chem. Soc. Rev.*2012, ASAP. DOI: 10.1039/C1CS15166E; (o)
- 7 (a) P. Jain, I. H. El-Sayed and M. A. El-Sayed, *Nano Today*2007, 2, 18; (b) C. J. Murphy, A. M. Golet, J. W. Stone, P. N. Sisco, A. M. Alkilany, E. C. Goldsmith, S. C. Baxter, *Acc. Chem. Res.* 2008, 41, 1721; (c) R. Badan, S. Lal, A. Joshi, N. J. Halas, *Acc. Chem. Res.* 2011, 44, 936-946; (d) A. Llevot, D. Astruc, *Chem. Soc. Rev.* 2012, 41, 242; (e) Y.C. Yeh, B. Creran, V.M. Rotello, *Nanoscale*,2012, ASAP. DOI:10.1039/C1NR11188D.
- 8 (a) C. Kojima, Y.Umeda, M. Ogawa, A. Harada, Y.Magata and K.Kono, *Nanotechnology*2010, 21, 245104; (b) C. Peng, L. Zheng, Q. Chen, M. Shen, R. Guo, H. Wang, X. Cao, G. Zhang, X. Shi, *Biomaterials*2012, 33, 1107; (c) E. Boisselier, A. K. Diallo, L. Salmon, C. Ornelas, J. Ruiz, D. Astruc, *J. Am. Chem. Soc.*2010, 132, 2729.
- 9 (a) Y. Matsumura, H. Maeda, *Cancer Res.*1986, 46, 6387; (b) R. Duncan, Y.-N. Sat, *Ann. Oncol.*1998, 9 (Suppl. 2) 39; (c) R. T. Poon, N. Borys, *Exp. Opin. Pharmacother.*2009, 10, 333-343.
- 10 K. R. Brown, A.P. Fox, M. J. Natan, *J. Am. Chem. Soc.* 1996, 118, 1154.
- 11 D. M. Mizrahi, M. Omer-Mizrahi, J. Goldshtein, N. Askinadze, S. Margel, *J. Polym. Sci., Part A: Polym. Chem.*2010, 48, 5468.
- 12 (a) D.V. Leff, P.C. Ohara, J.R. Heath, W.M. Gelbart, *J. Phys. Chem.*1995, 99, 7036; (b) A. Labande, J. Ruiz, D. Astruc, *J. Am. Chem. Soc.*2002, 124, 1782; (c) M.-C. Daniel, J. Ruiz, S. Nlate, J.-C. Blais, D. Astruc *J. Am. Chem. Soc.*2003, 125, 2617.

Supporting Information is available electronically on the CSJ-Journal Web site, <http://www.csj.jp/journals/chem-lett/index.html>.

Encapsulation of Water-soluble Vitamins by Gold Nanoparticles in Hydrophobic Media

Pengxiang Zhao,[§]Lionel Salmon,[&] Jaime Ruiz, [§]Didier Astruc^{§*}

[§]ISM, Univ. Bordeaux, 351 Cours de la Libération, 33405 Talence Cedex, France. E-mail:

d.astruc@ism.u-bordeaux1.fr

[&]Laboratoire de Chimie de Coordination, UPR CNRS N°8241, 205 Route de Narbonne, 31077 Toulouse Cedex, France

Supporting Information

1. Abbreviations of all chemicals	2
2. Determination of the numbers of ligands per AuNP.....	2
3. Encapsulation of the vitamins by the PEGylated AuNPs	2
4. Characterization of the AuNPs	2
4.1 UV-vis. spectrum of AuNPs.....	2
4.2 DLS of AuNPs	3
4.3 TEM of the AuNPs.....	3
4.4 IR spectrum of the AuNPs	4
4.4.1 IR spectrum of the AuNPs alone	4
4.4.2 IR spectrum of AuNPs containing encapsulated AA	4
4.4.3 IR spectrum of AuNPs containing encapsulated NA.....	6
4.4.4 IR spectrum of AuNPs containing encapsulated PN	7
4.4.5 IR spectrum of AuNPs containing encapsulated FA.....	7

1. Abbreviations

AA: ascorbic acid, vitamin C
NA: nicotinic acid, vitamin B₃
PN: pyridoxine, vitamin B₆
FA: folic acid, vitamin B₉
AuNPs: gold nanoparticles
DLS: dynamic light scattering
TEM: Transmission Electron Microscopy

2. Determination of the numbers of ligands per AuNP

Leff's method^{12a} provides the determination of the number of thiolate ligands:

Number n of Au atoms in each AuNP: $n(\text{Au}) = 4\pi(R-\delta)^3 / 3v_g = 8850$

(Diameter of AuNPs from TEM: $D = 6.6 \text{ nm}$; $v_g = 1.7 \times 10^{-2} \text{ nm}^3$; $R - \delta \approx D / 2$)

Number of thiol ligands in each AuNP: $n(\text{thiol}) = 4\pi(R-\delta)^2 / S_{\text{thiol}} = 639$

(Area of each thiol atom in the surface of AuNPs: $S_{\text{thiol}} = 0.214 \text{ nm}^2$)

$M(\text{AuNPs}) = n(\text{Au}) \times M(\text{Au}) + n(\text{thiol}) \times M(\text{thiol-mPEG}) = 2126850$;

3. Encapsulation of the vitamins by the PEGylated AuNPs

The four vitamins C, B₃, B₆ and B₉ were insoluble in dichloromethane in the absence of the AuNPs. For the four vitamins, the procedures of encapsulation were similar. In each case, the vitamin was progressively (slowly) added as small powdery portions into 10 mL of the dichloromethane solution containing 10 mg of the AuNPs, and the solution remained clear until the solid vitamin became insoluble in dichloromethane after a certain amount of vitamin was added. The amount of each encapsulated vitamin at the saturation point was 4.5 ± 0.5 equiv. vitamin C per ligand, 4.5 ± 0.5 equiv. vitamin B₃ per ligand, 2.5 ± 0.3 equiv. vitamin B₆ per ligand, and 1.5 ± 0.2 equiv. vitamin B₉ per ligand. The saturated vitamin@AuNP dichloromethane solution was filtered, and the UV-vis (in dichloromethane) and IR spectra (neat in KBr pellets following evaporation of dichloromethane) were recorded (see below).

4. Characterization of the AuNPs

4.1 UV-vis. spectrum of AuNPs

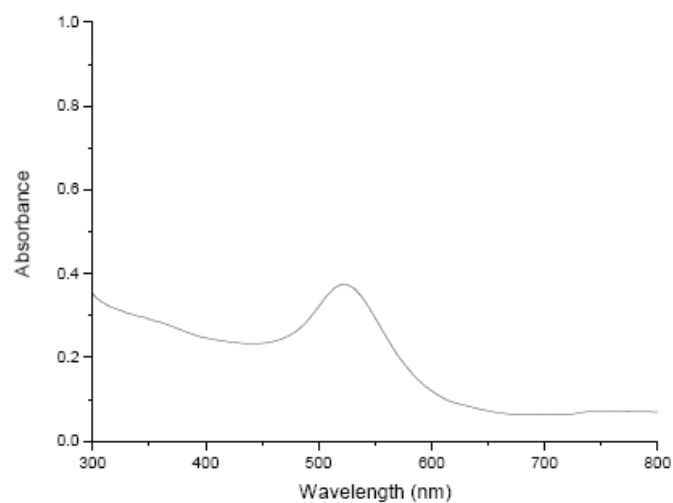


Figure 1. UV-vis. spectrum of the AuNPs in DCM. Plasmon band at 520 nm.

4.2 DLS of AuNPs

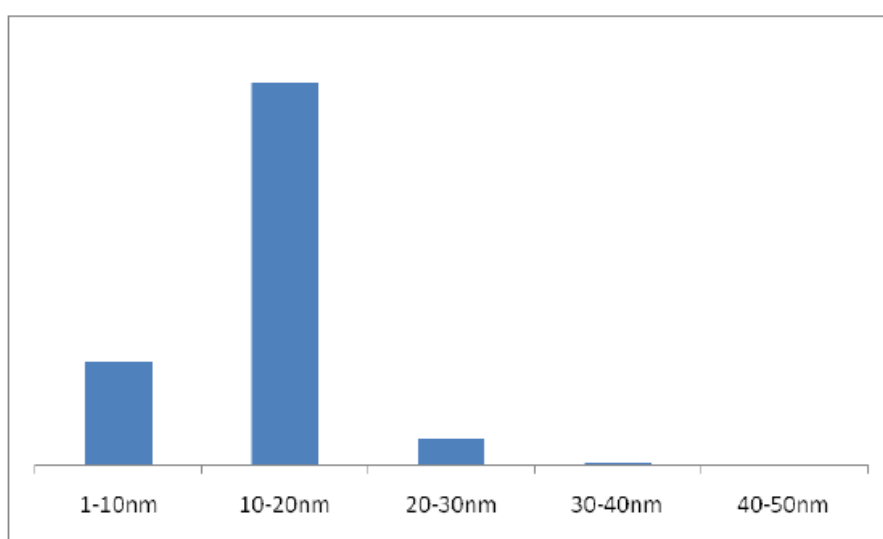


Figure 2. DLS of AuNPs. The average dynamic diameter of AuNPs is 19.2 ± 2 nm.

4.3 TEM of the AuNPs

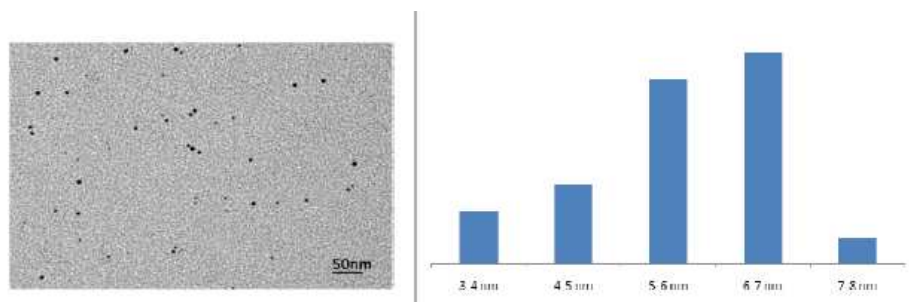


Figure 3. TEM picture (left) and histogram (right) of the AuNPs. The size of the AuNP core is 6.6 ± 0.5 nm.

4.4 IR spectrum of the AuNPs

4.4.1 IR spectrum of the AuNPs alone

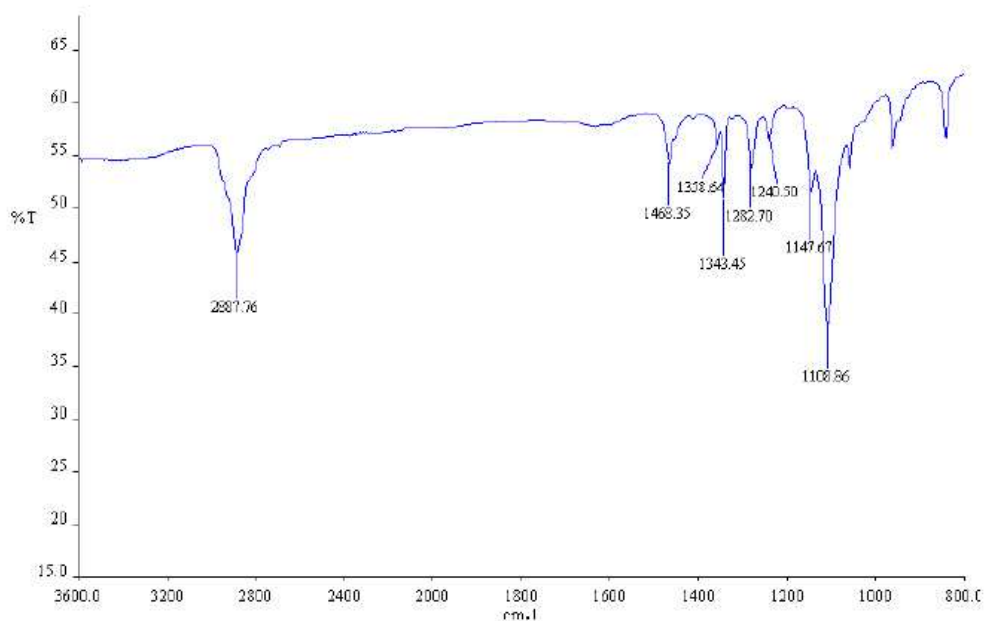


Figure 4. IR spectrum of the AuNPs alone in KBr pellets.

4.4.2 IR spectrum of AuNPs containing encapsulated AA

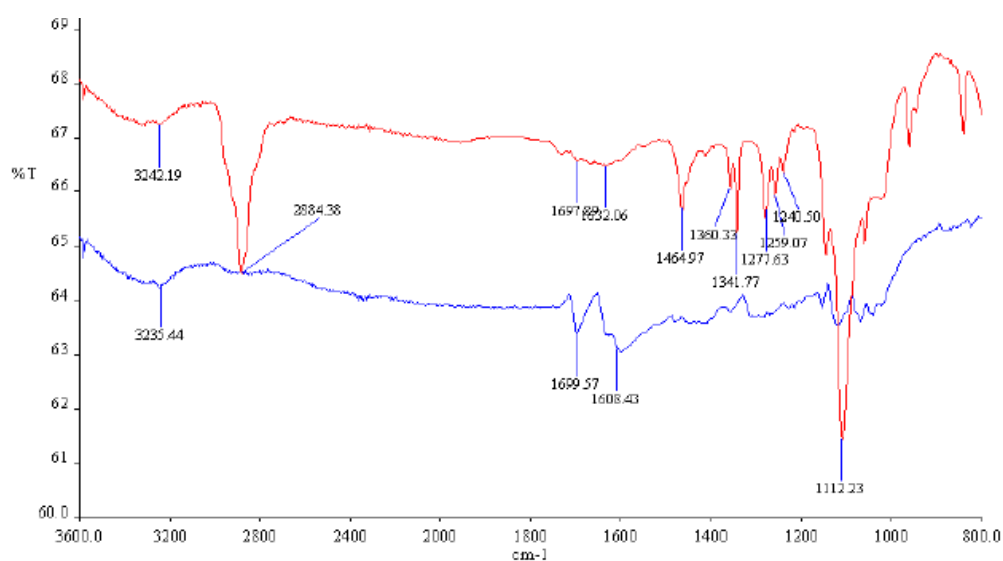


Figure 5. From bottom to up: IR of AA alone (blue) and AuNPs with encapsulated AA (red) in KBr pellets.

Table 1. Assignments of the IR absorption bands (KBr pellets) of the AuNPs alone (left column), AA alone (middle column) and the AuNPs with encapsulated AA (right column).^a

Frequency (cm ⁻¹)			Assignment
AuNPs	AA	AuNPs+AA	
1107(vs)		1112(vs)	v (C-H)
2887(vs)		2884(vs)	v (C-O-C)
1240-1468(vs)		1240-1464(vs)	δ(C-H)
	3235(m)	3242(m)	v (O-H)
	1608 (s)	1632 (w)	v(C=C) (in the aromatic ring)
	1699 (s)	1697 (w)	v (C=O)

^a Abbreviations: vs: very strong, s: strong, m: medium, w: weak, v: stretch, and δ: deformation.

4.4.3 IR spectrum of AuNPs containing encapsulated NA

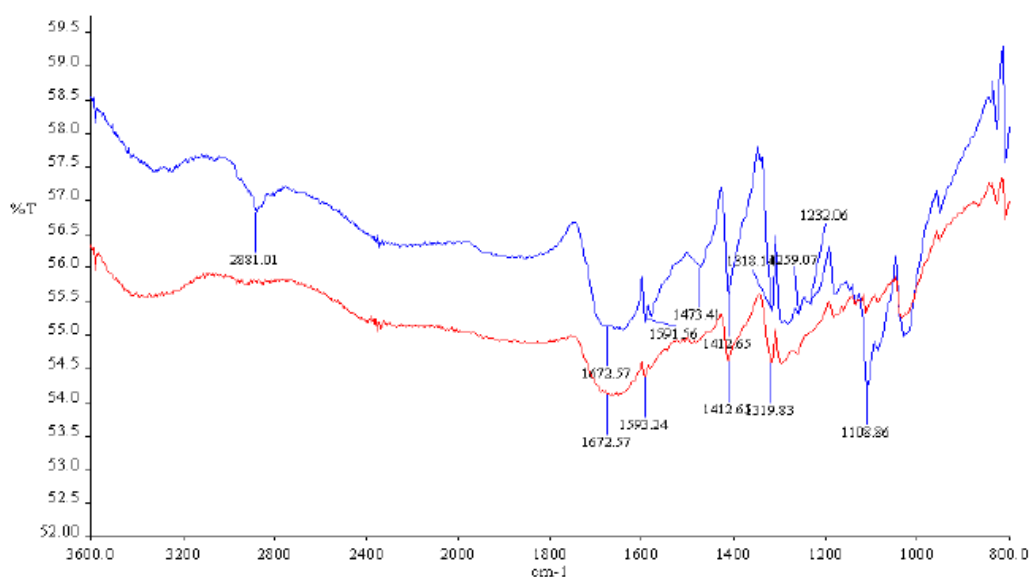


Figure 6. From bottom to up: IR of NA alone (blue) and AuNPs with encapsulated NA (red) in KBr pellets.

Table 2. Assignments of the IR absorption bands (KBr pellets) of the AuNPs alone (left column), NA alone (middle column) and the AuNPs with encapsulated NA (right column).^b

Frequency (cm ⁻¹)			Assignment
Au	NA	Au+NA	
1107(vs)		1108(vs)	ν (C-H)
2887(vs)		2881(s)	ν (C-O-C)
1240-1468(vs)		1232-1473(m)	δ (C-H)
	1593(m)	1591 (m)	ν (C=C) (in the aromatic ring)
	1672 (br)	1672 (br)	ν (C=O), ν (C=N)

^bAbbreviations: vs: very strong, s: strong, m: medium, br: broad, ν : stretch, and δ : deformation.

4.4.4 IR spectrum of AuNPs containing encapsulated PN

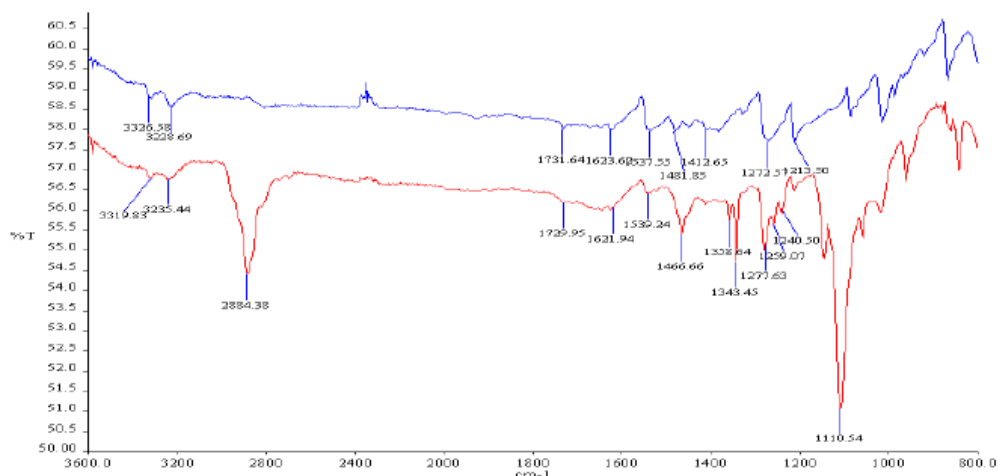


Figure 7. From up to bottom: the IR spectrum of PN alone (blue) and AuNPs with encapsulated PN (red) in KBr pellets.

Table 3. Assignments of the IR absorption bands (KBr pellets) of the AuNPs alone (left column), PN alone (middle column) and the AuNPs with encapsulated PN (right column).^c

Frequency (cm ⁻¹)			
Au	PN	Au+PN	Assignment
1107(vs)		1110(vs)	v (C-H)
2887(vs)		2884(vs)	v (C-O-C)
1240-1468(vs)		1240-1466(vs)	δ(C-H)
	3228, 3326(m)	3235, 3319(m)	v (O-H)
	1412-1537 (m)	1411-1539 (m)	v(C=C) (in the aromatic ring)
	1623, 1731 (m)	1621, 1729 (m)	v (C=N) (in the aromatic ring)

^cAbbreviations: vs: very strong, s: strong, m: medium, v: stretch, and δ: deformation.

4.4.5 IR spectrum of AuNPs containing encapsulated FA

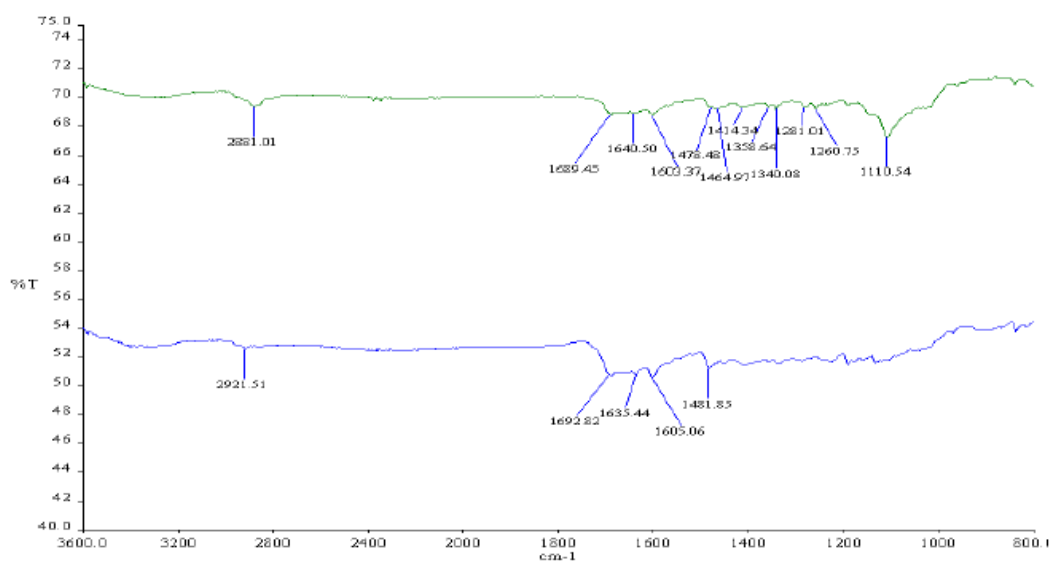


Figure 8. From bottom to up: IR spectrum of FA alone (blue) and AuNPs with encapsulated FA (green) in KBr pellets.

Table 4. Assignments of the IR absorption bands (KBr pellets) of the AuNPs alone (left column), FA alone (middle column) and the AuNPs with encapsulated FA (right column).^d

Frequency (cm ⁻¹)			Assignment
Au	FA	Au+FA	
1107(vs)		1110(vs)	v (C-H)
2887(vs)		2881(s)	v (C-O-C)
1240-1468(vs)		1260-1465(m)	δ(C-H)
	2921(w)		v (C-H)
	1605 (m)	1603 (m)	v(C=C) (in the aromatic ring)
	1635 (w)	1640 (w)	δ(N-H)
	1692 (w)	1689 (w)	v (C=O)

^dAbbreviations: vs: very strong, s: strong, m: medium, w: weak, v: stretch, and δ: deformation.



Chapter 4

The Application of AuNPs to Spin Cross-over Devices

4.1 Introduction and contribution

Spin cross-over devices are designed by Dr Azzedine Bousseksou's group as optical materials for memory storage resulting from hysteresis of the Fe(II) spin cross-over. Surface enhanced Raman spectroscopy or surface enhanced Raman scattering (SERS) is especially appropriate for the study of gold nanoparticles derived with such systems. It is a surface-sensitive technique that enhances Raman scattering by molecules adsorbed on rough metal surfaces (especially for Ag surface and Au surface). The enhancement factor can be as much as 10^{10} to 10^{11} , which means this technique may detect single molecules. Thus, chapter 4 contains a submitted article, in collaboration with the Laboratoire de Chimie de Coordination (LCC) in CNRS in Toulouse, Azzedine Bousseksou's group, including our contribution introduced below.

We have developed a specific SERS substrate, which was based on the introduction of AuNPs into the multilayer of the spin crossover (SCO) film. (See Figure 1) In the first step, benzene-1,4-dithiol was used to functionalize a gold surface by means of Au-S bonds. Then, the AuNPs were attached to the gold surface by the other S atom of the benzene-1,4-dithiol. In the next step mercaptopyridine was used to functionalize the "free surface" of AuNPs, also using the Au-S bonds. Afterwards, the substrate was immersed into ethanol solutions of $\text{Fe}(\text{BF}_4)_2$, $\text{K}_2\text{Pt}(\text{CN})_4$ and pyrazine step-by-step in order to assemble a continuous films of the SCO complex $\text{Fe}(\text{pyrazine})[\text{Pt}(\text{CN})_4]$. On the whole 5 layers of the complex were deposited.

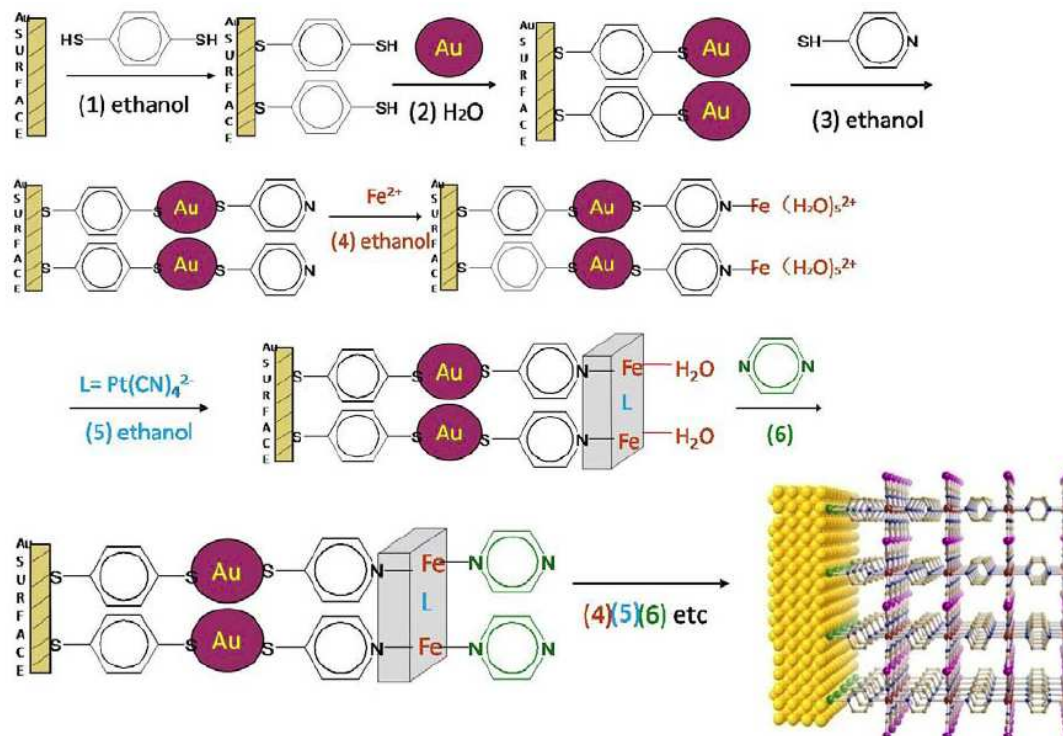


Figure 1. Scheme of sequential assembly of the SERS substrate and the multilayer of the compound $\text{Fe}(\text{pz})[\text{Pt}(\text{CN})_4]$

The AFM images (Figure 2) of the multilayer film revealed a mean roughness around 50 nm which is close to the expected total thickness for the multilayer [gold film (20 nm), a monolayer of AuNPs (18 nm) and 5 layers of the complex (5 nm)]. As we can be seen from the cross-section of the AFM image, objects with larger size (from a few hundreds of nm to a few tens of nm) are also observed, probably due to the aggregation of AuNPs and/or the precipitation of the iron complex.

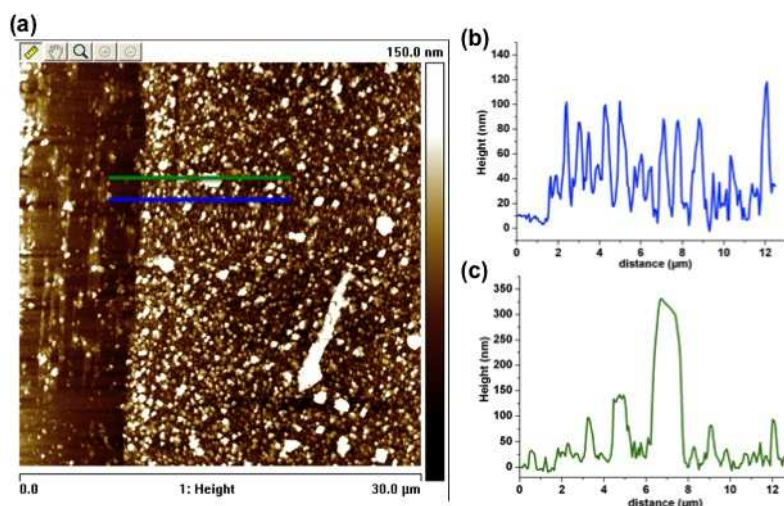


Figure 2. (a) AFM image of S5 surface with a stripe on the left. (b) and (c) are cross-sections corresponding to the blue and green lines on the AFM image, respectively. The depth of the stripe indicates the thickness of the gold layer deposited on silicon, i.e. 20 nm.

In order to detect the spin state switching for the 5 layers of the complex deposited on AuNPs, we have acquired Raman spectra at high and low temperatures (Figure 3). The Raman signature of silicon (broad band around $950\text{-}1000\text{ cm}^{-1}$) appears for both temperatures and both excitation wavelengths. At 532 nm excitation wavelength, we can see a clear Raman signal from the iron complex around 2200 cm^{-1} (CN stretching mode) at both temperatures. With the same conditions but with an excitation wavelength of 633 nm and a laser power of 12 mW, Raman spectra recorded at high and low temperatures are not very clean. Actually, with a red excitation, the Raman signal from 1,4-benzendithiol (main frequencies: $629, 738, 1056, 1092$ and 2560 cm^{-1}) is stronger than that of the iron complex. Moreover, the background produced by the silicon substrate is important in the range between $600\text{-}700\text{ cm}^{-1}$. For this reason it is very difficult to see the peaks at 645 or 675 cm^{-1} . Previous Raman experiments have highlighted that it is necessary to have a minimum of *ca.* 100 nm film thickness to detect the spectrum of the iron complex with our Raman spectrometer. From the AFM image we can safely deduce that the film thickness in the present case is certainly much less than 100 nm. Thus it is apparent that there must be an enhancement mechanism so as to observe Raman signal from this sample. We believe that this enhancement should be the plasmon resonance of gold nanoparticles (SERS effect).

The plasmon resonance for gold nanoparticles with 20 nm of diameter is around 520 nm, so the SERS effect will be maximal for the green excitation (532 nm). SERS effect can explain why we can detect Raman signal with only 5 deposited cycles. However, it is not the only effect as we can infer from the intensity difference between red and green excitation. Actually, this difference is detectable on the powder too. The other effect is the resonant Raman enhancement because the green spectral range corresponds to an absorption band of the iron complex. Indeed, the Raman signal of the iron complex is multiplied by *ca.* 6 when the excitation is at 532 nm (compared to 633 nm). We can thus tentatively distinguish surface-enhanced-resonance-Raman SERRS (532 nm) and SERS (633 nm) effects. One shall note also that the excitation at 785 nm did not allow us to observe a Raman signal from the sample. This observation is in agreement with the fact that the enhancement should decrease when the excitation wavelength is getting far from the green spectral region.

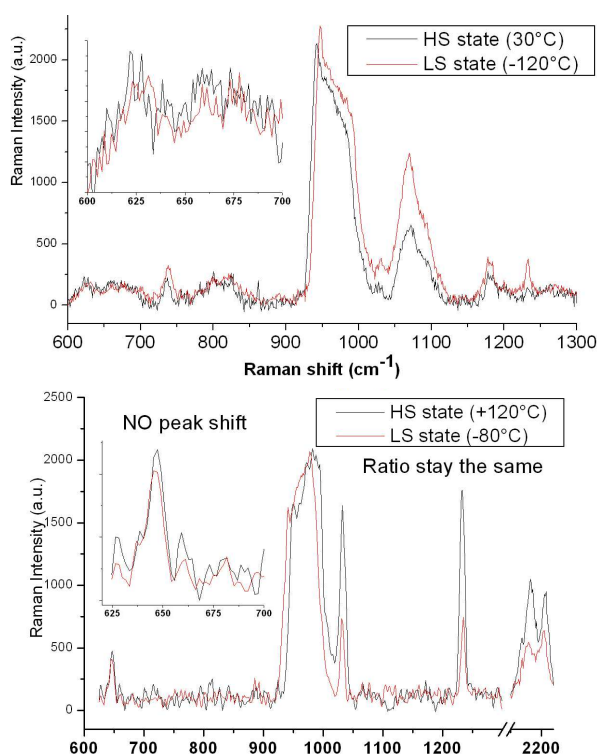


Figure 3 Raman spectra of FePt(pz) powder in the low spin and high spin states for excitation wavelengths of 632.8 nm (a) and 532 nm (b). (The background was removed.)

In summary, the Fe(pz)[Pt(CN)₄] system allowed us to demonstrate the usefulness of the SERS approach for obtaining the spectral signature of very thin (5 nm) layers of SCO complexes. On the other hand, a few drawbacks of the SERS approach have been also highlighted, which must be considered for the further development of this method in this field. First of all, the extreme surface sensitivity of the method leads to the exaltation of the signal mainly from the first deposited layer, which is often not representative for the ensemble of the film due to the possible presence of impurities,

anchoring layers (thiols in our case) or distorted/incomplete coordination environments around the Fe(II) ions. This fact – together with the modification of the selection rules - can explain the presence of additional peaks in the spectra when compared to the bulk complex. Resonance effects may be used to obtain more sample selectivity. In a few cases, we observed also strong spectral fluctuations and the emergence of broad bands between *ca.* 1000 – 1600 cm⁻¹. This phenomenon can be assigned to the formation of carbonaceous species formed by the alteration/decomposition of the deposited molecules (and/or contaminants) due to the high field enhancement. Even in the absence of decomposition problems, significant and uncontrolled sample heating and/or photoswitching may arise, which are of course undesirable phenomena in the context of spin transition studies. An optimization of the field enhancement seems thus inevitable in each case.

4.2 Submitted Article: Gold Nanoparticles on Spin Transition Device

Detection of molecular spin-state changes in ultra-thin films by photonic methods

I. A. Gural'skiy,^{1,2} C. Quintero,¹ K. Abdul-Kader,¹ M. Lopes,¹ C. Bartual-Murgui,^{1,3} L. Salmon,¹ Z. Pengxiang,⁴ G. Molnár,^{1,*} D. Astruc,⁴ A. Bousseksou^{1,*}

¹Laboratoire de Chimie de Coordination, CNRS UPR-8241 and Université de Toulouse, UPS, INP, F-31077 Toulouse, France

²Department of Chemistry, National Taras Shevchenko University, 01601 Kiev, Ukraine

³LAAS, CNRS & Université de Toulouse (UPS, INSA, IAES), 7 avenue du colonel Roche, 31077 Toulouse, France

⁴Université de Bordeaux, ISM, CNRS, UMR 5255, F-33405 Talence, France

* Corresponding authors: gabor.molnar@lcc-toulouse.fr, azzedine.bousseksou@lcc-toulouse.fr

Abstract. Ultrathin films of molecular spin crossover materials exhibit very appealing properties for a variety of photonic applications since the spin state switching is accompanied by a spectacular change of the complex refractive index in a wide spectral range. In this paper we discuss different optical spectroscopic approaches for the detection of spin state changes in nanometric films. We show that conventional light absorption measurements can be used down to the nanometer thickness if the oscillator strength of the transition is high, which is often the case for charge transfer transitions in the ultraviolet range. We discuss also methods based on fluorescence energy transfer and we show that this approach provides a straightforward means for detecting spin state changes in films in the visible wavelength range, even if photobleaching may be a problem for certain luminophores. Alternatively, refractive index changes accompanying the spin transition can be conveniently determined by surface plasmon resonance (SPR) spectroscopy, which can also provide very accurate film thickness determination. Plasmonic effects were also used, for the first time, to investigate spin crossover films by means of surface-enhanced Raman spectroscopy (SERS). We show that this technique can provide information not only on the spin state of the molecules in very thin layers, but also on their chemical composition and structure.

Keywords: spin crossover; thin films; luminescent doping; surface plasmon resonance; surface-enhanced Raman spectroscopy.

1 Introduction

Spin crossover (SCO) complexes of $3d^4 - 3d^7$ transition metal ions (Cr^{II} , Mn^{II} , Mn^{III} , Co^{II} , Co^{III} , Fe^{II} , Fe^{III}) represent an important class of bistable materials for which switching between high-spin (HS) and low-spin (LS) electronic configurations can be obtained by diverse external stimuli such as temperature change, light irradiation, application of pressure or magnetic fields, or even the adsorption of gas/vapor molecules.¹ The switching of molecular spin-states is accompanied with a spectacular change of various physical properties. For this reason the possible applications of these materials, including information storage, display and switching devices, pigments and sensors continue to draw much attention. Recently, considerable progress has been made in the synthesis of SCO nano-materials as patterned or continuous thin films, nano-composites or nanoparticles.²⁻³ This research aims to investigate size reduction effects on the spin crossover properties and also to integrate these materials into nanophotonic⁴⁻⁵ and nanoelectronic⁶⁻⁸ devices. For most photonic applications the ability to process the material as thin films is mandatory. However, the detection of spin state changes in very thin films (a few nm thickness) remains still a challenge in most cases. In addition, the chemical and structural characterization of these films is also a difficult task.

The simplest photonic approach is based on the detection of absorbance changes accompanying the SCO, but this may be hampered by the weak oscillator strengths of the electronic transitions. In a few cases, the absorbance changes were thus exploited in a less direct way, through luminescence doping, where the basic idea is to use a luminophore, whose luminescence is selectively quenched in a given spin state of the metal ions in the material due to a radiative or resonant energy transfer process.⁹ Refractive index changes associated with the SCO ($\Delta n_{\text{HL}} = n_{\text{HS}} - n_{\text{LS}}$, where n is the real part of the complex refractive index $n^* = n + ik$) provide probably even more interesting prospects for a range of photonic applications, but they remain largely unexplored. In this paper we discuss these different approaches and provide new strategies for further developments.

2 Experimental details

The preparation of the nanoparticle powders of the SCO complex $[\text{Fe}^{\text{II}}(\text{hptrz})_3](\text{OTs})_2$ (where hptrz = 4-heptyl-1,2,4-triazole, OTs = tosylate) as well as its homogeneous solution in chloroform were previously discussed in ref. [10]. Luminescent dyes were purchased from commercial sources and were added (1 %) to the ligand solution before the reaction with the iron salt. Thin films of $[\text{Fe}(\text{hptrz})_3](\text{OTs})_2$ were prepared by spin coating the chloroform solutions on quartz or gold-coated glass substrates. The film thickness was adjusted by changing the spinning velocity and the concentration of the complex. Thin films of the SCO complex $\text{Fe}^{\text{II}}(\text{pz})[\text{Pt}(\text{CN})_4]$ ¹¹ (where pz = pyrazine) were assembled on a gold nanoparticle (AuNP) functionalized surface as follows. The traditional Turkevich method¹² was used to synthesize AuNPs. The particle mean size (18 nm), determined by transmission electron microscopy, was found in agreement with the observed plasmon band at 520 nm. The substrates (Si wafer covered by 2 nm Ti and 15 nm Au) were first functionalized by submersing them overnight into a solution of 1 mM benzene-1,4-dithiol in ethanol. Then, the substrate was put into the AuNPs solution for 12 h. After this step it was submersed into a solution of 1 mM mercaptopridine in ethanol overnight. These wafers were soaked alternately (total of 5 cycles) in ethanol solutions of 100 mM $\text{Fe}(\text{BF}_4)_2$, 100 mM $\text{K}_2\text{Pt}(\text{CN})_4$ and 100 mM pyrazine at room

temperature (1 min in each solution), with rinsing in pure ethanol between steps (30 s). Finally they were dried under an Ar flow.

UV-visible absorption spectra were measured with a Cary 50 spectrophotometer equipped with a heating-cooling plate (Linkam PE120). A Fluoromax-4 (Horiba Jobin Yvon) spectrofluorimeter was used to acquire fluorescence excitation and emission spectra at room temperature, which were corrected for the instrument response (as implemented in the software). Variable temperature fluorescence intensity measurements were carried out using the fluorescence microscopy setup described in ref. [13]. Temperature dependent SPR spectra were acquired using a custom-built reflectivity setup,⁵ based on the conventional Kretschmann configuration. Raman spectra were collected by means of a LabRAM-HR (Jobin Yvon) Raman microspectrometer. The excitation source was either a HeNe (632.8 nm, 17 mW) or a Nd:YAG (532 nm, 50 mW) laser. The exciting radiation was directed through neutral density filters to reduce sample heating and was focused on the sample through a $\times 50$ objective (working-distance, WD = 10.6 mm, numerical aperture, NA = 0.5) or a $\times 100$ objective (WD = 1 mm, NA = 0.9). For Raman and fluorescence microscopy measurements the samples were enclosed under N_2 atmosphere in a variable temperature chamber (Linkam THMS600).

3 Results and discussion

3.1 Absorption spectroscopy

The change of the spin state of the molecule leads naturally to a complete change of its electronic absorption spectra, which can be used therefore conveniently to follow the spin state changes. In particular much attention has been focused on metal-centered $d-d$ (or ligand-field) transitions appearing in the visible (vis) or near infrared (NIR) spectral ranges.¹⁴ However, these transitions are relatively weak (Laporte forbidden) and the associated molar extinction coefficients (ϵ) span from 1 to $100 \text{ M}^{-1}\text{cm}^{-1}$. Taking into account the Lambert-Beer law (eq. 1), it is clear that metal-centered absorption bands cannot be observed for very thin films with thickness (d) below *ca.* $1 \mu\text{m}$, because their optical density (OD) will be very low, even if the concentration (c) of the metallic centers is high (*e.g.* pure, non-diluted compounds).

$$OD = 0.434\epsilon dc \quad (1)$$

On the other hand it is perhaps less widely recognized that charge transfer (CT) bands provide a possibility for detecting absorbance changes even in films with nanometric thickness, because ϵ can reach values as high as $10^4 - 10^5 \text{ M}^{-1}\text{cm}^{-1}$. For example, a chromophore with $\epsilon = 10^4 \text{ M}^{-1}\text{cm}^{-1}$ provides a signal in the $10^{-3} OD$ range for a 1 nm thick (continuous) film, which is readily measurable by conventional spectrophotometers. If CT transitions involve molecular orbitals located primarily on the metal ion, they will be also altered by the spin state of this latter. To highlight the potential use of this technique we have recorded the variable temperature optical absorption spectra of thin films of the spin crossover complex $[\text{Fe}(\text{hptrz})_3](\text{OTs})_2$ in the ultraviolet (UV) wavelength range for different film thicknesses (fig. 1). In the high temperature (*i.e.* high spin) state the films are nearly transparent through the whole $UV - vis - NIR$ spectral domain. On the other hand, in the low temperature (*i.e.* low spin) state they display an absorption band centered at 285 nm, which can be assigned thus to a

singlet CT band. As shown in fig. 1a-1b on the example of a 80 nm thick film, the temperature dependence of this absorption band reveals clearly an abrupt spin transition in the film around 338 K with a very small hysteresis loop. The variation of the absorbance at 285 nm as a function of the film thickness is shown in fig. 1c. A linear fit on the data yields an extinction coefficient of $1.0(2)\times 10^4 \text{ cm}^{-1}$. The main advantage of transmittance measurements is that they provide a quantitative determination of the spin fractions, the absorbance being closely proportional to the concentration of the chromophore. Furthermore, temperature and pressure dependent absorption measurements are easy to implement. On the other hand, they are limited to the study of films with high surface density of SCO complexes displaying HS and/or LS absorption bands of large oscillator strength. Moreover, such intense bands appear usually in the *UV* spectral range, which may represent a limitation for photonic devices.

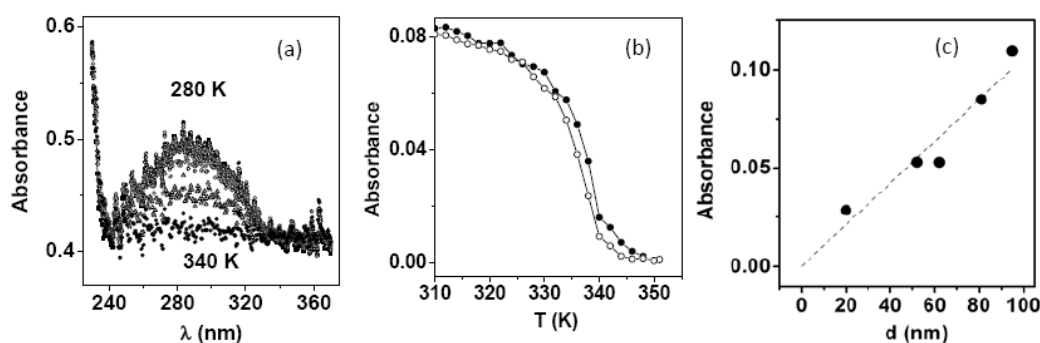


Fig. 1 (a) Selected temperature-dependent absorption spectra of a 80 nm thin film of the compound $[\text{Fe}(\text{hptrz})_3](\text{OTs})_2$ in the *UV* spectral region. (b) Temperature dependence of the absorbance of the same film at 285 nm ($dT/dt = 2 \text{ K/min}$). Open and closed symbols indicate the cooling and heating modes, respectively. (c) Variation of the absorbance (285 nm, room T) as a function of the film thickness. (The values of d were determined by atomic force microscopy.)

3.2 Fluorescent doping

For many applications detection of transmitted light intensity changes is not convenient. On the other hand, a luminophore dopant may be also used to probe the spin state of SCO materials. In general, luminescence can provide superior contrast and sensitivity for non-contact (remote) signal detection with fairly high spatial and temporal resolution. These assets can be used advantageously in various photonic applications. The luminescence signal may be modulated by the structural changes that occur on SCO, for example changes in the density (and hence rigidity) of the lattice can affect both the wavelength and intensity of the light emitted by the luminophore. Alternatively, the luminescence can be modulated directly due to the change in the electronic configuration of the SCO material during the transition. If the separation between a pair of energy levels associated with the luminophore matches closely an energy level spacing of the SCO centre (in a given spin state) the excited state energy can be transferred to the latter (fig. 2). For example, if the emission and/or excitation bands of the luminophore show significant overlap with the absorption bands of the SCO material, the luminescent response can be quenched via different energy transfer processes. Hence, through the judicious choice of a luminophore with suitable spectral overlap, it is possible to

modulate the luminescent response as a function of the spin state of the SCO centers. Key factors in optimizing the energy transfer mechanisms in these mixed materials include the nature (radiative or non-radiative) of the quenching process, the relative proportion of luminophores with respect to the spin-active centers as well as their separation.

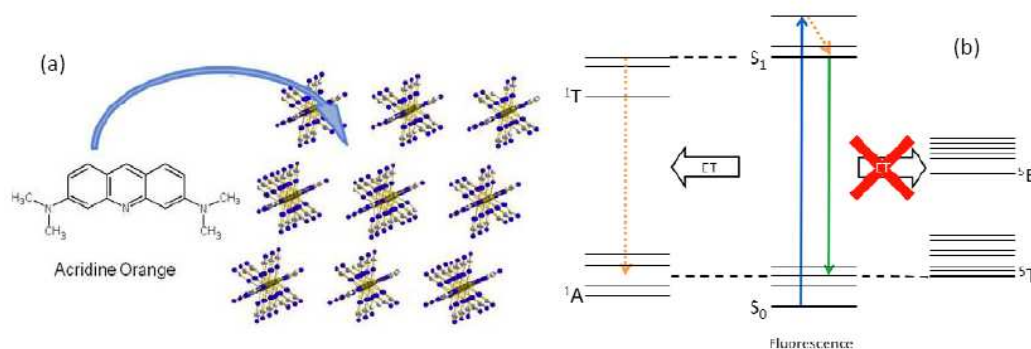


Fig. 2 (a) Schematic representation of the doping of a luminophore into the matrix of a spin crossover material. (b) Jablonski diagram showing excitation, fluorescence and energy transfer processes (ET) between a luminophore (S) and a spin crossover complex. The diagram shows the case when ET between the luminophore and the complex occurs in the LS (1A) state of the latter. Since the relaxation of the excited state of the complex ($^3T \rightarrow ^1A$) is a non-radiative process it leads to the quench of the fluorescence. When the complex is in the high spin (5T) state, ET is not efficient, *i.e.* the luminescence is not quenched.

Fig. 3 shows the chemical structure of different luminophores that we have tested in combination with the spin crossover complex $[\text{Fe}(\text{hptrz})_3](\text{OTs})_2$. These luminophores were chosen for their robust, intense luminescence in the green spectral region. Indeed, the inspection of the absorbance spectra in fig. 4 reveals that the emission bands of these luminophores overlap tightly with the broad absorption band of the complex in the LS state around 540 nm. The excitation spectra of the luminophores show also a partial spectral overlap at several wavelengths with the LS absorption bands of the complex. These features suggest that the spin state change of the complex from LS to HS should lead to a significant increase of the luminescence intensity for judiciously selected excitation and emission wavelengths.

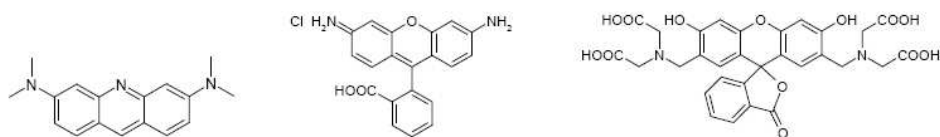


Fig. 3 Chemical structure of the luminophores used in this work. From left to right: acridine orange (AO), rhodamine 110 (RH110) and calcein.

The thermal variation of the luminescence intensity was measured at 543 nm (excited at 450 nm) for the nanoparticles of the compound $[\text{Fe}(\text{hptrz})_3](\text{OTs})_2$ doped with the different luminophores. At room temperature the complex is in the LS state, but upon heating it is transformed to the HS state

around 325 K. This spin state change involves the decrease of the absorbance at 543 nm and, as a result, an increase of the luminescence intensity at this wavelength for each dopant. When the sample is cooled back to room temperature it returns to the LS state as seen by the decrease of the luminescence intensity. One shall note that this thermal behavior is completely opposite when compared to the ordinary thermal extinction of the luminescence. Unfortunately, in the case of the calcein doped powder, we have been unable to obtain a stable, reproducible luminescence signal as a function of the temperature. This lack of stability is related mainly to photobleaching, but we observed sample ageing upon thermal cycling even in the dark, whose origin is not yet clear. On the other hand, the AO and RH110 doped powders display a fairly robust, reproducible thermal response (fig. 5a-5b). It is interesting to notice in these figures that the cooling and heating curves do not superpose: this thermal hysteresis is often observed in SCO materials due to the cooperative (first order) nature of the spin transition. Actually, as a function of the synthesis conditions, sample composition, morphology, solvents, etc. one may tune the transition temperature and also the form of the transition curves (gradual, abrupt, hysteresis) in a wide range,¹ which is a very useful asset for the different thermochrome applications.

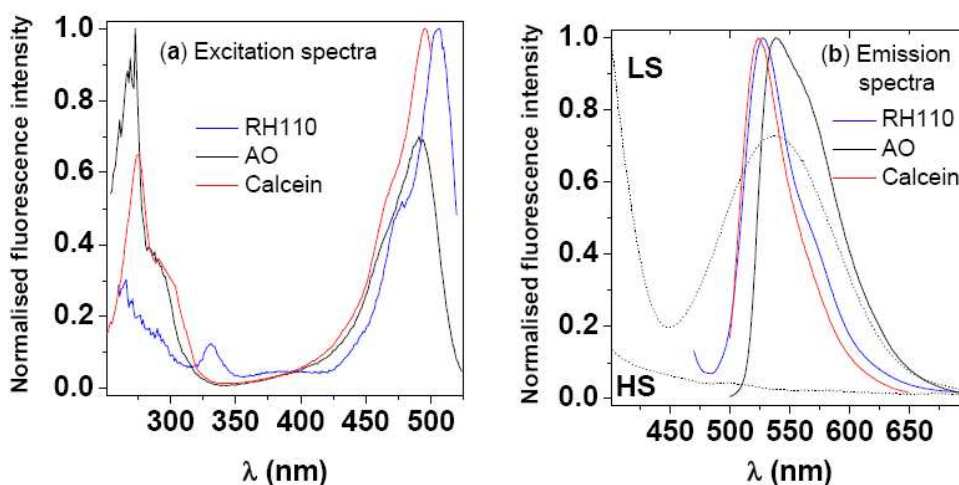


Fig. 4 Luminescence excitation (a) and emission (b) spectra of $[\text{Fe}(\text{hptrz})_3](\text{OTs})_2$ nanoparticles doped with different luminophores (295 K, chloroform solution). The spectra were recorded for 560 nm emission and 450 nm excitation wavelengths, respectively. The dotted lines show the absorption spectra of the complex in the LS and HS states.

We have also prepared thin films by spin coating the chloroform solution of the AO and also the RH110 doped complex on quartz substrates. The AO doped thin films were described in ref. [13]. Here we show the results with RH110 doping (fig. 5c). The spin transition curves obtained by fluorescence (fig. 5c) and by transmission (fig. 1b) measurements on two similar thin films (doped and undoped, respectively) are readily comparable. We shall also note that the RH110 doping in this system proved to be very efficient when compared to the results reported in ref. [15] for another Fe-triazole based system synthesized in reverse micelles. This observation highlights that beside the spectral overlap, which is nearly the same in the two cases, other parameters, such as the spatial

location of the luminophore should play also an important role in the energy transfer process in these systems.

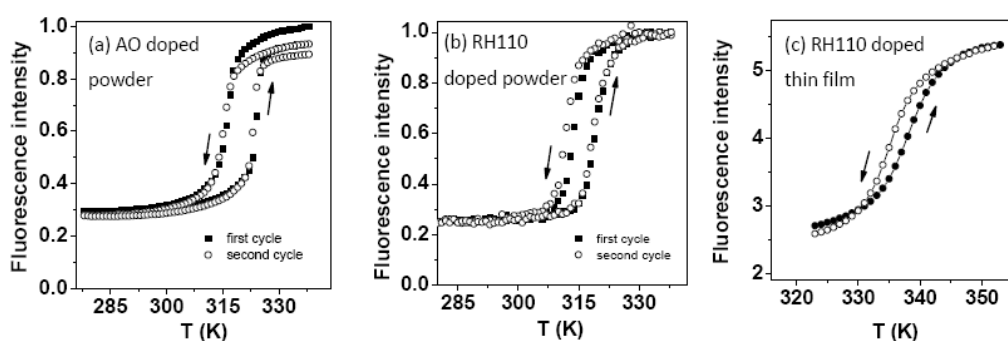


Fig. 5 Temperature dependence of the fluorescence intensity (excitation at 450 nm, emission at 543 nm) of the complex $[\text{Fe}(\text{hptrz})_3](\text{OTs})_2$ doped with different dopants in the heating and cooling modes ($dT/dt = 2 \text{ K/min}$). **(a-b)** powder samples, **(c)** thin film sample ($d = 150 \text{ nm}$).

3.3 Surface plasmon resonance (SPR) spectroscopy

SCO materials exhibit important changes of the refractive index through the whole $UV - vis - IR$ spectral ranges due primarily to the important density change accompanying the spin state change. This strong electron – lattice coupling arises from the different population of anti-bonding e_g and non-bonding t_{2g} orbitals of the Fe^{II} ion in the two spin states.¹ The volume of the octahedron defined by the six ligating nitrogen atoms around the iron(II) ion is typically 25–30 % higher in the HS state leading to a unit cell expansion $\Delta V_{\text{HL}}/V$ between 1 and 10 %, depending on the nature of the compound. As a consequence of this significant density change, one should expect a change of the real part of the refractive index upon SCO in the range between $\Delta n_{\text{HL}} = 0.01 - 0.2$. In addition to this material density change, one shall consider also the change of the electronic polarizability of the complex. This effect will be particularly important for wavelengths in the vicinity of intense charge transfer transitions.

Recently, we have demonstrated the possibility to follow the SCO phenomenon through the refractive index changes using optical diffraction, ellipsometry and SPR spectroscopy.⁴⁻⁵ This latter technique is particularly well adapted to study thin SCO films. For an appropriate combination of the wavelength, polarization and incidence angle of the exciting light beam a resonance is observed in the reflectance spectra. This is the so-called “simultaneous wavevector and frequency matching condition” for SPR spectroscopy. The corresponding minimum in the angular reflectance curve of the Au/SCO multilayer will be temperature dependent due to the ordinary thermal expansion of the material and, most importantly, due to the SCO phenomenon. When the temperature of the multilayer is increased the spin state of the SCO layer changes from LS to HS and the associated decrease of the refractive index leads to a shift of the resonance to lower angles. This phenomenon is shown in fig. 6a for a 30 nm thin film of the compound $[\text{Fe}(\text{hptrz})_3](\text{OTs})_2$ using the data reported in ref. [5]. One can observe that the shift of the reflectance intensity is virtually linear far from the spin

transition as expected for ordinary thermal expansion. On the other hand the discontinuity and the hysteresis loop around 320 K is a consequence of the thermal spin transition. This transition occurs at somewhat lower temperature when compared to the fluorescence (fig. 5c) and UV transmission (fig. 1b) curves. This difference is related most probably to the different degree of hydration of the films, because the SCO temperature in this hygroscopic compound is known to be very sensitive to its water content.¹⁰ It is important to note that the SPR spectra provide information not only on the spin state of the thin film, but allows also for the determination of its complex refractive index and its thickness. As an example, fig. 6b displays the SPR angle shift as a function of the thickness of the $[\text{Fe}(\text{hptrz})_3](\text{OTs})_2$ film. (The thickness was determined by fitting the reflection spectra of the multilayer by the Fresnel equations as described in ref. [5].)

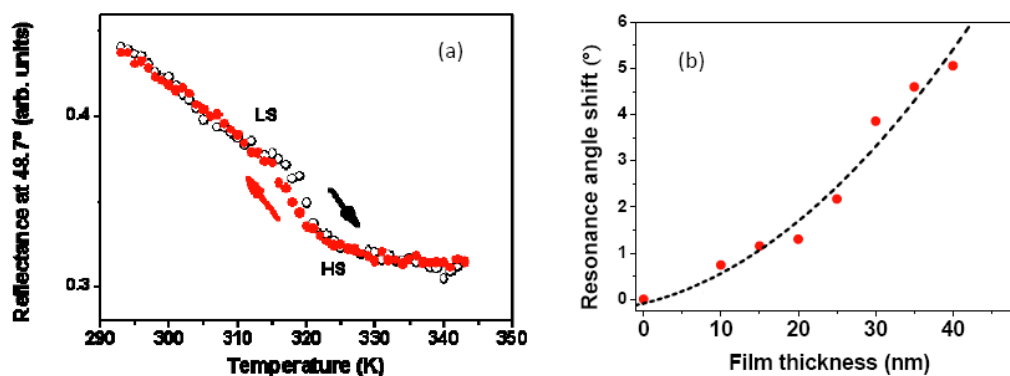


Fig. 6 (a) Temperature dependence of the reflectance intensity ($\lambda = 660 \text{ nm}$) at an incidence angle of 48.7° of the multilayer [glass / Ti (5 nm) / Au (45 nm) / $[\text{Fe}(\text{hptrz})_3](\text{OTs})_2$ (30 nm)] in the heating and cooling modes ($dT/dt = 2 \text{ K/min}$). (b) Variation of the resonance angle as a function of the film thickness ($\lambda = 660 \text{ nm}$, $T = 295 \text{ K}$).

3.4 Surface-enhanced Raman spectroscopy (SERS)

Besides the detection of molecular spin state changes in thin films of SCO compounds, another critical issue is the analysis of their composition and structure. Raman spectroscopy has been successfully employed at several occasions to infer structural information of continuous or patterned SCO films.² However, Raman scattering has inherently low cross-section, hence the idea of using an enhancement technique. Indeed, SERS refers to the fact that chemical species deposited on specifically prepared metal surfaces exhibit very intense Raman spectra exceeding by several orders of magnitude what is observed on “normal surfaces”. Today it is generally accepted that this high Raman scattering intensity arises in most cases primarily from the local electric field enhancement associated with the excitation of collective, plasma oscillations of free electrons in metals.¹⁶ Various different SERS active substrates (predominantly Ag or Au) have been described in the literature, including electrochemically roughened surfaces, lithographically patterned substrates as well as colloidal particles of various size, shape and composition, deposited in a more or less controlled manner. According to their enhancement factor they can be roughly categorized as “low sensitivity” or “high sensitivity” SERS substrates.¹⁷ The latter refers usually to substrates with “hot spots”, allowing for detection limits down to the single molecule level. However, such high sensitivity is

usually achieved at the expense of signal stability, reproducibility, excessive sample heating and even sample degradation. For this reason we decided to use a SERS substrate with a moderate sensitivity. Using standard electron-beam lithography and lift-off we elaborated arrays of gold nano-objects with the following nominal dimensions: length - 100 nm, width - 50 nm, height - 50 nm and period – 200/150 nm (fig. 7). A thin film (30 nm thickness) of the SCO complex $[\text{Fe}(\text{hptrz})_3](\text{OTs})_2$ was then spin coated on this substrate and its Raman spectra were recorded using 632.8 nm excitation, which is close to the plasmon resonance of the substrate around 642 nm (fig. 7).

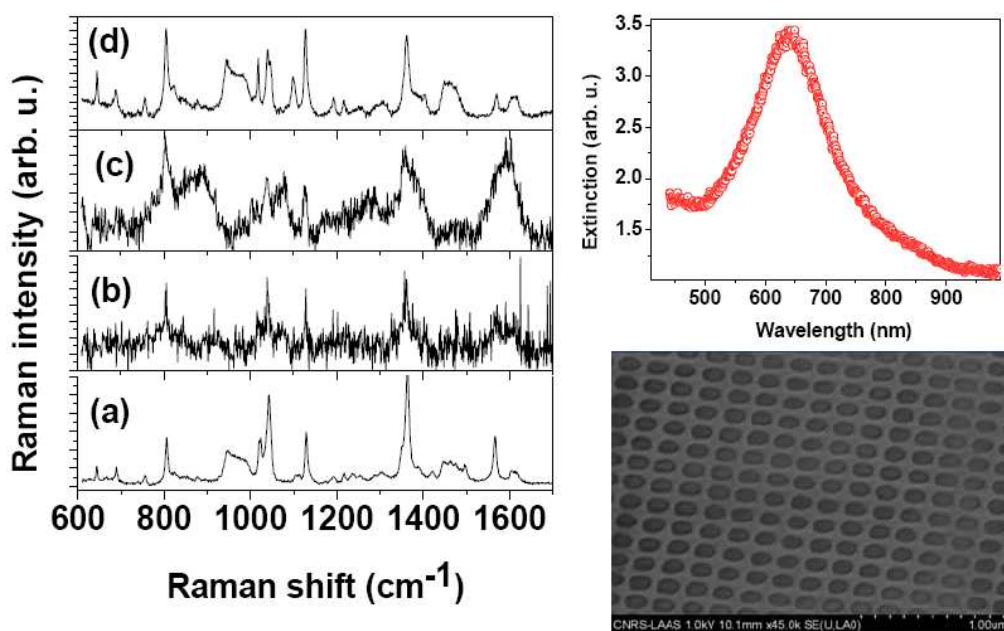


Fig. 7 Left panel: Raman spectra (632.8 nm excitation) of $[\text{Fe}(\text{hptrz})_3](\text{OTs})_2$ for the bulk powder (293 K – **a**, 353 K - **d**) and for a thin film sample ($d = 60$ nm) at 293 K on two different substrates: glass substrate (**b**), SERS substrate (**c**). The background of the spectra was removed. Right panel: The plasmon band (642 nm) and a SEM image of the lithographically patterned Au SERS substrate.

We have recorded Raman spectra of the deposited film both inside (fig. 7c) and outside (fig. 7b) of the SERS active region of the substrate in otherwise identical experimental conditions. For comparison we show also the Raman spectrum of the bulk powder (fig. 7a). The spectra of the films are very weak, but one can clearly recognize the spectral signature of the complex. We observe also a clear enhancement (*ca.* $\times 10$) due to the SERS substrate. In the case of the SERS spectrum we observe a few additional Raman modes as well, which may arise from impurities and/or due to the change of selection rules.¹⁶ For this complex, the spectral changes upon the SCO are rather subtle¹⁰ and it is difficult to assign the thin film spectra to the HS or LS states. To further investigate this question we have heated the film to 353 K, but no significant spectral change was observed. This suggests that the complex is already in the HS state at 293 K, due most probably to laser-induced heating. (Unfortunately, the very weak spectral intensity did not allow us to reduce the laser power.)

The confirmation of the SERS enhancement as well as the spin state identification for the

[Fe(hptrz)₃](OTs)₂ system turned out rather difficult. For this reason we decided to investigate by the SERS method thin films of the compound Fe(pz)[Pt(CN)₄], whose far-field Raman spectra have been extensively studied in our group.¹⁸ For this work we developed a specific SERS substrate, which was based on the introduction of gold nanoparticles (AuNPs) into a multilayer of the SCO film. (See fig. S1 in the Supporting Information for the schema of the assembly process.) In the first step, benzene-1,4-dithiol was used to functionalize a gold-coated substrate by means of Au-S bonds. Then, the AuNPs were attached to the surface by the other S atom of the benzene-1,4-dithiol. In the next step mercaptopyridine was used to functionalize the “free surface” of AuNPs, also using the Au-S bonds. Afterwards, the substrate was immersed into ethanol solutions of Fe(BF₄)₂, K₂Pt(CN)₄ and pyrazine step-by-step in order to assemble a continuous films of the SCO complex Fe(pz)[Pt(CN)₄], similar to the method described in refs. [11, 18]. On the whole 5 layers of the complex were deposited. The AFM images of the multilayer film revealed a mean roughness around 50 nm (fig. S2), which is close to the expected total thickness for the multilayer [Ti/Au (17 nm), 1 layer of AuNPs (18 nm), and 5 layers of the complex (5 nm)]. As one can see from the cross-section of the AFM image (fig. S2), objects with larger size (from a few hundreds of nm to a few tens of nm) are also observed, probably due to the aggregation of AuNPs and/or the precipitation of the iron complex.

The bulk powder of the Fe(pz)[Pt(CN)₄] complex was used to identify Raman markers of the spin transition for three different excitation wavelengths. Previous works have shown that, for an excitation at 632.8 nm, there are two useful markers. The first marker corresponds to the shift of a Raman mode from 645 cm⁻¹ in the HS state to 675 cm⁻¹ in the LS state. The second marker corresponds to the variation of the intensity ratio of two Raman modes at 1030 cm⁻¹ and 1230 cm⁻¹, the former (latter) being more intense in the HS (LS) state. Fig. S3 shows the Raman spectra of the bulk complex in the HS and LS states for two different excitation wavelengths. For the 532 nm excitation wavelength, the sole clear marker is the shift of the 645 cm⁻¹ mode. In contrast to the 633 nm excitation, the intensity ratio of the two other modes at 1030 cm⁻¹ and 1230 cm⁻¹ does not change much. For both excitation wavelengths, the LS state Raman signal is more intense than that of the HS state. In order to detect the spin state switching for the 5 layers of the complex deposited on AuNPs, we have acquired Raman spectra at high and low temperatures (fig. 8). The Raman signature of silicon (broad band around 950-1000 cm⁻¹) appears for both temperatures and both excitation wavelengths. At 532 nm excitation wavelength, we can see a clear Raman signal from the iron complex around 2200 cm⁻¹ (CN stretching mode) at both temperatures. With the same conditions but with an excitation wavelength of 633 nm and a laser power of 12 mW, Raman spectra recorded at high and low temperatures are not very clean. Actually, with a red excitation, the Raman signal from benzene-1,4-dithiol (main frequencies: 629, 738, 1056, 1092 and 2560 cm⁻¹) is stronger than that of the iron complex. Moreover, the background produced by the silicon substrate is important in the range between 600-700 cm⁻¹. For this reason it is very difficult to see the peaks at 645 or 675 cm⁻¹. Previous Raman experiments have highlighted that it is necessary to have a minimum of *ca.* 100 nm film thickness to detect the spectrum of the iron complex with our Raman spectrometer. From the AFM image we can safely deduce that the film thickness in the present case is certainly much less than 100 nm. Thus it is apparent that there must be an enhancement mechanism so as to observe Raman signal from this sample. We believe that this enhancement should be the plasmon resonance of gold nanoparticles (SERS effect). The plasmon resonance for gold nanoparticles with 18 nm of diameter is around 520 nm (fig. 8), so the SERS effect will be higher for the green excitation (532 nm).

SERS effect can explain why we can detect Raman signal with only 5 deposited cycles. However, it is not the only effect as we can infer from the differences between red and green excitation. The other effect is plausibly the resonant Raman enhancement because the green spectral range corresponds to an absorption band of the iron complex. Indeed, the Raman signal of the iron complex is multiplied by *ca.* 6 when the excitation is at 532 nm (compared to 633 nm). We can thus tentatively distinguish surface enhanced resonance Raman, SERRS (532 nm) and SERS (633 nm) effects. One shall note also that the excitation at 785 nm did not allow us to observe a Raman signal from the sample. This observation is in agreement with the fact that the enhancement should decrease when the excitation wavelength is getting far from the plasmon resonance.

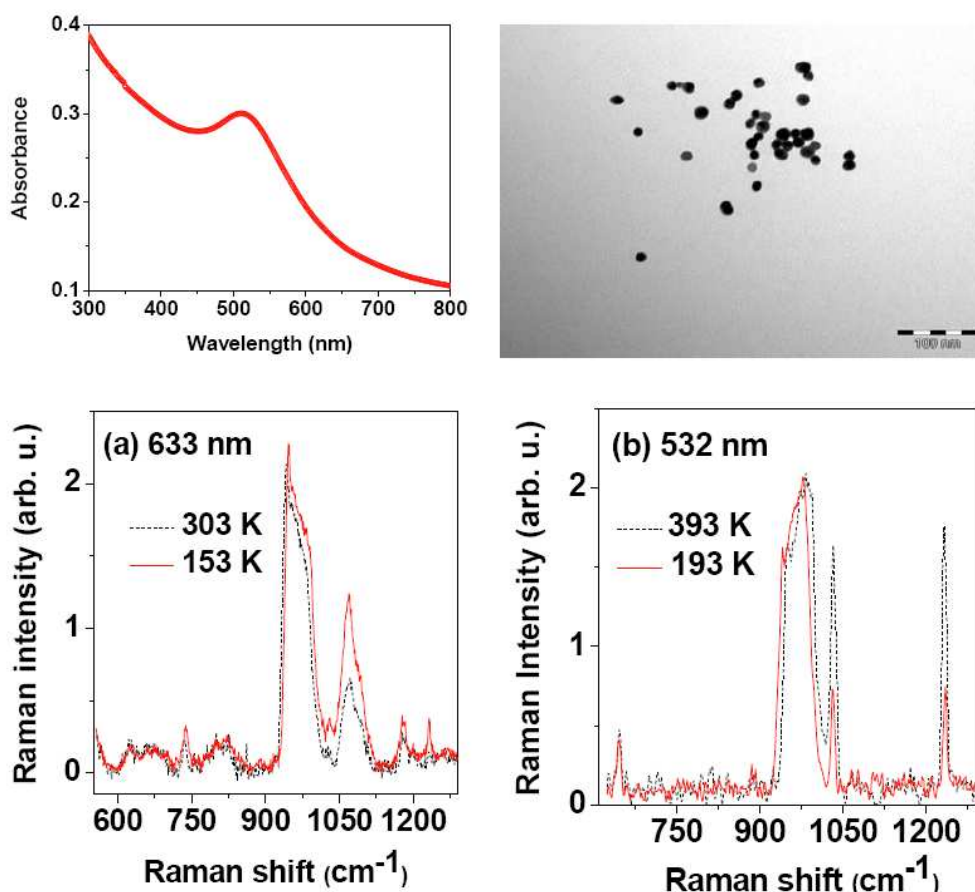


Fig. 8 (Top panel) The plasmon band (520 nm) and a TEM image of the Au nanoparticles used for the fabrication of SERS substrates. (Bottom panel) Raman scattering of a Fe(pz)[Pt(CN)₄] film deposited on the AuNP SERS substrate. Spectra were recorded at two different temperatures using an excitation wavelength of 632.8 nm (a) or 532 nm (b). The background of the spectra was removed.

On the whole, the Fe(pz)[Pt(CN)₄] system allowed us to demonstrate the usefulness of the SERS approach for obtaining the spectral signature of very thin (5 nm) layers of SCO complexes. On the

other hand, a few drawbacks of the SERS approach have been also highlighted, which must be considered for the further development of this method in this field. First of all, the extreme surface sensitivity of the method leads to the exaltation of the signal mainly from the first deposited layer,¹⁶ which is often not representative for the ensemble of the film due to the possible presence of impurities, anchoring layers (thiols in our case) or distorted/incomplete coordination environments around the Fe(II) ions. This fact – together with the modification of the selection rules - can explain the presence of additional peaks in the spectra when compared to the bulk complex. Resonance effects may be used to obtain more sample selectivity. In a few cases, we observed also strong spectral fluctuations and the emergence of broad bands between *ca.* 1000 – 1600 cm⁻¹. This phenomenon can be assigned to the formation of carbonaceous species formed by the alteration/decomposition of the deposited molecules (and/or contaminants) due to the high field enhancement.¹⁹ Even in the absence of decomposition problems, significant and uncontrolled sample heating and/or photoswitching may arise, which are of course undesirable phenomena in the context of spin transition studies. An optimization of the field enhancement seems thus inevitable in each case.

4 Conclusion

We have investigated nanometric thin films of the spin crossover complex [Fe(hptrz)₃](OTs)₂ by means of different optical methods. We have shown that standard transmission measurements can be very useful to follow the SCO phenomenon in the *UV* spectral range, where intense CT absorption bands occur. On the other hand, it is possible to use visible light as well, if one employs an appropriate luminescent dopant to report on the spin state changes through the luminescence intensity modulation. Besides a good spectral overlap between the luminophore and the SCO complex, however, one has to control also the spatial location and the stability of the luminophore within the SCO matrix. Alternatively, refractive index changes associated with the SCO can be also detected in the *vis-NIR* spectral range by, for example, surface plasmon resonance spectroscopy. From the SPR spectra we deduced not only the spin transition temperature, but also the thickness of the deposited film with nanometric precision. We have used surface plasmons also to analyze, for the first time, the composition and structure of SCO complexes in ultra-thin films *via* the SERS effect. On the other hand, the temperature-dependent SERS spectra did not allow us to evidence clearly the thermal spin crossover, probably due to excessive laser-induced heating in the regions of field enhancement. Further studies will be necessary to clarify this question. Finally we shall note that there is certainly also an interesting scope for complementary measurements in the infrared spectral range where the frequency dependence of the complex permittivity should provide rich and sensitive information on the properties of SCO thin films.

Acknowledgments

This work was supported by the ANR projects “NanoMol” and “CrossNanomat”.

References

-
- [1] P. Gütllich and H. A. Goodwin, "Spin Crossover - An Overall Perspective," *Top. Curr. Chem.* **233**, 1–47 (2004).
- [2] A. Bousseksou et al., "Molecular Spin Crossover Phenomenon: Recent Achievements and Prospects," *Chem. Soc. Rev.* **40**(6), 3313-3335 (2011).
- [3] M. Cavallini, "Status and Perspectives in Thin Films and Patterning of Spin Crossover Compounds," *Phys. Chem. Chem. Phys.* in press (2012), DOI: 10.1039/c0xx00000x.
- [4] A. Akou et al., "Soft Lithographic Patterning of Spin Crossover Complexes. Part 2: Stimuli-Responsive Diffraction Grating Properties," *J. Mater. Chem.* **22**(9), 3752-3757 (2012).
- [5] G. Félix et al., "Surface plasmons reveal spin crossover in nanometric layers," *J. Am. Chem. Soc.* **133**(39), 15342-15345 (2011).
- [6] T. Mahfoud et al., "Electrical properties and non-volatile memory effect of the [Fe(HB(pz)₃)₂] spin crossover complex integrated in a microelectrode device," *Appl. Phys. Lett.* **99**(5), 053307 (2011).
- [7] F. Prins et al., "Room-Temperature Electrical Addressing of a Bistable Spin-Crossover Molecular System," *Adv. Mater.* **23**(13), 1545-1549 (2011).
- [8] A. Rotaru et al., "Dielectrophoretic Organization and Charge Transport Measurements on Spin Crossover Nanorods: Towards Switchable Nanoelectronic Devices," submitted.
- [9] H. J. Shepherd et al., "Luminescent spin crossover materials," in *Spin-Crossover Materials: Properties and Applications* (ed. M. Halcrow), Wiley, (2012) in press.
- [10] I. A. Gural'skiy et al., "Synthesis of Spin-Crossover Nano- and Micro-objects in Homogeneous Media," *Chem. Eur. J.* in press (2012), DOI: 10.1002/chem.201201063.
- [11] C. Bartual-Murgui et al., "High quality nano-patterned thin films of the coordination compound {Fe(pyrazine)[Pt(CN)₄] deposited layer-by-layer," *New J. Chem.* **35**(10), 2089-2094 (2011).
- [12] J. Turkevich, P. C. Stevenson, and J. Hillier, "A study of the nucleation and growth processes in the synthesis of colloidal gold," *Discuss. Faraday. Soc.* **11**, 55-75 (1951).
- [13] C. M. Quintero et al., "Soft Lithographic Patterning of Spin Crossover Complexes. Part 1: Fluorescent Detection of the Spin Transition in Single Nano-Objects," *J. Mater. Chem.* **22**(9), 3745-3751 (2012).
- [14] A. Hauser, "Ligand Field Theoretical Considerations," *Top. Curr. Chem.* **233**, 49–58 (2004).
- [15] L. Salmon et al., "A novel approach for fluorescent thermometry and thermal imaging purposes using spin crossover nanoparticles," *J. Mater. Chem.* **20**(26), 5499 – 5503 (2010).
- [16] M. Moskovits, "Surface-enhanced spectroscopy," *Rev. Mod. Phys.* **57**(3), 783-826 (1985).
- [17] S. E. J. Bell and N. M. S. Sirimuthu, "Quantitative surface-enhanced Raman spectroscopy," *Chem. Soc. Rev.* **37**(5), 1012-1024 (2008).
- [18] S. Cobo et al., "Multilayer Sequential Assembly of Thin Films that Display Room-Temperature Spin Crossover with Hysteresis," *Angew. Chem. Int. Ed.* **45**(35), 5786-5789 (2006).
- [19] K. F. Domke, D. Zhang, and B. Pettinger, "Enhanced Raman Spectroscopy: Single Molecules or Carbon?," *J. Phys. Chem. C* **111**(24), 8611-8616 (2007).

SUPPLEMENTARY MATERIALS FOR

Detection of molecular spin-state changes in ultra-thin films by photonic methods

I. A. Gural'skiy,^{1,2} C. Quintero,¹ K. Abdul-Kader,¹ M. Lopes,¹ C. Bartual-Murgui,^{1,3} L. Salmon,¹ Z. Pengxiang,⁴ G. Molnár,^{1,*} D. Astruc,⁴ A. Bousseksou^{1,*}

¹Laboratoire de Chimie de Coordination, CNRS UPR-8241 and Université de Toulouse, UPS, INP, F-31077 Toulouse, France

²Department of Chemistry, National Taras Shevchenko University, 01601 Kiev, Ukraine

³LAAS, CNRS & Université de Toulouse (UPS, INSA, IAES), 7 avenue du colonel Roche, 31077 Toulouse, France

⁴Université de Bordeaux, ISM, CNRS, UMR 5255, F-33405 Talence, France

* Corresponding authors: gabor.molnar@lcc-toulouse.fr, azzedine.bousseksou@lcc-toulouse.fr

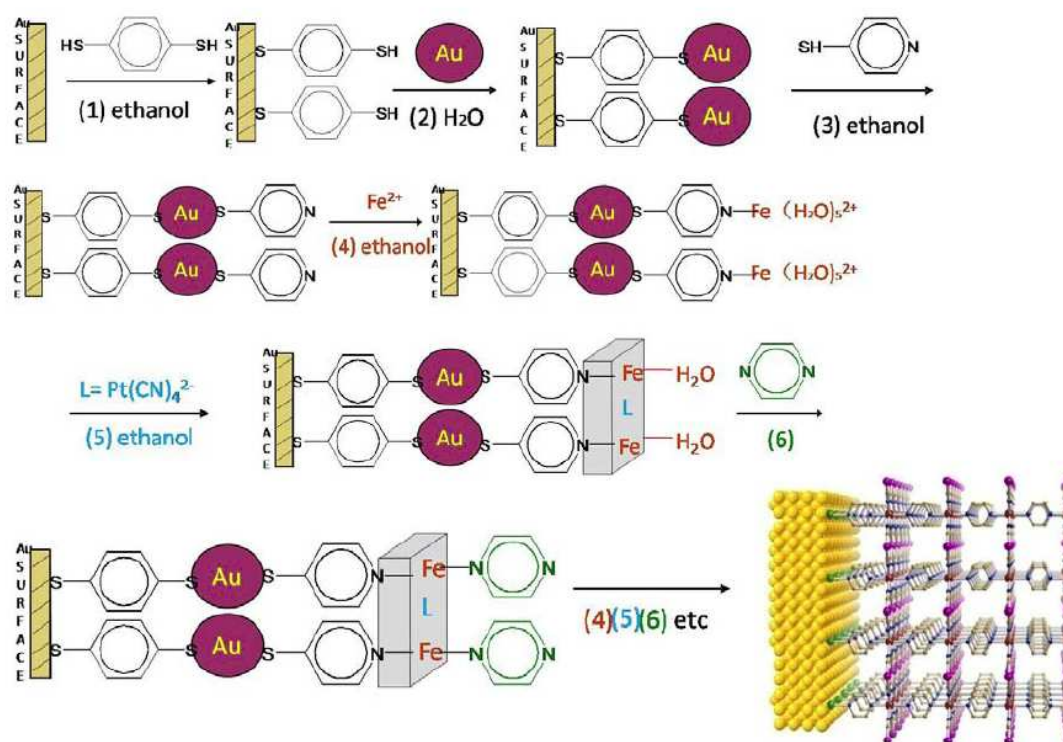


Fig. S1 Scheme of sequential assembly of the SERS substrate and the multilayer of the compound $\text{Fe}(\text{pz})[\text{Pt}(\text{CN})_4]$

14

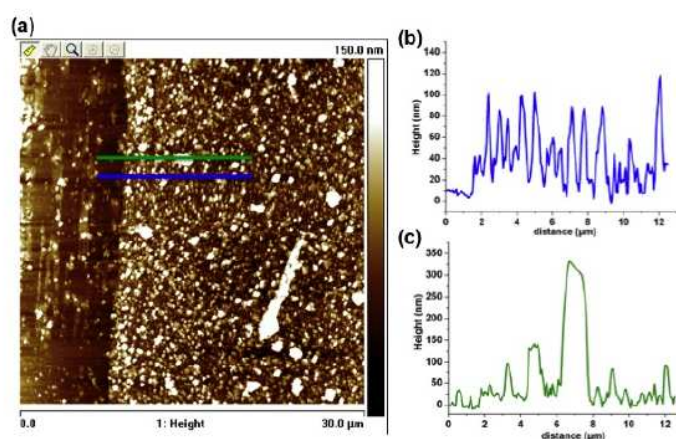


Fig. S2 (a) AFM image of the surface of the multilayer shown in fig. S1 with a stripe on the left. AFM cross-sections corresponding to the blue and green lines on the AFM image are also shown (b-c). The depth of the stripe indicates the thickness of the gold layer deposited on silicon, i.e. 20 nm.

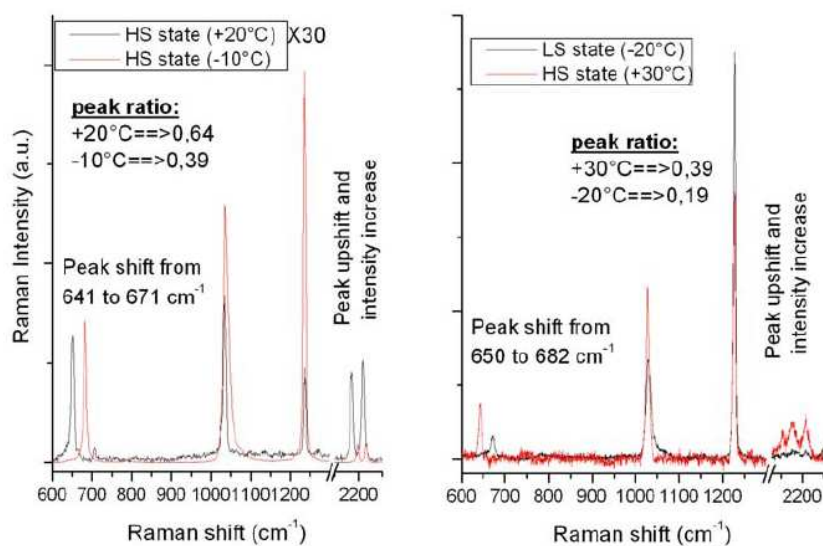


Fig. S3 Raman spectra of a Fe(pz)[Pt(CN)₄] powder sample in the low spin and high spin states for excitation wavelengths of 633 nm (left panel) and 532 nm (right panel).

Conclusions et perspectives - Conclusions and Perspectives

Au cours de cette thèse, nous avons recherché la synthèse et la fonctionnalisation de AuNPs ainsi que leurs applications dans divers domaines.

La première mise au point figurant dans le premier chapitre nous a donné l'occasion de nous pencher sur les très nombreuses méthodes de synthèse des AuNPs en fonction des applications souhaitées et de résumer et rassembler une bibliographie très fournie jusqu'à cette année et toujours en pleine croissance. Il est à présent possible, en particulier, de prédéfinir la taille et la morphologie des AuNPs ainsi que leur habillage.

La seconde mise au point a concerné la vectorisation du docétaxel à l'aide de l'ingénierie nanotechnologique. Étant donné les effets toxiques très sévères du taxotère, la formulation classique du docétaxel, de nombreuses recherches ont été menées afin de solubiliser et de vectoriser de façon la plus appropriée possible ce puissant médicament anti-cancer en optimisant la proportion administrée susceptible d'atteindre sélectivement les cellules cancéreuses. Ces recherches ont été menées afin de mettre au point de nouvelles formulations plus performantes que celles du taxotère. Il est remarquable de constater que, malgré une efficacité anti-cancéreuse au moins équivalente et sans doute même supérieure à celle du taxol, la formulation du paclitaxel, les tentatives d'essais cliniques sur de nouvelles formulations du docétaxel soit aussi nombreuses en regard de la littérature très fournie sur les recherches nanotechnologiques fondamentales de vectorisation.

Sur la base de ces études bibliographiques (chapitre 1), les travaux expérimentaux de thèse ont donné lieu à des synthèses et fonctionnalisations de AuNPs dans divers secteurs et rassemblés dans les trois chapitres 2-4.

D'une façon générale, après synthèse de AuNPs selon la méthode classique biphasique de Brust-Schiffrin, la fonctionnalisation est assurée soit par réaction "click" entre un azoture et un alcyne terminal, soit par couplage amidique covalent (plus classique, mais la plupart du temps de mise en oeuvre expérimentalement plus difficile), ou bien encore par interaction supramoléculaire, c'est-à-dire par liaison ionique, hydrogène ou encapsulation dans les branches de la AuNP. Toutes ces approches ont été réalisées dans ce travail de thèse selon les besoins.

Concernant la réaction "click" dont la mise en oeuvre est, par définition, si facile en chimie organique classique et moléculaire sub-nanoscopique selon le concept relevant de la chimie verte de Sharpless, l'extension aux AuNPs a posé d'énormes difficultés en raison de l'agglomération rédibitoire des AuNPs se trouvant au contact du catalyseur au Cu(I). Dans le catalyseur de Sharpless, le Cu(I) est très faiblement ligandé, ce qui résulte de la facilité affichée de mise en oeuvre à partir simplement de sulfate de cuivre et d'ascorbate de sodium en solvant organique ou aqueux. Dans ces

conditions, d'une part l'ion métallique est exposé à des interactions prononcées provoquant l'agglomération extensive, d'autre part son activité catalytique est modeste ou très insuffisante à température ambiante. Le nouveau catalyseur [Cu(I)(hexabenzyltren) Br permet à la fois de protéger le Cu(I) vis-à-vis de l'aggrégation par une bonne sphère de coordination tétradentate du ligand azoté et un accroissement de la densité électronique sur le centre métallique conduisant à une activité catalytique très accrue dès la température ambiante. Enfin le catalyseur est beaucoup plus facilement séparé des AuNPs que dans le système de Sharpless. Concrètement, ceci a abouti à un abaissement de la stoechiométrie en Cu(I) de 400% avec le catalyseur classique de Sharpless à 10% pour les fonctionnalisations variées avec notre catalyseur [Cu (I)(hexabenzyltren) Br pour la fonctionnalisation des AuNPs (chapitre 2).

Concernant la fonctionnalisation à l'aide du récepteur folate positionné en bout de chaîne polyéthylène glycol afin d'assurer un bon contact externe à l'approche des cellules cancéreuses, le couplage amidique déjà connu a été mis en oeuvre (chapitre 3).

La fonctionnalisation non covalente, supramoléculaire, est extrêmement utile, d'autant qu'elle est très facile de mise en oeuvre par simple contact pourvu que le système moléculaire ou nanoscopique ait été au préalable correctement organisé. C'est ainsi que nous avons avantageusement mis à profit les effets hydrophiles et hydrophobes respectifs de l'intérieur de la AuNP et du milieu extérieur (solvant) pour l'encapsulation et le transport de substrats tels que le docétaxel ou diverses vitamines (chapitre 3).

Enfin, l'expérience du laboratoire et la nôtre propre nous a permis de varier les modes de synthèse des AuNPs en comparer la méthode directe de synthèse à partir de HAuCl₄, mais qui n'est pas compatible avec la majorité des fonctions organiques et inorganiques, avec d'autres méthodes plus élaborées, mais bien plus efficaces.

C'est ainsi que nous avons étudié les différentes conditions d'échange de ligand thiolates par de nouveaux ligands fonctionnels thiols, accompagné par le transfert de l'atome d'hydrogène acide du ligand rentrant vers le thiolate sortant. Cette méthode mise au point à la fin des années 1990 par Murray a été souvent utilisée ici. Cependant, une méthode plus originale que cette dernière a été recherchée en raison du caractère limité des possibilités de la réaction d'échange de ligands de Murray.

Ainsi, les ligands "click", c'est-à-dire 1,2,3-triazoles ont été directement introduits sur les AuNPs par synthèse directe, et les nouvelles AuNPs ont été complètement caractérisées. Elles sont stables dans l'eau avec les ligands triazole-polyéthylène glycol, et elles peuvent facilement échanger rapidement tous leurs ligands avec des ligands thiolate fonctionnels ou un mélange en proportion précise de tels ligands fonctionnels.

Ces nouvelles AuNPs très originales comportant les nouveaux ligands 1,2,3-triazoles, de par leurs propriétés de stabilité et de labilité des ligands triazoles, possèdent des possibilités d'applications variées en tant que capteurs, comme nous l'avons démontré grâce à la variation de l'absorption plasmonique avec l'ATP et la vitamine C dans l'eau, et probablement en catalyse d'oxydation, en plus de leurs propriétés très utiles de substitution de ligands pour les synthèses les plus sophistiquées (chapitre 3).

L'introduction de complexes du Fe(II) à transition de spin constitue un exemple de synthèse de nanomatériaux. Cette collaboration a permis à l'équipe d'Azzedine Bousseksou d'envisager l'étude de la transition de spin entre les complexes à bas spin (zero) et haut spin (deux) en particulier par la méthode SERS (spectroscopie Raman exacerbée par le champ au voisinage immediate des AuNPs). La décroissance exponentielle de cet effet Raman au fût et à mesure de l'éloignement de la surface implique que les centres Fe(II) soient extrêmement proches de cette surface, ce que nous avons probablement sous-estimé dans une première approche. Cependant, le travail d'ensemble du groupe toulousain sur ces matériaux a récemment permis de soumettre un article en collaboration pour publication (chapitre 4).

Au bilan, notre thèse a permis des avancées dans la mise au point des connaissances actuelles sur la synthèse des AuNPs et la vectorisation du docétaxel et, sur le plan expérimental, de faire avancer de façon conséquente l'ingénierie d'élaboration et de fonctionnalisation des AuNPs, et ainsi d'ouvrir de nouvelles utilisations et d'applications potentielles des AuNPs dans les domaines de la nanomédecine et des nanomatériaux.

English

In this thesis, we investigated the synthesis and functionalization of AuNPs and their applications in various fields.

The first development in chapter 1 figure out the development has given us the opportunity to reflect on many methods for the synthesis of AuNPs according to desired applications and compile a summary of literatures until this year and still growing. It is now possible, in particular, to predefine the size and morphology of AuNPs.

The second development contained the vectorization of docetaxel using the nanotechnology engineering. Due to the severe toxic effects of taxotere, the classic formulation of docetaxel, a lot of investigations have been conducted to solubilize and vectorizing of docetaxel, which was considered to be the most appropriate way to deliver this powerful anti-cancer drug to cancer cells. This research was conducted to developed new formulations more efficiency than taxotere. It is remarkable noted that, the anti-cancer efficacy of docetaxel at least equivalent and probably even greater than that of Taxol, the paclitaxel formulation. However, a lot of literatures still attempt to investigate new formulations of docetaxel in clinical trials, which provided a basic nanotechnology research on vectorization.

Based on these literature reviews (Chapter 1), the experimental works led to synthesis and functionalization of AuNPs in different areas and gathered in the three chapter 2-4.

Generally, after synthesis of AuNPs using the traditional two phase Brust-Schiffrin method, the functionalization reaction is carried out by "click" between an azide and a terminal alkyne, or by covalent amide linkage (more classical, but always difficult in experiment), or alternatively by supramolecular interaction, that is to say by ionic bond, hydrogen or encapsulation in the branches of AUNP. All these approaches have been made in this thesis as required.

The "click" reaction is easily implemented in classical organic chemistry and sub-nanosopic molecular chemistry under the concept of green chemistry by Sharpless. The extension of AuNPs has posed enormous difficulties due to the agglomeration of AuNPs being contact with the catalyst Cu (I). In the Sharpless catalyst, Cu (I) is very weak liganded, easily generated from the copper sulfate and sodium ascorbate in aqueous or organic solvent. Under these conditions, the metal ion exposing to the interactions caused extensive agglomeration or AuNPs, on the other hand, its catalytic activity is modest or very poor at room temperature. The new catalyst [Cu (I) (hexabenzyltren)] Br allows both to protect the Cu (I) from the aggregation by a good coordination sphere of the tetradentate ligand nitrogen and increase in electron density on the metal center leading to an increased catalytic activity at room temperature. Finally the catalyst is easily separated from the AuNPs than that of the Sharpless system. In practice, this resulted in a decreasing of the

stoichiometry of Cu (I) 400 % with the conventional catalyst Sharpless to 10% for various functionalizations with our catalyst [Cu (I) (hexabenzyltren] Br for the functionalization of AuNPs (Chapter 2).

Concerning the folate functionalization of gold nanoparticles, the already known amide coupling was used to introduce the folate receptor at the termini of polyethylene glycol chain on gold nanoparticles to target the cancer cells. (Chapter 3)

The non covalent functionalization, supramolecular, is extremely useful, especially since it is very easy to prepare. The provided nanoscopic or molecular system has been properly organized in advance. Thus we have advantageously used the hydrophilic and hydrophobic effects related to the AuNP inside and the outside environment (solvent), respectively, for encapsulation and transportation of substrates as docetaxel or various vitamins (Chapter 3).

Finally, laboratory experience and our own knowledge allowed us to vary the methods of synthesis of AuNPs compared with the direct synthesis from HAuCl₄. However, it is not compatible with the majority of organic and inorganic functions, but compared with other more sophisticated methods, it is much more effective.

Thus, we studied the different conditions of thiolate ligand exchange with new functional thiol ligands, accompanied by the transfer of the acidic hydrogen atom in ligand returning to the leaving thiolate. This method developed in the end of 1990s by Murray was commonly used here. However, a more original method was investigated due to the limited possibilities of the Murray's ligand exchange reaction.

Thus, the ligands "click", 1,2,3-triazoles were directly introduced into the AuNPs by direct synthesis, and new AuNPs were fully characterized. They are stable in water with polyethylene glycol-triazole ligands, and can easily substitute all their ligands rapidly with thiolate ligands or with mixed thiolate ligands in precise proportion .

These very original AuNPs with the new ligands 1,2,3-triazoles have various potential applications as sensors (due to the variation of the plasmon absorption with ATP and vitamin C in water) and probably in oxidation catalysis. In addition, their useful properties on ligand substitution could be investigated in more sophisticated syntheses (Chapter 3).

The introduction of complexes of Fe (II) spin transition is an example of synthesis of nanomaterials. This work collaborated with Azzedine Bousseksou's group was aim to study the spin transition between low-spin complex (zero) and high spin (two) in particular by the SERS method (detected by Raman spectroscopy field in the immediate vicinity of AuNPs). The exponential decay of the Raman effect as and when the distance from the surface implies that the Fe (II) are extremely close to the surface, what we have probably underestimated in the first approach. However, the

overall work of the band from Toulouse on these materials has recently allowed us to submit an article for publication in collaboration (Chapter 4).

In sum, our thesis has led to advances in the development of current knowledge on the synthesis of AuNPs and the vectorization of docetaxel. Thus, the engineering of AuNPs on development and functionalization open a new utilization and potential application of AuNPs in nanomedicine and nanomaterials fields.